



HAL
open science

Role of retinal ephrin-As in the formation of visual maps

Élise Savier

► **To cite this version:**

Élise Savier. Role of retinal ephrin-As in the formation of visual maps. *Neurons and Cognition* [q-bio.NC]. Université de Strasbourg, 2016. English. NNT : 2016STRAJ042 . tel-01560670

HAL Id: tel-01560670

<https://theses.hal.science/tel-01560670>

Submitted on 11 Jul 2017

HAL is a multi-disciplinary open access archive for the deposit and dissemination of scientific research documents, whether they are published or not. The documents may come from teaching and research institutions in France or abroad, or from public or private research centers.

L'archive ouverte pluridisciplinaire **HAL**, est destinée au dépôt et à la diffusion de documents scientifiques de niveau recherche, publiés ou non, émanant des établissements d'enseignement et de recherche français ou étrangers, des laboratoires publics ou privés.

UNIVERSITÉ DE STRASBOURG

ÉCOLE DOCTORALE DE VIE ET SANTÉ

Institut des Neurosciences Cellulaires et Intégratives

UPR3212

THÈSE présentée par :

Elise SAVIER

pour obtenir le grade de : **Docteur de l'université de Strasbourg**

Discipline/ Spécialité : Neurosciences

**Rôle des éphrines-As rétiniennes dans la mise
en place des cartes visuelles**

THÈSE dirigée par :

M. REBER Michaël

Docteur, Institut des Neurosciences cellulaires et
Intégratives, Strasbourg

RAPPORTEURS :

M. DRESCHER Uwe

Professeur, King's College, MRC - Department of
Developmental Neurobiology, London

M. NICOL Xavier

Docteur, Institut de la Vision, UPMC, Paris

AUTRES MEMBRES DU JURY :

M. ISOPE Philippe

Docteur, Institut des Neurosciences cellulaires et
Intégratives, Strasbourg

M. WILLSHAW David

Professeur, Institute for Adaptive and Neural
Computation, School of Informatics, University of
Edinburgh

Role of retinal ephrin-As in the formation of visual maps

Elise SAVIER



"The brain is a world consisting of a number of unexplored continents and great stretches of unknown territory" – *Santiago Ramón y Cajal*

Acknowledgment

The present document would not have been possible without the help, encouragements and support of many persons. I thank all of them and I present them all my gratitude.

I would like to express my gratitude and appreciation to my thesis supervisor, Dr. Michaël Reber for advice and guidance.

I would like to thank Pr. Uwe Drescher, Pr. David Willshaw, Dr. Xavier Nicol and Dr . Philippe Isope for accepting to be a member of the jury of this thesis.

I would like to thank my colleagues, Frank Pfrieder, Martine Perraut and Amélie Barthélemy for technical advice and support.

I would like to thank my colleagues for stimulating discussions and inspiring comments. In this regard, I would like to especially thank Alvaro Sanz-Diez and Kevin Dorgans for help achieving some experiments and their support.

This work would have not been possible without collaboration with Stephen Eglen, to which I would like to express my gratitude.

I would like to thank my professors during initial training, especially Vincent Lelièvre, who has always been of great advice.

I would like to thank Richard Pinnell for spending time on the manuscript and also for being supportive.

Finally, I would like to thank my friends, and my mother, which always believed in me and supported me.

"Alone we can do so little, together we can do so much." – *Helen Keller*

Objective statement:

The following study addresses the role of retinal ephrin-As in the formation of visual maps. Unraveling the role of these molecules requires a quantitative approach which can only be permitted by disturbing in a quantitative manner, the gradient of ephrin-As in the retina. This was achieved by the generation of the Isl2-ephrin-A3 knock-in mouse model in which ephrin-A3 is over expressed in 50% of retinal ganglion cells creating an alternating gradient of retinal ephrin-As. The effect of this over-expression was then assessed on the formation of the retino and the cortico-collicular maps together with the behavioral consequences of altered visuotopic maps.

Table of content

Liste des abréviations en Français.....	1
List of abbreviations in English.....	1
Résumé détaillé en Français.....	4
Introduction.....	10
Maps in the nervous system.....	11
Anatomical description of the visual system.....	13
Retina	13
Vertical transmission of light information.....	13
Horizontal transmission of information.....	15
Retinal ganglion cells.....	16
Superior colliculus.....	19
Anatomy.....	19
Connectivity.....	21
Primary visual cortex.....	24
Anatomy.....	24
Connectivity.....	24
Retinotopy in the visual system.....	26
Retinotopy in the superior colliculus.....	26
Retinotopy in the primary visual cortex.....	26
Developmental timeline of retinotopy in the superior colliculus.....	28
Chemoaffinity hypothesis.....	29
The molecular biology of axon guidance.....	29
Identification of molecular cues.....	31
Eph and ephrins.....	33
Eph and ephrin family.....	33
Eph and ephrin signalling.....	35
EphAs and ephrin-As.....	39
Expression of EphA and ephrin-A in the visual system.....	39
Retina.....	39
Superior colliculus.....	41
Primary visual cortex.....	42
EphAs and ephrin-As in retino-collicular map formation.....	44
Eph and ephrins in cortico-collicular map formation and alignment.....	49
EphB and ephrin-B	51
Expression of EphB and ephrin-B in the visual system.....	51
Retina.....	51
Superior colliculus.....	53
EphB/ephrin-B in the formation of the retino-collicular map in mouse	55
Activity in the formation of visual maps.....	58
Spontaneous activity in the retina during development.....	60
Effect of altered activity in the retina.....	61
Effect of altered activity in the superior colliculus	63

Competition in the formation of visual maps: biology	67
Mechanistic models of retino-collicular map development.....	68
Forward signalling is relative	68
Counter-balancing repulsion	70
Competition.....	70
Theoretical modeling.....	71
Visual maps and behavior.....	74
Superior colliculus and behavior.....	74
Superior colliculus and attention deficits.....	74
Publications.....	76
Overview.....	77
Defective response inhibition and collicular noradrenaline enrichment in mice with duplicated retinotopic map in the SC.....	79
Overview.....	91
Estimating the location and size of retinal injections from orthogonal images of an intact retina.....	92
Overview.....	102
A Molecular Mechanism for the Topographic Alignment of Convergent Neural Maps	104
Complementary data.....	139
Ephrin-A3 expression on retinal ganglion cells axons	139
Ephrin-A3 expression in the superior colliculus	141
Termination zones morphology in <i>Isl2-ephrin-A3KI/KI</i>	145
Distance separation in cortico-collicular duplication in <i>Isl2-ephrin-A3KI/+</i> and <i>KI/KI</i>	146
Retino-collicular map in <i>Isl2-ephrin-A3KI</i> x <i>EphA4KO</i>	147
In silico modeling of the <i>Isl2-EphA3KI</i> cortico-collicular map.....	148
Discussion.....	149
Role of counter-gradients in the visual system.....	150
Role of retinal ephrin-As in the alignment of visual maps.....	152
Gradient matching and retinal-matching model.....	153
Stochasticity in molecular guidance.....	154
Behavior of the <i>Isl2-EphA3KI</i>	155
References.....	157

Index of figures and tables

Figure 1: Overview of the mouse primary visual system.....	12
Figure 2: Horizontal and vertical transmission of light information in the retina.....	14
Figure 3: Phototransduction.	14
Figure 4: Anatomy of the superior colliculus.	20
Figure 5: Major cell types in the superficial layers of the SC.	20
Figure 6: Schematic of the superior colliculus connectivity.	23
Figure 7: Principal connections to the primary visual cortex.	23
Figure 8: Anatomical retinotopy in primary visual system.	27
Figure 9: Developmental time of retino- and cortico-collicular maps.	27
Figure 10: Growth cone response to different molecular cues.....	30
Figure 11: Stripe assay.	30
Figure 12: Structure of Eph receptor and ephrin ligands.	32
Figure 13: Phylogenetic tree of Eph and ephrin family members and cross-talks.	32
Figure 14: Eph–ephrin signalling modes.	34
Figure 15: Intracellular activation upon Eph/ephrin activation.....	34
Figure 16: Overview of EphA/ephrin-A expression in the visual system.	40
Table 1: Summary of EphA and ephrin-A expression in the visual system	43
Table 2: Summary of mouse models used in the study of role of EphA/ephrin-A signalling in the formation of retino-collicular map.	48
Figure 17: Overview of EphB/ephrin-B expression in the visual system.....	52
Table 3: Summary of EphB and ephrin-B expression in the visual system	54
Figure 18: Refinement of projections by correlated activity.....	59
Figure 19: Propagation of retinal waves in the retina.	62
Table 4: Summary of the effects of altered activity on retinotopy in the superior colliculus in mouse...	65
Figure 20: Models of counter-balancing forces in retino-collicular mapping.	69
Figure 21: Theoretical model for neural map formation.....	69
Figure 22: Ephrin-A3 expression on RGCs entering the superior colliculus.....	139
Figure 23: Ephrin-A3 expression on optic nerve.	140
Figure 24: EphrinA3 expression in the superior colliculus.....	141
Figure 25: Ephrin-A3 expression in the superior colliculus.....	142
Figure 26: Ephrin-A3 staining in the superior colliculus.....	143
Figure 27: Ephrin-A3 staining in the superior colliculus.	143
Figure 28: EphrinA3 immunostaining in the superior colliculus.	144
Figure 29: Morphology of the retinal ganglion cells termination zones in the superior colliculus.....	145
Figure 30: Cortico- and retino-collicular termination zones.....	145
Figure 31: Distance separation between cortico-collicular termination zones in the superior colliculus in Isl2-ephrin-A3KI.....	146
Figure 32: Retino-collicular map of Isl2-ephrin-A3KI x EphA4KO.....	147
Figure 33: In silico modeling of the retino- and cortico-collicular map of Isl-EphA3KI/KI.	148

Liste des abréviations en Français

CGR	Cellule ganglionnaire de la rétine
Dil	1,1'-dioctadecyl-3,3,3',3'-tetramethylindocarbocyanine perchlorate
E	Jour embryonnaire
Eph	erythropoietin-producing human hepatocellular
Ephrin	Eph receptor-interacting proteins
Isl2/Islet-2	Insulin related protein 2
LGN	Corps genouillé latéral
P	Jour post natal
TDA/H	Trouble du déficit de l'attention/hyperactivité
V1	Cortex visuel primaire

List of abbreviations in English

Abi1	Abl interacting protein 1
AC1	Adenylate cyclase 1
Adam	A disintegrin and metalloproteinase
ADD	Attention-Deficit disorder
ADHD	Attention-Deficit/Hyperactivity disorder
AL	Anteromedial
AMPA	α -amino-3-hydroxy-5-methyl-4-isoxazolepropionic acid
AP	alkaline phosphatase
AP5	2-amino-5-phosphonopentanoic acid
ASD	Autism spectrum disorder
BDNF	Brain derived neurotrophic factor
Beta2	Beta 2 nicotinic receptor subunit
Brn3/Pou4f2	POU domain transcription factor
Cad8	Cadherin-8
cAMP	Cyclic Adenosine monophosphate
CAP	C-Abl associated protein
CB	Cone bipolar cell
CB	Cannabinoid receptor
Cdc42	Cell division control protein 42 homolog
Cg	Cingulate cortex
cGMP	Cyclic guanosine monophosphate
COS	CV-1 (simian) in Origin carrying SV40 genetic material.
CTB	Cholera toxin subunit B
D-AMPH	Dextroamphetamine
D1/D2	Dopamine receptor
Dil	1,1'-dioctadecyl-3,3,3',3'-tetramethylindocarbocyanine perchlorate
DOV	dorsally oriented vertical
Drd4	Dopamine receptor D4
DS	Direction-selective
dSC	Deep superior colliculus
DSGC	Direction-selective ganglion cell
DSM	Diagnostic and Statistical Manual of Mental Disorders
E	Embryonic day
Eph	Erythropoietin-producing human hepatocellular
ephrin	Eph receptor interacting protein
eTZ	Ectopic termination zone
Fc	Fragment crystallizable

fMRI Functional magnetic resonance imaging
 G-protein guanine nucleotide-binding proteins
 GABA Gamma-aminobutyric acid
 GCL Ganglion cell layer
 GDP Guanosine diphosphate
 GEF Guanine nucleotide exchange factor
 GPI Glycosylphosphatidylinositol
 Grb4 Growth factor receptor-bound protein
 GTP Guanosine triphosphate
 Hoxd10 Homeobox D10
 INL Inner nuclear layer
 IPL Inner plexiform layer
 ISH In situ hybridization
 Isl2/Islet2 Insulin related protein 2
 J-RGC Jam-B retinal ganglion cell
 JAM-B Junction adhesion molecule-B
 kcng Potassium voltage-gated channel subfamily G member
 KI knock-in
 KO knock-out
 LacZ LacZ β -galactosidase
 LC Locus coeruleus
 LGN Lateral geniculate nucleus
 LM lateralmedial
 LP Lateral posterior nucleus/pulvinar
 LTP Long term potentiation
 M opsin Medium wavelength-sensitive
 MAO-A Monoamine oxydase-A
 MAPK Mitogen-activated protein kinases
 mGluR Metabotropic glutamate receptor
 MPH Methylphenidate
 mRNA Messenger ribonucleic acid
 nAChR Nicotinic acetylcholine receptors
 Ndnf neuron-derived neurotrophic factor
 NF Narrow-field cell
 NMDA N-methyl-D-aspartate receptor
 ONL Outer nuclear layer
 OPL Outer plexiform layer
 OS Outer segment
 P Postnatal day
 P75NTR neurotrophin *receptor* p75
 PBGN Parabigeminal
 PDE Phosphodiesterase
 PI-PLC Phosphatidylinositol-specific phospholipase C
 PKA Protein kinase A
 PKG Protein kinase G
 PM Posteromedial
 PPRF Paramedian pontine reticular formation
 PV Parvalbumin
 RB Rod bipolar cell
 RGC Retinal ganglion cell
 riMLF Rostral interstitial nucleus of the medial longitudinal fasciculus
 RS Retrosplenial cortex
 RTK Receptor tyrosine kinase

S opsin Short wavelength-sensitive
 SAC Starburst amacrine cell
 SAI stratum album intermediale
 SAM Sterile alpha motif
 SAP Stratum album profundum
 SC Superior colliculus
 SFK Src family kinase
 SGI Stratum griseum intermediale
 SGS Stratum griseum superficiale
 SH2 *Src Homology 2*
 SO stratum opticum
 SPIG1/ SPARC-related protein containing immunoglobulin domains 1/
 FSTL4 Follistatin-like protein 4
 SPP1 Secreted Phosphoprotein 1
 sSC Superficial superior colliculus
 SST Somatostatin
 SZ Stratum zonale
 Ten-m3 Teneurin Transmembrane Protein 3)
 Thy1 Thymocyte antigen 1
 TK Tyrosine kinase
 TRHR Thyrotropin Releasing Hormone Receptor
 Trk Tropomyosin *receptor* kinase
 TTX tetrodotoxin
 TYW Thy1 regulatory elements driven expression of YFP, wheat germ
 agglutinin (WGA), and Escherichia coli β -galactosidase
 TZ Termination zone
 UV Ultraviolet
 V1 Primary visual cortex
 VIP Vasointestinal peptide
 WF Wide-field cell
 WT Wild-type
 X-gal 5-bromo-4-chloro-3-indolyl-beta-D-galactopyranoside

Résumé détaillé en Français

Notre capacité à nous représenter le monde extérieur et à interagir avec celui-ci dépend de notre perception sensorielle. Celle-ci résulte de l'intégration de nos sens et nécessite la conservation de la temporalité et de la spatialité de l'information sensorielle. La conservation de l'information spatiale est primordiale dans la vision qui constitue le sens dominant chez l'homme. Afin de conserver cette dimension, le système nerveux central est organisé sous forme de cartes nerveuses sensorielles au sein des systèmes visuel (rétinotopie), somato-sensoriel (somatotopie), et auditif (tonotopie).

Notre objet d'étude est la connectivité au sein du système visuel primaire, entre la rétine, le colliculus supérieur (dans le mésencéphale) et le cortex visuel primaire (V1) et le rôle des molécules de guidage de la famille des éphrines-A dans le maintien de la rétinotopie dans ce système de connexions.

Le colliculus est une structure sous-corticale majeure d'intégration multi-sensorielle, recevant des afférences visuelles, auditives et somatosensorielles. D'un point de vue physiologique, le colliculus supérieur est impliqué dans l'orientation du regard et la génération de saccades (mouvements rapides de l'oeil), et plus récemment, son rôle a également été démontré dans des processus cognitifs plus complexes, comme le contrôle de l'attention (Krauzlis et al., 2013).

Au cours du développement, dès le jour embryonnaire 15 (E15), les cellules ganglionnaires de la rétine (CGR) quittent la rétine par le biais du nerf optique et projettent dans le colliculus supérieur pour former une carte rétino-topique au 8e jour post-natal (P8) chez la souris. De P9 à P12 des projections en provenance de la couche V du cortex V1 viennent s'établir dans le colliculus supérieur et s'alignent avec les projections rétiniennes. Le colliculus supérieur présente ainsi deux cartes visuelles continues, les projections rétiniennes (carte rétino-colliculaire) et corticales (carte cortico-colliculaire). Les mécanismes de mise en place et d'alignement de ces cartes sont encore peu caractérisés.

La relation spatiale entre les CGR au niveau de la rétine se retrouve dans les connexions synaptiques dans le colliculus supérieur : l'axe nasal-temporal de la rétine projetant le long de l'axe rostral-caudal du colliculus supérieur et l'axe dorsal-ventral de la rétine projetant le long de l'axe médio-latéral. Cette topographie est également maintenue dans la carte cortico-colliculaire, l'axe latéro-médial de V1 projetant le long de l'axe caudal-rostral du colliculus supérieur, tandis que l'axe antéro-postérieur projette sur l'axe latéro-médial. Parmi les problématiques soulevées, l'organisation spatiale des projections rétino-topiques du colliculus supérieur demeure centrale et sa compréhension ouvre de nombreuses perspectives fondamentales mais également biomédicales, dans le cadre des maladies du neurodéveloppement (Trouble du déficit de l'attention, autisme)(Mathis et al., 2014).

Des études antérieures ont démontré un rôle essentiel des Ephs et éphrines dans la mise en place des projections de la rétine vers le colliculus supérieur (carte rétino-colliculaire). Plus précisément les EphAs/éphrines-A sont chargées de la mise en place de l'axe nasal-temporal tandis que les EphBs/éphrines-B organisent l'axe dorsal-ventral. Les EphAs sont des récepteurs tyrosine kinase qui reconnaissent avec un degré d'affinité similaire les différentes éphrines-A. Leur mode de signalisation est bidirectionnel, les récepteurs Ephs pouvant être activés par les ligands (éphrines) et réciproquement. L'expression des EphAs se fait selon un gradient croissant nasal-temporal au niveau de la rétine, tandis que les éphrines-A sont exprimées de façon croissante selon l'axe rostral-caudal au niveau du colliculus supérieur et activent les récepteurs EphAs portés par les axones rétiniens. Une particularité du système EphAs/éphrines-A est la présence d'un contre-gradient d'éphrines-A (temporal → nasal) dans la rétine et de EphAs (caudal → rostral) dans le colliculus supérieur, dont le rôle est encore à ce jour mal connu.

Optimisation de la localisation des coordonnées rétiniennes :

L'étude de la mise en place des cartes visuelles nécessite des techniques de traçage précises afin de mettre en relation les coordonnées rétiniennes avec les coordonnées des sites de projections dans le colliculus supérieur. L'obtention des coordonnées rétiniennes s'effectue grâce à une mise à plat de la rétine après dissection. Cette méthode, laborieuse, introduit de nombreux biais. De plus, il est nécessaire ultérieurement de projeter les coordonnées selon l'axe nasal-temporal, induisant une perte d'information supplémentaire. Afin d'optimiser l'acquisition de ces coordonnées rétiniennes, nous avons participé à la validation d'une méthode informatique intitulée IntactEye.

En collaboration avec Stephen Eglén et Johannes Hjort du département de Mathématiques Appliquées et de Physiques Théoriques de Cambridge, un algorithme permettant de localiser le site d'injection a été développé. Cette méthode permet, à partir de rétines intactes, encore sphériques de localiser avec précision le site d'injection à partir de deux images et de calculer sa position le long de l'axe nasal-temporal, sans procéder à la mise à plat de la rétine. Un article présentant cette méthode a été publié (Hjorth et al., 2015).

Rôle des éphrine-As rétiniennes dans la mise en place des cartes visuelles.

Afin d'élucider la fonction du gradient d'éphrine-As rétiniennes, un modèle de souris knock-in a été généré. Ces souris sur-expriment le ligand éphrine-A3, sous le contrôle du promoteur du gène *Isl2*, un facteur de transcription présent dans 50% des CGR. Ce modèle murin, les souris *Isl2*-éphrine-A3 knock-in (KI) présente deux populations de CGR, l'une avec un niveau endogène d'éphrines-A (éphrine-A2/A3/A5) et l'autre présentant une sur-expression d'éphrine-A3 qui s'ajoute au niveau endogène d'éphrines-A, perturbant ainsi de manière quantitative le gradient d'éphrines-A rétiniennes.

Caractérisation moléculaire du modèle *Isl2*-éphrine-A3KI :

Le modèle murin *Isl2*-éphrine-A3KI a été caractérisé d'un point de vue moléculaire selon deux approches : quantification des ARNm par PCR quantitative et mise en évidence de l'expression protéique d'éphrine-A3 et d'*Isl2* par techniques d'immunofluorescence. Les résultats obtenus confirment que la sur-expression d'éphrine-A3 ne perturbe pas les niveaux de transcription endogène des EphAs/éphrines-A et que le motif d'expression d'éphrine-A3 co-localise avec la présence d'*Isl2*, induisant une surexpression ectopique. Ainsi, il a été possible de démontrer la présence de deux sous-populations au niveau des CGR dans le modèle *Isl2*-éphrine-A3KI : l'une exprimant des niveaux endogènes d'éphrines-A/EphAs, l'autre sur-exprimant éphrine-A3 sous le contrôle d'*Isl2*. Une fois le modèle validé, la caractérisation phénotypique de la carte rétino-colliculaire a pu être établie.

Carte rétino-colliculaire des *Isl2*-éphrine-A3KI:

La carte rétino-colliculaire de ce modèle a été caractérisée par injection d'un traceur lipophile (Dil) au niveau de la rétine. Pour chaque injection, la localisation de la zone de terminaison dans le colliculus supérieur a été identifiée par microscopie confocale, mesurée et mise en relation avec la localisation de l'injection au niveau de la rétine après mise à plat. Cette étude a été réalisée sur des animaux à P8. Une cartographie a ainsi pu être réalisée chez les homozygotes, les hétérozygotes *Isl2*-éphrine-A3KI, ainsi que les souris contrôles. Nos données révèlent une absence d'effet de la sur-expression d'éphrine-A3 dans les CGR sur la carte rétino-colliculaire, suggérant qu'éphrine-A3 n'est pas directement impliquée dans la formation des connexions rétino-colliculaires.

Caractérisation des projections rétino-géniculaires :

Des injections sub-rétiniennes focales de Dil ont permis la localisation des sites de terminaison au sein du corps genouillé latéral (LGN), une autre cible majeure des projections de la rétine. L'analyse par correspondance topographique en comparaison au souris sauvage ainsi que la morphologie des sites de terminaison n'ont révélé aucune différence chez les souris Isl2-épinephrine-A3KI.

Caractérisation de la ségrégation ipsi et contralatérale des projections :

Des injections intra-oculaires de toxine cholérique couplée à un fluorophore permettent de marquer dans leur intégralité les projections en provenance de la rétine et de déterminer leur domaine d'occupation dans le LGN ainsi que dans le colliculus supérieur. Ce type de marquage permet de vérifier la ségrégation des entrées en fonction de leur provenance. En effet, chez la souris, 5% des CGR projettent de manière ipsilatérale et les épinephrine-A ont été impliquées dans leur ségrégation (Pfeiffenberger et al., 2005). Cette caractérisation n'a révélé aucun défaut chez la souris Isl2-épinephrine-A3KI quant à la séparation des projections.

Mise en évidence d'un chevauchement des sites de projection rétino et cortico-colliculaires:

Afin de mettre en évidence une interaction entre les projections en provenance de la rétine et du cortex visuel primaire un double marquage a été réalisé. La totalité des projections rétiniennes a été marquée à l'aide de la toxine cholérique couplée à un fluorophore tandis que les projections en provenance de l'aire primaire visuelle ont été marquées par un traceur lipophile (Dil). Ce double marquage démontre un chevauchement et en conséquence une interaction entre ces deux types de projections. Ces résultats ont ensuite été confirmés par une transfection par des adénovirus exprimant une protéine fluorescente.

Caractérisation des projections cortico-colliculaires :

Des études antérieures portant sur les épinephrine-A ont mis en évidence que celles-ci étaient impliquées dans l'établissement de la carte cortico-colliculaire ($V1 \rightarrow SC$) (Cang et al., 2005a) et que la mise en place de cette dernière dépendait également de l'activité neuronale de la carte rétino-colliculaire (Triplett et al., 2009). En effet, d'un point de vue développemental, les projections du cortex vers le colliculus supérieur arrivent plus tardivement que les projections de la rétine. La duplication de la carte rétino-colliculaire observée chez les mutants Isl2-EphA3 entraîne également une duplication des projections originaires de l'aire visuelle primaire V1 (Triplett et al., 2009). L'hypothèse émise par ces auteurs suggérait alors un rôle de l'activité neuronale de la carte rétino-colliculaire dans le contrôle de la formation de la carte cortico-colliculaire.

En conséquence, les projections cortico-colliculaires chez le modèle Isl2-épinephrine-A3 ont été caractérisées par le biais d'injections de traceur neuronal dans V1 chez des souris à P15 pour lesquelles la carte cortico-colliculaire est mature. De manière intéressante, des duplications ont été observées chez 47% des animaux homozygotes et 43% des animaux hétérozygotes, bien que la carte rétino-colliculaire soit similaire aux contrôles. De plus, la distance de séparation des zones de projection est doublée chez les homozygotes par rapport aux hétérozygotes (7 et 13% de la longueur de l'axe colliculaire), suggérant un effet dépendant du nombre de copies de l'allèle. Cette observation serait en faveur d'un rôle important de la signalisation moléculaire, en plus de l'activité neuronale rétino-colliculaire, pour la mise en place des projections cortico-colliculaires. L'hypothèse mécaniste suggère que le ligand épinephrine-A3 est transporté dans le colliculus supérieur par les axones rétiniens

et fournirait une information positionnelle aux axones corticaux en provenance de V1. Le décalage de maturation des cartes rétino et cortico-colliculaire au cours du développement (P8 versus P12) plaide en faveur d'un tel mécanisme.

La pénétrance partielle du phénotype pourrait s'expliquer par la nature stochastique de la formation des cartes au sein du système visuel, supportée par d'autres travaux récents (Owens et al., 2015). En effet, l'activité neuronale de la carte rétino-colliculaire étant normale, celle-ci pourrait contrebalancer, dans une certaine mesure, la séparation induite par la signalisation moléculaire. De plus la présence de zone de terminaisons dupliquées et simples a pu être observée au sein du même animal, excluant une différence due à la pénétrance génique du phénotype.

Carte rétino-colliculaire des *Isl2-EphA3KI* x *Isl2-éphrine-A3KI*

Le modèle *Isl2-éphrine-A3KI* a ensuite été croisé avec le modèle *Isl2-EphA3KI* qui lui sur-exprime dans la même sous population de CGR le récepteur EphA3. Cette mutation seule entraîne une duplication de la carte rétino-colliculaire chez les mutants homozygotes, et une duplication partielle chez les mutants hétérozygotes, caractérisée par la présence de duplications au niveau caudal et de terminaisons simples au niveau rostral (Brown et al., 2000; Reber et al., 2004). Nous avons pu constater après réalisation de la cartographie chez les doubles hétérozygotes *Isl2-EphA3/éphrine-A3*, une réversion du phénotype *Isl2-EphA3KI*, en d'autres termes, une absence de duplication sur la totalité de l'axe rostral-caudal. Ce phénotype révèle que la co-expression d'éphrine-A3 (au sein de la *même* CGR) provoque une interaction en *cis* entre éphrine-A3 et EphA3 suffisante pour inactiver EphA3 localement.

Carte cortico-colliculaire des *Isl2-EphA3KI* x *Isl2-éphrine-A3KI*

La cartographie cortico-colliculaire des doubles mutants a également été réalisée. L'absence de détection de duplication indique une réversion du phénotype *Isl-éphrine-A3KI/+*, confirmant l'inactivation conjointe du ligand éphrine-A3 ainsi que du récepteur EphA3.

Modélisation in silico :

Afin de valider la pertinence du modèle mécaniste proposé, une adaptation d'une modélisation in silico existante a été réalisée. Le modèle original (Koulakov and Tsigankov, 2004) permet de modéliser la formation de la carte rétino-colliculaire en fonction des gradients d'EphA et d'éphrine-A et de l'activité neuronale. Afin de reproduire la formation de la carte cortico-colliculaire qui arrive séquentiellement après la formation de la carte rétino-colliculaire, nous avons dans un premier temps modélisé les projections rétino-colliculaires, puis transposé le gradient d'éphrine-A rétinienne dans le colliculus supérieur sur cette carte ainsi établie. Cette carte sert ensuite de support, fournissant les informations positionnelles nécessaires pour guider la mise en place de la carte cortico-colliculaire. Cette signalisation se fait donc en fonction des gradients d'EphA présents dans le cortex visuel primaire et des gradients d'éphrine-A originaires de la rétine, transposés dans le colliculus supérieur. Cette modélisation séquentielle permet de simuler la mise en place des cartes chez les animaux sauvages mais reproduit également nos observations, avec un taux de duplication et une distance de séparation des projections similaires à ceux caractérisés chez les homozygotes et les hétérozygotes.

Conclusion :

En conclusion, mes travaux ont pu identifier le rôle des éphrines-A rétinienne, jusque là controversé, en mettant en évidence un nouveau mécanisme moléculaire d'alignement des cartes rétino-topiques impliquant ces molécules. Plus généralement, une carte sensorielle de référence

fournit l'information moléculaire nécessaire à l'alignement d'une seconde carte sensorielle. D'un point de vue conceptuel, ce mécanisme permet un ajustement précis des cartes sensorielles en compensant la variabilité naturelle de la carte de référence.

Etude comportementale du modèle murin Isl2-EphA3KI

Le modèle murin Isl2-EphA3KI

Le modèle murin Isl2-EphA3KI qui surexprime une molécule de guidage (EphA3) dans une sous-population de cellules ganglionnaires de la rétine, a permis des avancées conceptuelles majeures dans la compréhension des mécanismes moléculaires contrôlant la mise en place des cartes visuelles (Bevins et al., 2011; Brown et al., 2000; Owens et al., 2015; Reber et al., 2004; Triplett et al., 2009). D'un point de vue anatomique, ces souris présentent une duplication des projections visuelles de la rétine et de l'aire corticale V1 vers le colliculus supérieur situé dans le mésencéphale. Ces projections visuelles vers le colliculus sont organisées de manière topographique, en d'autres termes, la topographie de l'espace visuel est représentée et conservée au sein du colliculus supérieur (figure 1). Dans le cas du mutant Isl2-EphA3KI, cette duplication anatomique entraîne la formation de deux cartes, donc une représentation double de l'intégralité de l'espace visuel dans le colliculus supérieur. Cette duplication provoque, lors de la stimulation d'un point de l'espace visuel, une activation conjointe de deux zones distinctes dans le colliculus supérieur, induisant une hyperstimulation visuelle de celui-ci (Owens et al., 2015; Triplett et al., 2009).

Caractérisation comportementale

Afin de déterminer quelles étaient les conséquences comportementales de l'hyperactivation de ce centre d'intégration, nous avons réalisé des études comportementales et moléculaires chez le mutant Isl2-EphA3KI (Mathis et al., 2015). Nous avons ainsi pu démontrer que les capacités visuelles et mnésiques, la locomotion et l'apprentissage ne sont pas altérés. Néanmoins, le modèle murin Isl2-EphA3KI présente des troubles attentionnels, mis en évidence et confirmés par deux tests spécifiques (le test de boîte claire/obscur et la tâche de Go/No Go). Ces souris présentent donc, d'un point de vue comportemental, une impulsivité augmentée et une tendance à la distractivité, en particulier envers un distracteur visuel (Mathis et al., 2015).

Signalisation cathécholaminergique

Afin de vérifier si notre modèle murin présentait une altération de la signalisation monoaminergique (dopamine, sérotonine, adrénaline et noradrénaline), nous avons effectué la quantification de ces molécules, de leurs récepteurs, des enzymes métaboliques ainsi que des transporteurs dans différentes structures. Nos résultats ont révélé une absence de différences significatives concernant l'expression des récepteurs, enzymes métaboliques et transporteurs. En revanche, une augmentation significative (d'un facteur 2) de la noradrénaline dans les couches visuelles du colliculus supérieur, où est présente la duplication rétinotopique, a été démontrée chez le mutant homozygote.

Considérations thérapeutiques

Les symptômes que le modèle Isl2-EphA3KI présente sont similaires à ceux observés chez l'homme dans le trouble du déficit de l'attention (TDA). Le TDA est, d'après le DSM-V, un mode persistant d'inattention souvent accompagné d'hyperactivité-impulsivité qui apparaît au cours du développement de l'enfant avec une prévalence en France entre 3% et 5%. Ces troubles altèrent durablement la vie scolaire, sociale et familiale. persistent à l'âge adulte dans près de 65% des cas.

Les résultats d'analyse génétique chez l'homme ne montrent pas d'association significative avec un gène ou une famille de gènes donnés. L'hypothèse majeure actuelle quant à l'étiologie de cette psychopathologie repose sur un déséquilibre de la balance monoaminergique, et notamment la dopamine (Biederman, 2005; del Campo et al., 2011). Ces résultats proviennent de dosages sériques chez des patients ainsi que sur le mode d'action des traitements pharmaceutiques efficaces pour cette pathologie. En effet, le traitement de référence demeure le méthylphénidate, qui agit comme un inhibiteur des transporteurs de la dopamine et de la noradrénaline responsables de la recapture de ces molécules. Ces traitements n'apportent qu'un bénéfice modéré (Organisation Mondiale de la Santé) et comportent de nombreux effets secondaires, notamment sur le système cardio-vasculaire. Prenant en considération ces différents éléments, de nouvelles approches thérapeutiques sont nécessaires.

Cette altération de la noradrénaline est en accord avec la littérature, qui suggère qu'un déséquilibre de la voie noradrénergique pourrait être responsable des troubles comportementaux observés chez les patients. En parallèle, des travaux ont montré une implication du colliculus supérieur dans les troubles attentionnels. Des études chez l'humain montrent qu'une hyperactivation du colliculus supérieur est corrélée à une augmentation de la distractivité (Overton, 2008). Chez le rat, il a été mis en évidence que le méthylphénidate induit une modification de la qualité du traitement de l'information sensorielle dans le colliculus (Briggs et al., 2013; Dommett et al., 2009).

Conclusion

Considérant ces résultats, le mutant *Isl2EphA3KI* semble être un modèle de choix pour le TDA/H. Il présente en effet des symptômes similaires ainsi que les conséquences physiopathologiques retrouvées dans ce trouble. Ce modèle murin constitue une approche audacieuse comparé aux modèles basés sur une altération des voie monoaminergiques (Sontag et al., 2010). En effet, nos résultats démontrent qu'une altération du système sensoriel, en l'occurrence la vision, est suffisante pour reproduire ces symptômes chez l'animal, suggérant que la disruption de la balance noradrénergique pourrait n'être qu'une conséquence, et non pas la cause de la pathologie. Cette approche sensorielle est souvent négligée en psychiatrie et ouvre de nouvelles pistes thérapeutiques. Les troubles de la perception pourraient également induire d'autres pathologies du développement chez l'enfant, notamment l'autisme qui présente une forte comorbidité avec la synesthésie, un désordre sensoriel.

Introduction

Maps in the nervous system

During development, cells have to find their precise location and differentiate in order to establish functional organs. This is the result of the execution of a precise genetic program, orchestrated in a specific temporal order. Cells also exchange a variety of information through both cell-cell contacts and the secretion of molecules. As far as the nervous system is concerned, being specialized and at the right place is not enough. Neurons have to send projections across long distances in order to establish functional connections between the various structures within the brain. Projections also emanate from the periphery, in order to transfer information about the environment and the global state of the organism. How such connections are established at the right place and at the right time remains one of the most fundamental, yet unanswered, questions in neuroscience, as the overall structure and connectivity is the substrate for functions of the brain. Furthermore, fully understanding how projections are established during development would allow for new strategies to be devised regarding nerve regeneration, as well as providing an insight into ways for “rewiring” the brain in some pathological states.

Our ability to interact and evolve in our environment depends on the accuracy of our representation of the external world. This requires both spatial and temporal coding of a variety of stimuli for ensuring an appropriate response. Temporal coding is performed by the responding elements, with a variation in frequencies and delays, while spatial coding depends on the wiring of the network, and how these connections are established. This wiring across long distance mostly takes place during development. These long range projections will allow functional connectivity and an accurate response through signal processing by different relays, each with a specific role.

A striking feature of the organization of the nervous system is the maintenance of spatial order across different structures. This is often referred to as the “topographic order”, which is the maintenance of the spatial relationship between input neurons and their projecting sites in the target structure; taking the form of maps. These maps can be found at different levels in the brain and allow for an appropriate sensory representation as well as integration. They can take a variety of forms, such as a discrete or continuous representation of the sensory space (Luo and Flanagan, 2007).

Topographic maps appear during development and seems to be linked through this process. This form of organization seems to be appropriate for spatiotemporal computation, as well as proper sensory representation and integration. Another functional aspect is sensory discrimination (Kaas, 1997).

Maps in the brain are topographic at the global level and modular at the local level. The first step seems to be guided by molecular cues, (Flanagan, 2006; Wei et al., 2013) whilst the second step seems to be refined by activity-dependent mechanisms (Katz and Shatz, 1996).

Considering the energetic cost of establishing neuronal connections, optimization of the distance between functionally related neurons is required. This aspect has led to the formation of a variety of maps in the nervous system, where afferences are organized according to different features. Indeed, in the olfactory system, neurons with similar response properties end up projecting toward the same cluster in the next relay, whereas in the auditory system, projections are organized according to the tonotopy (frequency tuning). In the visual system, the spatial relationship is the key wiring constraint, which allows a representation of the environment according to space. This retinotopic organization allows neurons representing adjacent parts of the visual field to interact over short axonal and dendritic pathways (Chklovskii and Koulakov, 2004).

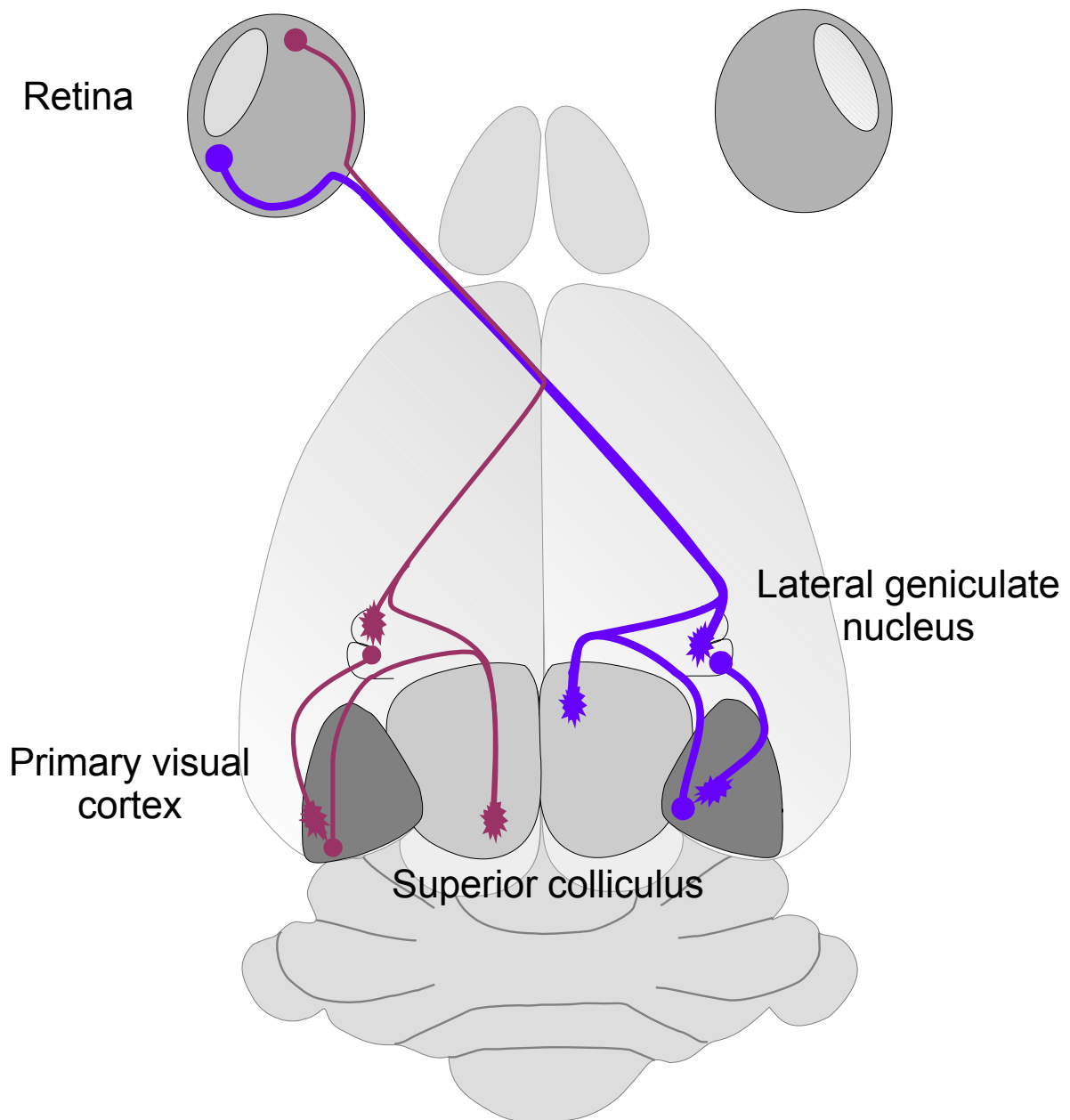


Figure 1: Overview of the mouse primary visual system. Light is sampled by the retina and transferred in parallel to the lateral geniculate nucleus and superior colliculus. Projections from the retina target mostly the contralateral side (blue). 5% of retinofugal projections target the ipsilateral side in mouse (purple). From the lateral geniculate nucleus, projections are sent to the V1. The superior colliculus receives in turn feedback from the primary visual cortex.

Anatomical description of the visual system

Vision is an active and constructive process that starts with sampling of the scenery. This is possible with the coordination of eye-movement and attention. All visual information regarding the outside world reaches the brain through the eye (Figure 1), where light is captured by a thin light-sensitive sheet of cells called the retina. Our internal representations are built upon information transmitted by the retinal ganglion cells (RGCs) after computation through the different cell layers of the retina.

Retina

The retina is made of 3 layers of cells and two layers of connections which are called the plexiform layers. The light information is gathered at the back of the eye by photoreceptors before being transduced and computed to the RGCs, which are the sole retina outputs to the brain. Two types of information transmission can be considered: vertical and the horizontal (Figure 2).

Vertical transmission of light information

The outer part of the retina is made of photoreceptors, which are the light detectors. Their outer segments, where the phototransduction operates, form the photoreceptor outer segments (OS). The rods and cone cell bodies form the outer nuclear layer (ONL), and make contact in the outer plexiform layer (OPL) with bipolar cells that form the inner nuclear layer (INL). Bipolar cells contact RGCs in the inner plexiform layer (IPL), and their cell bodies make the ganglion cell layers (GCL) (Figure 2).

Rods and Cones:

Light is detected in the retina by two types of photoreceptors: rods and cones. Rods are specialized for low-light vision and are highly sensitive, whereas cones mediate daylight vision and display a higher temporal resolution. In mice, rods represent 97% of the photoreceptors in the retina (Carter-Dawson and LaVail, 1979). Light sensitivity is conferred by visual pigments (opsins), for which three types can be found in mice photoreceptors. Rhodopsin is expressed in rods, while cones express two different types of opsins. The medium wavelength-sensitive (M) opsin has the highest sensitivity at 508nm, whereas the short wavelength-sensitive (S) opsin responds mostly at 360nm, and is in the UV spectrum (Nikonov et al., 2006; Tan et al., 2015). These two opsins display a segregated distribution along the dorsal-ventral axis (Applebury et al., 2000; Szél et al., 1992). According to this differential expression, the mouse retina can be divided into three parts:

- Dorsal retina, containing mainly MS cones with very little S opsin co-expression
- Central zone, in which the S/M opsin co-expression ratio increases
- Ventral retina, which strongly expresses S opsins

This particular distribution has been shown to be optimal for the processing of the visual scenery, with the dorsal part of retina responding essentially to green light and the ventral part responding to blue light (Baden et al., 2013).

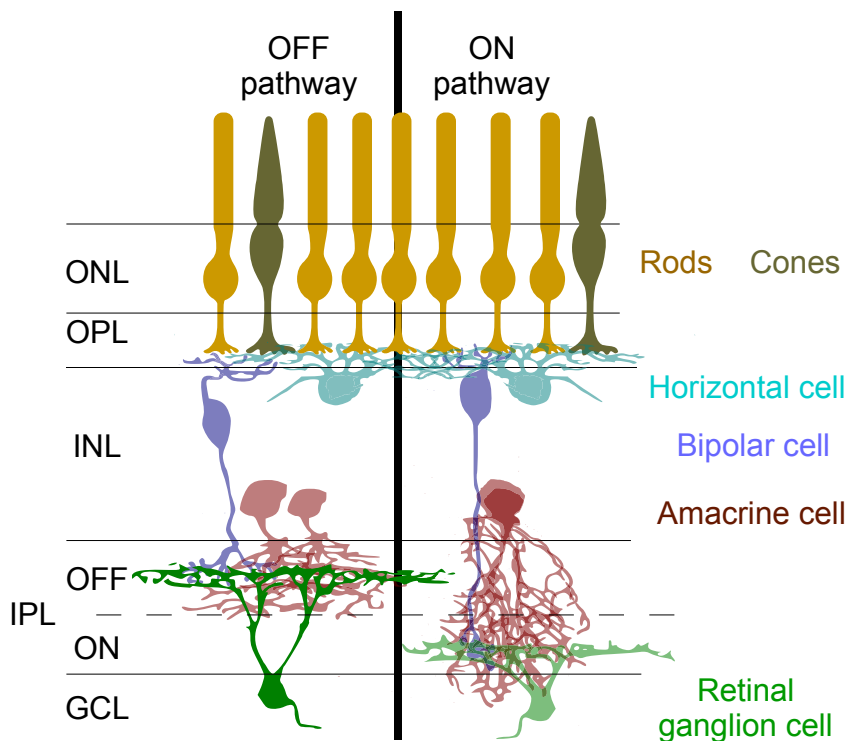


Figure 2: Horizontal and vertical transmission of light information in the retina. The OFF (left) and the ON (right) pathways and specific connectivity patterns are represented. Light information is sampled by rods (yellow) and cones (brown), located in the outer nuclear layer (ONL) which target OFF and ON bipolar cells (purple), forming the inner nuclear layer (INL). These connections, the outer plexiform layer (OPL) are modulated by horizontal cells (blue). Retinal ganglion cells (green), forming the ganglion cell layer (GCL) receive inputs in the inner plexiform layer (IPL) from bipolar cells modulated by amacrine cells (red).

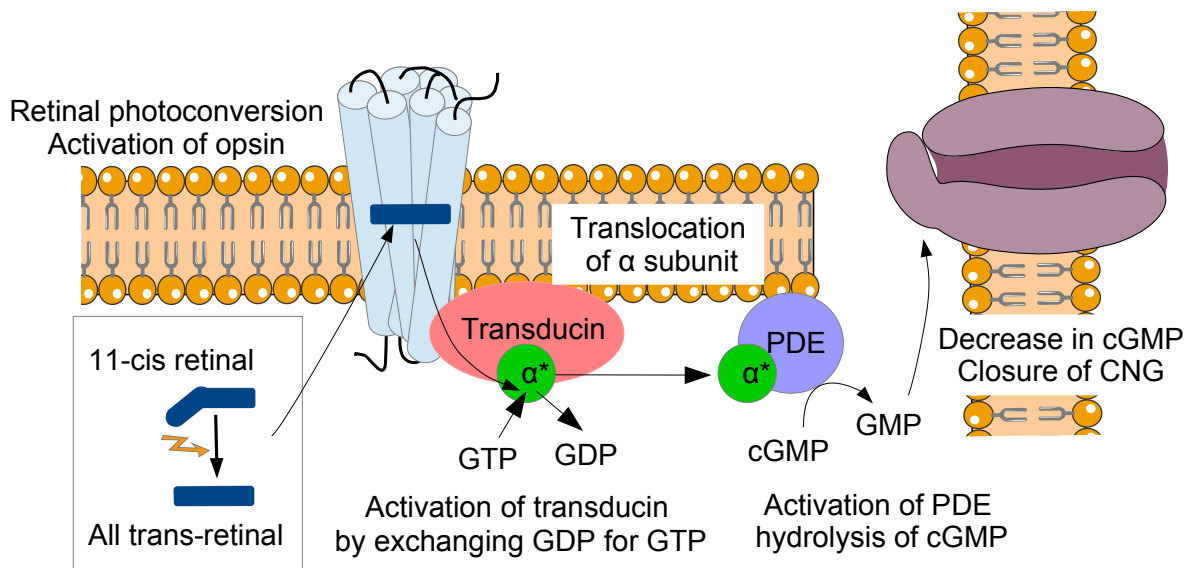


Figure 3: Phototransduction. Photoconversion of 11-cis retinal to all-trans retinal activate opsin. The α subunit of transducin is activated by exchanging GDP for GTP and translocates to activate phosphodiesterase (PDE). This lead to a decrease in cGMP levels which induces the closing of cyclic nucleotide gated channel (CNG).

Phototransduction

The outer layer of the retina is composed of photoreceptors that can detect photons via the activation of opsins. These visual pigments bind to retinal (retinaldehyde), which changes conformation when hit by photons: from 11-cis retinal to the all-trans configuration. Once activated, opsins interact with the G-protein transducin, which promotes the exchange of GDP to GTP, leading to the active form of the alpha subunit. This subunit activates phosphodiesterase (PDE), which hydrolyzes cGMP, leading to the reduction of the overall cytosolic cGMP concentration. This reduction induces a closure of cyclic nucleotide-gated channels, which in turn reduces the Na⁺ and Ca²⁺ influx, subsequently leading to the hyperpolarization of the cell and a reduction in glutamate release (Figure 3). Consequently, photoreceptors facilitate glutamate release in darkness, and reduces glutamate release when activated by light.

Bipolar cells

Photoreceptors transfer light detection to bipolar cells. These cells can be mostly ON or OFF and have different response properties to glutamate. OFF cells have ionotropic receptors (AMPA-kainate receptors mostly), and glutamate release in darkness depolarizes these cells. ON cells invert this response through G-coupled metabotropic receptors (mGluR6), which lead to the closure of cation channels (Euler et al., 2014). For these cells, glutamate release induces a hyperpolarization. ON and OFF bipolar cells target different parts of the IPL; the OFF cells making connections in the outer part, and the ON cells making connections in the inner part (Figure 2). In addition, bipolar cells can be divided in two groups according to their connections to either rods or cones. In mice, 12 types of bipolar cone (CB) cells and one type of bipolar rod (RB) cell can be found (Ghosh et al., 2004).

Horizontal transmission of information

Light information is gathered by photoreceptors and transferred to the RGCs via two parallel pathways: the ON pathway and the OFF pathway (Figure 2). However, many different features of vision are already extracted and sent through specialized types of RGCs, which is described below. Part of this computation is already performed in the retina through lateral connections. These connections are established by both horizontal and amacrine cells, which have their cell bodies in the inner nuclear layer and make connections in the outer and inner plexiform layers respectively.

Horizontal cells

Horizontal cells modulate the connections between photoreceptors and bipolar cells, and maintain the sensitivity of light detection over a broad range of intensities. This cell type is GABAergic, and generates a linear surrounding inhibition in the first synaptic layer of the retina through feed-forward excitation and inhibition (Thoreson and Mangel, 2012). Only one type of horizontal cell can be found in mice – the so-called B type – which has an axon terminal postsynaptic to rods. Even if still debated, current hypothesis suggest that the depolarization of horizontal cell dendrites suppresses glutamate release from photoreceptors, allowing adaptation for different light intensities (Demb and Singer, 2015a).

Amacrine cells

32 different types of amacrine cells have been identified, with their diversity highlighting their variety of functions (Cherry et al., 2009). These interneurons are either GABAergic or glycinergic, and can co-release dopamine or acetylcholine. These cells are broadly classified as either narrow- or wide-field, on the basis of the diameter of their dendritic trees. Narrow-field cells are commonly

glycinergic and wide-field cells are commonly GABAergic (Zhang and McCALL, 2012). Amacrine cells are postsynaptic to bipolar cells and are responsible for the acquisition of specific features, such as light motion detection and direction selectivity through local computation (Demb and Singer, 2015b). A particular type – the starburst amacrine cell (SAC) – enables a direction-selective computation in the retina. Both horizontal and vertical information are transferred to RGCs, the output of the retina.

Retinal ganglion cells

All visual information exits the retina through the RGCs. Both the connections and the spiking patterns established by these cells are the sole output of the retina to the brain, regarding the visual scenery. Current studies have revealed that RGCs are feature detectors, and send through parallel pathways images, which are partially processed. To date, 30 functional output channels have been identified according to both their morphology (Coombs et al., 2006) and their electrophysiological response properties (Baden et al., 2016). Recently, a lot of effort has been made towards the classification of RGCs, linking morphological types to molecular properties and to the type of stimuli to which these RGCs respond (Sanes and Masland, 2015). Here, the major classes of RGCs will be reviewed, with a particular focus on RGCs targeting the superior colliculus (SC).

Despite their diversity, RGCs share common properties. Their cell bodies are located in the ganglion cell layers, their dendritic arborizations extend into the inner plexiform layer, while their axons exit the retina through the optic nerve. From a molecular aspect, some pan-markers have been identified, notably Thy1 and Brn3 (Liu et al., 1996; Xiang et al., 1995). Their transmission to brain targets is mostly glutamatergic. A particular feature of RGC types is their homogeneous distribution across the retinal space which forms so-called mosaics. As a consequence, visual information is encoded by the same number of different RGC types.

On-Off DSGC:

At least 4 subtypes of ON-OFF direction-selective ganglion cells (DSGC) have been identified (Sanes and Masland, 2015). This group expresses commonly the gene that encodes the neuropeptide CART (cocaine- and amphetamine- regulated transcript) (Kay, 2011), in addition to different markers according to their response properties in the retina (Posterior: CART, Mmp17, Upward: CART, Col25a1, Cdh6, Downward: CART, Col25a1, Cdh6) (Dhande et al., 2015). ON-OFF DSGC respond to both increases and decreases in light intensities, in a specific direction. This selectivity is believed to be acquired from the direction-selective process of amacrine cells (Vaney et al., 2012). ON-OFF DSGC have a bistratified dendritic tree with one dendritic arbor targeting the ON sublamina of the inner plexiform layer (IPL), adjacent to the ganglion cell layer (GCL), whereas the other arbor stratifies in the OFF sublamina, adjacent to the inner nuclear layer (INL) (Famiglietti, 1992).

ON-OFF DSGC target both dorsal and ventral lateral geniculate nucleus (LGN), and present a laminar segregation in the SC where they target preferentially the upper parts of the SGS (stratum griseum superficiale), rather than the lower part. These RGCs do not project to the superchiasmatic nucleus, nor to the accessory optic nuclei or most of the pretectal nuclei (Hong et al., 2011; Kay, 2011).

ON DSGC:

Some DSGC only respond to ON stimuli; for example, moving light spots and moving light rather than dark spots and dark edges (Sun et al., 2006). They can be divided into three groups, according to their directional preference (upward, downward, or forward motion), and have a monostratified dendritic tree in the inner plexiform layer, where ON amacrine starburst cells can be

found. One of these subgroups can be specifically labeled with Hoxd10 and SPIG1, and targets the accessory optic system, which mediates optokinetic responses for stabilizing images according to self-motion (Dhande et al., 2013).

OFF DSGC

These cells are also named J-RGC, due to the expression of JAM-B (junction adhesion molecule B), and they present an asymmetric dendritic arbor along the dorsal-ventral axis of the retina. This induces a particular type of response: they respond to stimuli moving along the direction from the soma to the dendrite, and have an OFF center and a highly asymmetric ON surround (Kim et al., 2008a).

α RGCs

Three types of α RGCs have been described according to their response preferences (Van Wyk et al., 2009). These commonly coexpress the markers Spp1 (secreted phosphoprotein osteopontin) and kcng4 (a voltage-gated potassium channel subunit), are monostriated, and have different targets inside the IPL. These RGCs are center-surround spot detectors.

- Sustained ON α RGCs dendritic arborization target the lower IPL and express low levels of melanopsin
- Sustained OFF α RGCs target the central part of the IPL and share the TYWY7 (W7) marker with the transient OFF α RGCs
- Transient OFF α RGCs detect looming objects, and correspond to PV-5 or approach-sensitive RGCs. Their dendritic arborization can be found in the upper part of the IPL and express specifically CB2 (Huberman et al., 2008)

Local edge detectors or object motion sensing

W3B RGCs have small dendritic fields and target the center of the IPL. These cells have the properties to distinguish a moving object from moving stimuli generated by head or eye movements. This operates by suppressing their firing when both surround and center stimuli are moving at the same time. These are specifically labelled in the TWY3 (W3) transgenic line (Zhang et al., 2012).

ipRGCs

5 different types of RGCs (M1-M5) are intrinsically photosensitive and express melanopsin. They have a large dendritic arbor and project essentially to the suprachiasmatic nucleus (SCN), where they play a role in synchronizing circadian rhythms.

Other RGC types

Whilst other types of RGCs can also be found, they are not to date fully characterized; among them some are chromatically sensitive or orientation sensitive. Other morphologically inferred types have been observed in the retina but have not been linked to a particular type.

Retinal ganglion cells target to the brain

RGCs target 46 different brain regions, among which are image forming and non-image forming areas. In mice, the most densely innervated are:

- In the hypothalamus: peri-supraoptic nucleus, retrochiasmatic area and suprachiasmatic nucleus. These areas regulate circadian rhythm photo-entrainment and use light information as cues for the time of the day.

- In the thalamus: dorsal lateral geniculate nucleus, intergeniculate leaflet, para-habenular zone peripeduncular nucleus and ventral lateral geniculate nucleus. It is from these entries that sensory information will be relayed to cortical area.
- Pretectum, accessory optic system and all the layers of the SC except SGI (Stratum griseum intermediale) (Morin and Studholme, 2014).

Interestingly, a single RGC can innervate both LGN and SC (Dhande et al., 2011). However, differences can be found in the functional properties of RGCs that innervate the SC but not the dLGN (Ellis et al., 2016).

Laminar specificity

When RGCs reach their target, they still have to find the proper laminar in which to establish their connections. This phenomenon has been studied in the retino-recipient structures, mainly: the LGN and the SC. Here, the laminar specificity will only be reviewed in the SC.

Superior colliculus

The lamina-specific targeting of some RGC subtypes has been characterized. Using CB2 as a marker, the establishment of connections for OFF- α RGCs was studied. These RGCs establish their final connections in the lower SGS but at P4-P5, and their arborization can also be found in the upper SGS. At P12, the specific stabilization of appropriate targeted axon arbors is believed to occur through the molecular compatibility between pre- and post-synaptic partners, and leads to the arbor retraction and synapse elimination (Cheng et al., 2010).

The morphology and position of axonal arborizations have been characterized and linked to RGCs subtypes in the SC. Combining a morphological and a molecular approach, the distribution of J and BD RGCs in the SC was identified. Interestingly, these RGC cell types segregate into different parts of the SGS, suggesting the existence of functional submaps in the SC. J-RGCs target between 37-95 % of the SC height, while FSTL4-RGCs target between 45-100 % of the SC map. DSGC are known to establish most of their connections to the upper part of the SC, in which DS residing cells can be found. A cluster analysis has been performed according to the maximum height reached by different morphological subtypes of RGCs. Among well-defined types, the following segregation was observed from top to bottom (Hong et al., 2011), and confirmed in other studies:

- LED (W3) (Kim et al., 2010)
- OFF DSGC (J-RGC) (Kim et al., 2008b, 2010), ON-OFF DSGC (FSTL4, DRD4, TRHR) (Dhande et al., 2013; Huberman et al., 2009; Kay, 2011; Kim et al., 2010; Rivlin-Etzion, 2011)
- transient OFF alpha (CB2+) (Huberman et al., 2009), sustained OFF alpha (W7) (Kim et al., 2010), sustained ON alpha RGC and M3, and other melanopsin cells (Hattar et al., 2006)
- ipsilateral

No systematic relationship could be established between the laminar position of RGCs dendrites and the laminar position of axonal arbors. However, a correlation was found between the size of RGC dendritic fields and the depth at which axonal arborizations are established. RGCs with large dendritic fields target lower parts of the SGS (Hong et al., 2011).

In addition to finding the appropriate lamina into the target, RGCs need to find their appropriate location relative to each other, in order to maintain the topographic organization of the retina and the appropriate location at which a stimulus was detected. This is based on three major mechanisms: molecular gradients, cell-cell interaction (competition), and refinement by activity. One of the key goals of neuroscience is to understand how these connections are established and maintained across structures.

Superior colliculus

Anatomy

The superior colliculus (SC), located on the dorsal part of the midbrain, is one of the major centers for multi-sensory integration. This structure is well conserved across species and plays a fundamental role in attention, and in controlling orienting responses. The superficial layers that receive essentially visual inputs, operate as a salience detector. This information is transferred toward the deeper layers, which contains an eye movement map as well as converging auditory and somatosensory inputs. This information is integrated and can result in the orientation of the eyes and the head toward salient stimuli. Here, a particular focus will be made on the superficial layers of this structure.

Laminae

This laminated structure is composed of seven alternating fibrous and cellular laminae, which are distributed from dorsal to ventral as follows:

- stratum zonale (SZ), with a small density of cells
- stratum griseum superficiale (SGS), which receives visual input from retina and visual cortex
- stratum opticum (SO) – where the fibres enter the SC

These three layers compose the superficial layers of the SC. Below the SO, the intermediate layers stratum griseum intermediale (SGI) and stratum album intermediale (SAI) can be found. The stratum griseum profundum (SGP) and stratum album profundum (SAP) are designated deep layers. Classically, the SC is divided into two different parts: the superficial layers (above the stratum opticum, sSC) and the deeper layers (dSC)(Figure 4).

Cell types

Among the cell types that can be found in the superficial layers, 4 major types have been morphologically characterised, notably by Golgi studies (Langer and Lund, 1974) (Figure 5):

- Wide-field (WF) cells have their somas in the deepest portion of the sSC (the optic fibre layer), and extend thin, elaborately branched dendrites obliquely to the dorsal surface of the sSC. These cells have receptive field properties and project mostly to the pulvinar, while responding to small moving stimuli.
- Horizontal cells have long, horizontally extending dendrites with relatively sparse branching. These cells are GABAergic, which suggests that this cell type might be responsible for the receptive field properties of WF. They have large receptive fields, respond to large stationary or swiftly moving stimuli, and project to dorsal and ventral LGN (Lateral geniculate nucleus) and PBGN (Parabigeminal nucleus) (Gale and Murphy, 2014).
- Narrow-field (NF) cells have thick primary dendrites that extend ventrally (into the optic fibre layer) and dorsally to the sSC surface. NF cells exhibit a strong direction-selectivity, which might be due to their connections with DS RGCs. They project toward the deeper layers of the SC. NF cells have small spatial receptive fields, prefer small stimuli, are often direction selective, and project to the PBGN and deeper layers of the SC
- Stellate cells have a limited field of thin dendrites and show no preferred orientation. Stellate cells, like NF cells, have small receptive fields, prefer small stimuli, and project to the PBGN; but unlike NF cells, they also project to LGN.

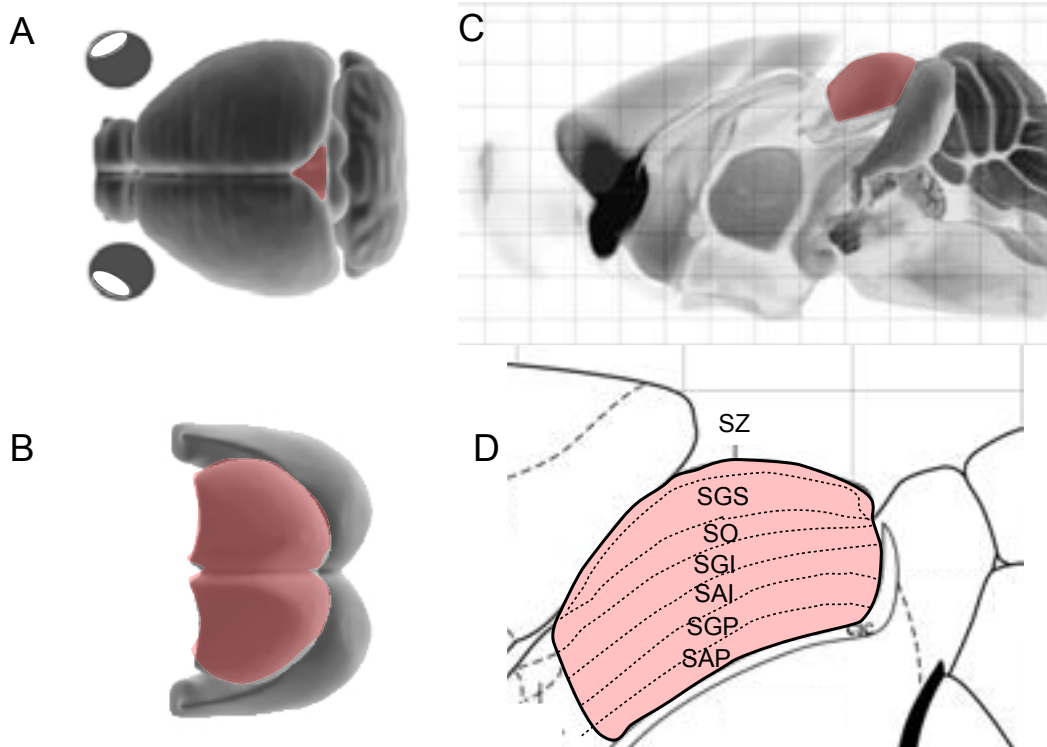


Figure 4: Anatomy of the superior colliculus. SC highlighted in red in all views. A. Location of the SC in the brain. Top view. B. Isolated SC. In gray, inferior colliculus. C. Sagittal view of the brain, showing location of the SC in situ. D. Sagittal view of the SC showing the different layers. SZ: Stratum zonale, SGS: Stratum griseum superficiale, SO: Stratum opticum, SGI: Stratum griseum intermediale, SAI: Stratum album intermediale, SGP: Stratum griseum profundum, SAP: Stratum album profundum. Adapted from the Allen Brain Atlas.

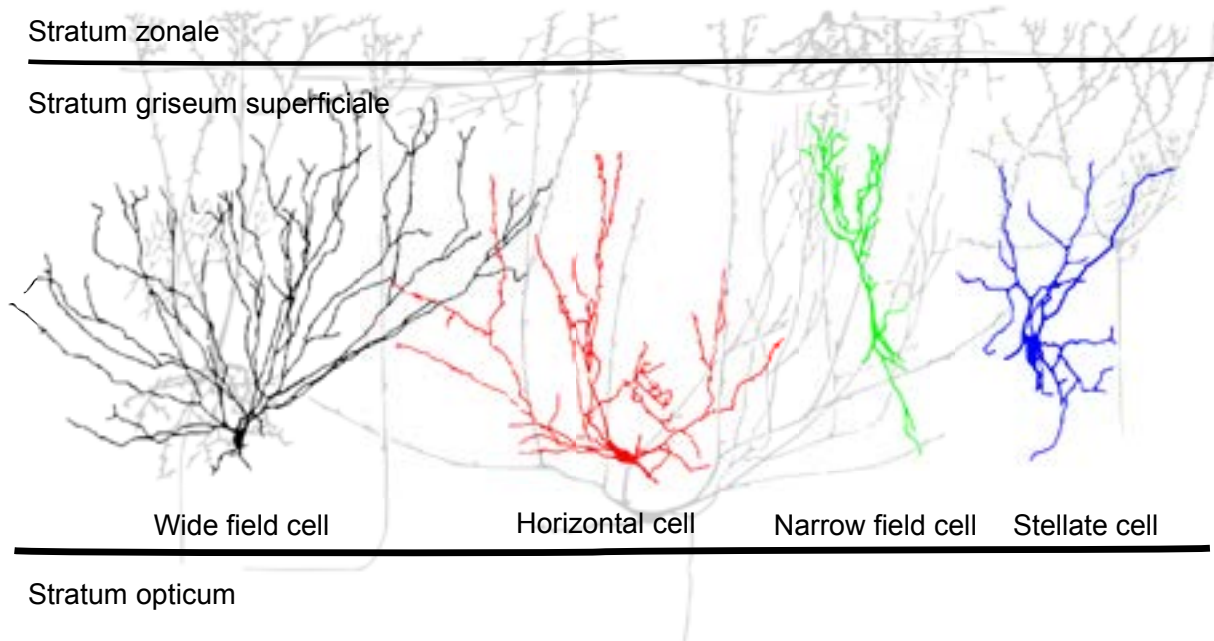


Figure 5: Major cell types in the superficial layers of the SC. Cell bodies are located in the stratum griseum superficiale (SGS). Major types are wide field cells (black), horizontal cells (red), narrow field cells (green) and stellate cells (blue)

From an evolutionary perspective, the distribution of these cells is conserved. However, the morphology of WF cells varies across species, notably with a decrease in dendritic field size for animals that rely more on vision (Hilbig et al., 2000). Interestingly, these 4 morphological cell classes correspond to distinct electrophysiological characteristics and have been recently linked to molecular markers in the mouse. These cell types also display different response properties, with wide-field cells responding to movement and slow speed, horizontal cells to fast speed, stellate cells to slow speed, while narrow field cells show a strong direction-selectivity (Gale and Murphy, 2014). In deeper layers, multipolar cells can be found as well as small horizontal cells, but have not yet been subject to extensive classification (May, 2006).

The superficial layers of the SC contain a high density of GABAergic cells, which represent almost 50% of the cells in this region (Mize, 1992). These cell types have been extensively classified in a variety of species (ferret, cat, rabbit, dog, hamster) (Behan et al., 1992, 2002; González-Soriano et al., 2000; Lee et al., 2006; Mize et al., 1992) according to the expression pattern of calbindin, parvalbumin and calretinin; however this data is not available in the mouse. These cells display different electrophysiological properties and variable spiking patterns, including regular spiking, burst spiking, and fast spiking patterns (Endo et al., 2003). In addition, a population of cells located in the uppermost part of the SC displays a high direction selectivity, which decreases in deeper layers, suggesting a laminar-specific organization of DS neurons (Inayat et al., 2015). Orientation columns can also be found in the sSC, with groups of cells preferentially responding to a particular orientation (Feinberg and Meister, 2015).

Connectivity

The superficial layers are mainly visual and receive inputs from the retina and cortical areas, while auditory and somatosensory inputs are restricted to the deeper layers of the SC. Visual information is later on transferred to these layers where they are aligned with other sensory modalities.

Afferences

The majority of visual afferents enter the SC through the SO and form connections in the SGS. These inputs come directly from the retina and originate from the RGCs. In the mouse 70% of RGCs target the SC (Hofbauer and Dräger, 1985) in a topographic and mostly contralateral manner. Another source of visual information comes from cortical areas, with primary visual cortex (V1) providing retinotopically organized inputs to the SGS and SO in different species (e.g. cat, monkey, rat, mouse), and originate from layer V pyramidal cells. In rats, area 18a extends to the SGI while other areas (18b) reach deeper layers of the SC.

The SC also receives inputs from the auditory system in the deeper layers, which originate from various areas including: external nucleus of the inferior colliculus, nucleus of the brachium of the inferior colliculus, nuclei of the lateral lemniscus, periolivary nucleus, and sagulum; according to species. These auditory inputs are modulated by visual inputs originating from the SGS, as demonstrated by cooling experiments in cats (Lomber et al., 2001).

A representation of the somatosensory periphery from a visual perspective can also be found in the intermediate to deeper layers of the SC (Dräger and Hubel, 1976), and originate from the cuneate and the gracile nuclei; while the head representation comes from the trigeminal nucleus. Part of the deeper layers of the SC is dedicated to multi-sensory integration, with cells displaying multi-sensory responses located in the SGI and SGP. These cells display a stronger response when different modalities are spatially close to each other. Inputs come from different cortical regions, notably from the auditory cortex, somatosensory cortex, and the insular cortex (Wallace et al., 1993).

Intrinsic connectivity and processing

Intralaminar: Lateral inhibition

A notable response property of the SC is the suppression of responses in the SGS when a distractor is presented in its response field (Lovejoy and Krauzlis, 2010). This feature is believed to operate through a winner-takes-all mechanism through the entire visual space, which requires the existence of long range inhibitory projections inside the SC (Trappenberg et al., 2001). These projections have been identified and can be either excitatory or inhibitory. Furthermore, when two different sites in the sSC are stimulated, sites in close proximity facilitate the excitation, while the stimulation of remote sites inhibit the excitation induced by stimulation of a closer point. These lateral interactions can enhance the spatial contrast of a visual stimulus, and suggests that the SC is organized to localize salient stimuli (Phongphananee et al., 2014).

Interlaminar: Columnar organization

One of the major outputs for the superficial layers of the SC is the SGI. Indeed, NF cells send their projections to the deeper layers (SGI), and target cells displaying similar response properties (Isa, 2002). This was first demonstrated in tree shrew, in which electrical stimulation in the SGS elicited excitatory synaptic responses in the SGI (Lee et al., 1997). Interestingly, the response amplitude was at its highest when the stimulation and recording sites were vertically aligned, which suggests a columnar-like organization of the interlaminar connection (Isa and Saito, 2001).

Efferences

The sSC presents 3 major outputs in mice: LGN (Harting et al., 1991), pulvinar (Tohmi et al., 2014), and parabigeminal nucleus (Gale and Murphy, 2014) (Figure 6). Most of these projections are topographically organized. More precisely, the SGS sends projections to the parabigeminal nucleus ipsilaterally, which in turn projects back bilaterally to the superficial SC (May, 2006). SGS also sends projections to the thalamus, notably to the dLGN, with a high conservation of topography (Harting et al., 1991). The ventral part of the LGN is also a major target but displays a high variability across species. Another output is the nucleus of the optic tract, the posterior pretectal nucleus and the olivary pretectal nucleus, and are involved in the control of saccades.

The major output of the SC is the control of saccadic eye movement, which can be decomposed into two major components: the horizontal and the vertical components. The intermediate and deep layers send descending outputs to the brainstem reticular formation and spinal cord, where the gaze center can be found.

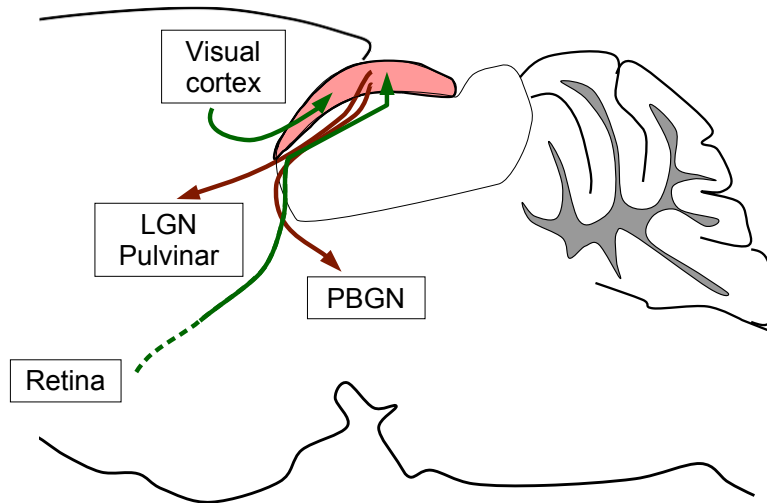


Figure 6: Schematic of the superior colliculus connectivity. The superficial layers of the SC (red) receives visual afferences (green) from the visual cortex and the retina. These layers project to deeper layers, lateral geniculate nucleus (LGN), pulvinar (LP) and parabigeminal nucleus (PBGN) (red).

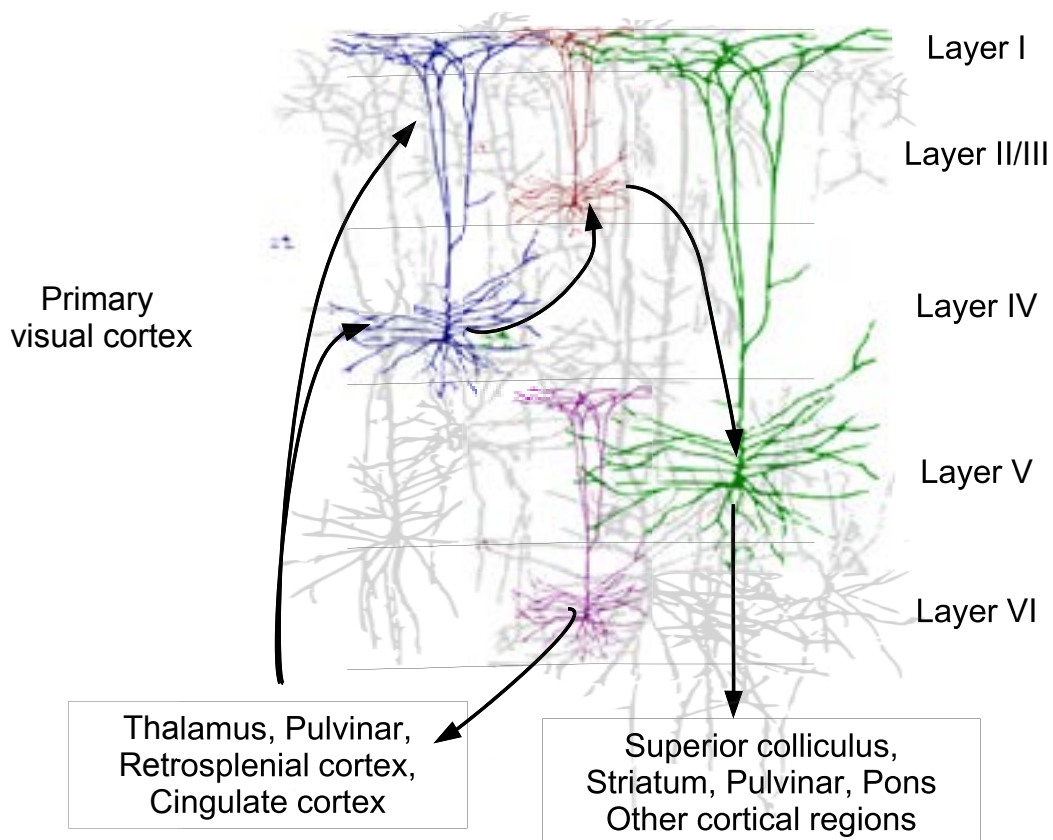


Figure 7: Principal connections to the primary visual cortex. Thalamus send projection to layer I and IV, along with other cortical areas. Thalamic input from layer IV is transferred to layer II/II and finally to layer V and VI. Layer V pyramidal neuron target the superior colliculus, striatum, pulvinar and other cortical region. Layer VI cell project back to the thalamus.

Primary visual cortex

Anatomy

The primary visual cortex also called V1, striate cortex, or area 17, and is one of the most studied areas of the brain. This structure is located in the caudal part of the cortex, partially covering the SC. Since Hubel and Wiesel's original work on receptive field properties and binocular matching in the cat visual cortex (Hubel and Wiesel, 1962), much effort has been made to understand how the visual field is represented in this structure, as well as which features of vision are encoded. V1 is the first cortical area to receive visual information, which is later transferred to other cortical areas.

Mice have proven to be a valuable model to study vision (Huberman and Niell, 2011), even though some differences can be found with cats and monkeys. Indeed, mice lack the large-scale map of orientation selectivity, namely orientation columns (Métin et al., 1988), as well as having reduced visual acuity than other species that are used as a model of vision (Prusky and Douglas, 2004). Despite these differences, mice share many other features with mammals (Niell and Stryker, 2008), and can contribute to a better understanding of visual processing.

Cell types

Recently, all cell types from the mouse visual cortex have been characterized through transcriptomic analysis. This study revealed the existence of 19 types of glutamatergic cells, classified according to their layer distribution as well as 23 types of GABAergic cells (Tasic et al., 2016). Inhibitory cells can be distinguished by the expression of classical molecular markers, PV⁺ (parvalbumin), SST⁺ (somatostatin), VIP⁺ (Vasointestinal peptide) and Ndnf⁺ (neuron-derived neurotrophic factor).

- SST⁺ cells corresponds largely to Martinotti cells and target layer I apical dendrites of pyramidal cells, as well as other inhibitory neurons
- PV⁺ consist of two classes of morphological cells, basket cells, which target the soma of pyramidal cells, and chandelier cells which target the axon initial segment of pyramidal cells (Runyan et al., 2010)
- VIP⁺ and Ndnf⁺ interneuron roles are to date not well defined in the visual cortex

Connectivity

Intrinsic connectivity and processing

V1 represents the classical neocortex organization, with 6 different layers of excitatory cells (Douglas and Martin, 2004). The majority of inputs received by inhibitory and excitatory cells in V1 are intrinsic connections (Liu et al., 2013). A canonical circuit following the excitatory connectivity has been characterized (Figure 7), in which thalamic inputs arrive in layers IV and pyramidal cells make short range projections to layers II/III. These cells in turn project to layer V, which in turn projects to layer VI and to layers II/III and VI (Van Hooser, 2007).

Afferences

V1 receives inputs from the thalamus (Clascá et al., 2012), more precisely from dLGN, which are tuned to orientation and direction (Sun et al., 2015). Both inhibitory and excitatory neurons also receive projections from the LP (lateral posterior nucleus, pulvinar) (Liu et al., 2013). Comparable to cats and monkeys, parallel pathways from the LGN can also be found in mice (Gao et al., 2010), with a specific one for direction selectivity, originating from the shell of the LGN and preferentially targeting the superficial layers of the visual cortex (layers I and II) (Cruz-Martín, 2014). Projections originating from the core of the LGN target the deeper layers, mostly layer IV, but also layer V and VI (Kondo and

Ohki, 2015).

In addition to local connections, V1 also receives inputs from other cortical regions, notably from the RS (retrosplenial cortex) and Cg (Cingulate cortex) (Liu et al., 2013). Notably, the cingulate region of mouse frontal cortex has been shown to influence sensory processing in V1, through long-range projections that activate local γ -aminobutyric acid–ergic (GABAergic) circuits (Zhang et al., 2014).

Efferences

V1 sends projections not only to other cortical areas – most of which are involved in visual processing – but also to the cingulate cortex, retrosplenial cortex and somatosensory cortex. For most of these projections, the topographic order is maintained (Wang and Burkhalter, 2007).

When looking at the response properties of these cortico-cortical projections, they are functionally distinct according to the area that they target. More precisely, cortico-cortical neurons targeting lateral-medial, anterolateral and postero-medial areas differ in their spatial and temporal frequency tuning according to projecting site (Glickfeld et al., 2013).

Layer V pyramidal neurons in mice V1 target other brain regions including the striatum, the SC, the pulvinar, the pons, as well as various cortical regions. These cells also show a difference in orientation tuning and contrast sensitivity, according to their targets (Lur et al., 2016).

Finally, layer VI neurons send feedback signals to all cortical layers and some subcortical structures, such as the LGN. Layer VI contains at least two distinct morphological subclasses of pyramidal cells that in turn project to either the cortex, or provide feedback to the thalamus. These two subclasses display different tuning properties. Layer VI cortico-cortical neurons show broad orientation tuning while layer VI cortico-thalamic neurons show an extremely narrow orientation tuning, and generally sparse activity (Vélez-Fort et al., 2014). Taken together, these results demonstrate that cells in V1 are functionally specific according to their downstream target, suggesting parallel processing of different features of the visual scene.

Visual information received in V1 is transferred to surrounding areas. In mice, the densest cortico-cortical projections from V1 terminate in visual cortical areas LM (lateromedial), AL (anterolateral) and PM (posteromedial) (Wang and Burkhalter, 2007). Similar to other mammalian species, two major pathways can be found regarding visual information processing: the ventral and the dorsal stream – which are often referred as the “where” and the “what” components of vision. The LM and AL areas are distinct areas which have been shown to be the starting point of these two distinct streams of information (Wang et al., 2011). These results support the notion that LM and AL are distinct areas of extrastriate visual cortex in terms of architecture, topography, and connectivity, and that they are the gateways for the ventral and dorsal streams, respectively. This information will ultimately be transferred to temporal circuits for object recognition and posterior parietal networks, for visually guided actions.

Retinotopy in the visual system

In addition to finding their appropriate laminar target in the structures they innervate, axons also need to be organized relative to each other. Topography is the maintenance of the spatial relationship between input neurons to their projecting sites. In the case of the visual system, the maintenance of spatial order in the retina is referred as retinotopy. This spatial organization is found in most retino-recipient structures.

Retinotopy in the superior colliculus

Retino-collicular map

The topographic organization of retinal afferents to the SC has been demonstrated in mice through electrophysiological approaches. These studies demonstrated a representation of the entire retinotopy in the SC, which is aligned with other sensory modalities (Dräger and Hubel, 1975, 1976). Since the connections between the retina and the SC are monosynaptic, retinotopy can be assessed directly through anatomical tracing. Lipophilic tracers allow direct visualization of RGC termination zones (TZ) in the SC and constitute a robust and reliable way to quantify the retinotopic arrangement of projections (Simon and O'leary, 1992). Functionally, the entire colliculus can also be visualized and monitored using optical intrinsic imaging (Cang et al., 2008a). With this technique, the changes of the intrinsic optical properties due to neuronal activity are visualized, displaying the entire map of the retinotopic space during visual stimulation.

In the SC, retinal afferents are organized as following: the nasal-temporal axis of the retina projects onto the caudal-rostral axis of the SC, whereas the dorsal-ventral axis maps onto the lateral-medial axis (Figure 8).

Cortico-collicular map

Layer V pyramidal neurons from V1 send projections to the SC (cortico-collicular fibers), in which they align into the retino-collicular map. The organization cortico-collicular projections was first described in rat (Lund, 1966), and found to be topographically matched with retinal inputs. This was later on described in mice also through anatomical studies (Rhoades et al., 1985). More precisely, the lateral-medial axis of V1 aligns on the rostral-caudal axis of SC, while the rostral-caudal axis maps onto the medial-lateral axis (Figure 8).

Retinotopy in the primary visual cortex

V1 receives inputs mostly from dLGN, and also presents a continuous representation of the visual space. Evidence for a retinotopic organization of V1 come from electrophysiological studies performed in mice. Retinotopy in V1 was characterized by the identification of receptive fields which revealed a uniform cortical magnification factor across visual space with low inter-individual variability (Dräger, 1975; Wagor et al., 1980). Optical intrinsic imaging is also a technical approach that revealed the retinotopy in V1 (Kalatsky and Stryker, 2003; Schuett et al., 2002) that has been extensively used, and has led to refinements of the mapping. This method is now the standard to validate other technical approaches. The effect of wakefulness on retinotopy was also assessed, and revealed that the intensity of hemodynamic responses depends critically on anesthesia and wakefulness (Pisauro et al., 2013). Retinotopy in V1 has also been characterized with other approaches like voltage-sensitive dye (Polack and Contreras, 2012), and genetically encoded voltage indicator (Carandini et al., 2015) and 2-photons imaging using genetically-encoded calcium indicators (Marshall et al., 2011). Retinotopy in V1 can be found as a projection of the nasal-temporal axis onto the medial-lateral axis, whereas the dorsal-ventral axis projects onto the antero-posterior axis (Figure 8).

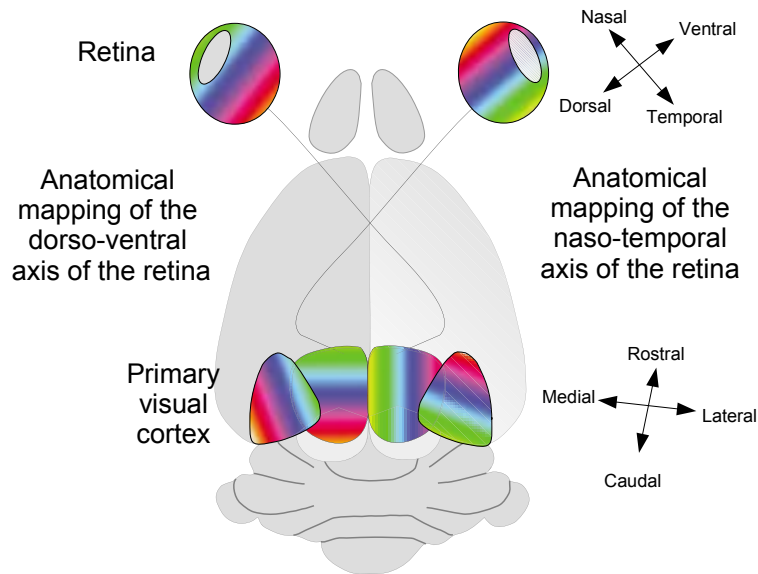


Figure 8: Anatomical retinotopy in primary visual system. dorsal-ventral axis of the retina projects along lateral-medial axis of the SC, which corresponds to the rostral-caudal axis of V1 (anterior-posterior)(left). nasal-temporal axis of retina projects along caudal-rostral axis of SC, corresponding to the lateral-medial axis of V1 (right).

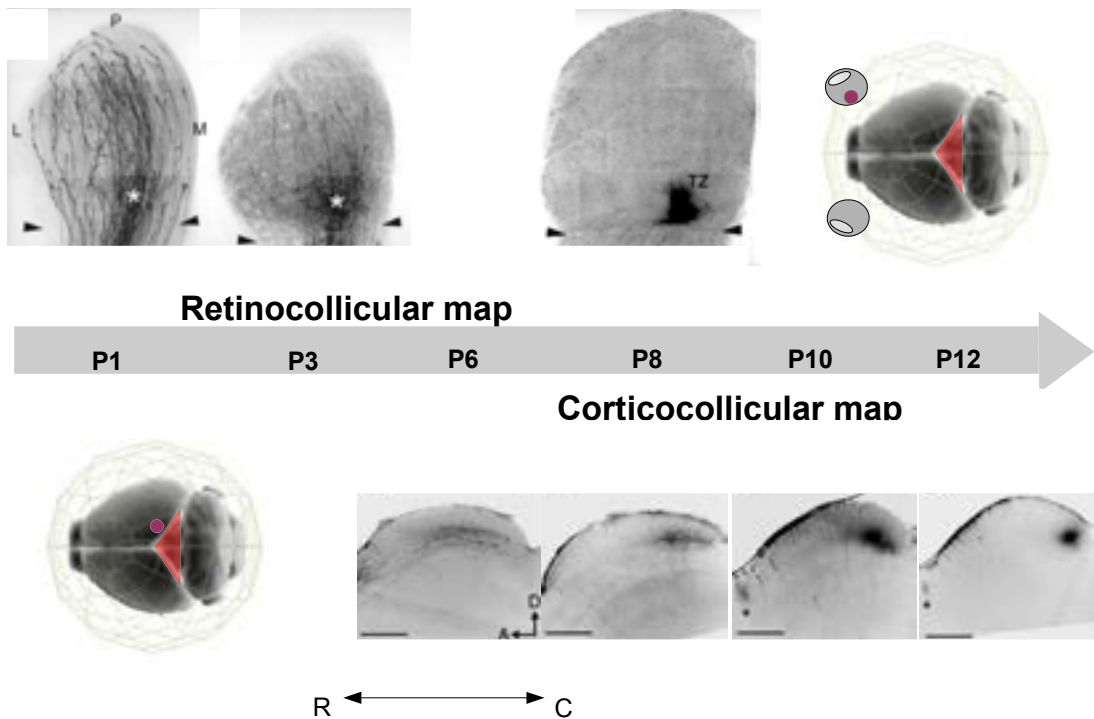


Figure 9: Developmental time of retino- and cortico-collicular maps. Retino-collicular (top) map formation starts with an overshooting of projections. At P1, the entire collicular space is filled and termination zone refine at P8. In parallel, starting from P6, axons from primary visual cortex enter the SC to form cortico-collicular map and refine at P12. Adapted from Hindges et al., 2002 and Triplett et al., 2009.

Developmental timeline of retinotopy in the superior colliculus

Retino-collicular map

RGCs leave the retina at embryonic day 15 (E15) and reach the rostral edge of the SC at E17-E18 (Simon and O'leary, 1992). In a first phase occurring at P0-P1 – which is called the overshoot (Figure 9, A) – axons extend to the caudal end of the SC and fill the entire collicular space. Interstitial branches are formed along the lateral-medial axis, in both directions at the level of the future TZ. At P3, branches have reached the TZ, a retraction of the overshoot has begun to occur, and a higher density of arborization at the topographically correct locations can be found (Yates et al., 2001) (Figure 9, B). At P8, TZs are dense and focus and occupy less than 5% of the rostral-caudal axis (Figure 9, C) (Triplett et al., 2009). All arborizations that were not in the topographically correct location have been eliminated and the retino-collicular map is considered as mature (Hindges et al., 2002).

Cortico-collicular map

Projections from the V1 enter the SC later during development, after the formation of the retino-collicular map. These projections enter the SC by the rostral end through the SO at P6 (Figure 9, D). A broad TZ can be observed at P8 (Figure 9, E). The refinement of these projections starts at P10 (Figure 9, F) and they can be considered as mature by P12 (Figure 9, G) (Triplett et al., 2009).

Taken together, these observations have indicated that when cortico-collicular projections reach the SC, the retino-collicular map is already established, presumably providing support for the mapping of these projections. To establish these maps during development, positional information needs to be instructed to ingrowing axons, in order to find their correct location. Development involves the execution of a genetic program, with many temporal and spatial constraints. The precise mechanism through which projections are guided has been the subject of extensive studies, specifically in topographic mapping. This mapping requires a precise guidance through development of ingrowing axons.

Chemoaffinity hypothesis:

How connections are established during development has been a matter of debate for decades. Classically, two opposite views have been confronted, namely Sperry's chemoaffinity hypothesis and Hebb's rule. Sperry's chemoaffinity hypothesis (Sperry, 1963), proposed the following: *"...an orderly cytochemical mapping in terms of two or more gradients of embryonic differentiation that spread across and through each other with their axes roughly perpendicular. These separate gradients successively superimposed on the retinal and tectal fields and surroundings would stamp each cell with its appropriate latitude and longitude expressed in a kind of chemical code with matching values between the retinal and tectal maps."* On the other hand Hebb's rule, "cells that wire together, fire together" seems to point toward the requirement of activity to establish functional connections. Evidence has built up that both phenomena are indeed required.

The molecular biology of axon guidance:

During development, axons have to travel long distances to find their appropriate targets and establish connections. The way directional information is integrated by the ingrowing cell is through the growth cone. Initially discovered by Santiago Ramon y Cajal, the growth cone can be found at the distal tip of the axon, and is characterized by both widening and extensions. The growth cone comprises two types of processes: filopodia and lamellipodia. Filopodia can be found at the periphery of the growth cone and are thin extensions that constantly extend and retract. Lamellipodia can be found between these filopodia and are also highly dynamic (Maskery and Shinbrot, 2005)(Figure 10). Time lapse microscopy allowed real-time visualization of growth cones which revealed a highly dynamic process (Aletta and Greene, 1988; Goldberg and Burmeister, 1986). The growth cone is made of filamentous actin and tyrosinated microtubule which confers it its motility, based on cytoskeletal rearrangement (Dent and Gertler, 2003; Maskery and Shinbrot, 2005).

Molecular cues are known to be involved in axonal pathfinding both during development and regeneration (Politis et al., 1982; Tessier-Lavigne et al., 1988). These environmental cues can be either diffusible or membrane-bound, and are integrated by the growth cone and induce modifications of the cytoskeleton (Dent and Gertler, 2003). The growth cone responds in different ways to extracellular molecular cues, which can be either attractive or repulsive (Figure 10). First, receptors are activated by such cues, effectors are activated, and this signal is transduced to actin binding, leading to the modulation of actin dynamics. The way molecular cues signal the growth cone and remodel cytoskeleton rearrangements has been intensively studied, leading to the identification of key downstream effectors.

Four major groups of receptors are known to induce subsequent changes at the growth cone: netrins, semaphorins, slits and ephrins (Dickson, 2002). These families of molecules induce activation or inactivation of pathways that lead to the Rho family of small GTPases, which will in turn direct the assembly and disassembly of actin filaments. Attractive cues generally signal through the activation of Rac and Cdc42, which will promote actin polymerization and induce growth cone extension. Repulsive cues will trigger Rho activity which decreases actin polymerization and cause growth cone retraction.

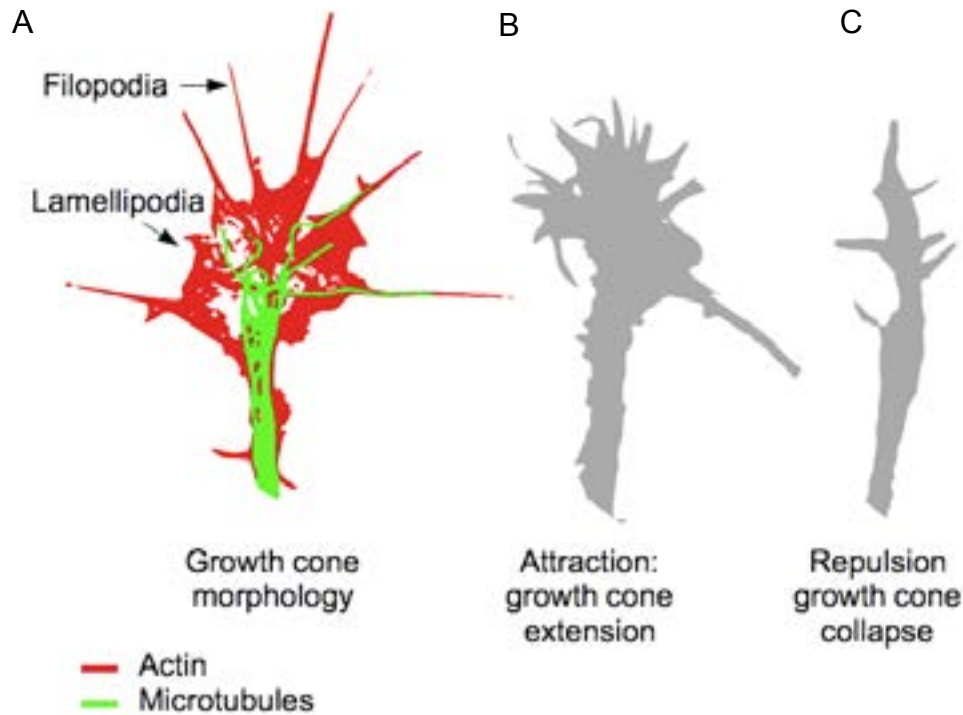


Figure 10: Growth cone response to different molecular cues. **A.** Morphology of growth cone. Filopodia are thin extensions made of filamentous actin (red) and lamellipodia can be found between them. Microtubules (green) can be found at the base of the growth cone. **B.** Shape of the growth cone in extension, in response to an attractive cue. Filopodia can be found. **C.** Growth cone collapse in response to a repulsive cue. Filopodia are retracted.

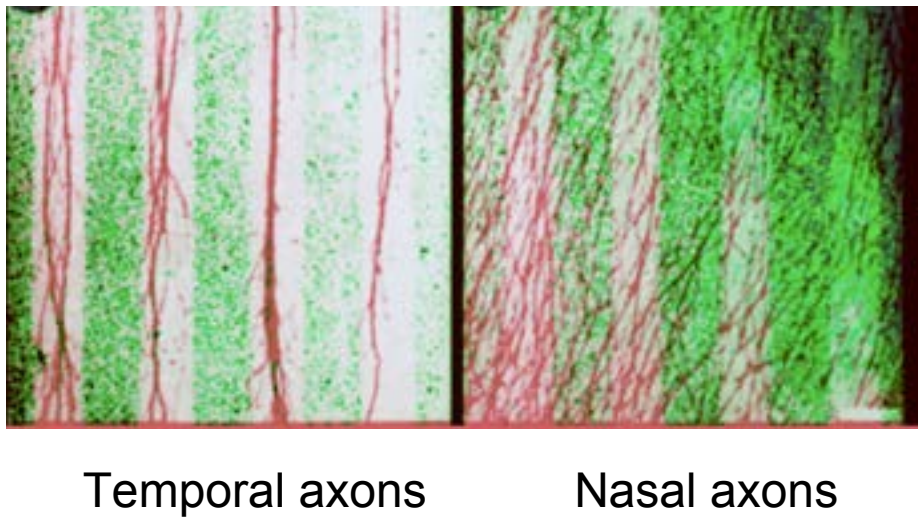


Figure 11: Stripe assay. Pseudocolor image adapted from (Walter et al., 1987a). **A.** Temporal and **B.** nasal axon (red) are allowed to grow on alternating stripes of caudal (green) and rostral (white) tectal membranes.

This rather simplistic view (one molecule triggers one type of response) does not take into account a variety of factors that are responsible for the complexity of axon guidance. Indeed most studies have been conducted *in vitro*, putting in contact ingrowing axons with a single molecule as *in vivo* the environment is much more complex. Different actors will interact with each other, eliciting a broad range of responses. In addition, the same molecule can trigger different responses, either being attractant or repellent. Furthermore, the same axon response properties can also change through time and space. As a consequence, the spatial and temporal variation can reverse the growth cone's response from attractive to repulsive. Among factors that can modulate the growth cone's response properties, are the level of cyclic nucleotides. For example, the repulsive effect of netrin-1 can be modulated through cAMP and PKA activity, while Sem3A is sensitive to cGMP and PKG. More generally, reducing the levels of cAMP or cGMP, or inhibiting PKA or PKG, converts an attractive response to a repulsive one; whereas elevating cAMP or cGMP, or activating PKA or PKG, switches repulsion to attraction (Dickson, 2002; Ming et al., 1997; Song et al., 1998, 1997). Taken together, many different elements can contribute to the guidance of ingrowing axons.

Identification of molecular cues

Before molecular cues were identified, the adhesive properties of ingrowing axons were studied, and were believed to play a key role in axonal pathfinding. The cell recognition of ingrowing axons was highlighted in *in vitro* studies. When ingrowing axons originating from embryonic chick retina were given a choice between a monolayer of tectal or retinal cells *in vitro*, a clear preference for the *in vivo* target can be seen (Bonhoeffer and Huf, 1980). Later on, the positional preference was demonstrated using different parts of the retina and the tectum. More precisely, nasal axons were shown to display different response properties when compared to temporal ones, which can recognize tectal cells according to positions along the rostral-caudal axis of the tectum. Even when using non innervated tecta, from an earlier embryonic stage, temporal retinal axons can still demonstrate a preference for the anterior tectum (Bonhoeffer and Huf, 1982).

Key experiments that led to the identification of guidance cues involved in topographic mapping are the so-called stripe assays, which set the basis of understanding on cell-cell mediated signaling (Walter et al., 1987a). In these experiments, growing axons were given the choice between alternating layers of different substrates (Figure 11). This experimental paradigm demonstrated that temporal axons had shown a preference for rostral tectum membranes whilst avoid the caudal one, whereas nasal axons had shown no preference. It was later suggested that this was not a preference, but rather a repulsive effect of the caudal part of the tectum. This repulsive effect could be abolished by heating the membranes (Walter et al., 1987b), or by PI-PLC treatment (Walter et al., 1990). These experiments confirmed the postulated idea by Sperry that gradients of molecules are expressed in the target structure in order to inform growing axons of their location through repulsive signalling.

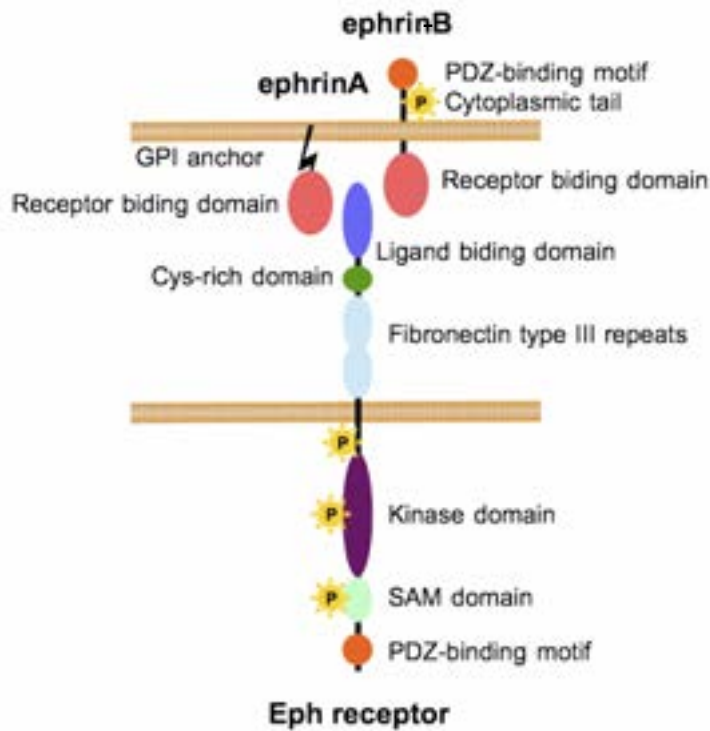


Figure 12: Structure of Eph receptor and ephrin ligands. **Top:** Ephrins are divided into A and B classes: the A class is linked to the membrane via a glycosylphosphatidylinositol (GPI) linkage, whereas the B class has a cytoplasmic tail and a PDZ-binding motif. On the extracellular side, both are composed of a receptor binding domain. **Bottom:** EphA and EphB receptors have a common structure. On the extracellular side, a ligand-binding domain, which binds to the receptor-binding domain of ephrins, followed by a Cys-rich domain and two fibronectin type III repeats. The intracellular side of Eph receptors is composed of a kinase domain (TK), a sterile alpha motif (SAM) and a PDZ binding motif. Phosphorylation sites are also highlighted.

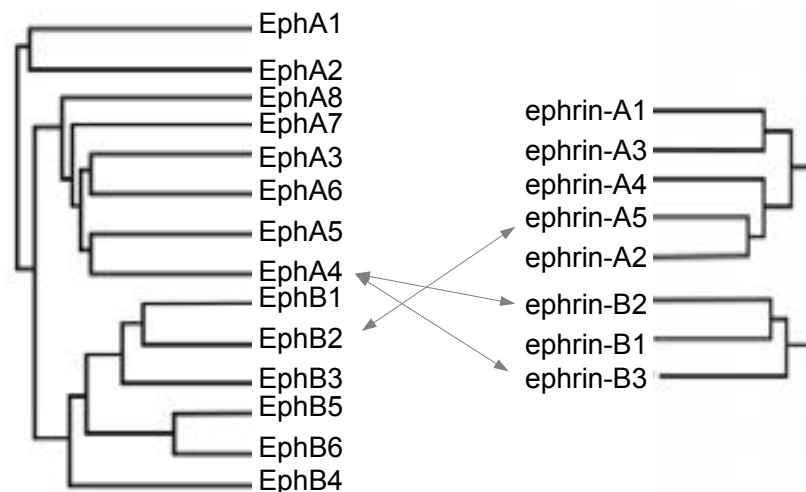


Figure 13: Phylogenetic tree of Eph and ephrin family members and crosstalks. Eph and ephrins can be divided into A and B classes based on sequence conservation. These receptors and ligands show affinity within each class according to their homology, but can also interact with each family. Cross-talks between A and B subclasses are highlighted.

Eph and ephrins

Discovery of Eph/ephrins and their involvement in retino-collicular mapping:

Pioneer experiments in the identification and characterization of Eph receptor (erythropoietin-producing human hepatocellular receptors) and ligands were initially performed in chicks (Tessier-Lavigne, 1995). Eph receptors have for a long time been orphan receptors, without an identified ligand. The first to be characterized was ELF-1 (ephrin-A2) in chick (Cheng and Flanagan, 1994), and was found to interact with Mek4 (EphA3) and Sek (EphA4). Ephrin-A2 expression was characterized and found to be expressed in complementary gradients to EphA receptors in the retina and tectum (Cheng et al., 1995). RAGS (ephrin-A5) was later on identified, and its involvement in retino-tectal mapping was demonstrated using ephrin-A5-expressing COS cells, which have a repulsive effect in stripe assay on both temporal and nasal retinal axons *in vitro* (Drescher et al., 1995). Their discoveries in different species led to a variety of names which were unified in 1997, with receptors being named Eph, and ligands being named ephrins (Eph interacting protein) (Eph nomenclature committee, 1997).

Eph and ephrin family

Ephs constitute the largest family of tyrosine kinase receptors, which transduce signals from the surface by activating a tyrosine kinase in the cytosol. They can be divided in two families according to homology and ligand affinity: EphA (A1 to A8) and EphB (B1 to B6) receptors (Figure 13). On the other hand, their membrane-bound ligands are subdivided into two families according to their anchoring to the membrane ephrin-As (A1 to A5), which are GPI anchored; and ephrin-Bs (B1 to B3), which have a cytoplasmic tail (Davis et al., 1994; Flanagan and Vanderhaeghen, 1998).

Among the most remarkable features of Eph/ephrin signaling, is the existence of a so-called reverse signaling. This is where the Eph receptor acts as a ligand to activate ephrins, and the redundancy between the different ligands and receptors leads to a cross-talk among them. Taken together, these different features add to the complexity of this signaling process, which makes the task of determining the identification and roles of these molecules more difficult.

Eph receptor and ephrin ligand structure

EphA and EphB receptors share the same structure. These tyrosine kinase receptors display on the extracellular part a ligand binding domain, a cystein-rich region, 2 fibronectin type III repeats, and a transmembrane domain. On the intracellular part, two conserved tyrosine residues can be found on the juxtamembrane region, as well as a protein kinase domain, a sterile alpha motif (SAM, involved in the formation of dimers and oligomers) and PDZ binding domain (consensus binding region) (Figure 14, bottom).

Their ligands, ephrin-A and ephrin-B both display a receptor binding domain. Ephrin-As are GPI anchored, whereas ephrin-Bs have cytoplasmic regions in addition to a PDZ binding domain (Figure 14, top). This difference in structure is at the origin of the division of the 2 subclasses of EphA and EphB, which can also be found in terms of affinity.

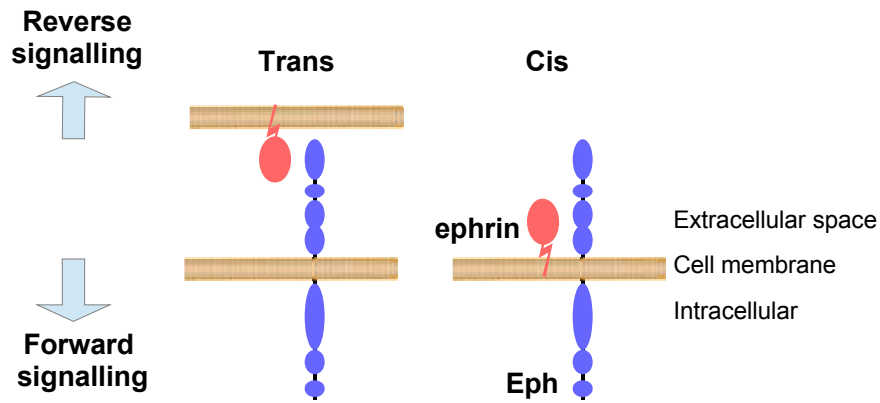


Figure 14: Eph–eprin signalling modes. Eph and eprin can occur between two cells (**Trans**, left) or within the same cell (**Cis**, right). In addition, the Eph receptor bearing cell (**Forward signalling**, bottom) or the eprin ligand bearing cell (**Reverse signalling**, top) can transduce the signal upon activation.

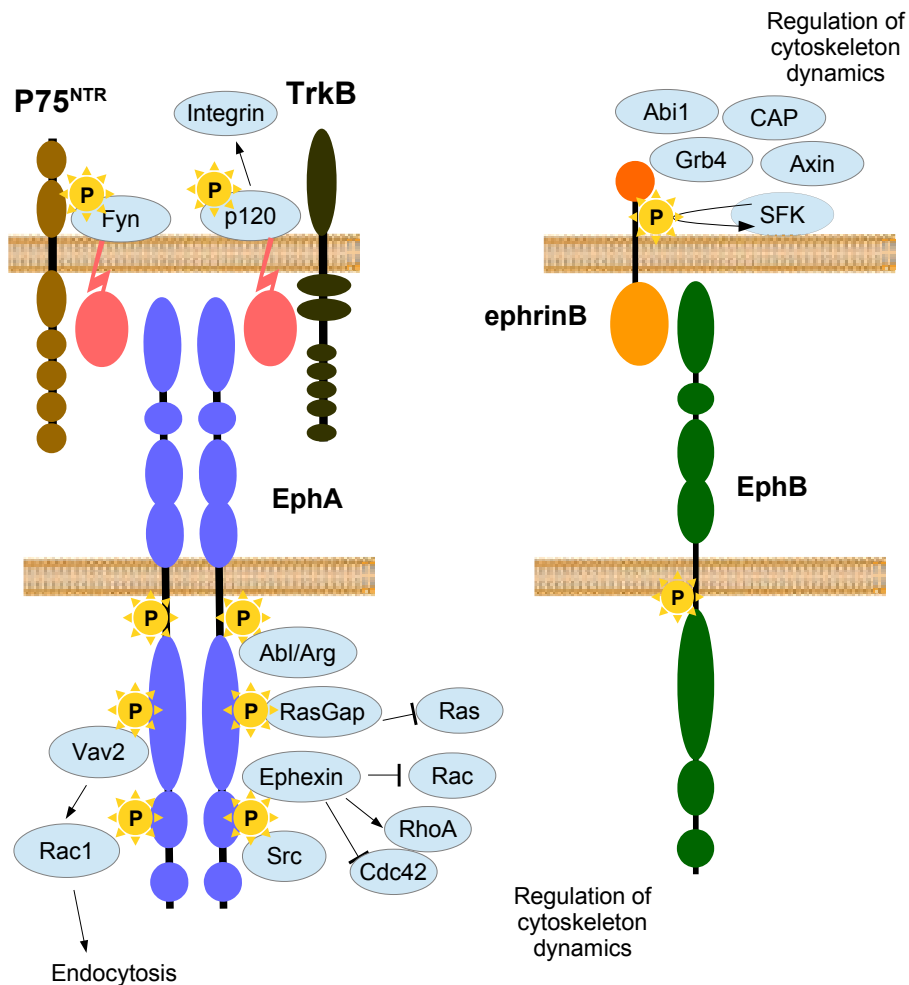


Figure 15: Intracellular activation upon Eph/eprin activation. A. EphA and eprin-A forward (Bottom) and reverse signalling (Top). eprin-A can interact with P75^{NTR} and TrkB during reverse signalling while EphA forward signalling leads to the activation of effectors which regulate cytoskeleton dynamics. Endocytosis is regulated by Vav2. **B. eprin-B reverse signalling.** Activation of the ligand leads to the phosphorylation of the cytoplasmic tail through Src family kinase (SKF) and recruitment of effectors.

Affinity between Eph/ephrin

Eph and ephrin show a variable degree of affinity within each family. Most EphA and ephrin-A can interact with each other due to the high homology between them, and the same stands true concerning EphB and ephrin-B. In addition, some members of the A group can interact with the B group (Figure 13). Indeed, EphA4 is able to recognize ephrin-B2 and ephrin-B3, thus increasing the possibility of interactions. More recently an interaction between EphB2 and ephrin-A5 has also been demonstrated, increasing the different identified cross-talks (Gale et al., 1996; Himanen et al., 2004).

Eph and ephrin signaling

The way Eph/ephrin signaling operates to guide axons during development has been the subject of intensive research, whilst providing insights into the intrinsic mechanisms of signaling. This signaling process is quite versatile. Not only can Eph and ephrin can act as both ligands and receptors, but they can interact by cell contact (trans) or within the same cell (cis)(Figure 14). Concerning the effect on the growth cone guidance, EphA-mediated signaling through activation by ephrin-As acts to induce a growth cone collapse or a turning (Weinl et al., 2003). On the other hand ephrin-A activation can either promote growth cone extension or collapse, according to the system and interactions with other receptors. In addition, an effect of dosage has been observed, with low concentrations of ephrin-A leading to attraction, and higher concentrations leading to repulsion (Hansen et al., 2004). Taken together, these findings highlight the complexity of Eph/ephrin signaling. Here, interactions and downstream signaling that are relevant for axon guidance will be highlighted.

Forward signaling

Eph receptors are activated by clusters of membrane-bound ephrin ligand and dimerize (Egea et al., 2005). Upon activation, each monomer autophosphorylates juxtamembrane tyrosine residues (Ellis et al., 1996), leading to full activation of the receptor (Fang et al., 2008; Kullander et al., 2001). This creates binding sites for SH2 domain-containing proteins (like Src family kinase), which transmit the signal inside the cell (Arvanitis and Davy, 2008). Blocking Src family kinase abolishes the repulsion of retinal axons by posterior tectal membranes in the stripe assay (Knoll, 2004).

Activation of Eph receptors can also be transferred through Abl and Arg, which regulate actin polymerization, can associate with Eph receptors directly through the SH2 domain and tyrosine phosphorylation, or indirectly through other proteins (Yu et al., 2001). Eph receptor activation results in the recruitment of RasGAP, which then inactivates Ras and suppresses ERK activation (Elowe et al., 2001). Stimulation of endogenous EphA kinases with ephrin-A1 inhibits the Ras/MAPK cascade (Miao et al., 2001). Adenylate cyclase-1 has also been demonstrated to be essential for ephrin-A5 elicited axon retraction (Nicol, 2006).

The guanine nucleotide exchange factor (GEF) ephexin1 interacts with EphA4, and has been suggested to mediate the effect of EphA on the activity of both Rho GTPases (key regulators of the cytoskeleton) and axon guidance, through activation of RhoA and inhibition of Rac and Cdc42 (Sahin et al., 2005; Shamah et al., 2001). Inhibiting Rho GTPase reduces ephrin-A5 induces growth cone collapse (Wahl et al., 2000).

Cleavage of Eph and ephrin:

The process through which Eph/ephrin signaling is terminated, is believed to operate through Vav2, a guanosine exchange factor that activates Rac1. Indeed, to achieve repulsion, the binding between Eph and ephrin has to be terminated through endocytosis – for which Vav is required. In addition, RGCs from Vav2^{-/-}-Vav3^{-/-} mice fail to respond to ephrin-A stimulation in culture, suggesting

an important role for Vav in the regulation of growth cone collapse (Cowan et al., 2005).

Another process for terminating Eph/ephrin signaling, is the cleavage of this complex. Adam10 has been demonstrated to either interact with ephrin-A2 (Hattori et al., 2000) or EphA3 (Janes et al., 2005) upon EphA/ephrin-A interaction, resulting in either the cleavage of ephrin-A2 in the juxtamembrane domain, or leading to the internalization of the receptor respectively.

Reverse signaling

One of the most striking features of Eph/ephrin interactions is reverse signaling. In this particular configuration, the ligand, ephrin, acts as receptor and induces an intracellular response. First discovered in ephrin-B (that has an intracellular domain), evidence has built up concerning this phenomenon in GPI-anchored ephrin-A also (Figure 14).

Ephrin-B

Ephrin-B cytoplasmic tail has 5 invariant tyrosine residues which suggested interaction with other proteins. These residues on ephrin-B are phosphorylated by SFK (Src family kinase)(Palmer et al., 2002) upon activation by EphB (Bruckner et al., 1997; Holland et al., 1996). Once phosphorylated, Grb4 SH2/DH3 domain can be associated with the ephrin-B cytoplasmic domain, and recruit different effector like Axin, Abi1 (Abl interacting protein 1) and CAP (c-Abl associated protein) which regulate cytoskeleton dynamics (Cowan and Henkemeyer, 2001; Xu and Henkemeyer, 2009).

The ephrin-B cytoplasmic tail also has a PDZ domain binding site. Point mutations impairing this site results in the agenesis of the corpus callosum, which suggests an important role for this signaling process *in vivo* (Bush and Soriano, 2009). Upon activation, PTP-BL (Protein Tyrosine Phosphatase, containing a PDZ domain) is recruited and ephrin-B is dephosphorylated. This allows the recruitment of other cytoplasmic effectors (Palmer et al., 2002) (Figure 15).

Ephrin-A

Ephrin-As (which are GPI-anchored) can also transduce a signal when activated by EphA receptors. This leads to the activation of integrin (Davy, 2000) through a 120kDa protein (p120), which is phosphorylated upon ephrin-A activation (Huai and Drescher, 2001).

Activated ephrin-A also recruits the SKF Fyn (Davy et al., 1999), which leads to an increase in cell adhesion. Ephrin-A has been demonstrated to interact with P75^{NTR} (a receptor for neurotrophin), and induces axon repulsion. In P75^{NTR} knock-outs, EphA7 mediated repulsion is abolished in stripe assays, suggesting that P75^{NTR} is required for this repulsive effect. When looking at the retino-collicular map of these animals, TZs are shifted rostrally. Interactions between ephrin-A2 and P75^{NTR} results in an increase in Fyn phosphorylation (Lim et al., 2008)(Figure 15). This effect is reversed by proBDNF and BDNF (Marler et al., 2010).

Another BDNF mediated signaling through the ephrin-A ligand has also been shown. Indeed, ephrin-A interacts with and inactivates TrkB in cis, following activation by EphA receptors (Figure 15). TrkB responds to BDNF and promotes axon branching, when interacting with ephrin-A5. This effect is reversed upon activation by EphA, through a decrease in PI3 kinase activity (Marler et al., 2008).

The modulation of TrkB receptor by ephrin-A is not the only interaction in cis that is known for the Eph/ephrin family. Indeed, when co-expressed in the same cell, Eph and ephrin are also able to interact with each other through a process called "cis-interaction" (Figure 14).

Cis interaction:

Evidence for a role of retinal ephrin-A and cis-interactions is derived from *in vitro* studies in chicks. Whenever ephrin-A5 or ephrin-A2 is over-expressed in RGC, temporal RGCs lose their sensitivity to ephrin-A repulsive signaling in stripe assay with alternating caudal and rostral tectum. This is correlated with an increase in EphA receptor phosphorylation. In addition, removal of ephrin-A by PI-PLC treatment renders nasal axons sensitive to ephrin-A, through a supposed EphA mediated mechanism. This has been further confirmed by the observation of targeting errors in the tectum, when ephrin-A2 was over-expressed in the retina. Temporal axons overshoot their target, while nasal ones are unaffected (Hornberger et al., 1999). Similar results were obtained with the over-expression of ephrin-A5, with targeting defects observed for both temporal and nasal axons (Dütting et al., 1999).

In spite of this evidence, nasal axons from ephrin-A2/A5 knock-out mice gain in responsiveness in stripe assays, containing anterior and posterior SC stripes from wild-type mice (Feldheim et al., 2000), suggesting that ephrin-As are involved in silencing EphA receptors.

Co-expressed EphA4 receptors and ephrin-A2 results in a reduction of both EphA3-FC and ephrin A5-FC binding on HEK293 cells, when compared to a single expression. This interaction operates through the receptor-binding domain that becomes inaccessible upon cis-interactions between ephrin-A2 and EphA4. To exclude the effects of cleavage, the GPI-anchor was replaced by a SC1 transmembrane domain (Yin et al., 2004). The finding that Eph and ephrin can interact in cis in an artificial expression system has raised questions regarding the function, relevance, and physiological significance of such interactions *in vivo*, and how such signaling could be untangled.

In developing motor axons, the co-expression of Eph receptors and ephrin-A ligands can also be found. Application of both the extracellular domain of EphA7 and EphA3-FC leads to growth cone enlargement, whereas the application of the clustered extracellular domain of ephrin-A1-Fc induces growth cone collapse. When ephrin-As are removed by PI-PLC treatment, the EphA7-FC-induced spreading is abolished, suggesting that it is indeed mediated by ephrin-As. These opposing effects can be explained by the segregated localization of EphA and ephrin-A proteins within the plasma membrane. When misaddressing the ligand to the receptor-enriched sites – and vice versa – by the generation of chimeric proteins, cis-attenuation can be observed. Taken together, these results suggest that in motor axons, cis-attenuation does not operate since both the ligand and receptors are segregated (Marquardt et al., 2005).

Despite these findings, this segregation process has not been demonstrated in RGCs. This study suggests that the receptors and ligands are spatially segregated, leading to reductions cis interactions, which would then lead to silencing whilst actually increasing the versatility of Eph and ephrin signaling. In addition, this study has also suggested that ephrin-A reverse-signaling is attractive, whereas EphA signaling is repulsive. However, when EphA7-Fc is applied on RGC ingrowing axons, a repulsion effect can be observed (Rashid et al., 2005). In chick, EphA3 has been demonstrated to interact in cis with ephrin-A5 through a ligand-binding domain-independent process, leading to the desensitization of trans-signaling (Carvalho et al., 2006).

Conclusion

Much evidence highlights the versatility of Eph and ephrin signaling. Indeed, most of the receptors and ligands can interact with each other within each group, and furthermore some cross-talks can also be found. This renders the study of specific roles for each particular member somewhat difficult. In addition, both forward- and reverse-signaling can be found, which makes the identification of each member's contribution in different physiological phenomena quite difficult. Furthermore, the co-expression of both ligands and receptors within the same cell and the existence of cis interactions

increases the number of possibilities through which Eph and ephrin can signal.

Taken together, all of these different aspects of Eph/ephrin signaling renders difficult the interpretation of their respective contribution to biological phenomena. In addition, most of the systems used to reveal some of these interactions are cell culture assays, in which the level of expression of these receptors and ligands is way above physiological concentrations. This could lead to interactions that are not possible *in vivo*, notably due to the segregation of these different actors (Marquardt et al., 2005). In addition, a dose-effect phenomenon has been described *in vitro* (Hansen et al., 2004), which makes this interpretation even more difficult. Today, the contribution of ephrin-A reverse-signaling remains controversial, due to the lack of direct evidence, as well as the plethora of different possible interpretations.

EphAs and ephrin-As

Expression of EphA and ephrin-A in the visual system (Table 1 and Figure 16)

Sperry's postulate states that cells express molecular tags which allow them to recognize each other and gives them guiding instruction regarding which directions to follow, through mechanisms of repulsion and attraction. These genetically encoded labels should be expressed by both target and projecting structure leading to a unique concentration of both, therefore giving precise localization. Several candidates belonging to the Eph and ephrin family fulfilling these criteria have been identified. Most members of this RTK family can be found expressed in complementary gradients along the visual system, among which some have been implied in the formation of visual maps. Here, the temporal and spatial expression of different Eph members that are found in the visual system will be described, as well as gradient orientation. The direction of gradient orientation indicates low to high expression (ex: caudal-rostral → low caudal to high rostral expression).

Retina

EphA receptors and ephrin-As have been described in the retina with different methods and at different stages of development. Originally, EphA receptors have been demonstrated to interact with collicular ephrin-As, which is referred as forward signalling. Later on, the presence of molecules able to bind EphA receptors in the retina suggested the existence of countergradients, which are complementary expression of ligands and receptors. The role of these gradients is still debated.

EphAs

Different technical approaches have been extensively used to demonstrate the presence of EphA receptors in the retina: *in situ* hybridization, ephrin-A-AP binding, reporter lines and immunostaining. *In situ* hybridization reveals the presence of mRNA with a high spatial resolution and specificity, but does not reveal the amount of protein that are translated and inserted at the membrane. Ephrin-A-AP and ephrin-A-Fc binding consists in applying ligands of EphA receptors coupled to an alkaline phosphatase or fused to the Fc portion of human immunoglobulin. However the high redundancy of the Eph/ephrin family and the numerous cross-talks make it hard to point out a specific receptor in case of a positive signal. Reporter lines carrying the lacZ gene, coding for β galactosidase were also used to monitor the endogenous expression of EphA receptors. Immunostaining studies are quite recent, as no specific antibody were available for a long time. However their sensitivity is not sufficient to detect graded expression considering the scattering of receptors across the entire cell structure, especially when compared to mRNAs, which are mostly concentrated in cell bodies.

Early evidence pointing to the presence of gradients of EphA receptors came from binding study. Initially in mouse, ephrin-A4 and ephrin-A1-FC were reported to display a graded binding in the retina along the nasal-temporal axis, suggesting a corresponding gradient of EphA receptors (Marcus et al., 1996). This was latter on confirmed using ephrin-A2 and ephrin-A5-AP which revealed a graded binding activity in a nasal-temporal gradient in the retina (Feldheim et al., 1998). Direct evidence came from *in situ* hybridization with which several EphAs have been identified in the retina:

- EphA3 can be found in the retina at P0 in an ungraded manner but not in the RGC layer (Brown et al., 2000; Feldheim et al., 1998)
- EphA4 is expressed in the ganglion cell layer, however, no gradient can be found at P0 and P1 (Feldheim et al., 1998; Reber et al., 2004)
- EphA5 expression has been reported in a nasal-temporal gradient in the retina by ISH in wild-

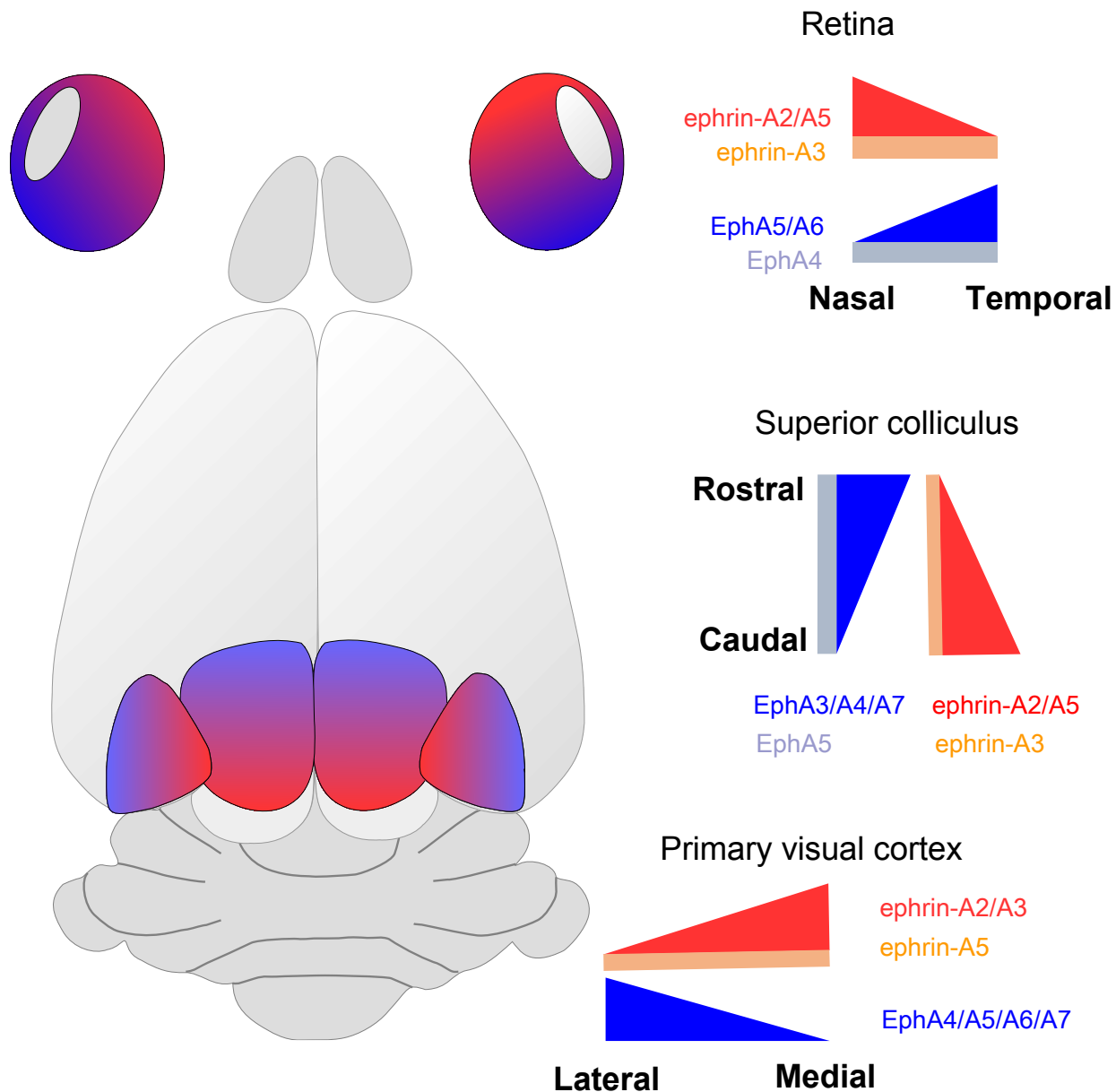


Figure 16: Overview of EphA/ephrin-A expression in the visual system.

Counter-gradients of EphAs and ephrin-As can be found in the retina, the superior colliculus and primary visual cortex. In the retina, EphA5 and EphA6 are expressed in low-nasal to high-temporal gradient while EphA4 is ungraded. Ephrin-A2 and ephrin-A5 are expressed in the opposite orientation (temporal → nasal), and ephrin-A3 is ungraded. In the superior colliculus, EphA3, EphA4 and EphA7 are expressed in a low-caudal to high-rostral gradient while EphA5 expression is constant along the rostral-caudal axis. Ephrin-A2 and ephrin-A5 are expressed in low-rostral to high-caudal gradient and ephrin-A3 expression is constant. In primary visual cortex, EphA4, EphA5, EphA6 and EphA7 have a graded expression from low-medial to high-lateral. Ephrin-A2 and ephrin-A3 form a lateral-medial gradient and ephrin-A5 expression is ungraded.

type mice in the RGC layer at P0 and P1, suggesting this receptor as a potential candidate for the formation of topographic maps (Brown et al., 2000; Feldheim, 2004; Feldheim et al., 1998; Reber et al., 2004). The level of expression is 2.6-fold higher at the temporal pole as compared to the nasal pole (Diaz et al., 2003)

- EphA6 is expressed in a similar graded manner, with a low nasal-temporal gradient, at P0 in the RGC layer (Brown et al., 2000; Feldheim, 2004; Feldheim et al., 2000; Reber et al., 2004). Expression is 2.8-fold higher at the temporal pole than at the nasal pole (Diaz et al., 2003)
- EphA7 shows no obvious expression at P0 in the retina (Feldheim et al., 1998)

The summed concentration of all EphA receptors across the retina has revealed a 2.75 fold increase in expression between the nasal and the temporal pole, at the mRNA level (Reber et al., 2004). Some of these expressions were confirmed by other approaches. For example, the graded expression of EphA5 was further confirmed with EphA5lacZ/lacZ mice by galactosidase staining (Feldheim, 2004), as well as at the protein level with immunostaining from E11 to E17, with a strong signal at E17 in the GCL (Cooper et al., 2009).

ephrin-As

The presence of EphA-Fc receptor binding in the retina has suggested the presence of ephrin-As. The E16.5 mouse retina shows an affinity for EphA7-Fc, with a stronger expression on nasal axons when compared to temporal (Rashid et al., 2005), and indeed, a similar activity has been reported for both EphA receptor fusion proteins EphA5-Fc and EphA2-Fc (Marcus et al., 1996).

- ephrin-A2 is expressed in the GCL at P1 in an ungraded manner (Pfeifferberger et al., 2006).
- ephrin-A3 was not initially detected in the retina by ISH (Marcus et al., 1996), although more recent studies have found its presence at P1 in an uniform distribution in the GCL (Pfeifferberger et al., 2006)
- ephrin-A4 could not be detected in the retina (Marcus et al., 1996)
- ephrin-A5 can be found in a temporal-nasal gradient (Marcus et al., 1996)

Ephrin-A5 expression was further confirmed at the protein level by immunostaining at E16.5, with a stronger signal at the nasal pole than at the temporal pole of the retina, in the GCL (Deschamps et al., 2010). Receptor-AP staining in the ephrin-A2/ephrin-A5KO double mutants did not succeed at detecting any binding, suggesting that ephrin-A2 and ephrin-A5 are the most abundant ligands that are present inside the retina (Feldheim et al., 2000).

Superior colliculus

EphAs

Similar to ephrin-As in the retina, countergradients of EphA receptors have also been identified in the SC. These gradients have either been detected by ISH or by immunostaining.

- EphA3 mRNA exhibit a caudal-rostral gradient in the SC at P1, and appears weaker in signal as compared to EphA7 (Rashid et al., 2005)
- EphA4 RNA is detected in a caudal-rostral gradient at E12 (Yun et al., 2003), and broadly expressed at high levels in a very shallow gradient at P1 (Rashid et al., 2005). EphA4 protein can be found in the SC from E11 to P6 (Greferath et al., 2002)
- EphA5 expression was also reported in the developing mouse SC from E9 to E17 at the protein level, as well as at adult stage (Cooper et al., 2009)
- EphA7 mRNA can be found at E12 in a caudal-rostral gradient (Feldheim et al., 2000; Yun et al., 2003), stable from E16 to P6 to become barely detectable at P11 (Rashid et al., 2005)

EphA7 was also detected by receptor affinity probe staining *in situ* in the SC between E12.5 and E14.5, and at P1 (Rogers et al., 1999), and also by western blot, with a stronger signal at the rostral pole than the caudal pole (Rashid et al., 2005)

ephrin-As

Similar to the identification of EphA receptors in the retina, binding assays in the SC have revealed a single rostral-caudal gradient. Using an EphA3-AP fusion protein, a staining was identified in the SC at E18 (Feldheim et al., 1998). This gradient was further characterized by ISH and immunostaining.

- ephrin-A2 is present at the mRNA level in a rostral-caudal gradient at E12 (Yun et al., 2003), E15, and E18, with a high point of expression at the SC/IC boundary (Feldheim et al., 1998, 2000; Hansen et al., 2004). Ephrin-A2 is expressed 2.2-fold more in the caudal region than in the rostral region of the SC (Diaz et al., 2003)
- ephrin-A3 can be found at low level in the SC at P1 and ungraded (Pfeiffenberger et al., 2006)
- ephrin-A5 is expressed in a rostral-caudal gradient at the mRNA level at E16 and P1 (Feldheim et al., 2000; Hansen et al., 2004; Rashid et al., 2005; Yun et al., 2003). Quantification of RNA has revealed a 5.5-fold increase from rostral to caudal (Diaz et al., 2003). Ephrin-A5 can also be found at the protein level at E14.5 and E16.5 in the SC, but immunostaining has failed at detecting a graded expression (Deschamps et al., 2010)

ISH was also performed against ephrin-A1, A3, and A4, and could not detect any expression in the SC (Feldheim et al., 2000). EphA3-AP or EphA5-AP binding assays on ephrin-A2/ephrin-A5KO double mutants could not detect any binding above the background level (Feldheim et al., 2000).

Primary visual cortex

The presence of retinotopic maps in V1 suggest a patterned organization of projections that require a precise mapping mechanism. Molecules from the EphA/ephrinA family have been identified in this structure, suggesting a role in the formation of these topographic projections.

EphAs

Few studies have addressed the expression of EphA receptors specifically in V1. However, whole brain studies have revealed a graded expression at different stages. At P0, ISH staining of EphA4, EphA5, EphA6 and EphA7 mRNA shows a medial-lateral gradient across the posterior cortex, while EphA3 seems to be expressed at a constant weak level; although boundaries of V1 are difficult to determine (Yun et al., 2003). EphA4 receptors have been characterized at the protein level in the developing mouse. Its expression can be found in the posterior cortex from E11 to P6, with a strong peak of expression at E15 and E17.5 (Greferath et al., 2002). ISH at P0 in the posterior cortex has revealed a strong expression of EphA7 (Rash and Grove, 2006). More specifically in V1, *in situ* hybridization at P4 has revealed a staining for EphA7 and EphA4 that is similar to Cad8 expression, a marker for V1. This expression is graded along the medial-lateral axis, with a slight peak that could mark the border between V1 and V2 (Cang et al., 2005b).

ephrin-As

Expression of ephrin-A2 and ephrin-A3 mRNA can be found at P4 in the V1 in a lateral-medial gradient (Cang et al., 2005b; Pfeiffenberger et al., 2006), whereas ephrin-A5 is expressed in a complementary manner to Cad8, EphA4, and EphA7; suggesting a role in boundary formation of the visual cortex (Cang et al., 2005a; Deschamps et al., 2010; Pfeiffenberger et al., 2006).

Gene	Technique	Age	Gradient	Reference
Retina				
EphA4	ISH	P0	Ungraded	(Feldheim et al., 1998)
EphA5	ISH	P0	Nasal → Temporal (2.6 fold)	(Brown et al., 2000; Cooper et al., 2009; Diaz et al., 2003; Feldheim, 2004; Feldheim et al., 1998)
	Immunostaining	E11-E17		
EphA6	ISH	P0	Nasal → Temporal (2.8 fold)	(Brown et al., 2000; Diaz et al., 2003; Feldheim, 2004; Feldheim et al., 2000)
ephrin-A2	ISH	P1	Ungraded	(Pfeiffenberger et al., 2006)
ephrin-A3	ISH	P1	Ungraded	(Pfeiffenberger et al., 2006)
ephrin-A5	ISH	E15	Temporal → Nasal	(Marcus et al., 1996)
	Immunostaining	E16.5		
Superior colliculus				
EphA3	ISH	P1	Caudal → Rostral	(Rashid et al., 2005)
EphA4	ISH	E12 and P1	Caudal → Rostral	(Greferath et al., 2002; Rashid et al., 2005)
	Immunostaining	E11- P6		
EphA5	Immunostaining	E9-E17	Ungraded	(Cooper et al., 2009)
EphA7	ISH	E12-P11	Caudal → Rostral	(Feldheim et al., 2000; Rashid et al., 2005; Rogers et al., 1999; Yun et al., 2003)
ephrin-A2	ISH	E12-E15- E18	Rostral → Caudal	(Diaz et al., 2003; Feldheim et al., 1998; Hansen et al., 2004; Yun et al., 2003)
ephrin-A3	ISH	P1	Ungraded	(Pfeiffenberger et al., 2006)
ephrin-A5	ISH	E16-P1	Rostral → caudal	(Deschamps et al., 2010; Feldheim et al., 2000; Hansen et al., 2004; Rashid et al., 2005; Yun et al., 2003)
	Immunostaining	E14.5-E16.5	Ungraded	
Primary visual cortex				
EphA4	Immunostaining	E11 → P6	Medial → Lateral	(Cang et al., 2005a; Greferath et al., 2002; Yun et al., 2003)
	ISH	P0		
EphA5	ISH	P0	Medial → Lateral	(Yun et al., 2003)
EphA6	ISH	P0	Medial → Lateral	(Yun et al., 2003)
EphA7	ISH	P0 and P4	Medial → Lateral	(Cang et al., 2005a; Rash and Grove, 2006; Yun et al., 2003)
ephrin-A2	ISH	P4	Lateral → Medial	(Cang et al., 2005a; Pfeiffenberger et al., 2006)
ephrin-A3	ISH	P4	Lateral → Medial	(Cang et al., 2005b; Pfeiffenberger et al., 2006)
ephrin-A5	ISH	P4	Ungraded	(Cang et al., 2005a; Deschamps et al., 2010; Pfeiffenberger et al., 2006)

Table 1: Summary of EphA and ephrin-A expression in the visual system

EphAs and ephrin-As in retino-collicular map formation

Since the discovery of molecular gradients and their implication in topographic mapping, a lot of effort has been made towards understanding the contributions of the members of the Eph and ephrin family. Here the major *in vitro* and *in vivo* findings, alongside the mouse models that have been generated to study relative implications of EphAs and ephrin-As, will be described (Table 2).

In vitro

ephrin-A2

The implication of ephrin-As in retino-collicular mapping has come from the identification of their graded expression and their effect *in vitro* in stripe assays on ingrowing chick RGCs. When given the choice between an alternating stripe of 293T cells – either mock transfected or expressing ephrin-A2 temporal axons – they show a preference for lanes without ephrin-A2, whereas nasal axons show no preference at all (Monschau, 1997; Nakamoto et al., 1996). Similar results were obtained in mice with the same experimental paradigm, with temporal axons avoiding lanes that contain ephrin-A2.

ephrin-A5

Similar to ephrin-A2, ephrin-A5 is also repulsive for temporal chick RGCs. Interestingly, nasal axons also show a sensitivity to this molecule, with a decrease in response when compared to temporal explants (Drescher et al., 1995; Monschau, 1997). In mice, wild-type E14-16 retinal explants grown on homogeneous carpets of P0-P2 SC membranes from either WT or ephrin-A5KO, and they do not display a difference in neurite outgrowth (Frisén et al., 1998). However, a difference can be observed in stripe assays. Indeed, when temporal RGCs are given a choice between stripes of mock-transfected, or ephrin-A5 expressing 293T cells, a preference can be seen for the absence of ephrin-A5. This preference is abolished for nasal axons (Feldheim et al., 1998).

ephrin-A2 and ephrin-A5

Stripe assays were also performed with material originating from double mutants which lack both ephrin-A2 and ephrin-A5. In this experimental paradigm, the retina and SC originated from either wild-type or double mutant animals. When WT temporal axons are grown on ephrin-A2/ephrin-A5KO alternating SC stripes, caudal stripes lose their repulsive effect. Conversely, when nasal retinal axons from the double mutants are grown on WT SC, they gain in responsiveness, showing a preference when nasal axons are otherwise insensitive to repulsion (Feldheim et al., 2000).

EphA5

To study the involvement of EphA5 in retino-collicular mapping, an EphA5LacZ mutant was generated. In this approach, the intracellular domain of EphA5 was replaced by β -galactosidase, leaving intact the extracellular domain. This approach only alters the forward signaling. In stripe assays using WT SC stripes, temporal RGCs derived from EphA5LacZ/LacZ mutants show a decrease in repulsion sensitivity, when compared to WT and heterozygotes mutants. Nasal axons show no obvious changes in the EphA5lacZ/lacZ mutants, remaining unresponsive to SC membranes (Fig. 4 E). Similar experiments were performed using wild type RGC on EphA5KO SC membranes, but showed no difference with the wild-type. This could be due to reverse signaling, since the extracellular domain of EphA5 is intact, and thus one cannot rule out the implication of EphA5 in reverse signaling through ephrin-As. These results suggest an implication of EphA5 forward signaling in the repulsion of temporal RGC and in the formation of retino-collicular map (Feldheim, 2004).

EphA7

EphA7, which is expressed only in the SC also shows a repelling activity *in vitro*. Using EphA7-Fc and Fc stripes, retinal axons had shown a preference for Fc stripes, without any differences between nasal and temporal axons (Rashid et al., 2005)

In vivo

EphA3

To study the involvement of retinal EphAs specifically in the formation of the retinotopic map, a gain of function mutant was generated (Brown et al., 2000). This model takes advantage of the expression pattern of *Isl2*, which can be found in 50% of RGCs that target contra-laterally to the SC. More specifically, *Isl2* is expressed in OFF α RGCs (CB2 +), but not in ON-OFF DSGC (DRD4 -), and innervate the entire depth of the SC (Triplett et al., 2014). As a consequence, in this mouse model, the *Isl2-EphA3KI*, EphA3 is overexpressed in 50% of RGCs. This leads to a striking phenotype, where projections along the nasal-temporal axis of the retina segregate into two distinct zones along the rostral-caudal axis of the SC, leading to a duplication of the overall retino-collicular map. Interestingly, heterozygotes only display a partial duplication of the retino-collicular map, with a collapse point at 76% of the rostral-caudal axis (Brown et al., 2000; Reber et al., 2004). In addition neither projections target the correct TZ, with wild-type projections being shifted caudally.

EphA5

In *EphA5LacZ/LacZ* mutants, targeting errors can be found in axons originating from both the temporal and the nasal pole of the retina, with the formation of ectopic sites in 42 and 51% of the animals, respectively. Ectopic sites are shifted rostrally for the nasal projections and caudally for the temporal projections. Similar results were also obtained for central injections, with multiple arborizations in 75% of the cases for homozygotes. No such phenotypes were observed in *EphA5LacZ/+* mutants. In *EphA5LacZ* mutants, forward signaling is specifically targeted, since only the intracellular part of the receptor is replaced with a β -galactosidase (Feldheim, 2004).

EphA7

In *EphA7-/-*, ectopic TZ can be found with anterograde tracing in 62% of the animals, as well as an extended scattering when RGCs are labelled retrogradely. Since EphA7 is only expressed in the SC, these results suggest a role for reverse signaling in the formation of the retino-collicular map through the suppression of branching that is located rostrally to future TZs. (Rashid et al., 2005)

Compound mutants

Isl2-EphA3KIxEphA4KO

Generation of compound mutants, heterozygous for EphA3 in *Isl2* positive cells and *EphA4-/+*, has provided insights into signaling mechanisms. In these double mutants, the collapse point is shifted at 88% of the rostral-caudal axis, compared to 76% in the *Isl2-EphA3KI*; while the distance separation between duplicated projections is increased from 20% of the rostral-caudal axis in *Isl2-EphA3KI/+* to 75% in the *Isl2-EphA3KI/+*, *EphA4+/-*. These results have revealed a participation in the overall signaling of EphA4, in which expression is ungraded in both the retina and the SC during RC map formation (Reber et al., 2004); and has thus further identified the basic principles of the mapping formation. Indeed, this study suggests that a dominant RGC (expressing the highest level of EphA receptors) drives the mapping through comparing EphA relative signaling between RGCs.

Isl2-EphA3KlxEphA5KO

Further insights in signaling mechanisms has come from studies of another compound mutant: the Isl2-EphA3KlxEphA5KO. In these double mutants, at a heterozygote state for both alleles, a shift in the collapse point when compared to the single EphA3KI/+ mutant, can be found. This also suggests a relative signaling model with the participation of EphA5 in the formation of the retino-collicular map (Bevins et al., 2011), and further suggests that EphA receptors can be considered as functionally equivalent in this system.

Role of ephrin-A5 in retino-collicular mapping

To study the role of ephrin-A5 in retino-collicular mapping, a knock out was generated. In these animals, the expression of ephrin-A2 – which also shows a grade expression in the SC – is unaltered. In homozygotes, the mapping of projections originating from the temporal pole of the retina revealed in 50% of cases that the formation of an eTZ has shifted caudally, close to the main TZ site. In addition, some axons overshoot towards the most caudal part of the SC, at the border with the inferior colliculus. Retrograde tracing from the caudal pole of the SC has also revealed an increase in the scattering of the retrolabeled RGCs (Frisén et al., 1998). The mapping of projections originating from the nasal part of the retina has revealed stronger mapping defects in ephrinA5^{-/-} (91% penetrance), with an eTZ that is shifted rostrally (Feldheim et al., 2000).

Recently, a conditional mutant for ephrin-A5 was generated. In this model, ephrin-A5 is either specifically removed from the retina or the SC. For axons originating from the temporal pole of the retina, deletion of the collicular ephrin-A5 leads to minor targeting defects, with eTZ close to the topographically correct location, but shifted caudally with a 100% penetrance. In 40% of cases, a rostrally shifted eTZ could be found for projections from the temporal part of the retina for the ephrin-A5 retinal KO. For nasal axons, a collicular deletion of ephrin-A5 leads to a formation of eTZs that are shifted rostrally to the topographically correct location. However, the absence of retinal ephrin-A5 does not induce targeting defects for projections from the nasal pole of the retina (Suetterlin and Drescher, 2014).

Role of ephrin-A2 in retino-collicular mapping

Similarly, the ephrin-A2KO was generated. In these animals, mapping defects can be found, with the formation of eTZ being shifted more caudally in 57% of homozygous, for axons originating from the temporal pole of the retina. However, no mapping defects can be found concerning the nasal pole of the retina (Feldheim et al., 2000).

Role of ephrin-A2 and ephrin-A5 in retino-collicular mapping

The generation of compound mutants, by crossing ephrin-A2 and ephrin-A5KO, has revealed a more striking phenotype that has a high penetrance. In double heterozygous animals, ephrin-A2^{+/-} ; ephrin-A5^{+/-}, caudally shifted eTZ can be observed with 55% of penetrance. When nasal axons are labeled, no mapping defects could be found. In ephrin-A2^{-/-};ephrinA5^{-/-} mutants, mapping defects are more severe in nasal RGCs than in temporal RGCs, with 92 and 85% penetrance, respectively. Interestingly, eTZs are shifted in an opposite way, with temporal TZs shifted caudally and nasal TZs shifted rostrally (Feldheim et al., 2000).

In addition, multiple ectopic sites can be found in double mutants, whereas a single site can be found in the single homozygous mutants. These eTZs were also shifted along the medial-lateral axis, which could be explained by an interaction between ephrin-A5 and EphB2 (Himanen et al., 2004); the latter being involved in the mapping of the lateral-medial axis (Hindges et al., 2002).

Role of ephrin-A3 in retino-collicular mapping

The retino-collicular map of ephrin-A3KO mice has also been assessed. In these animals, both the nasal and temporal axons target their correct locations without the formation of eTZ (Pfeiffenberger et al., 2006). However, in triple homozygous knock-outs – ephrin-A2/A3/A5 – the absence of ephrin-A3 has worsened the mapping deficits on the double homozygous ephrin-A2/A5KO mutants (Pfeiffenberger et al., 2006).

Mutant	Mapping defect		References
	(Penetrance) Nasal	(Penetrance) Temporal	
ephrin-A2KO	No mapping defect	(57%) Caudal shift	(Feldheim et al., 2000)
ephrin-A3KO	No mapping defect	No mapping defect	(Pfeiffenberger et al., 2006)
ephrin-A5KO	(91%) Rostral shift	(50%) Caudal shift	(Frisén et al., 1998)
ephrin-A5 retinal KO	No mapping defect	(40%) Rostral shift	(Suetterlin and Drescher, 2014)
ephrin-A5 collicular KO	Rostral shift	Caudal shift	(Suetterlin and Drescher, 2014)
ephrin-A2/ephrin-A5KO	(92%) Rostral shift	(85%) Caudal shift	(Feldheim et al., 2000)
EphA3 ^{KI/+}	Duplication	Collapse point at 76%	(Brown et al., 2000)
EphA3 ^{KI/KI} x EphA4 ^{-/-} or EphA5 ^{-/-}	Duplication	Duplication	(Bevins et al., 2011) (Reber et al., 2004)
EphA3 ^{KI/+} x EphA4 ^{+/-}	Duplication	Collapse point at 88%	(Reber et al., 2004)
EphA3 ^{KI/+} x EphA4 ^{-/-}	Duplication	Collapse point at 95%	(Reber et al., 2004)
EphA3 ^{KI/+} x EphA5 ^{+/-}	Duplication	Collapse point at 85%	(Bevins et al., 2011)
EphA3 ^{KI/+} x EphA5 ^{-/-}	Duplication	Collapse point at 90%	(Bevins et al., 2011)
EphA5KO	(51%) Rostral shift	(42%) Caudal shift	(Feldheim, 2004)
EphA7KO	(62%) Rostral shift	No mapping defect	(Rashid et al., 2005)

Table 2: Summary of mouse models used in the study of role of EphA/ephrin-A signalling in the formation of retino-collicular map.

EphA and ephrin-As in cortico-collicular map formation and alignment

During development, retinal inputs form the retino-collicular map between P0 and P7, followed by the formation of the cortico-collicular map, originating from layer V pyramidal cells in V1. These two maps are topographic, and aligned in the SC, and represents the same part of the visual field. The alignment and formation of the cortico-collicular map seems to depend on retinal inputs, since its formation occurs at a later stage. In addition, mapping defects can be found in the absence of retinal inputs and molecules of the Eph/ephrin family have been involved in the formation of this map.

Interactions between the retino- and the cortico-collicular map

Inputs from the retina and the V1 target to the same layers in the SC, mostly the SGS and the SO (Lund, 1972). These projections are aligned in this structure, with a correspondence between their respective axes (Rhoades et al., 1985). The medial-lateral axis of V1 aligns onto the rostral-caudal axis of the SC, both of which reflects the nasal-temporal axis of the retina. Evidence suggests that both the retino-collicular and cortico-collicular inputs converge on the same cells in the SC; and electron microscopy studies have shown that cortico-collicular fibers contact small-caliber, non-GABAergic dendrites in the SC (Boka et al., 2006). At the cellular level, both cortico-collicular and retino-collicular fibers have been found to synapse on dorsally-oriented vertical (DOV) cells by co-localization studies (Phillips et al., 2011) in the SC.

From a functional aspect, collicular neurons respond to a single impulse from V1, demonstrating a direct functional connectivity (Bereshpolova, 2006). Recent studies have also highlighted the coupling of oscillations between V1 and SC (Stitt et al., 2015), and also that cortico-collicular projections can modulate the magnitude of responses in the SC (Zhao et al., 2014). Furthermore, when these fibers are silenced in awake animals, a decrease in collicular neuronal responses can be observed, with no alteration observed in anesthetized animals (Zhao et al., 2014). Since cortical inputs are aligned onto retinal inputs and modulate their response, the receptive field of the cortical afferents need to overlap with the receptive field of the collicular cells they contact.

Role of EphA and ephrin-As in V1 formation and alignment of projections

EphAs and ephrin-As present graded expression in V1, and topographic defects in V1 can also be found in the ephrin-A2/A3/A5KO. An *in situ* hybridization study has revealed the presence of EphA4 and EphA7 in a medial-lateral gradient, while ephrin-A2, -A3, -A5 can be found in a lateral-medial gradient in V1. This graded expression suggests that these molecules could be used throughout different structures in order to initiate the formation of topographic maps (Cang et al., 2005a).

Retinotopy in V1 was also assessed in ephrin-A deficient mice, using optical intrinsic imaging. These triple ephrinA2/A3/A5 mutants display an increase in scattering for both the elevation and azimuth; a bigger cortical magnification factor and a shifted orientation for V1 (Cang et al., 2005a). In addition, ectopic expression of ephrin-A5 in V1 disrupts the internal topography, while when expressed in the lateral cortex, the positioning of V1 is altered (Cang et al., 2005a).

When looking at the alignment of V1 and SC in ephrinA2/A5 homozygote deficient mice, mis-targeting can also be found in the projections from V1 (Wilks et al., 2010). Formation of eTZ occurs at a lower frequency for cortico-collicular projections, when compared to retino-collicular projections, suggesting a misalignment between the two maps. This could be due to the existence of non-functional eTZs from the retina (Haustead et al., 2008), which would fail to establish/align connections from V1.

Isl2-EphA3KI

The Isl2-EphA3KI mouse model presents a duplicated retino-collicular map in the SC, as demonstrated both at anatomical (Bevins et al., 2011; Reber et al., 2004) and functional levels (Owens et al., 2015; Triplett et al., 2009). This duplication is due to an ectopic expression of EphA3 in 50% of the RGCs, leaving the endogenous gradients EphAs/ephrinAs in the SC unaltered. Interestingly, the topography within V1 is not altered in Isl2-EphA3KI, with a single representation of the retinotopy (Triplett et al., 2009). However, mapping defects can be found in the projections from V1 to the SC (the cortico-collicular projections). Remarkably, a duplication of the cortico-collicular projections has been shown in these animals, mimicking the duplication of the retino-collicular map. These results have suggested that cortico-collicular map alignment in the SC is instructed by correlated retinal activity. However at this point, a role of retinal guidance cues in cortico-collicular map alignment cannot be excluded.

Models of altered retinal inputs:

To investigate the contribution of retinal inputs towards the formation of the cortico-collicular map in the SC, mouse models that feature decreased retino-collicular inputs have been studied.

- In anophthalmic mice, cortico-collicular axons are still able to reach the SC, however these inputs are disorganized (Khachab and Bruce, 1999).
- In monocularly enucleated animals at birth, projections from V1 reach the superficial layers of the SC prematurely (Grant et al., 2016). When animals are enucleated at P6, these projections are still able to form a coarse topography, with TZs at least four times larger than for wild-type (Triplett et al., 2009).
- In Math5^{-/-} mice, only 5 to 10% of RGCs remain (Lin et al., 2004). In these animals, cortico-collicular projections are also unrefined similarly to enucleated animals (Triplett et al., 2009).

These studies suggest that retinal inputs are required for the formation of refined projections, since a coarse topography can still be found. This phenomenon could be attributed either to the absence of spontaneous correlated activity or to molecular instruction coming from the retina.

Indeed, two major hypotheses could explain how the retino- and cortico-collicular maps are aligned in the SC. A gradient matching model suggests that projections from V1 are guided by gradients expressed in the SC, using the same type of molecules than that used for the mapping of the retino-collicular projections. This mechanism would allow for the alignment of both maps through shared molecular cues.

A retinal matching model suggests that cortico-collicular projections are guided by activity, and align through Hebbian mechanisms. Correlated activity for the same part of the retinotopic space would drive the establishment of projections, and would allow their alignment. In addition, recent studies have highlighted the necessity of reciprocal inputs for the formation of interconnected maps along the visual system, which suggests an interdependence of maps for proper alignment (Shanks et al., 2016).

EphB and ephrin-B

Expression of EphB and ephrin-B in the visual system (Table 3)

EphA and ephrin-A have been identified as key actors in the organization of retinotopic projections in the visual system. However, their expression by itself cannot account for the organization of the entire retinotopic map that can be found in the SC. Indeed, EphA/ephrin-A organize solely the nasal-temporal axis, while having little or no influence on the mapping of the dorsal-ventral axis of the retina onto the lateral-medial axis of the SC. Molecules from the EphB subclass have been found to be expressed as gradients along this axis.

Retina

The graded expression of EphBs along the dorsal-ventral axis of the retina, as well as their effect on axon growth have suggested an implication in the formation of the retino-collicular map.

EphB

Experiments in the chick have shown a graded expression of EphBs along the dorsal-ventral axis, (Braisted et al., 1997), suggesting an implication in the mapping of the lateral-medial axis in the SC. Following this study, the expression of the EphB receptor was investigated in the mouse retina. The generation of EphB1 and EphB2 reporter lines have allowed further study of receptor expression.

- EphB1 is expressed uniformly along the dorsal-ventral axis at the mRNA level in the GCL at E14.5 and E16 (Birgbauer et al., 2000), while X-gal stains in EphB1LacZ mutants at E16.5, P1 and P8 had shown a high expression in the ventral-temporal region of the embryonic retina, which becomes uniformly distributed at postnatal stages (Thakar et al., 2011)
- EphB2 mRNA is initially distributed in an ungraded manner at E13, but by E16, a ventral-dorsal difference in expression can be detected (Birgbauer et al., 2000) The graded expression of EphB2 is progressive as reported, when monitoring EphB2- β -gal protein expression from E13 to E16 retinas, with a dorsal-ventral gradient appearing at E16 (Birgbauer et al., 2000). EphB2 expression is at its strongest at the mRNA level at P0, found at P4 (Hindges et al., 2002) and can still be detected by galactosidase staining at P8 (Thakar et al., 2011)
- EphB3 receptor mRNA is expressed uniformly along the dorsal-ventral axis in the retina at both E13 and E16 (Birgbauer et al., 2000). A peak in expression can be found at P0, while mRNA can still be detected at P4 (Hindges et al., 2002)
- EphB4 mRNA expression is detected at E14, but does not appear to be graded. A shallow dorsal-ventral gradient can be found at P0 and P4 (Hindges et al., 2002)
- EphB6 mRNA is not detected in the retina (Hindges et al., 2002)

ephrin-B

Similar to ephrin-As, a counter-gradient of ephrin-B can be found in the retina.

- Ephrin-B1 is expressed in the GCL of both dorsal and ventral retina. (Birgbauer et al., 2000) At P0, ephrin-B1 is expressed in a ventral-dorsal gradient in the GCL, which can still be found at P4 (Hindges et al., 2002)
- Ephrin-B2 is not detected in the GCL at embryonic stages (Birgbauer et al., 2000), but at P0, a ventral-dorsal gradient can be found in the RGC layer that remains at P4 (Hindges et al., 2002). β -gal stains at E17.5, P0 and P8 show a graded expression of ephrin-B2 in a ventral-dorsal gradient in the retina (Thakar et al., 2011).
- Ephrin-B3 is expressed in the GCL uniformly along the dorsal-ventral axis at E14.5 (Birgbauer et al., 2000).

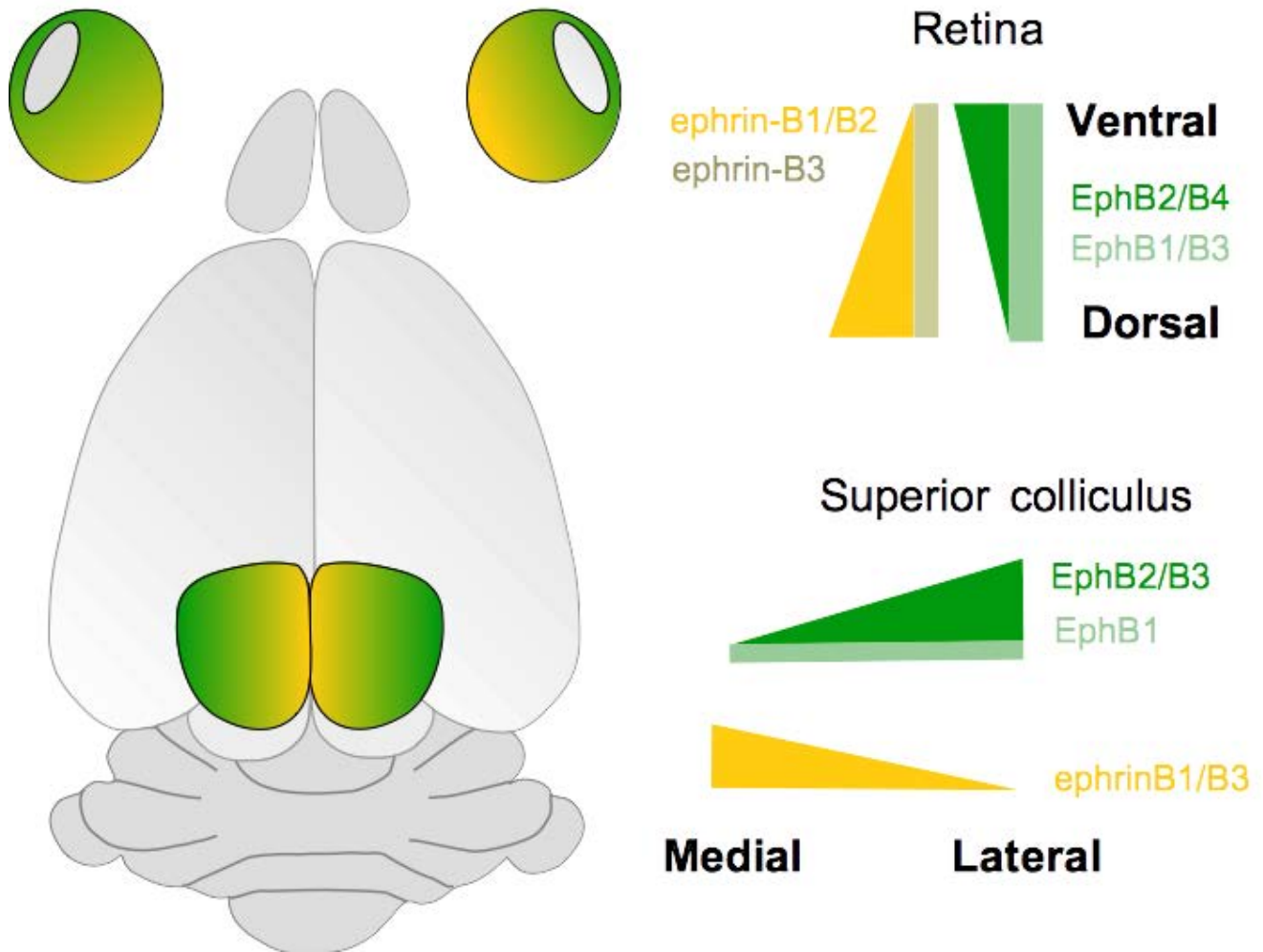


Figure 17: Overview of EphB/ephrin-B expression in the visual system.

Counter-gradients of EphBs and ephrin-Bs can be found in the retina and the superior colliculus. In the retina, EphB2 and EphB4 are expressed in low-dorsal to high-ventral gradient while EphB1 and EphB3 expression is ungraded. Ephrin-B1 and ephrin-B2 are expressed in the opposite orientation (ventral → dorsal), and ephrin-B3 is ungraded. In the superior colliculus, EphB2 and EphB3 are expressed in a low-medial to high-lateral gradient while EphB1 expression is constant along the medial-lateral axis. Ephrin-B1 and ephrin-B3 are expressed in low-lateral to high-medial gradient.

Superior colliculus

Complementary expression of EphB and ephrin-B can be found in the SC. These graded expressions in the target structure has suggested their implication in the formation of the retinotopic map.

EphB

- EphB1 expression was detected in the EphB1LacZ mutants in which X-gal stains had shown a strongly uniform expression, within cells of the SC (Thakar et al., 2011).
- EphB2 mRNA is expressed in a medial-lateral gradient in the SC ventricular zone at P0 and P4 (Hindges et al., 2002), while EphB2- β -gal fusion protein was reported to be expressed uniformly in the SC at P1 and P8 (Thakar et al., 2011).
- EphB3 mRNA was detected in medial-lateral gradient in the SC ventricular zone at P0 and P4 (Hindges et al., 2002)

ephrin-B

- Ephrin-B1 mRNA is expressed in a lateral-medial gradient across the SC at P0 that persists at P4 (Hindges et al., 2002). Immunostaining has failed to detecting a gradient, as well as finding a low immunoreactivity in the SC (Buhusi et al., 2009; Migani et al., 2009)
- Ephrin-B2 expression was not detected in the SC (Hindges et al., 2002)
- Ephrin-B3 is strongly expressed at P0 at the midline, separating the left and right SCs (Hindges et al., 2002)

Gene	Technique	Age	Gradient	Reference
Retina				
EphB1	ISH	E14.5-E16	ventral-temporal	(Birgbauer et al., 2000; Thakar et al., 2011)
		Postnatal	Ungraded	
EphB2	ISH	E13-E16	Ungraded	(Birgbauer et al., 2000)
		P0,P4,P8	Dorsal → ventral	
EphB3	ISH	E13-E16	Ungraded	(Birgbauer et al., 2000; Hindges et al., 2002)
EphB4	ISH	E14	Ungraded	(Hindges et al., 2002)
		P0-P4	Dorsal → Ventral	
ephrin-B1	ISH	P0-P4	Ventral → Dorsal	(Birgbauer et al., 2000; Hindges et al., 2002)
ephrin-B2	ISH	P0-P4	Ventral → Dorsal	(Birgbauer et al., 2000; Hindges et al., 2002)
ephrin-B3	ISH	E14.5	Ungraded	(Birgbauer et al., 2000)
Superior colliculus				
EphB1	X-gal staining in EphB1LacZ mutant	P1-P8	Ungraded	(Thakar et al., 2011)
EphB2	ISH	P0-P4	Medial → Lateral	(Hindges et al., 2002; Thakar et al., 2011)
	X-gal staining in EphB2LacZ mutant	P1-P8	Ungraded	
EphB3	ISH	P0-P4	Medial → Lateral	(Hindges et al., 2002)
ephrin-B1	ISH	P0-P4	Lateral → Medial	(Hindges et al., 2002)
ephrin-B3	ISH	P0	Midline	(Hindges et al., 2002)

Table 3: Summary of EphB and ephrin-B expression in the visual system

EphB/ephrin-B in the formation of the retino-collicular map in mouse

Evidence for a role of EphB/ephrin-B signaling in organizing the lateral-medial axis of the SC has come from the graded expression of EphB in the retina along the dorsal-ventral axis, and the corresponding gradient of ephrin-Bs in the SC along the lateral-medial axis. As a consequence, projecting cells expressing high level of EphB target zones of the SC that express high levels of ephrin-B. In addition, counter-gradients of ephrin-B in the retina and EphB in the SC can also be found. Few studies have addressed the role of EphB/ephrin-B signaling in the formation of the retino-collicular map in mice. Most evidence is derived from *in vitro* studies, and loss of function studies of EphBs, by global knock-out approaches and point mutations.

In vitro

Graded expression is not sufficient by itself to imply a causal role in the formation of topographic map. Indeed, these molecules are also required to elicit a response from ingrowing axons, either repulsive or attractive. *In vitro* studies have addressed the interactions between EphB and ephrin-B in order to elucidate their mechanisms of action. Retinal explants, originating from different parts of the retina were placed into contact with ephrin-B2. Ephrin-B2 induces a rapid growth cone collapse, and sustained axon retraction of ventral-temporal RGCs, but has little effect on dorsal-temporal RGCs (Petros et al., 2010).

This effect can be selectively reversed by using EphB4-Fc, which specifically blocks ephrin-B2 mediated inhibition of neurite outgrowth (Williams et al., 2003). Ephrin-B1, B2 and B3 show inhibitory effects on neurite outgrowth for RGCs originating from the ventral-temporal part of the retina. Taken together, these results suggest that EphB/ephrin-B signaling is a good candidate for organizing the lateral-medial axis of the SC.

In vivo

EphB1

Retino-collicular mapping in EphB1 protein null mutants (Williams et al., 2003) have revealed a mapping defect for RGCs, with the formation of eTZ originating from the ventral part of the retina with a penetrance of 65% for homozygous animals, and 38% of heterozygous animals (Thakar et al., 2011). The implication of forward signaling was pinpointed by a similar characterization in the EphB1 Tau-LacZ (Chenau and Henkemeyer, 2011), in which the intracellular domain of EphB1 was replaced by β -galactosidase. In these animals, forward EphB1 signaling is impaired, while reverse signaling is maintained. Mapping defects could still be found in 59% of homozygous and 20% of heterozygous animals, suggesting an implication of EphB1 forward signaling in retino-collicular mapping (Thakar et al., 2011).

EphB2:

Evidence for the implication of EphB2 in dorsal-ventral mapping has come from the characterization of EphB2 null mutants (Henkemeyer et al., 1996), which display mapping defects originating from the ventral-temporal retina, in 21% of the homozygous animals and in 6% of the heterozygous animals (Thakar et al., 2011). Further evidence has been derived from the characterization of the EphB2LacZ mutant (Henkemeyer et al., 1996), in which the intracellular domain of EphB2 was replaced by β -galactosidase; selectively disrupting forward signaling while maintaining reverse signaling.

A higher phenotype penetrance was observed when RGCs originate from the ventral-temporal retina, with 62% penetrance in homozygous and 32% penetrance in heterozygous animals. A dominant negative effect has been reported previously in EphB2LacZ animals (Cowan et al., 2000; Dravis et al., 2004; Hindges et al., 2002), which can also be observed here with an increased frequency of mapping errors, when compared with the EphB2 null protein mouse model. These mapping defects are not found when injections are performed in the dorsal part of the retina, suggesting that EphB2 is involved mainly in the mapping of ventral projections.

Further analysis of the different signaling pathways in point-mutated EphB2 mutants have revealed the implication of the tyrosine kinase domain. EphB2K661R mutants (Genander et al., 2009) have a point mutation that disrupts tyrosine kinase catalytic activity. Targeting defects from the ventral-temporal zone can be found in 50% of homozygotes and in 21% of heterozygotes. These results confirm the implication of EphB2 forward signaling, and indicates that the tyrosine kinase catalytic activity is a key component in this signal transduction process (Thakar et al., 2011).

The involvement of the PDZ domain could not be excluded. To investigate this aspect, the retino-collicular map of EphB2 Δ VEV mutants (Genander et al., 2009) was characterized. These mutants lack the ability to bind PDZ domain-containing proteins. Since no increase in the percentage of animals displaying eTZ was found on the EphB3KO background, this binding site was considered not to participate in the retino-collicular mapping (Thakar et al., 2011).

Analysis of the EphB2 F620D mutant that displays a constitutively active EphB2 (Holmberg et al., 2006) has revealed in 29% of the animals, the formation of an eTZ along the lateral-medial axis (Thakar et al., 2011), confirming the implication of the tyrosine kinase activity in retino-collicular mapping.

EphB3:

Anatomical tracing in EphB3KO has revealed eTZ, originating from the ventral-temporal part of the retina in 20% of animals, suggesting its implication in retino-collicular mapping (Thakar et al., 2011).

ephrin-B1:

Given that ephrin-B1 is an X-linked gene, hemizygous male and heterozygous female ephrin-B1KOs (Davy et al., 2004) were used to assess the implications of ephrin-B1 in retino-collicular map formation. No mapping defects were found regarding RGCs that originate from the dorsal part of the retina in these ephrin-B1 mutants. However, mapping defects that originate from the ventral part of the retina were found in 25% of the ephrin-B1 hemizygous males and in 33% of heterozygous females.

ephrin-B2:

To test the implication of ephrin-B2 reverse signaling with regards to the guidance of the RGC to the SC, the ephrin-B2 mutants that lack the intracellular domain of the ligand, was utilized (Dravis et al., 2004; Thakar et al., 2011). In these animals, forward signaling is still functional whereas reverse signaling is impaired. ETZ can be found shifted medially to the main TZ in dorsal injections in 11% of the heterozygotes, and in 27% of the homozygotes, and suggests that ephrin-B2 reverse signaling is required for the dorsal RGC axon retino-collicular mapping. Mapping defects can also be found in projections originating from the ventral part of the retina (42% of double mutants).

Compound mutants:

Analysis of EphB1/EphB2KO double mutants have revealed severe mapping abnormalities for projections originating from the ventral retina, with a lateral-caudal shift featuring a 100% penetrance of the phenotype. Penetrance is decreased when EphB1KOs are crossed with the EphB2-LacZs (75% for homozygotes, 66% for heterozygotes). However, no eTZs were found for projections originating from the dorsal part of the retina.

In EphB2;EphB3KO double homozygous knock-outs, eTZs can be found shifted laterally in roughly 40% of the animals. Further insights come from the use of EphB2KI, in which the intracellular part of the receptor has been replaced by a β -galactosidase, which removes the function of downstream signaling whilst retaining the function of upstream signaling. In double homozygous EphB3KO;EphB2KI, laterally shifted TZs can be found in 60% of the animals, while 29% of the EphB2KI^{-/-}; EphB3^{-/-} mice display mapping defects (Hindges et al., 2002).

Conclusion

EphB and ephrin-B have been demonstrated to play a fundamental role in the mapping of the RGC, from the ventral-temporal region of the retina, onto the medial-lateral axis of the SC. EphB1 and EphB2 forward signaling is involved in the targeting of the ventral-temporal axons, as demonstrated by studies in which the TK domain was specifically impaired, whereas EphB2 PDZ domain shows little involvement. These results suggest an essential role for the tyrosine kinase activity in the formation of the retino-collicular map. EphB3 seems to be involved also, although its ungraded expression in the retina suggests that it is probably not carrying positional information by itself. This signaling is believed to occur through interactions with ephrin-B1, as loss of function studies of this ligand unravel defects in the mapping of the ventral-temporal axons. Ephrin-B2 is the only receptor to induce defects from the dorsal part of the retina, and for which reverse signaling seems necessary for proper axon targeting.

The different responses can be explained by the expression of distinct molecules, according to their location in the retina. Indeed, ventral-temporal axons are positive for EphB1, EphB2 and EphB3, while dorsal-temporal axons are EphB3 and EphB2 positive. This spatial restriction suggests the presence of combinatorial effects of these different receptors, regarding specific targeting in the SC. The synergistic effects observed in compound mutants highlight the interplay between receptors and ligands, which probably act together in order to instruct the final topographic location.

The temporal dimension of the expression seems to play an important role in the different implications of EphB and ephrin-B signaling. Gradients are subject to a variation during development, and some only appear at particular time points, only to become uniform at later stages. Indeed, EphB/ephrin-B signaling is also involved in the formation of the optic chiasm where in mice, 5% of the RGCs project ipsilaterally. Evidence has accumulated concerning the role of EphB1 (Petros et al., 2009) and EphB2 (Chenau and Henkemeyer, 2011) in the formation of these ipsilateral projections. This signaling takes place through interactions with ephrin-B2, expressed at the level of the optic chiasm by radial glial cells (Williams et al., 2003).

Deciphering the relative contribution of each of the actors to these different processes is a daunting task. The spatial-temporal expression pattern may provide insights into these mechanisms, the same molecules being expressed at different time points, and localization being involved in different processes, which together add to the complexity of EphB and ephrin-B signaling in the formation of the retino-collicular map.

Activity in the formation of visual maps

The formation of appropriate connections is essential for proper sensory processing. Even if molecular cues play a fundamental role in establishing topological and topographic order, these projections are later reshaped by activity. In particular, evidence has accumulated concerning the role of activity during the formation of the retino-collicular map. Originally considered as mutually exclusive mechanisms, a consensus has emerged whereby molecular cues are establishing a rough map, during which activity is being involved in the refinement of the map (Cline, 2003; Tsigankov and Koulakov, 2010).

Hebb theory

The contribution of activity towards the formation of appropriate connections both during development, and later during learning, has been the subject of intensive study in the field of neuroscience. The underlying debate involves the relative roles of nature (genetically encoded developmental program) versus nurture (experience). Current viewpoints in the domain suggest a cooperative process occurring at the interface between activity-dependent mechanisms and molecular guidance cues. These two forces are acting together to properly wire the nervous system. Historically, Hebb's initial postulate (Hebb, 2002) is often summarized as "Cells that fire together, wire together", states that the correlated activity between two cells will lead to a remodeling of their connection pattern, leading to either a decrease, or an increase, in their connections (Figure 18). This mechanism, which is believed to be the cellular basis of learning and plasticity, allows individuals to adapt to their environment in respect to optimization of sensory circuits (Cline, 2003).

This universal mechanism has also been studied in the context of map formation. More specifically, the role of activity was investigated in the formation of the retino-geniculate (eye-specific segregation) and retino-collicular map (retinotopy). The visual system displays some interesting features for understanding the contribution of activity in the formation of the appropriate connections during development. Indeed, from embryonic stages, the retina displays a spontaneous activity with a high spatial and temporal correlation ("cells that fire together"), which are transferred to the target structures. Indeed, a correlation between retinal waves and spontaneous activity in the SC and V1 has been demonstrated, confirming the propagation of this activity (Ackman et al., 2012). This link was confirmed by enucleation and pharmacological blockade of retinal inputs, leading to an altered correlated activity in downstream targets (Ackman et al., 2012; Colonnese and Khazipov, 2010; Siegel et al., 2012). These characteristics would maintain and refine the topographic order across brain regions, because the connections between neighboring cells are strengthened ("wire together"), whereas the connections from more distant cells are lost (Eglen et al., 2003).

The relative contribution of either molecular or activity-based cues has been a subject of intensive debates over the years. Two different aspects will be described here: eye specific segregation in the LGN and retinotopy in the SC.

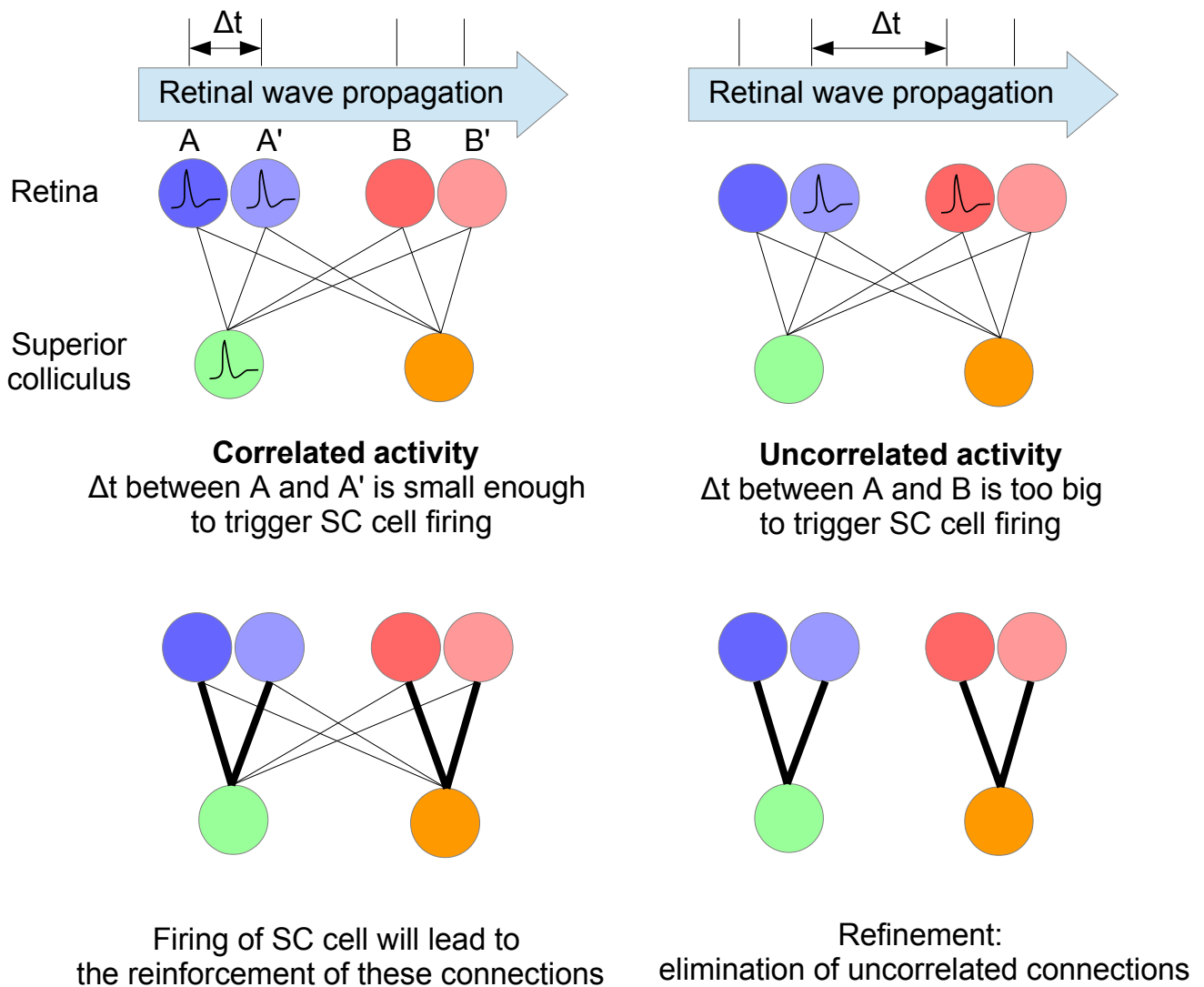


Figure 18: Refinement of projections by correlated activity. During development, correlated activity propagates in the retina, leading to the sequential activation of neighboring cells. **Correlated activity (top, left).** When adjacent cells fire together, this leads to the activation of the corresponding collicular cell. This will lead to the reinforcement of connections. **Uncorrelated activity (top, right).** When distant cell fire, their activity is uncorrelated. Connections are not maintained and are eliminated.

Spontaneous activity in the retina during development

Retinal waves (Ford et al., 2012; Torborg and Feller, 2005)

The role of activity in the formation of connections in the nervous system came from Hebb's postulate. In the development of the visual system, this activity takes a particular form in the source structure; the retina. Evidence for spontaneous activity in the retina came from recordings of neonatal rabbit retinæ, which display spontaneous bursting activity (Masland, 1977). Later on, a strong correlation among neighboring RGCs was identified in fetal rat retina (Galli and Maffei, 1988; Maffei and Galli-Resta, 1990; Meister et al., 1991). The simultaneous recordings of a large cell population by electroretinogram, and optical recordings of intracellular calcium levels revealed a strong spatial and temporal correlation of this activity, which became the so-called retinal waves (Feller, 1999, Wong, 1999). Further characterization of these waves revealed that they could start at any random location and spread through the entire retinal space (Feller et al., 1996; Meister et al., 1991; Wong et al., 1993). This correlated bursting activity was also found in the developing mouse retina and demonstrated to be transferred to the LGN (Mooney et al., 1996).

Cells involved in the propagation of these waves were also characterized. Blockade of cholinergic transmission alters these waves, which suggested a cholinergic transmission, thus highlighting a potential implication of starburst amacrine cells (Feller et al., 1996). The implication of RGCs was confirmed by a patch-clamp technique, suggesting that these waves may be conveyed to downstream targets in the developing visual system (Feller et al., 1996; Wong et al., 1993). Both amacrine and RGC display synchronized oscillations as demonstrated by calcium imaging (Wong et al., 1995). Compelling efforts have been made to understand the mechanisms through which these waves originate and propagate. Indeed in mice, these retinal waves can be separated into three distinct stages, from E16 to P0 (stage I), P0-P11 (stage II) and P11-P21 respectively.

Stage I waves

Stage I retinal waves are large propagating waves that occur between E16 and P0 in mice prior to the formation of retinal synapses, and initiated by RGCs. These waves can be reduced by nAChR antagonists (Bansal et al., 2000), suggesting that they are partially driven by acetylcholine. Other components involved may depend on gap junctions and adenosine, since 18 β -GA (a blocker of gap junction coupling) completely abolishes stage I waves in the rabbit retina (Syed et al., 2004).

Stage II waves

Stage II retinal waves are mediated by cholinergic transmission (Feller, 2002; Feller et al., 1996; McLaughlin et al., 2003; Zhou, 2001), and occur during the first postnatal week in mice. These waves start at a random location and propagate across the entire retina (Feller et al., 1997). They are initiated by spontaneous depolarization of starburst amacrine cell (SACs), which display a transient recurrent excitatory connectivity in rabbits (Zheng et al., 2004, 2006). This recurrent network of SACs was also confirmed in mice (Ford et al., 2012; Xu et al., 2016). To demonstrate the implication of SACs, selective ablation of these cells was performed in ferrets (Huberman et al., 2003), leading to a decrease in the correlation of activity in neighboring SACs. Depolarization of a single SAC triggers the initiation of stage II waves, and occurs through volume release of acetylcholine that will depolarize both neighboring RGCs and SACs, allowing the propagation of these waves. (Ford et al., 2012). Additionally, the $\alpha 3\beta 2$ nAChR subunit has been demonstrated to be a requirement for the propagation of these waves. Indeed $\alpha 3^{-/-}$ mice have altered spatiotemporal retinal waves with 2 distinct types of waves (large and small), whereas $\beta 2$ KO have no correlated waves (Bansal et al., 2000).

Stage III waves

Stage III waves occur between P10 and P15, are mostly glutamatergic, and are initiated by bipolar cells (Firth et al., 2005; Kerschensteiner, 2016). These waves are no longer sensitive to AchR antagonists, and the switch from cholinergic to glutamatergic transmission correlates with the maturation of bipolar cells (Miller et al., 1999; Wong et al., 2000). Recently, All amacrine cells have been involved in the generation and propagation of glutamateric retinal waves (Firl et al., 2015). The propagation of these waves is mediated by the volume release of glutamate (Blankenship et al., 2009; Firl et al., 2013). Gap junctions are also involved in the dynamics of retinal waves. Indeed, the absence of Connexin36 – a major component of the gap junction gates – leads to an altered firing pattern during the second postnatal week (Akrouh and Kerschensteiner, 2013; Torborg et al., 2005).

Effect of altered activity in the retina

Effect on retinotopy: Chemical studies

Early evidence pointing toward the implication of activity in the formation of topographic maps in the visual system was derived from drug-induced activity blockade, during development. In mammals, tetrodotoxin (TTX) injections, which specifically block voltage-gated sodium channel, has an effect on the refinement of the projections. Indeed, when blocking RGCs activity in rats with TTX, targeting errors are maintained due to the overshooting (O'Leary et al., 1986). More specifically, epibatidine application (a cholinergic antagonist) in ferrets (Huberman et al., 2003; Penn et al., 1998) and mice (Cang et al., 2005b; Chandrasekaran, 2005; Rossi et al., 2001; Sun et al., 2008a) blocks stage II retinal waves, leading to a reduced refinement of the termination zones (TZ) of the projecting RGCs to the SC, and in the LGN. However, the retinotopic location of these TZs is maintained. Controversies were raised when epibatidine was shown not only to block retinal waves, but also by silencing only 50% of RGCs while increasing the remaining spontaneous activity (Sun et al., 2008a).

Effect on retinotopy: genetic studies

Chemical studies have demonstrated the implication of cholinergic transmission in the propagation of retinal waves and on the refinement of retino-collicular projections. Many studies have been conducted using the $\beta 2$ knock-out mouse model ($\beta 2^{-/-}$). These animals lack the $\beta 2$ subunit of the nicotinic receptor (nAChR), which is involved in stage II retinal waves. As a consequence, these mice display spontaneous uncorrelated firing, which disrupts the spatial feature of retinal waves (Bansal et al., 2000; McLaughlin et al., 2003; Rossi et al., 2001). Stage II retinal waves in $\beta 2^{-/-}$ animals are mediated by gap junctions that display different spatiotemporal properties, as compared to cholinergic waves (Kirkby et al., 2013; Sun et al., 2008a; Torborg and Feller, 2005).

In contrast to WT animals, P4 $\beta 2^{-/-}$ mice show a reduced correlation in the firing patterns between neighboring retinal neurons (McLaughlin et al., 2003). Further investigation revealed that correlated activity is still present in these animals, with an increase in frequency of the traveling waves, and a lack of direction preference (Stafford et al., 2009; Sun et al., 2008b). This suggests that wave directionality coupled to short-range correlated bursting patterns of RGCs, work together to refine retinofugal projections (Stafford et al., 2009)

Anatomical characterization of $\beta 2^{-/-}$ animals by Dil tracing showed abnormally diffuse TZs in the SC at the topographically correct location. When looking at single RGCs arborizations, a larger axonal arborization can also be found in these knock-outs (Dhande et al., 2011). Furthermore this improper refinement could still be observed at P20 after eye opening, suggesting that it is not rescued by stage III retinal waves (McLaughlin et al., 2003a).

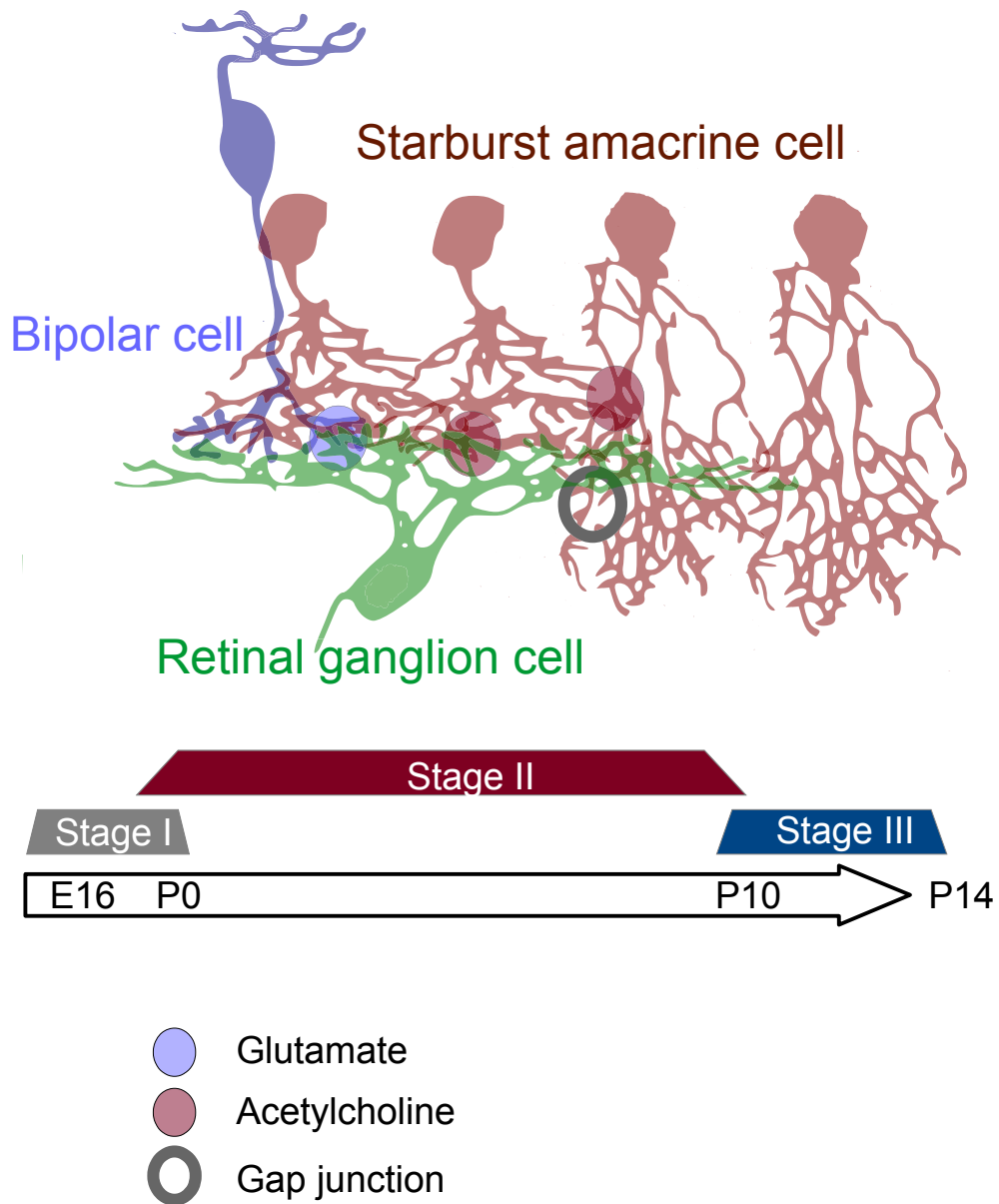


Figure 19: Propagation of retinal waves in the retina. Stage I retinal waves occur between E16 and P0 in mice and are transmitted by gap junction. Stage II retinal are initiated by starburst amacrine cells and occur between P and P10. Spontaneous depolarization is transmitted by acetylcholine to retinal ganglion cells. Stage III retinal waves occur between P10 and P14, are glutamatergic and depend on bipolar cells.

Electrophysiological recordings in $\beta 2^{-/-}$ animals also demonstrated larger receptive fields (Chandrasekaran, 2005). Functional imaging showed that regions activated by a single visual stimulus are larger and more diffused when compared to wild-type. In addition, a distortion of the overall map can be found (Mrsic-Flogel, 2005). Together these results suggest that the cholinergic-driven waves during the first postnatal week are required for retinal axon refinement in the SC (Firth et al., 2005).

Effect on eye specific segregation: Chemical studies

Activity is also involved in the eye-specific segregation in the LGN. Early evidence came from prenatal chronic diffusion of TTX in cats, which lead to the abolition of eye-specific segregation in the LGN (Shatz and Stryker, 1988). However, binocular TTX injections from birth to P10 are shown to delay, but not prevent eye-specific segregation in ferrets (Cook et al., 1999). In mice and ferrets treated with epibatidine, an overlap of ipsi and contralateral axons can be observed in the LGN, suggesting the involvement of stage II retinal waves in eye-specific segregation (Penn et al., 1998; Rossi et al., 2001). Interestingly, if these animals are kept until the occurrence of stage III retinal waves, this segregation is partially rescued with the formation of patchy, random patterns of eye-specific zones in the LGN (Huberman et al., 2002; Muir-Robinson et al., 2002). A decrease in correlation by a specific removal of SAC, is not sufficient to alter the eye specific segregation, indicating that the presence – but not the normal pattern – of spontaneous RGCs discharges, is required for eye-specific retino-geniculate segregation (Huberman et al., 2003). When activity is increased in one eye by elevating cAMP levels, a spreading of the eye-specific zone in the LGN in ferrets can be found (Stellwagen and Shatz, 2002).

Genetic studies

Eye-specific segregation was also studied in the $\beta 2$ KO animals. Eye-specific segregation fails to occur in the normal time frame (Cang et al., 2005a; Chandrasekaran, 2005; Grubb et al., 2003; Muir-Robinson et al., 2002; Pfeiffenberger et al., 2005; Rossi et al., 2001), suggesting an implication of activity in eye patterning. In another model, the $Cx36^{-/-}$ mice exhibit an altered spontaneous firing activity, and displays tonic firing at low rates between bursts. In these animals a normal eye-specific segregation in the LGN can be found, suggesting that high-frequency bursts that are synchronized across nearby RGCs are correlated with eye-specific segregation, whereas additional asynchronous spikes do not inhibit segregation (Torborg et al., 2005).

Effect of altered activity in the superior colliculus

In *Xenopus*, a specific blockade of NMDA receptors in the tectum by AP5 (a selective NMDA receptor antagonist) alters the early development of the tectal cell's dendritic arbor. At later stage both AMPA and NMDA blockade decrease the dendritic arbor branch length, consistent with the role of glutamatergic synaptic transmission in maintaining dendritic arbor structure (Rajan and Cline, 1998). In rats, chronic treatment of an NMDA-receptor antagonist reduces the elimination of mistargeted axonal arborization (Simon et al., 1992).

The topography of the retinotopic maps in the hamster with a partially ablated SC (via an electric lesion), was determined by multi-unit mapping and was subsequently found unaltered. NMDA receptor blockade increases the receptive field size of single units in normal maps (Huang and Pallas, 2001), but does not affect the velocity or the size tuning (Razak, 2003). In addition, when NMDA receptors are blocked during development in rats, the size of retinal axon's synapse are increased at P6, P8 and P10 (Colonnese and Constantine-Paton, 2006).

Conclusion

The instructive versus permissive role of activity in the establishment a refined topographic map has been controversial. A permissive role would suggest that activity by itself does not induce subsequent changes, whereas an instructive role suggests that activity is required for specific targeting of the projections. Untangling both process remains challenging. Indeed, if activity is solely permissive (allowing other types of signaling), alteration could induce changes in molecular signaling, which would mimic an instructive role.

However, evidence for an instructive role for activity has built up recently (Chandrasekaran, 2005; Xu et al., 2011). Historically, experiments in amphibians have demonstrated that forcing two eyes to innervate the same tectal lobe results in the formation of ocular dominance bands that can be reversed by blocking the activity. These results suggest that this segregation is induced by the correlated activity within each eye (Constantine-Paton and Law, 1978; Reh and Constantine-Paton, 1985).

As described above, improper refinement can be observed in many cases in the absence of activity. Further evidence has come from the fact that a disrupted activity also induces subsequent changes. Indeed, $\beta 2$ KO were initially thought to lack correlated activity in stage II retinal waves, but more recent studies demonstrated that residual correlated activity could still be found in these mutants. As mentioned earlier, they present unrefined retino-collicular TZs, strongly suggesting that the presence of activity is not only required for the refinement of retino-collicular projections, but that it must follow specific spatial-temporal features (Stafford et al., 2009, Shah and Crair, 2008). $\beta 2$ rescued animals – in which $\beta 2$ expression is restored solely in RGCs – display altered cholinergic retinal waves (Xu et al., 2011), which result in an impaired refinement of the retino-collicular projections; suggesting that stage II retinal waves must originate within SACs for proper correlation.

Concerning the role of activity in the formation of the retino-collicular map, patterned activity may be solely involved in the elimination of eTZs. Furthermore, concerning eye specific segregation, a partial recovery can be observed when animals are allowed to reach adult stages, suggesting a delay in maturation rather than a disruption in the refinement process (Huberman et al., 2003). Experiments altering the activity at the level of the SC also lead to an increase in ectopic arborization.

The mechanisms through which correlated activity shapes the refinement of the retino-collicular projections are still under investigation. The presence of correlated firing both from a temporal and spatial aspect suggest an instructive role of activity. Indeed, according to Hebbian-based processes, these retinal waves will make RGCs that are close to each other to fire together and reinforce their synaptic strength, leaving those that are far apart with a temporal delay in firing and no synaptic reinforcement. As a consequence, the timing of correlated firing indicates that RGCs are close neighbors in the retina, suggesting that retinal waves also carry spatial information from the retina to the SC (Butts and Rokhsar, 2001). Support for the requirement of a specific temporal pattern and such a mechanism come from *in vitro* induction of LTP among immature synapses in the SC, by mimicking retinal waves. (Shah and Crair, 2008)

In addition, these waves have been demonstrated to travel to downstream targets. However, little is known about the mechanism by which these waves could be read out in the target structure. Indeed, among Hebbian rules that could apply in this condition, the phenomenon of spike-time dependent plasticity (Bi and Poo, 1998) (that can be considered as a coincidence detector) gives a particular time window for synaptic reinforcement to occur. This type of plasticity is believed to be NMDA receptor-mediated. NMDA receptors have been demonstrated to be involved in the refinement of retinotopic projection and selective branch elimination (Ruthazer et al., 2003).

Manipulation	Retinal activity	Retinotopic refinement	Reference
Binocular epibatidine in mouse	Stage II retinal wave blockade	Reduced refinement	(Cang et al., 2005b; Rossi et al., 2001; Sun et al., 2008a)
β 2-nAChR KO in mouse	Gap junction-mediated retinal waves with reduced nearest neighbor correlations; increased uncorrelated firing between waves	Reduced refinement	(McLaughlin et al., 2003; Muir-Robinson et al., 2002; Rossi et al., 2001)
Rescue of β 2-containing nAChRs in RGCs of β 2-nAChR KO mouse	Small-range cholinergic retinal waves	Normal refinement	(Xu et al., 2011)
AC1 KO mouse (lacks the calcium-dependent adenylate cyclase 1)	Normal retinal waves	Reduced refinement	(Dhande et al., 2012; Plas et al., 2004)
MAOA KO mouse (lacks monoamine oxidase A resulting in excess serotonin)	Unknown	Reduced refinement	(Upton et al., 1999, 2002)
Altered ephrin expression/signaling in mouse	Normal	Disrupted targeting but normal refinement	(Cang et al., 2008a; Huberman et al., 2005; Pfeifferberger et al., 2005, 2006)
Ten-m3 KO and Ten-m2 KO mice (lack members of teneurin family of glycoproteins)	Normal retinal waves	Altered ipsilateral mapping	(Leamey et al., 2007; Young et al., 2013)

Table 4: Summary of the effects of altered activity on retinotopy in the superior colliculus in mouse

Controversies regarding the instructive role of activity came from *in vitro* study in which ephrin-A5 collapse response was altered in the presence of TTX (Nicol et al., 2007), demonstrating that neuronal activity modulates the repellent action of ephrin-As through the downstream second messengers calcium and cAMP. Taken together, these results suggest that activity is required for the proper read-out of molecular cues.

Activity-dependent refinement processes seem to occur at a local rather than a global refinement of TZs. Indeed, topographically incorrect termination sites can be found in molecular guidance mutants, which would otherwise be eliminated by correlated activity. Indeed eTZs, which are located far from the topographically correct location, should not be strengthened throughout this process. A way to test the contribution of activity in the refinement of projections would be to pharmacologically block the activity in ephrin-As KO mutants. If activity is involved in the elimination of eTZs, this would lead to an increase in the number of these sites by blocking the process of collateral elimination. Indeed, even if this has already been tested in compound $\beta 2$ /ephrin-A2/A3/A5KO, eTZs are likely to be refined by locally correlated activity, which is still present $\beta 2$ KO.

Isl2-EphA3KI heterozygotes could also be used as a read-out of the contribution of activity. In these animals, projections from the nasal pole of the retina are duplicated, while projections from the temporal pole are single. The existence of this collapse point has been suggested to be due to a counterbalancing effect originating from correlated activity. By altering activity in these animals, the relative contribution of each mechanism can be better understood.

In summary:

Concerning spontaneous activity:

- RGCs present a correlated activity during development
- This correlated activity spreads to downstream targets

Altering/blocking activity in the retina or in the SC leads to:

- Unrefined TZs
- Larger receptive fields
- Compressed map
- Increased number of synapses
- Same tuning properties

Competition in the formation of visual maps: biology

Competition for space seems to be an important process for the formation of a retino-collicular map. This mechanism is indeed required to explain map expansion and compression as observed in original experiments with partial ablation of either the retina (Attardi and Sperry, 1963), or the SC (Yoon, 1971). If positional information was solely carried by molecular tags, maps would not be able to adapt to changes in the collicular space. In addition, in the absence of a counter-balancing force, all axons would target the rostral pole of the SC, where the ephrin-As repulsion is the lowest. An interaction and a competition for space between these entering fibers is therefore required to order themselves relative to one another, and to fill the entire collicular space.

In models with decreased retinal inputs, the competitive strength is decreased. In these cases, axons tend to occupy more space, making extended TZs.

Math5^{-/-}

In the Math5^{-/-} mutant, only 5-10% of the RGC population remains, and is evenly distributed throughout the retina (Lin et al., 2004). When tracing the entire population of RGCs, only the rostral-medial part of the SC is innervated (Triplett et al., 2011), suggesting that the projections are highly repulsed by ephrin-As at the caudal pole of the SC, and attracted medially by EphB gradient. These forces need to be counterbalanced by competition in order to yield an ordered topographic map. Indeed, when tracing focal zones in the SC with retrograde tracing by CTB (Cholera toxin B subunit), RGCs in Math5^{-/-} animals are spread across the entire retina, with a broad distribution, suggesting that projections lose their topographic location. Similarly, anterograde labeling reveals a sparse and unrefined TZ, suggesting that in absence of competition, projections are not able to refine properly and to reach their topographically correct position.

Dicer

A conditional deletion of retinal progenitor cells also gave an insight into the competitive mechanisms driving retino-collicular map formation. Using Pax6 α as a driver for the deletion of Dicer1, retinal progenitor cells are specifically ablated in the distal-most nasal and temporal pole of the retina. In these animals, 40% of the RGCs remains, but whole eye-fill tracing reveal that projections occupy 85% of the collicular space, leading to an expansion of the map. In this case, the general retinotopy is maintained, but retrograde labeling show an increased dispersion of RGCs in the retina as compared to wild-types (Maiorano and Hindges, 2013).

Mechanistic models of retino-collicular map development

The presence of complementary gradients of EphAs and ephrin-As in both projecting and target structures, along with their opposite gradients of expression within a given structure, their forward and reverse signalling modes, their ligand-receptors binding similarities and the controversies between *in vitro* and *in vivo* observations; has dramatically increased the complexity of the identification and design of mechanistic models of action of EphA/ephrin-A signaling. However, the use of elaborated genetic studies (conditional knock-outs, knock-ins, compound knock-in/knock-out, multiple knock-outs) led to many recent insights, notably regarding the signaling mode (relative vs absolute) and the counter-balancing forces required for robust mapping mechanisms (competition vs dual-gradient vs servomechanism).

Different hypotheses have been made regarding contribution of forward signalling (retinal EphA receptors interacting with collicular ephrin-As) to the formation of the retino-collicular map. Indeed different forces are required to explain plasticity and phenotypes observed in mouse models, in which Eph/ephrin signalling is partially disrupted. Theoretical work has given many insights into the requirements and constraints for establishing topographic maps.

Forward signalling is relative

Gain-of-function studies and genetic approaches gave a further explanation on how maps can be plastic, such as in-map compression or ablation studies, or respond to gradient perturbation. These experiments provided an insight into the signaling mode through which EphA and ephrin-As interact to provide positional information. Forward signaling is characterized by the binding of retinal EphAs to collicular ephrin-As, inducing a repulsive response. As a consequence, RGCs with the highest level of EphA receptors connect to collicular targets that carry the fewest amount of ephrin-As, and vice versa. Indeed, ephrin-As are chemorepellent (especially for temporal axons), which will establish connections in the rostral pole of the SC. First evidence for the operation of forward signaling in the establishment of the retino-collicular map *in vivo* came from the characterization of ephrin-A2KO. Indeed, ephrin-A2 expression is only graded in the SC and mapping defects, with the presence of eTZs, can be observed in these mutants. These observations corroborate with the implication of forward signaling.

Relative signaling

Evidence for a relative signaling principle came from the generation of the *Isl2-EphA3KI* mice (Brown et al., 2000). In this mutant, EphA3s are selectively expressed in 50% of RGCs that induce a map duplication, due to the differential segregation of two RGCs sub-populations: the *Isl2*-positive RGCs that express wild-type levels of EphAs, and ectopic EphA3 and *Isl2*-negative RGCs, which express the wild-type level of EphAs. In heterozygous animals, the retino-collicular map is partially duplicated, with the appearance of a collapse point along the rostral-caudal axis of the SC for retinal projections arising from the temporal end of the retina ($\geq 76\%$ of the nasal-temporal axis). This suggest that the *Isl2*-positive RGCs that express high levels of EphA receptors, still map in the SC independently of their absolute level of EphAs. Moreover, the presence of a collapse point in the heterozygous animals suggest that the superimposed level (spikes) of EphA3 beyond the collapse point ($\geq 76\%$ of the nasal-temporal axis) is too low, relative to the high endogenous EphA4, A5 and A6 level of expression, in order to allow the system to discriminate between an EphA3 (*Isl2*-positive) and a wild-type (*Isl2*-negative) RGC. In addition, both projecting sites in homozygotes are shifted from wild-type projections, which means that wild-type RGCs are also displaced from their correct location in the SC. These observations suggest a competition between ganglion cells for the

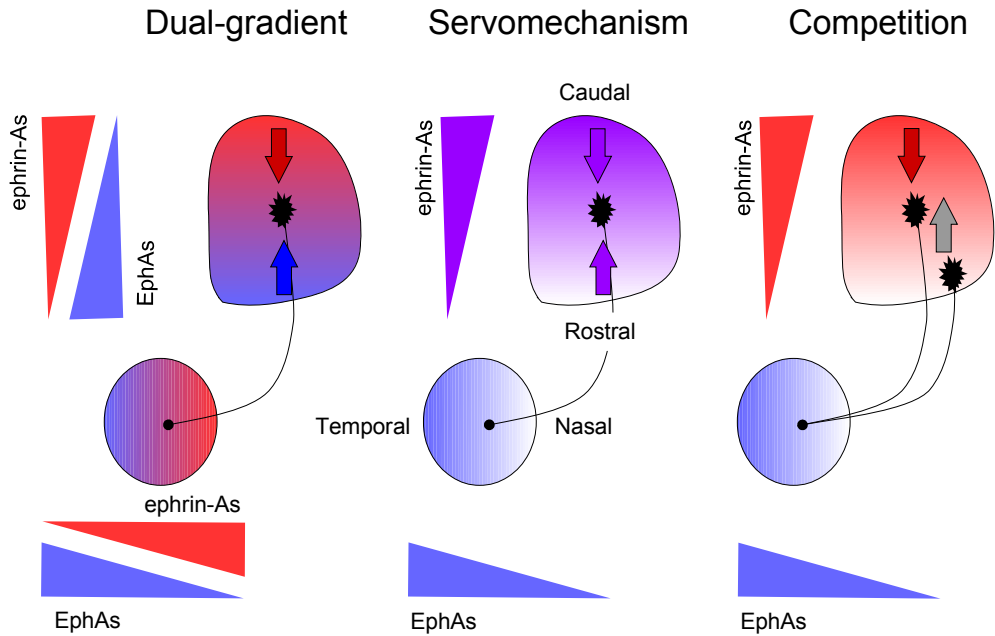


Figure 20: Models of counter-balancing forces in retino-collicular mapping. Repulsion from forward EphA/ephrin-A signalling (retinal EphAs, (blue) and collicular ephrin-As (red or purple)) need to be counter balanced. **Dual-gradient.** In this model, retinal ephrin-As (red) signal with collicular EphAs (blue), exerting a repulsive force originating from the rostral pole of the superior colliculus. **Servomechanism model.** In this model, collicular ephrin-As (purple) have a bifunctional signalling, where they can either exert repulsive or attractive forces (purple arrow). **Competition model.** RGC can interact with each other and repel other toward the caudal pole of the superior colliculus.

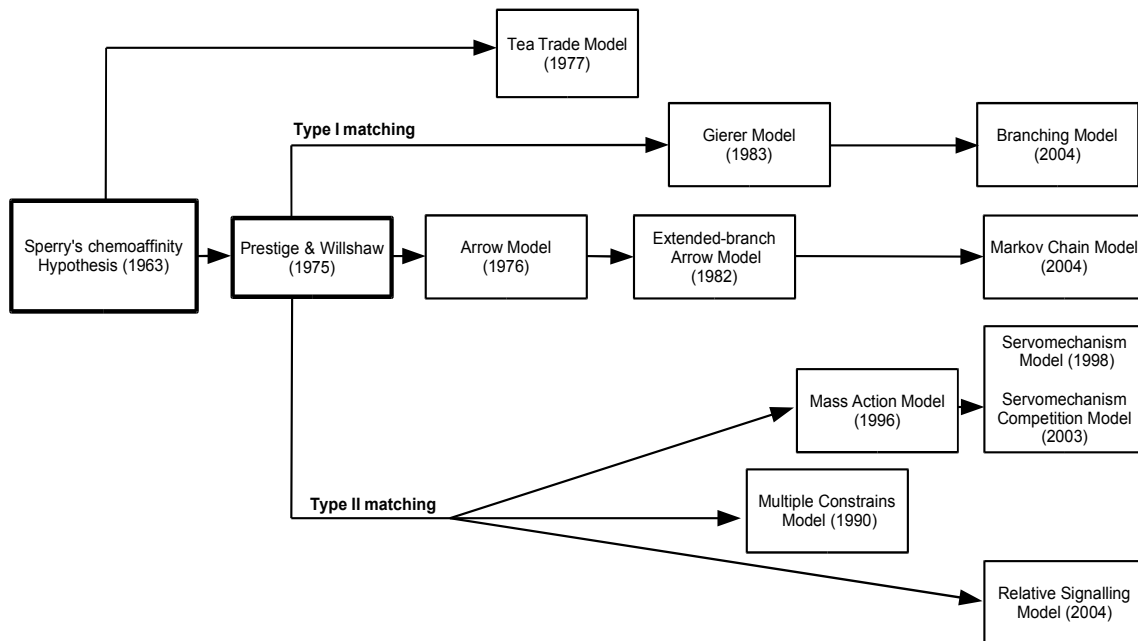


Figure 21: Theoretical model for neural map formation.

innervation of the SC. These results provided a strong support for the Relative signaling model, in which RGCs compete for termination sites along the rostral-caudal axis of the SC through a comparison of relative, or ratio-based differences in the EphA signaling intensity. This model was also tested and validated in compound mutants in which EphA4 (Reber et al., 2004) and EphA5 (Bevins et al., 2011) was removed.

This suggests that EphA and ephrin-A signaling operates through a relative rather than an absolute-forward signaling mode, and that competition is involved in the formation of the retino-collicular map.

Counter-balancing repulsion

Servomechanism model

In the absence of a counterbalancing force, RGCs would all target to the rostral pole of the SC, since the caudal pole exerts repulsion. One way to counter-act this repulsion would be to have the same molecular mechanism exert a differential role according to the concentration. Servomechanism models posit that a single graded molecule can have both positive and negative effects that serve to guide retinal axons to their correct position. This hypothesis is supported by *in vitro* findings, which demonstrated that the repulsive effect of ephrin-A2 and ephrin-A5 varies continuously with retinal position, and can either inhibit or promote neurite outgrowth (Hansen et al., 2004). Another possibility would be that the optimal concentration of EphA/ephrin-As would be permissive for BDNF-induced branching. However, this differential response to different levels of ephrin-A2 is observed in the membranes of 293T cells transfected with ephrin-A2, compared to wild-type rostral membranes, and does not promote axonal outgrowth in an absolute way (Weth et al., 2014).

Dual gradient model

A possible way to counter-balance EphA/ephrin-A forward repulsive signaling from the caudal pole of the SC, would be the presence of another repulsive gradient running in the opposite direction. The presence of counter-gradients of EphAs in the SC and ephrin-As in the retina suggest that they could fulfill this role. EphA7 is only expressed in the SC, and loss-of-function studies of this receptor has revealed the formation of eTZs; further confirming the implication of reverse signaling in retino-collicular mapping (Rashid et al., 2005). This suggests that retinal ephrin-As are activated by collicular EphAs, leading to a repulsive reverse signaling. However a bidirectional signaling that is fully based on dual gradients (reverse and forward signalling) as suggested here, would preclude the entry of nasal axons into the SC, since they carry high levels of ephrin-As, and would therefore encounter a high level of EphAs. However, as observed *in vitro*, nasal axons might be desensitized in a first step and acquire their sensitivity to collicular EphAs in the SC in a second step.

Competition

Another way to account for the necessity of a counter-balancing force is through competition. If the chemical cues are read in a relative manner and all projections show a differential (graded) affinity towards the source target, then competition plays a fundamental role in the organization of the retino-collicular map.

Axonal interaction

Even if competition seems to be a required process for the formation of the retino-collicular map, molecular cues involved in this particular process remain to be elucidated. A good candidate to sort out axons relative to each other is axon/axon interactions. *In vitro* experiments in chick, in which

ingrowing axons were given a choice between temporal or nasal axons to grow along, had demonstrated that growth cones from the temporal half of the retina preferentially grew along temporal axons, whereas nasal retinal axons do not distinguish between nasal and temporal ones (Bonhoeffer and Huf, 1985). Axon-axon interactions could occur in the SC during the over-shooting phase, and the presence of gradients and counter-gradients strongly suggests these interactions.

A recent *in vitro* study demonstrated that temporal growth cones collapse when contacting nasal axons. This retraction can be prevented by PI-PLC treatment, suggesting an implication of ephrin-As. In addition, a conditional ephrin-A5KO was generated, where ephrin-A5 can be either specifically removed from the retina or the SC. The phenotype observed suggests that nasal axons repel temporal axons from the caudal pole of the SC through an axon-axon interaction (Suetterlin and Drescher, 2014). Some ephrin-As could be engaged in axon/axon mediated repulsion, according to their localization on the axon shaft, while other ephrin-As could interact with collicular gradients of EphAs.

Theoretical modeling

Theoretical modeling of the retino-collicular map formation, and to a greater extent of topographic maps relies essentially on 3 aspects which have been developed earlier: 1) Chemoaffinity 2) Competition 3) Correlated activity. Prestige and Willshaw (1975) were the first to formalize notions of chemospecific matching suggested by Sperry's hypothesis and to computationally investigate the importance of competition in this context. They defined a crucial distinction between two forms of chemical matching termed "type I" and "type II". In "type I" matching each retinal cell has an affinity for just a small neighborhood of tectal cells, with a peak affinity for the topographic matching cell in the target tissue. In schemes of "type II" matching, all axons have high affinity for making connections at one end of the tectum and progressively less for tectal cells elsewhere. Conversely, tectal cells have high affinity for axons from one pole of the retina and less from others; there is graded affinity between the two sets of cells. However, constraints about the number of connections each cell can make is important. If this number is not limited, then no map results, but introducing competition, by restricting the total connections, does lead to a map. These key concepts led to the formulation of different computational models. Here only computational models based on Eph/ephrin-A chemoaffinity will be considered.

Servomechanism model

The "Mass Action Model" (Nakamoto et al., 1996) proposed that axons stop growing across the SC whenever they encounter a standard value of a negative signal from a receptor (i.e. law of mass action, $[RL] = K_A[R][L]$, with receptor concentration, R, ligand concentration, L, and K_A , affinity constant). This is purely a "type I" model, specifying when axons should stop growing, however it does not address how they seek out appropriate targets. Developing axons carry a particular value of receptor (R) according to their position along the nasal-temporal axis, and encounter different amounts of ligand across the rostral-caudal axis of the SC (L) and compare it to a standard signal strength (S). To simulate the formation of the map at each step, a new value of ligand is encountered and the repulsive strength is computed as follow, $|R \cdot L - S$. If the repulsive strength is smaller at the new site, then the axon terminal migrates towards it, otherwise it remains on the same site. This procedure is repeated until repulsion is minimized. This model is type I, and cannot account for map plasticity. An extended version of this model was developed that added competition (Honda, 2003), although some of its assumptions are arbitrary and its explanatory power is limited.

Arrow model and extensions

In the original “Arrow Model” (Hope et al., 1976), axons exchange position if they are relatively in the wrong location. This mechanism was originally described as instructions given to soldiers that need to be lined up according to their size:

“Choose either of your neighbours:

If you have chosen your left-hand neighbour, then
if he is taller than you stay put;
if he is shorter than you change places.

If you have chosen your right hand neighbour, then
If he is taller than you, change places;
If he is shorter than you stay put. “

In this case, only one connection can be established in the SC, which is considered as a discrete space. A randomization is also implemented. This model failed to account for translocated maps since it relies exclusively on local rather than global information. Overton and Arbib (1982) presented a more sophisticated version of the “Arrow Model”, termed the “Extended Branch-Arrow Model”, which is much more realistic as it considers the tectum as a continuum rather than a discrete array of positions. An additional force that directs axons to their appropriate position was also added.

More recently, a probabilistic version of combined Arrow models and a servomechanism model was proposed (Koulakov and Tsigankov, 2004), based on a stochastic interchange between neighboring axon terminations in the SC – The Markov Chain Model. In this model, axons exchange their connections in order to minimize their energy levels, according to the amount of receptors and ligands. This Markov Chain Model models the formation of disturbed maps generated by EphA mis/over-expression. However, the weakness of this model resides in the lack of robustness in the constraints, varying according to the type of mis/over-expression.

Marker induction model

Von der Malsburg and Willshaw (1977) proposed the “Tea Trade Model” based on the idea that map formation might be dependent on induction of molecules from the retina into the tectum. There are no pre-existing tags encoding position in the tectum, it is assumed that retinal markers are transported to the tectum via induction. Subsequent experimental data have made it clear that there are pre-existing gradients in the tectum and that these play a crucial role in retino-tectal mapping.

Gierer model (Counter-gradient model)

Gierer (1983, 1987) proposed a model based on the matching of pre-existing gradients in retina and tectum based closely on Sperry’s chemoaffinity hypothesis and introducing the concept of counter-gradients (two gradients running in the opposite direction in the tectum). However, competition and axon-axon interaction were not considered, and the rigidity of the matching strongly limits its explanatory power.

Branching model

Following experimental data (Yates et al., 2001), a computational model in which topographic specificity is based on axonal branching, was developed (Yates et al., 2004). In this “Branching Model”, counter-gradients of both branch-promoting/inhibiting (counter-gradients of ephrin-As and EphAs in the tectum) molecules are required in the SC to generate topographic specificity. This is mostly a type I model, where branching occurs probabilistically, with some flexibility due to the ability of axons to interact.

Relative signaling model

Based on experimental data acquired in the Isl2-EphA3KI, the “Relative signaling Model” was proposed (Reber et al., 2004), based on relative signaling and competition between axons for collicular innervation (“type II matching model”). However, this model does not account for the dynamics of the mapping during development.

Balancing reverse and forward signaling

Another model was also proposed recently (Gebhardt et al., 2012), in which chemoaffinity is extended to include ephrin-A/EphA-based fiber/fiber chemospecificity, eventually out-competing fiber/target interactions. This model takes into account signals generated from axon–target, axon–axon, and intra-axon interactions between ephrin-As and EphAs.

Most of the theoretical formulations of Sperry's chemoaffinity hypothesis done so far find their roots in the pioneering work of Prestige and Willshaw, representing a hallmark in the field of theoretical neurobiology.

Visual maps and behavior

Originally, the SC gained interest with the description of a contralateral neglect of visual stimuli following a lesion of this structure, despite the fact that other visual pathways were intact (Sprague and Meikle, 1965). Further studies demonstrated that the SC, through its projections, controls essentially two components that are involved in attention: saccades and head movement.

Saccades are rapid, ballistic eye movements that abruptly change the point of fixation, during which the eye is relatively stationary and gathering visual information. The circuit for saccade generation has been extensively characterized in cats and monkeys, but fewer studies have been conducted in mice. Indeed, the laterality of the eyes suggested that head movement was mostly used for gaze orientation. However, electrical stimulation of the SGI can induce eye movements similar to a saccade in mice, suggesting the existence of saccade generator circuits downstream of the mouse SC, in a similar manner to that of cats and monkeys.

The SC plays an essential role in orientation through representations of space, in integration of different sensory inputs, and in sending direct motor outputs. These spatial representations take the form of maps, which can be found along the height of the SC, with superficial layers receiving visual inputs, and deeper layers receiving auditory and somatosensory inputs. This multi-sensory integration is also subject to modulation from cortical regions. Due to the small amount of studies conducted in mice, results obtained in two other species of rodents, hamsters and rats, will also be considered.

Superior colliculus and behavior

A behavioral study in mice demonstrated that unilateral optogenetic activation or inhibition of one half of the intermediate and deep layers of the SC can lead to a significant shift in the movement direction during a sensorimotor decision task. A contralateral bias could be induced when the corresponding half of the SC was activated, while inhibition resulted in an ipsilateral bias (Stubblefield et al., 2013).

Catecholaminergic modulation of the superior colliculus

The SC receives noradrenergic innervation from the locus coeruleus (LC) and RGCs, dopaminergic innervation from the substantia nigra, as well as serotonergic innervation from the raphe nucleus (May, 2006). When the colliculus is activated by environmental stimuli (mostly visual and auditory), signals triggered by these stimuli have to be above the background firing in order to be processed and integrated. A high signal-to-noise ratio is required to retain salient (strong) stimuli and to weaken distractible stimuli (Dommett et al., 2009). Dopamine is known to increase the signal-to-noise ratio in striatal cells (Volkow et al., 2001), and is believed to play a similar role in the SC (Gowan et al., 2008). Recently, a segregation in the distribution of D1 and D2 receptors in the superficial and intermediate layers of the SC has been demonstrated. Dopamine in the SC originates from small diencephalic cell group called A13, and appears primarily inhibitory to SC neurons (Bolton et al., 2015). Accordingly, D-AMPH and MPH increase the signal-to-noise ratio in the SC of rats (Dommett et al., 2009). From a behavioral aspect, an altered signal-to-noise ratio can transform a non-salient stimulus into a salient stimulus, leading to inappropriate responses and increased distractibility.

Superior colliculus and attention deficits

The SC plays a fundamental role in orientating gaze towards salient stimuli, and is known to control and generate saccadic eye movements (May, 2006). More recently, it has been shown to participate in visuo-spatial orientation and attention (Lovejoy and Krauzlis, 2010). Consistent with its

role, dysfunction of the SC has been involved in several psychological diseases and syndromes such as epilepsy (Ross and Coleman, 2000), schizophrenia (Cutsuridis et al., 2014), supranuclear palsy (Armstrong, 2011) and ADHD (Dommett et al., 2009; Miller, 2009; Overton, 2008).

Attention deficits

Considered as the first psychiatric disorder to be diagnosed in children, Attention Deficit/Hyperactivity Disorder (ADHD) is a neurodevelopmental disease, generally diagnosed before the age of 7, of complex etiology. It affects 8-12% of children – of which half retain ADHD symptoms as adults – and also it shows a 75% of heritability and a sex ratio of 3 to 6 males for 1 female (Biederman, 2005). Patients show increased impulsivity, distractibility and activity (Himelstein et al., 2000).

Although the etiology of this disease is not fully understood, therapeutic effects of MPH (methylphenidate) and D-AMPH (dextroamphetamine) suggest that noradrenergic and dopaminergic transmission is impaired (Volkow et al., 2001). MPH is known to inhibit both dopamine (DAT) and noradrenalin transporters (NAT), leading to increased levels of dopamine and noradrenalin in the synaptic cleft. D- AMPH has a non-specific action as it increases both noradrenalin release and reduces monoamine oxydase activity (MAO - involved in monoamine catabolism) (del Campo et al., 2011). Structural and functional imaging have also pointed out a dysfunction in fronto-cortical pathways (Biederman, 2005). Even if some findings regarding noradrenalin levels in ADHD are conflicting (decrease or increase), an important aspect seems to be the balance between the catecholamines rather than their absolute concentrations. Indeed, relationship between catecholamine levels and performance is often viewed as a U-shaped function (del Campo et al., 2011), meaning that both an increase or a decrease can lead to impaired performance. In addition the balance between dopamine and noradrenalin seems to be critical for ensuring an optimal performance (Aston-Jones and Cohen, 2005). Recent findings suggest that ADHD symptoms (in particular impulsivity and distractibility) are the result of a collicular hyperstimulation (Overton, 2008). Supporting this idea, ADHD patients are often unable to produce certain saccadic types (anti-saccade and express saccade), and show an increased distractibility in tasks linked to the colliculus (Overton, 2008).

Collicular dysfunction in animal models of ADHD

Recently, the characterization of visual responses in animal models of ADHD, the New Zealand genetically hypertensive rat (GH) (Sutherland et al., 2009) and the spontaneously hypertensive rat (SHR) (Sagvolden, 2000) has been conducted. In both strains, an increased responsiveness of the superficial layers of the SC was observed, with an increased response amplitude to whole field light flashes in GH rats (Clements et al., 2014), and a longer response duration without desensitization in SHR rats (Brace et al., 2015). In GH animals, this response change could be reduced by a widely used treatment of ADHD: D-Amphetamine.

Behavior in mice with altered visual maps: ephrin-As deficient mice

Ephrin-A5/ephrin-A2KO has been suggested as a mouse model of Autism Spectrum Disorders (ASD), since they display a repetitive grooming behavior (Wurzman et al., 2015). The single ephrin-A2KO also presents a particular learning deficit. Even if these mice have similar learning rates and sensitivity to a stimulus when compared to WT mice during the initial acquisition of a visual discrimination task, they employ a different learning strategy during reversal learning (Arnall et al., 2010). However, these animals present other altered pathways than the retino-collicular map, due to the general expression of ephrin-As throughout the brain during development.

Publications

Defective response inhibition and collicular noradrenaline enrichment in mice with duplicated retinotopic map in the SC.

Mathis, C., Savier, E., Bott, J. B., Clesse, D., Bevins, N., Sage-Ciocca, D., Geiger, K., Gillet, A., Laux-Biehlmann, A., Goumon, Y., Lacaud, A., Lelièvre, V., Kelche, C., Cassel, J.C., Pfrieder, F. W., Reber, M. (2014). *Brain Structure and Function*, 220(3), 1573-1584.

Isl2-EphA3KI mice

The SC is involved in attentional processes as well as gaze orientation, but behavioral consequences of an altered retinotopy specifically has not been investigated. The Isl2-EphA3KI over-expresses EphA3 (an EphA receptor), in Isl2+ cells that represent 50% of retinal ganglion cells, that are homogeneously spread throughout the retina. This leads to a strong phenotype in both the cortico- and the retino-collicular map, due to the differential responses of Isl2 + and Isl2- RGCs during the formation of visual maps, which carry different levels of EphAs. As a consequence, both maps are duplicated (Brown et al., 2000; Reber et al., 2004). This anatomical duplication is also functional, with the coexistence of two maps in the SC covering the entire retinotopic space, leading to the activation of two distinct zones for the stimulation of a single part of the visual field (Owens et al., 2015; Triplett et al., 2009).

Behavioral characterization

To investigate behavioral consequences of an over-stimulation of the SC, a behavioral and molecular characterization study was conducted. This study demonstrated that visual acuity, locomotion and memory are unaltered in the Isl2-EphA3KI. However, attentional defects were revealed through two different tests: the Go/No Go and the dark/light box test. These mutants displayed an enhanced impulsivity in addition to a tendency towards distractibility, especially in the presence of visual distractor.

Monoaminergic signaling

Monoaminergic signaling was also characterized in these animals through a quantification of dopamine, serotonin, adrenalin and noradrenalin, their receptors, metabolic enzymes, and transporters. These results had revealed no subsequent changes in expression at the mRNA level in the structures under study. However, a 2-fold increase in noradrenalin was found in the superficial layers of the SC in homozygote mutants, where the duplication can be found.

Therapeutic considerations

Behavioral defects found in the Isl2-EphA3KI mouse model are similar to symptoms observed in humans with attention deficit disorders (ADD). ADD is, according to DSM-V, a persisting attention deficit, that is often associated with hyperactivity and impulsivity, occurring during development. To date, GWAS studies have not associated this disorder with any particular gene. Current hypothesis concerning etiology suggest an imbalance in monoaminergic signaling, especially in dopamine levels. These results come from quantification of monoamines levels in patients and therapeutic effects of current drug treatment for this pathology (del Campo et al., 2011). Indeed, the most widely used treatment to date is methylphenidate, which acts as an inhibitor of dopamine and noradrenalin transporters. These treatments have limited benefits and strong side effects, notably on the cardiovascular system. Taking into consideration these different aspects, new therapeutic approaches are required.

Noradrenergic imbalance found in the Isl2-EphA3KI mouse model is in line with the literature,

which suggests that such impairments could be responsible for the symptoms observed in patients. In addition, other studies have revealed an implication of the SC in attentional defects. FMRI studies in patients shown that a collicular hyper-activation increases distractibility (Overton, 2008). In rats, methylphenidate has been shown to alter the signal-to-noise ratio in the SC (Dommett et al., 2009).

Conclusion

Considering these results, the *Isl2-EphA3KI* mouse seems to be good candidate as a model for ADD. Indeed, both symptoms and pathophysiological consequences can be found. In addition, when compared to other model that is available based on altered catecholaminergic transmission, the approach is quite innovative. Our results demonstrate that an alteration in sensory integration – in this particular case, vision – is sufficient to mimic ADD symptoms as well as a noradrenalin balance disruption. This suggests that catecholamine imbalance could be a consequence rather than a cause in this pathology. Furthermore, sensory processing disorders are often neglected in the etiology of psychiatric disorders and could be, at least in part, responsible for these troubles.

Defective response inhibition and collicular noradrenaline enrichment in mice with duplicated retinotopic map in the superior colliculus

Chantal Mathis · Elise Savier · Jean-Bastien Bott · Daniel Clesse · Nicholas Bevins · Dominique Sage-Ciocca · Karin Geiger · Anaïs Gillet · Alexis Laux-Biehlmann · Yannick Goumon · Adrien Lacaud · Vincent Lelièvre · Christian Kelche · Jean-Christophe Cassel · Frank W. Pfrieger · Michael Reber

Received: 5 February 2014 / Accepted: 28 February 2014 / Published online: 20 March 2014
© The Author(s) 2014. This article is published with open access at Springerlink.com

Abstract The superior colliculus is a hub for multisensory integration necessary for visuo-spatial orientation, control of gaze movements and attention. The multiple functions of the superior colliculus have prompted hypotheses about its involvement in neuropsychiatric conditions, but to date, this topic has not been addressed experimentally. We describe experiments on genetically modified mice, the *Isl2-EphA3* knock-in line, that show a well-characterized duplication of the retino-collicular and cortico-collicular axonal projections leading to hyperstimulation of the superior colliculus. To explore the functional impact of collicular hyperstimulation, we compared the

performance of homozygous knock-in, heterozygous knock-in and wild-type mice in several behavioral tasks requiring collicular activity. The light/dark box test and Go/No-Go conditioning task revealed that homozygous mutant mice exhibit defective response inhibition, a form of impulsivity. This defect was specific to attention as other tests showed no differences in visually driven behavior, motivation, visuo-spatial learning and sensorimotor abilities among the different groups of mice. Monoamine quantification and gene expression profiling demonstrated a specific enrichment of noradrenaline only in the superficial layers of the superior colliculus of *Isl2-EphA3* knock-in mice, where the retinotopy is duplicated, whereas transcript levels of receptors, transporters and metabolic enzymes of the monoaminergic pathway were not affected. We demonstrate that the defect in response inhibition is a consequence of noradrenaline imbalance in the superficial layers of the superior colliculus caused by retinotopic map duplication. Our results suggest that structural abnormalities in the superior colliculus can cause defective response inhibition, a key feature of attention-deficit disorders.

Electronic supplementary material The online version of this article (doi:10.1007/s00429-014-0745-5) contains supplementary material, which is available to authorized users.

C. Mathis · J.-B. Bott · K. Geiger · A. Gillet · C. Kelche · J.-C. Cassel

Laboratory of Adaptive and Cognitive Neurosciences, CNRS, University of Strasbourg UMR 7364, 67000 Strasbourg, France
e-mail: chantal.mathis@linc.u-strasbg.fr

E. Savier · D. Clesse · A. Laux-Biehlmann · Y. Goumon · A. Lacaud · V. Lelièvre · F. W. Pfrieger · M. Reber (✉)
Institute of Cellular and Integrative Neurosciences, CNRS UPR 3212, University of Strasbourg, 5, rue blaise Pascal, 67084 Strasbourg, France
e-mail: michael.reber@inserm.fr

N. Bevins
Molecular Neurobiology Laboratory, The Salk Institute,
La Jolla, San Diego, CA 92037, USA

N. Bevins
Department of Neurosciences, University of California, La Jolla,
San Diego, CA 92039, USA

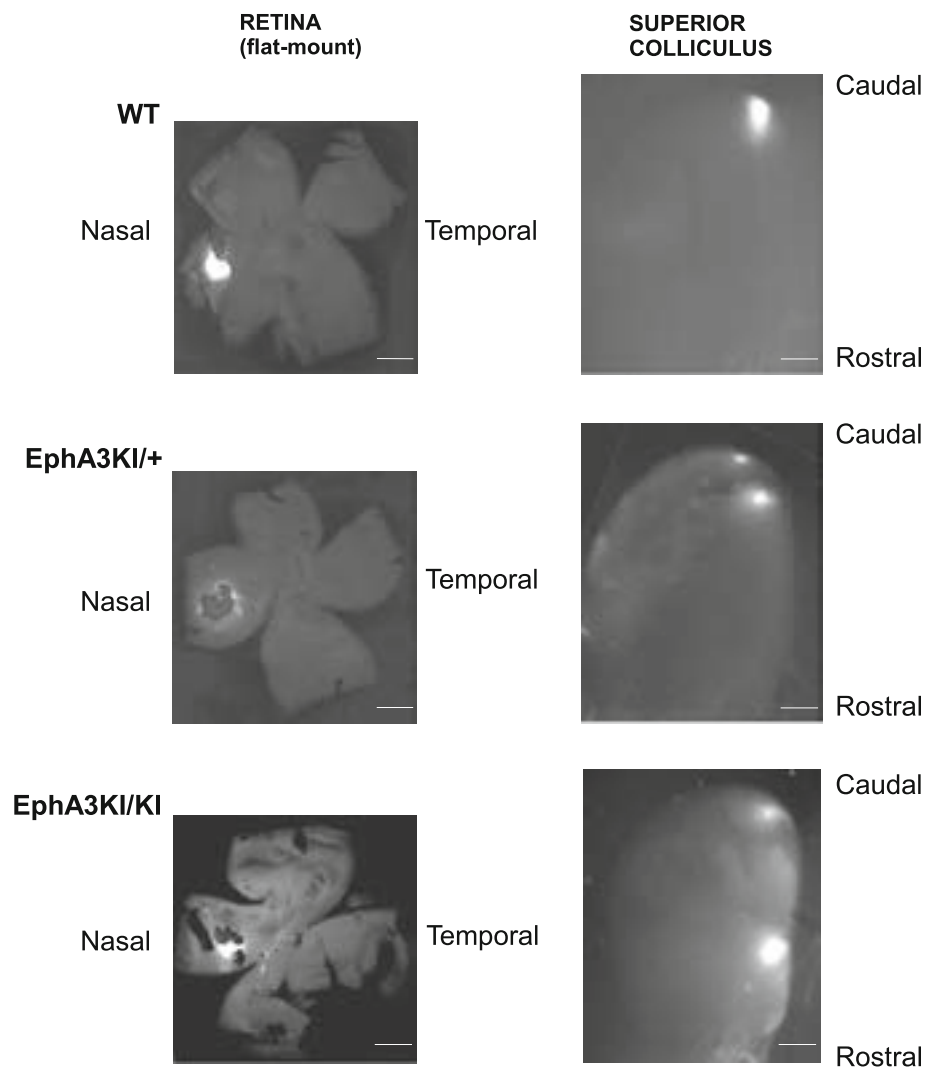
D. Sage-Ciocca
Chronobiotron, UMS 3415, CNRS, 67084 Strasbourg, France

Keywords Retinotopy · Visual system · EphA signaling · Superior colliculus · Noradrenaline · Response inhibition · Attention-deficit disorders

Introduction

The superior colliculus (SC) is a midbrain structure that integrates sensory inputs from multiple modalities (Wallace et al. 1993; Holmes and Spence 2005; May 2006) and plays a central role in visuo-spatial orientation, attention and sensorimotor processing (Stein 1984; May 2006; Gandhi and Katnani 2011). Defects in SC function have

Fig. 1 Topographic retino-collicular projections in WT and Isl2-EphA3KI animals. Micrographs illustrate nasal 1,1'-dioctadecyl-3,3,3'-tetramethylindocarbocyanine perchlorate (Dil) injections in P8 retinas and the corresponding termination zone(s) in the SC. *Top* an injection in nasal WT retina leads to a single caudal termination zone in the SC. *Middle* an injection in a nasal EphA3KI/+ retina leads to two caudal termination zones in the SC. *Bottom* an injection in a nasal EphA3KI/KI retina leads to two distant termination zones in the SC. Scale bars 1 mm



been associated with a number of neuropathological and neuropsychiatric disorders including epilepsy (Ross and Coleman 2000), schizophrenia (Fuentes 2001) and autism spectrum disorder (ASD) (Kleinmans et al. 2011). Recently, collicular hyperstimulation has been proposed to underlie attention-deficit/hyperactivity disorder (ADHD) symptoms, especially the impulsivity and distractibility associated with the disorder (Overton 2008; Miller 2009; Dommett et al. 2009). However, direct experimental evidence for such a link remains elusive.

The SC presents a particular feature, namely the topographic organization of its sensory inputs (Sperry 1963; Lemke and Reber 2005; May 2006). Axons of retinal ganglion cells (RGCs) project to the superficial layers of the SC along spatial axes reflecting their position along corresponding axes in the retina (the retino-collicular map). Layer V neurons of the V1 cortex also project in a topographic manner to the superficial layers of the SC, the cortico-collicular map, which is in register with the retino-

collicular map (May 2006; Triplett et al. 2012). This creates a topographic representation of the visual field in the superficial layers of the SC, also called retinotopy. Auditory and somatosensory afferents projecting to deep layers of the SC are also aligned with the visual maps (Meredith and Stein 1985; King et al. 1998; May 2006) enhancing perception of salient stimuli and influencing decision and overt behavior (Stein et al. 2009).

We took advantage of a specific disruption of the retinotopy in the superficial layers of the SC that has been observed in the Isl2-EphA3 knock-in mice (Fig. 1; Brown et al. 2000). In this mouse model, the EphA3 tyrosine kinase receptor, which acts as a guidance molecule during map formation, is over-expressed by a subset of RGCs. This leads to a well-characterized duplication of the retino-collicular and cortico-collicular maps along the anterior–posterior axis of the SC. Over-expression of the EphA3 receptor neither affects retinal organization and integrity, nor the topography of collicular somatosensory inputs

(Brown et al. 2000; Reber et al. 2004; Triplett et al. 2009; Bevins et al. 2011; Triplett et al. 2012). The duplicated visual maps are functional as single visual stimuli trigger the activation of two distinct areas in the SC (Triplett et al. 2009). Unlike other mouse models that target Eph/ephrin signaling (Dottori et al. 1998; Feldheim et al. 2000; Feldheim 2004), the genetic modification in the Isl2-EphA3 knock-in mice affects only a subset of RGCs and does not affect other structures in the brain (Brown et al. 2000; Reber et al. 2004, Thaler et al. 2004).

To determine if hyperstimulation of the SC, due to duplication of the retinotopic projections, influences collicular-related behavior, wild-type (WT), heterozygous (EphA3^{KI/+}) and homozygous (EphA3^{KI/KI}) Isl2-EphA3KI mice were subjected to a series of well-established behavioral tests. As a first approach, we tested general visual ability (cliff test, optokinetic reflex, Morris water maze with visible platform) as the effects of disrupted EphAs gradients in the RGCs and duplicated retinotopy in the SC on visual perception have never been described before. We then focused on general sensorimotor (locomotor activity, circadian rhythmicity, light/dark box test) and integrative features (beam walking test) and on collicular-related behavior, especially visuo-spatial orientation and memory (Morris water maze with hidden platform) and response inhibition (Go/No-Go task). Our results show that EphA3^{KI/KI} mutant mice exhibit defective response inhibition when compared to WT or EphA3^{KI/+} littermates. Visual acuity, sensorimotor activity, visuo-spatial learning, motivation and memory were similar in the different genotypes. Molecular characterization demonstrated elevated noradrenaline levels in the superficial layers of the SC in EphA3^{KI/KI} animals where the retinotopy is duplicated. Expression levels of receptors, transporters and enzymes of the monoaminergic signaling pathway were similar to WT littermates. Interestingly, these changes resemble specific symptoms of the adult and predominantly inattentive-type of ADHD patients (Diamond 2005; Biederman and Faraone 2005).

Materials and methods

Animals

Mice were bred and housed in our mouse facility (Chronobiotron, UMS 3415, CNRS, Strasbourg) and tested during the light phase (ZT2–ZT10) of their light/dark cycle except for indicated experiments. All procedures were in accordance with national (council directive 87/848, October 1987) and European community (2010/63/EU) guidelines. Official agreement numbers for animal experimentation were 67-292 for CM, 67-215 for J-CC and

67-358 for KG, AG was under their responsibility. Mice were genotyped by PCR of genomic DNA from tail biopsies as described previously (Reber et al. 2004). Four- to seven-month-old male littermates of each genotype (EphA3^{KI/KI}, EphA3^{KI/+} and WT) on a mixed genetic background (C57/Bl6 × 129Sv/J) were subjected to behavioral tests and molecular analyses. Standard laboratory rodent food and water were available ad libitum throughout all experiments, except for the Go/No-Go task, for which all mice were kept at 85 % of their free-feeding weight.

Behavioral tests

Three distinct cohorts of 4- to 7-month-old WT, EphA3^{KI/+} and EphA3^{KI/KI} males littermates were characterized using fixed sequences of test ranging as much as possible from the least to the most invasive test. Inter-test intervals (ITI) varied along the sequences to limit order effect. The first cohort of 4- to 7-month-old males littermates ($n = 6–9$ per group) was first tested in the light/dark box test (Boeuf et al. 2009) (ITI 5 days) and then only in the Go/No-Go task (Meziane et al. 1993). The second cohort of 4- to 7-month-old males littermates ($n = 7$ per group) was dedicated to sensorimotor evaluations. They were first tested for circadian wheel running activity (Mendoza et al. 2008) and general locomotor activity (Yassine et al. 2013) (ITI 15 days) followed by the Morris water maze paradigm (Moreau et al. 2008) (ITI 15 days), the beam walking test (Moreau et al. 2008) (ITI 3 days) and the visual cliff test (Gibson and Walk 1960) (ITI 21 days). The optokinetic reflex (Douglas et al. 2005) was studied on a third cohort of 4-month-old ($n = 7–10$) male littermates. Detailed descriptions can be found in Online resource 1.

Molecular analysis

Transcript levels were analyzed by semi-quantitative PCR and monoamine levels were measured by high-pressure liquid chromatography as described in the Online resource 1.

Statistical analysis

Unless otherwise indicated, data were analyzed by analysis of variance with repeated measure factors to study interactions between genotype and side, trial, day, 15-min block, quadrant, runway (rANOVA). All statistical outcomes were confirmed by a Kruskal–Wallis test applied on the light–dark single factors or within each repeated measure, as group sizes in behavioral studies were relatively small. When required, post hoc analyses were performed with the Newman–Keuls (NK) multi-comparison test

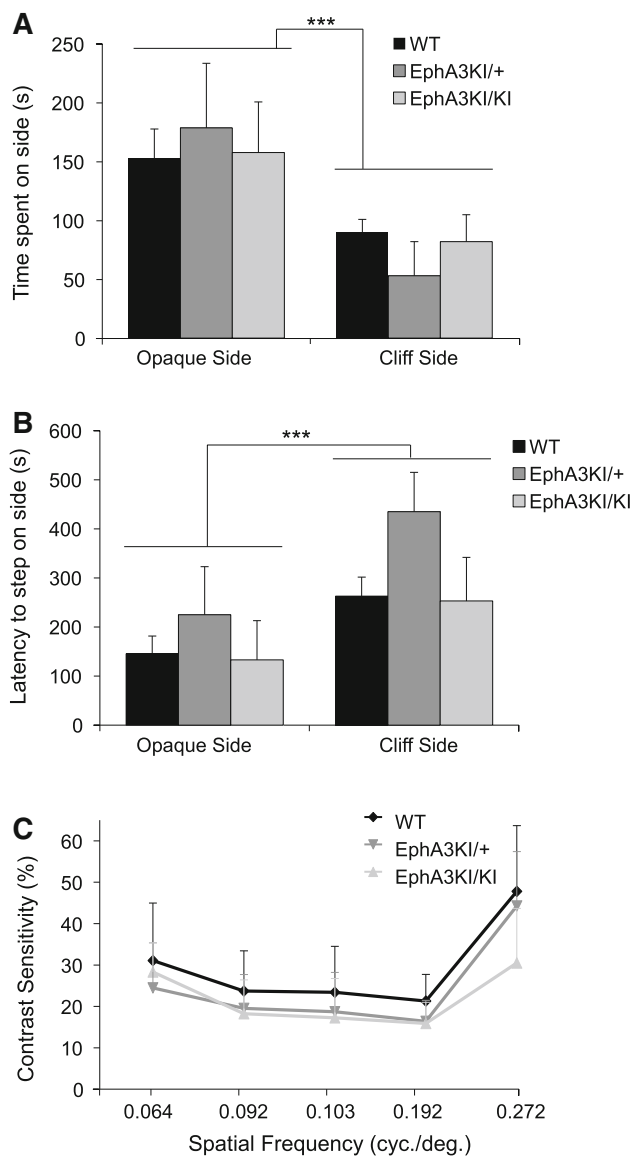


Fig. 2 Visual acuity in *Isl2-EphA3* knock-in mice. **a** In the visual cliff test, WT, *EphA3KI/+* and *EphA3KI/KI* mice spent significantly more time on the opaque side compared to the cliff side. The three groups of mice did not differ in terms of mean time (s) spent on the opaque side and cliff side during the 10 min session. **b** The latency to step down toward the opaque side was significantly lowered compared to the cliff side, but similar in all genotypes. **c** In the OKR test, the average contrast sensitivity (threshold contrast as %, y axis) for spatial frequencies ranging from 0.064 to 0.272 cycles/degree (x axis) varies similarly in the three groups of mice. *** $p < 0.0001$

(Statistica 8.0; Statsoft, Inc., Tulsa, OK). The time spent in the goal quadrant of the water maze was compared to the 15-s chance value by means of a *t* test. The 15-s chance value corresponds to the time spent for random search in four quadrants during the 60 s probe test. All behavioral data are expressed as mean \pm standard error of the mean (SEM). HPLC and qPCR data were analyzed using the

non-parametric Kruskal–Wallis (KW) test. All expression data are represented using boxplots (min, q1, median, q3, max).

Results

The functional contribution of the SC in specific behavior has been investigated in a variety of experiments, including electrophysiological recording, inactivation and lesion approaches (Binns 1999; Huberman and Niell 2011) but little has been done at a more integrated level in animal models with congenital defects.

Visual acuity

We first asked whether the modified collicular retinotopy affects visual acuity using the visual cliff test, which measures visual depth perception in rodents. Mice from all three experimental groups spent significantly more time on the opaque side compared to the cliff side (side: $F_{1,18} = 10.15$, $p = 0.005$; Fig. 2a) and stepped earlier onto the opaque side than onto the cliff side (side: $F_{1,18} = 16.61$, $p < 0.001$; Fig. 2b) indicating normal visual perception. There was no significant difference between genotypes for the latency to step down and the time spent on either the checkered side or the cliff side (no genotype effect or genotype \times side interaction). We next tested visual acuity by stimulating and measuring the optokinetic reflex (OKR). This reflex mediates compensatory head motions elicited by moving full-field visual stimuli, to maintain a constant image on the retina. Mice from all three genotypes showed similar threshold values for the minimum contrast that triggers an OKR at spatial frequencies ranging from 0.064 to 0.272 cycles/degree (Fig. 2c). Together, these results indicated normal visual acuity in *EphA3^{KI/KI}* and *EphA3^{KI/+}* mice.

General locomotor activity, sensory motor coordination and circadian rhythm

We next tested locomotor activity using horizontal cage activity and wheel running. Mice of each experimental group showed a similar decrease in locomotor activity over the course of a 3-h session corresponding to habituation to the new cage (15-min block: $F_{11,198} = 55.17$, $p < 0.0001$; Fig. 3a) and no significant effect of the genotype was observed in total wheel running activity, all three genotypes showing normal rhythmic activity (Fig. 4b, Online resource 2). The key role of the SC in the integration of sensorimotor modalities led us to test sensorimotor coordination. All three genotypes underwent the beam walking test and showed similar latencies to leave the start segment

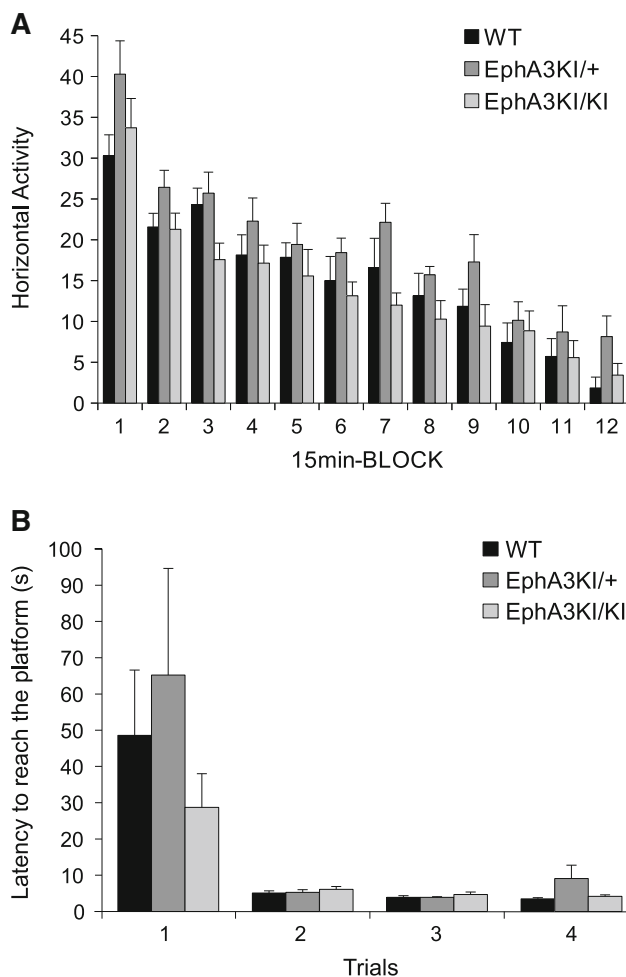


Fig. 3 Locomotor activity and sensorimotor coordination in *Isl2-EphA3* knock-in mice. **a** During the 3-h habituation phase, *EphA3KI/KI* and *EphA3KI/+* mice did not differ from their WT littermates in terms of exploration of a new environment (expressed as mean horizontal activity per 15-min block). **b** *EphA3KI/KI* mice did not differ from their WT littermates in terms of mean time per trial to reach the platform over 4 trials of the beam test. In all three genotypes, this parameter decreased significantly over consecutive trials

(genotype \times trial: $F_{6,54} = 0.65$, $p > 0.10$, not shown) and to reach the platform, which decreased significantly during subsequent trials (trial: $F_{3,54} = 16.48$, $p < 0.0001$; Fig. 3b). Sensorimotor coordination and latency to leave the start segment were similar among genotypes. Moreover, we tested whether the running activity of knock-in mice follows light-entrained and endogenous circadian patterns. All three genotypes showed similar running activity in 12 h light–dark and dark–dark cycles with similar endogenous period (WT: 23.57 ± 0.26 h, *EphA3^{KI/+}*: 23.76 ± 0.35 h and *EphA3^{KI/KI}*: 23.69 ± 0.26 h; Fig. 4). Together these results indicate normal locomotor activity, sensory motor processing and circadian activity in *EphA3^{KI/KI}* and *EphA3^{KI/+}* animals.

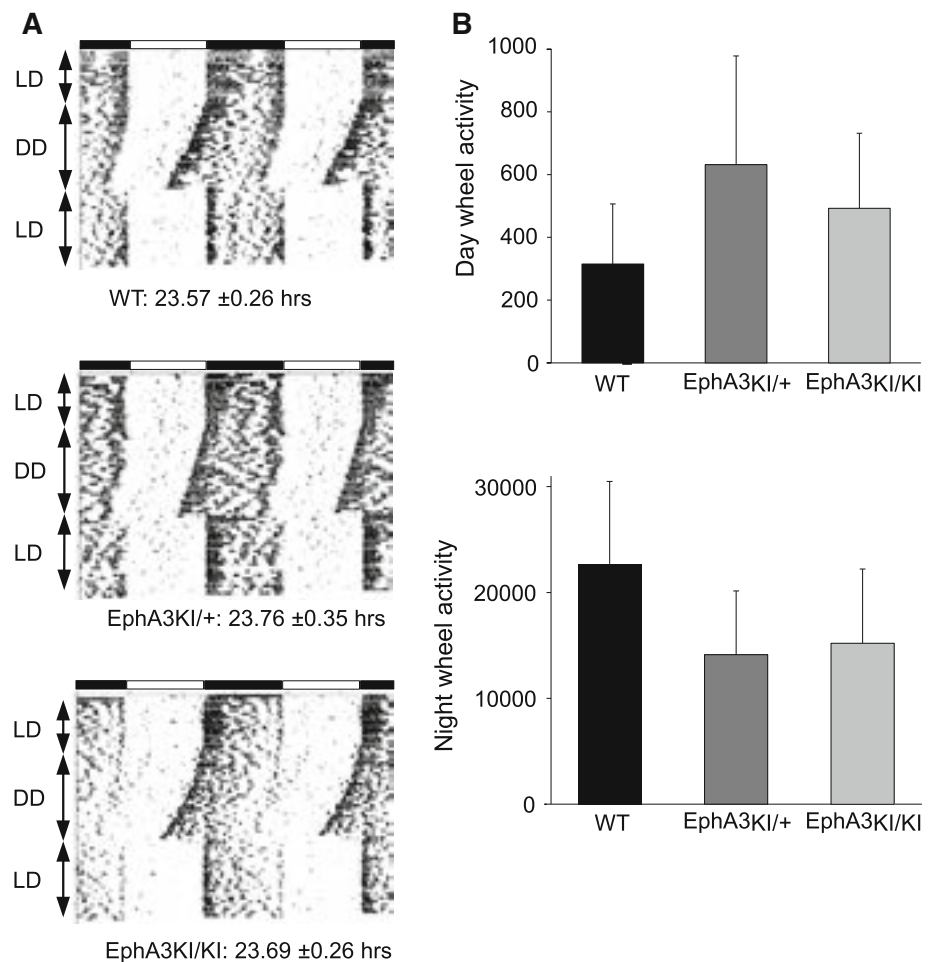
Visuo-spatial orientation and memory

We then tested vision and motor skills using the Morris water maze visible platform test, where mice must locate a cue at close range, and swim toward it. After 2 days of habituation, mice were tested for their performance in reaching a visible platform. Swim speed and distance were measured in four trials. Swim speed remained stable and similar for all groups. Swimming distance was similarly reduced among all groups over the four consecutive trials (trial: $F_{3,54} = 16.07$, $p < 0.0001$). No significant difference was observed among genotypes or genotype \times trial interactions (Fig. 5a). Next we used a variant of the Morris water maze test where the platform is hidden to evaluate visuo-spatial learning and memory. Here, mice must find the hidden platform based on distant visual cues outside the pool. Over the course of the four training days, mice of all three genotypes showed similar swim speeds and learned the position of the hidden platform equally well (day: $F_{3,54} = 20.67$, $p < 0.0001$; Fig. 5b). No difference was observed between genotypes, suggesting that *EphA3^{KI/+}* and *EphA3^{KI/KI}* animals are able to learn a task requiring visuo-spatial orientation abilities. In a probe test performed 24 h later, all mice showed a clear bias toward the target quadrant where they spent significantly more time than the 15-s chance level (WT: $t_6 = 6.68$, $p = 0.0005$, *EphA3^{KI/+}*: $t_6 = 4.62$, $p = 0.004$; *EphA3^{KI/KI}*: $t_6 = 6.01$, $p = 0.001$; Fig. 5c). Taken together, these results indicated normal visuo-spatial orientation, preserved motivation to reach a visible and hidden platform and intact spatial learning and memory in *EphA3^{KI/KI}* and *EphA3^{KI/+}* mice.

Anxiety, response inhibition

As the behavioral output in several tasks (e.g., visual cliff, Go/No-Go and Morris water maze) can be modulated by levels of anxiety, they were determined in the *Isl2-EphA3* knock-in mice using the light/dark box test (Crawley 2007). This conflict test evaluates anxiety based on the tendency of a mouse to explore a novel environment against the aversive effect of a brightly lit open field (the light box). We measured both the time spent in the light box (aversive environment) and the number of attempts to enter this box (defined as an incomplete body entrance). Animals from the three genotypes spent a similar amount of time in the aversive environment (the light box) indicating comparable levels of anxiety (Fig. 6a). In support of that, habituation times in a novel activity cage and latency to leave the start segment in the beam walking test, presented above, did not differ between the three genotypes further suggesting that the *Isl2-EphA3KI* animals exhibit normal levels of anxiety. Surprisingly, *EphA3^{KI/KI}* and *EphA3^{KI/+}* mice made significantly fewer attempts to enter

Fig. 4 Circadian activity in Isl2-EphA3 knock-in mice. All three groups of mice showed similar endogenous periods after a 15 days of light–dark (LD) cycle followed by 10 days of constant darkness (DD) (a) and similar diurnal and nocturnal wheel running activity (b)



the light box (incomplete body entrances) compared to their WT littermates (attempts: $F_{2,21} = 4.24$, $p < 0.05$, NK post hoc: $p < 0.05$; Fig. 6b). In other words, EphA3^{KI/KI} and EphA3^{KI/+} mice were less hesitant and entered the light box more readily suggesting that they fail to refrain from exploring an aversive environment. In addition, EphA3^{KI/KI} and EphA3^{KI/+} mice showed a decreased latency for complete body entrance into the light box compared to WT littermates (latency: $F_{2,21} = 3.24$, $p = 0.06$; Fig. 6c). This provides further evidence that they did not hesitate to enter an aversive environment. However, EphA3^{KI/KI} mice showed no increase in time spent in the light box and no impairment in the visual cliff test, optokinetic reflex and both versions of the water maze in which performance depends on intact visual abilities (Yassine et al. 2013). Alternatively, reduced hesitation to enter the light box could be related to a diminished response inhibition, a key feature of impulsivity (Chamberlain and Sahakian 2007).

To confirm defects in response inhibition of knock-in mice, we performed a Go/No-Go task. Go/No-Go paradigms are based on a cue discrimination conditioning and

are commonly used to assess attention and response inhibition, but also learning and memory functions in humans and mice (Meziane et al. 1993; Aron and Poldrack 2005; Gubner et al. 2010; Loos et al. 2010). This test required food restriction, during which the mice were kept at 85 % of their weight to ensure motivation for food reward. Mice of all three genotypes showed similar weight loss and motivation for food during food restriction (not shown) (Meziane et al. 1993). In our version of the task, mice were conditioned to run successively down two runways differing in colors, one color runway being always baited with food (Go trail) and the other never baited (No-Go trial). Both EphA3^{KI/+} and WT littermates progressively learned to discriminate between the reinforced (Go trials) and non-reinforced (No-Go trials) runways as indicated by a significant decrease in running time on Go trials and stable running times on No-Go trials (Go trials: $F_{2,34} = 18.9$, $p < 0.0001$; Fig. 7a, b) as usually observed in this task (Meziane et al. 1993). This suggested normal learning, motivation and response inhibition in EphA3^{KI/+} and WT mice. Running duration of EphA3^{KI/KI} animals decreased similarly than WT and EphA3^{KI/+} littermates on Go trials. Surprisingly, and in

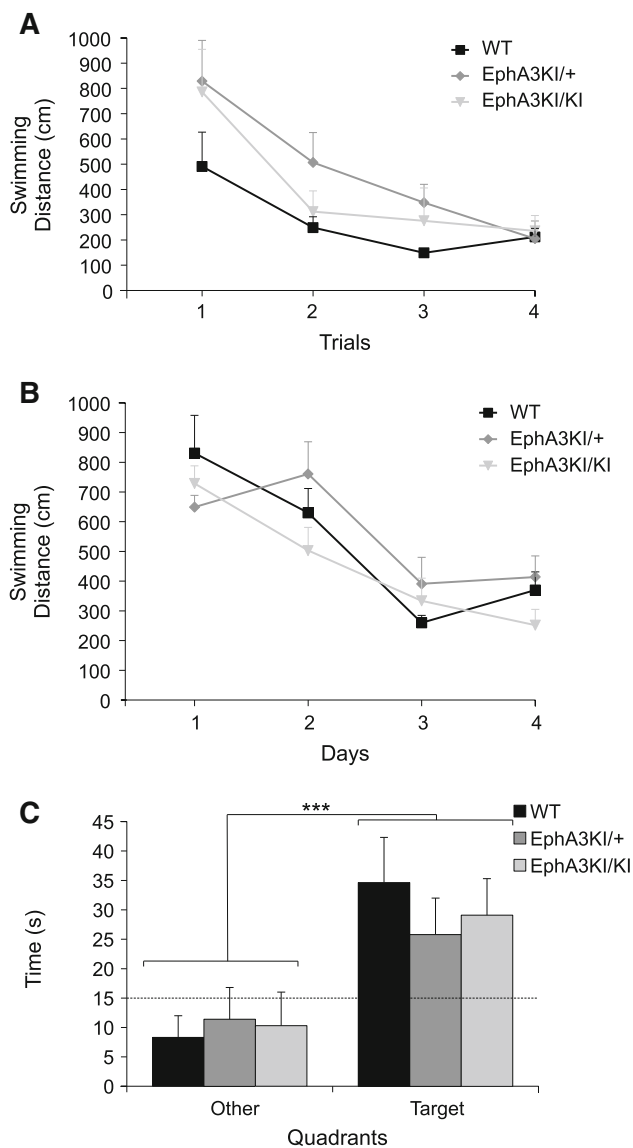


Fig. 5 Visuo-spatial orientation, spatial navigation, learning and memory in *Isl2-EphA3* knock-in mice. **a** In the visible platform test of the Morris water maze paradigm, all three groups of mice required similar mean swimming distances per trial to reach the visible platform and showed a similar decrease in the swimming distance over consecutive trials. **b** During the 4-day-long training period in the hidden platform test of the Morris water maze paradigm, *Isl2-EphA3* knock-in mice and their WT littermates required similar swimming distances to reach the platform and showed a similar decrease over consecutive trials. **c** In the 60-s probe test without platform, mice spent significantly more time in the target quadrant compared to the mean time in other quadrants regardless of their genotype. *** $p < 0.0001$

contrast to WT and *EphA3^{KI/+}*, *EphA3^{KI/KI}* running times also significantly decreased on No-Go trials (No-Go trials: $F_{4,34} = 4.03$, $p < 0.01$, NK $p < 0.05$; Fig. 7a, b) indicating their failure to refrain themselves from running in the non-reinforced runway on No-Go trials. Preserved performances of the *EphA3^{KI/KI}* animals on Go trials suggested intact motivation for food and efficient learning. A

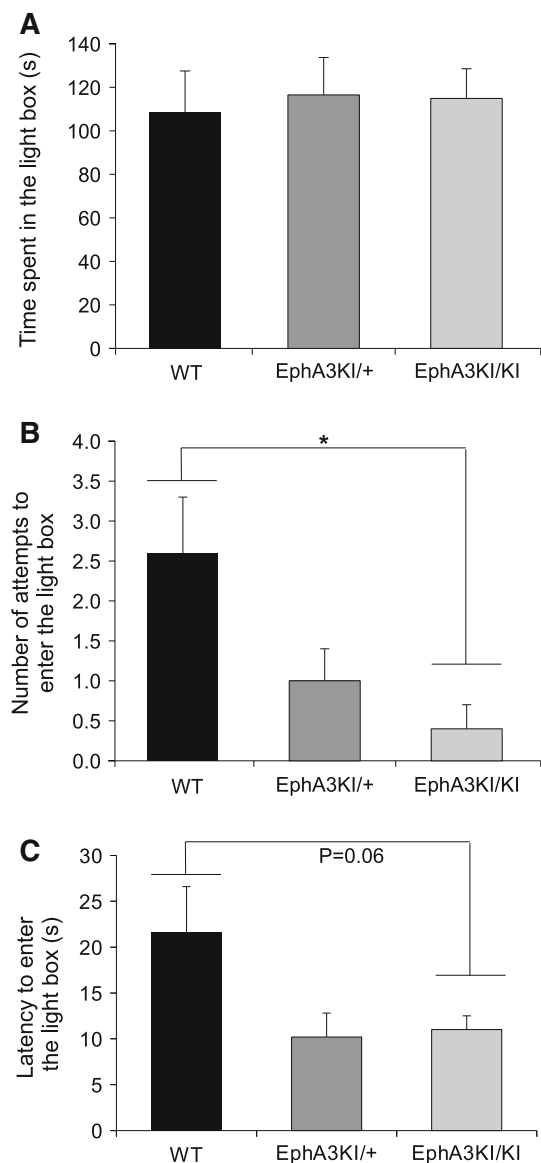
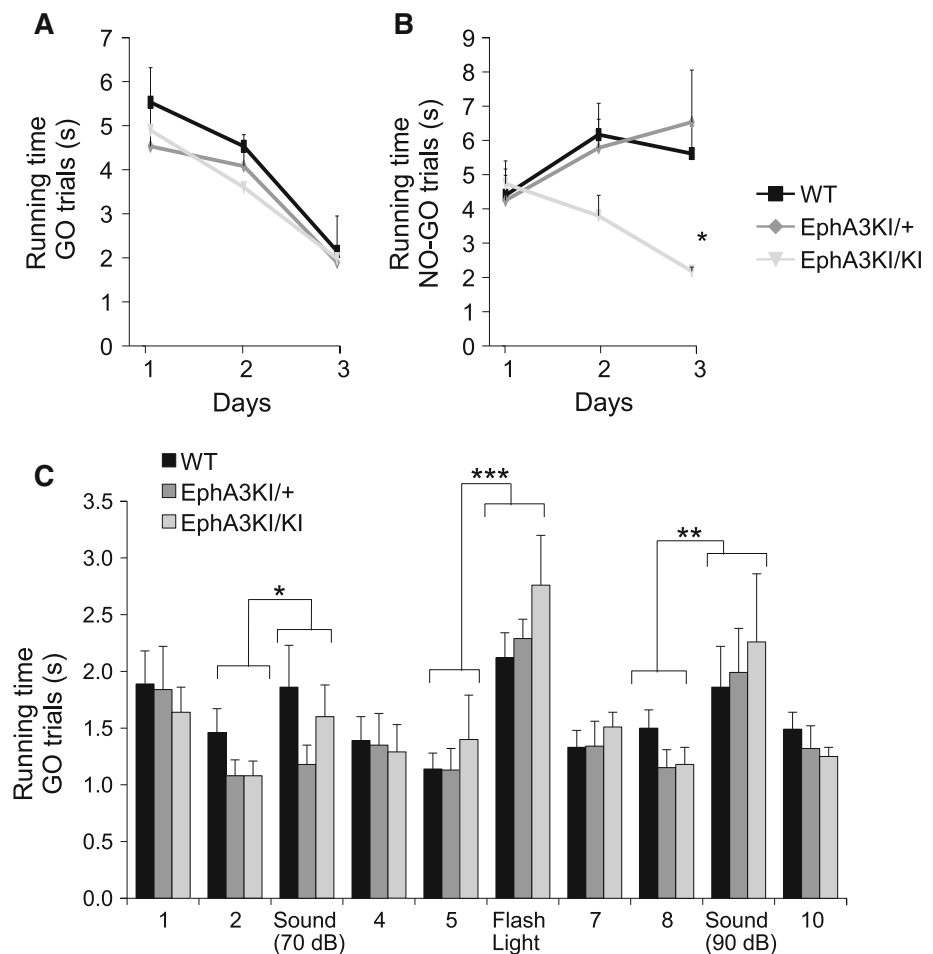


Fig. 6 Anxiety-related behavior in *Isl2-EpA3* knock-in mice. **a** In the light/dark box test, *Isl2-EpA3* knock-in mice spent the same amount of time (s) in the light box as their WT littermates. **b** *EphA3KI/KI* animals showed a significant decrease in the number of attempts to enter the light box compared to the WT littermates. **c** *EphA3KI/KI* and *EphA3KI/+* animals showed a tendency to a decreased latency (s) to enter the light box compared to their WT littermates. * $p < 0.05$

discrimination learning deficit in these mice is unlikely since amnesic treatments are known to affect essentially Go running times (Meziane et al. 1993, 1998). In addition, their performance in the visible and hidden versions of the Morris water maze as well as in the visual cliff test and optokinetic reflex suggests that their visual acuity and visuo-spatial memory are comparable to those of WT and *EphA3^{KI/+}* littermates. Taken together, these results further support the hypothesis of a defective response inhibition in the *EphA3^{KI/KI}* animals.

Fig. 7 Go/No-Go performance in Isl2-EpA3 knock-in mice. **a** Over the three sessions, WT, EphA3KI/+ and EphA3KI/KI mice reduced their mean running time per trial in the reinforced Go trials. **b** Over the three sessions, WT and EphA3KI/+ mice show stable mean running time in the non-reinforced No-Go trials, as opposed to EphA3KI/KI littermates, which also reduced their running times in No-Go trials NK $*p < 0.05$. **c** Auditory (70, 90 dB tone) and visual (flash light) distractors led to significant increases in the running times in Go trials of all three genotypes. Note that EphA3KI/KI mice appeared slightly more sensitive to a visual distractor than their littermates. $*p < 0.05$; $**p = 0.01$; $***p < 0.0001$



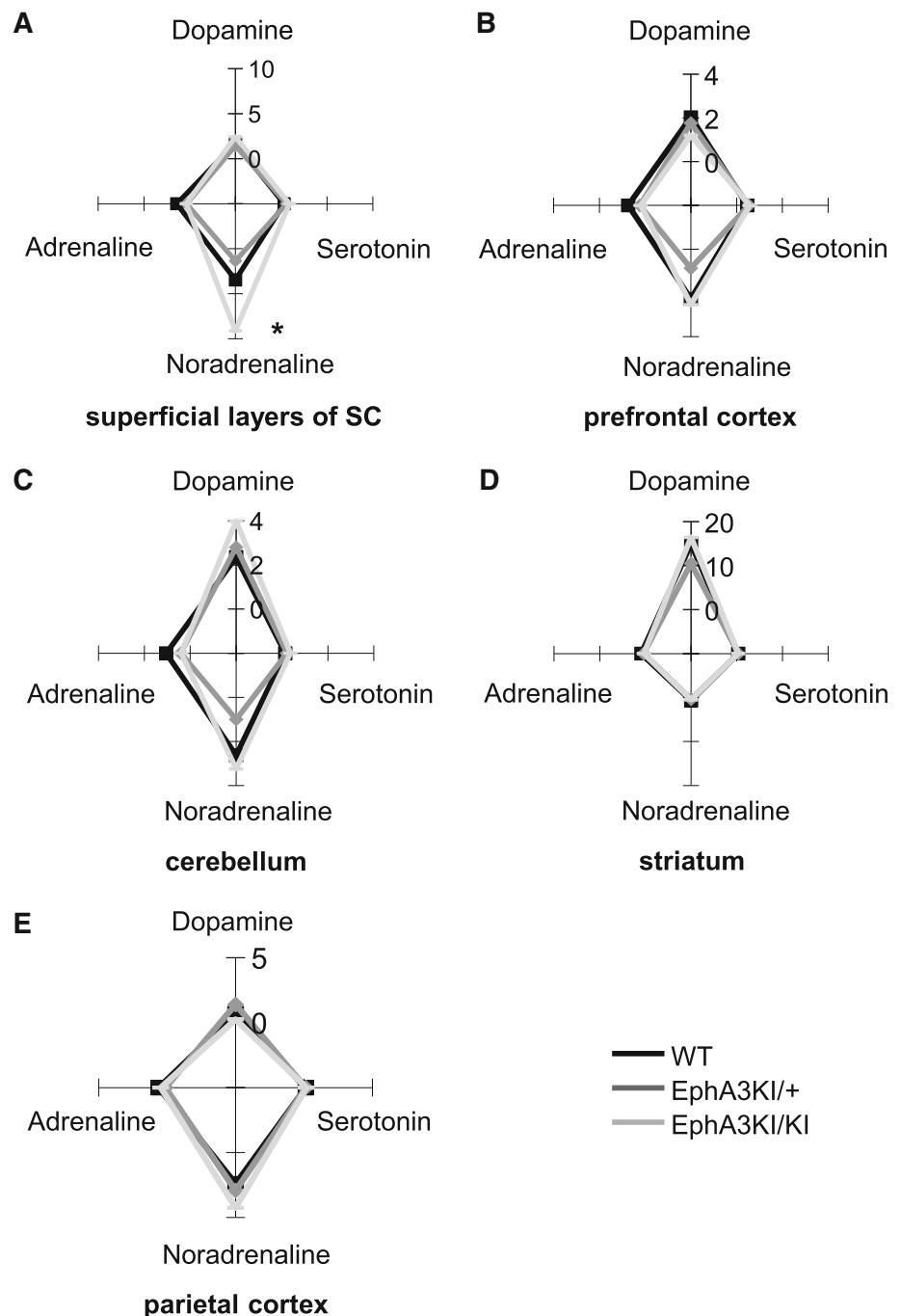
In principle, this defective behavior could be caused by impaired attention or increased distraction (Barkley 2004). To test this possibility, we repeated the reinforced Go task, but added visual (flashing light) and auditory (tone) distractors. Mice of all genotypes showed significantly increased running times by reducing their speed in trials with tones (70 dB tone: $F_{1,18} = 5.48$, $p < 0.05$; 90 dB tone: $F_{1,18} = 9.18$, $p < 0.01$; Fig. 7c) and flash lights ($F_{1,18} = 92.06$, $p < 0.0001$; Fig. 7c) compared to non-distracted trials. Notably, all EphA3^{KI/KI} mice increased their running times when exposed to a flashing light, (one mouse stopped to look toward the origin of the stimulus) although the difference between EphA3^{KI/KI} and WT littermates did not reach statistical significance (Flash latency: $F_{2,18} = 1.17$, $p = 0.33$; Fig. 7c). These data indicate that a flashing light and loud tones are effective distractors during the Go task.

Analysis of regional monoamine levels

The observed defective response inhibition in EphA3^{KI/KI} mice, corresponding to an ADHD phenotypic feature, could

be induced by abnormal catecholamine levels (van der Kooij and Glennon 2007; Sontag et al. 2010). To test this possibility, we determined levels of monoamine neurotransmitters in distinct areas of the mouse brain, namely the superficial layers of the superior colliculus (SC), the prefrontal cortex, the striatum, the parietal cortex and the cerebellum, all involved in attentional processes and motor control (Hemelstein et al. 2000; Aron and Poldrack 2005; Biederman and Faraone 2005; Overton 2008). Levels of dopamine, adrenaline and serotonin were not significantly different between genotypes in the five structures studied (Fig. 8; Online resource 2). In contrast, the levels of noradrenaline were significantly increased in the superficial layers of the SC of EphA3^{KI/KI} compared to their EphA3^{KI/+} and WT littermates (KW test $p < 0.05$; Figs. 8a, 9). The increase in noradrenaline in the superficial layers of the SC prompted us to examine the expression of receptors, transporters and enzymes that are involved in monoaminergic metabolism and associated with attention-deficit diseases (Hemelstein et al. 2000; Biederman and Faraone 2005). All three genotypes showed similar expression of transporters, metabolic enzymes and downstream receptors of dopamine, noradrenaline, adrenaline and

Fig. 8 Monoamine concentrations in selected brain regions of Isl2-EphA3 knock-in mice. Radar-plot representation of total dopamine, adrenaline, noradrenaline and serotonin content (median values, ng/mg of proteins) in the **a** superficial layers of the SC, **b** prefrontal cortex, **c** cerebellum, **d** striatum and **e** parietal cortex. The noradrenaline content was significantly increased in superficial SC layers of EphA3KI/KI compared to EphA3KI/+ and WT littermates. * $p < 0.05$ KW test. SC superior colliculus



serotonin in the superficial layers of the SC and in other brain regions (Online resource 2).

Discussion

Our study provides first evidence for specific behavioral and molecular changes in mice with genetically altered retinotopy in the superior colliculus and consequently enhanced visual inputs. In the Go/No-Go task, EphA3^{KI/KI} mice performed normally on Go trials by increasing their

running speed, but they were completely unable to inhibit their running response on No-Go trials.

In the light/dark box test, EphA3^{KI/KI} mice entered the aversive light box more readily than control mice. Altogether, our behavioral tests revealed that EphA3^{KI/KI} mice exhibit defective response inhibition, a form of impulsivity. The observation that heterozygous EphA3^{KI/+} mice behave like WT littermates in the Go/No-Go task suggests that a partial duplication of the retino-collicular map (Brown et al. 2000) is not sufficient to trigger defective response inhibition. The observed behavioral changes were remarkably

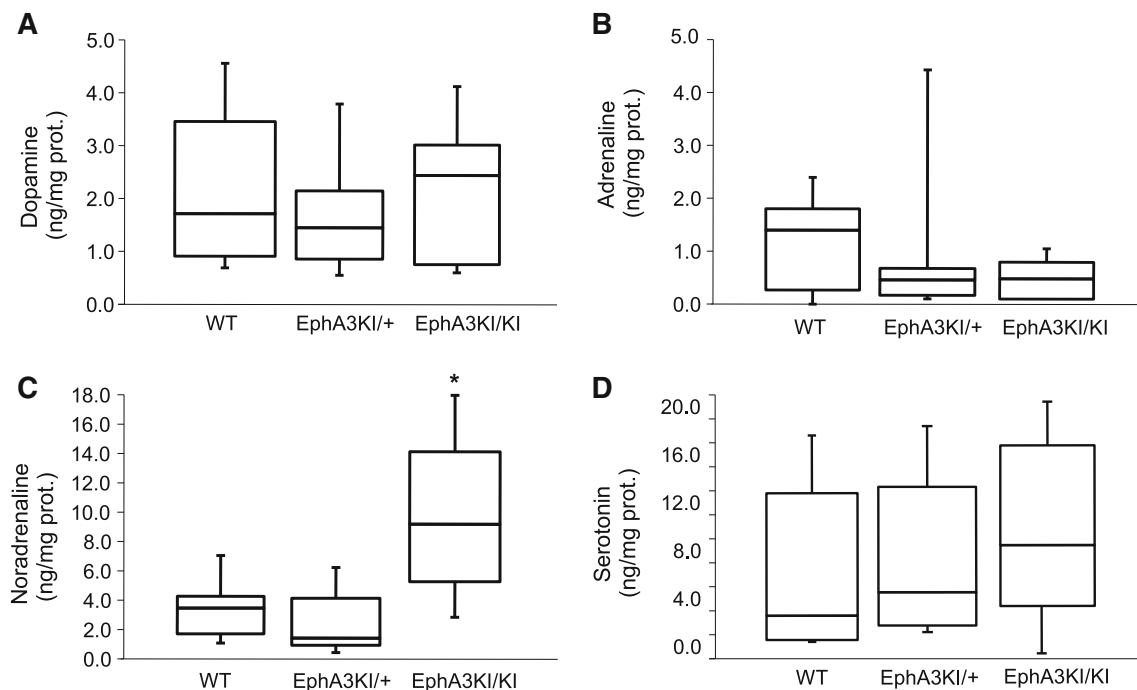


Fig. 9 Monoamine content in the SC of Isl2-EphA3 knock-in mice. Boxplot representation (min, q1, median, q3, max) of total **a** dopamine, **b** adrenaline, **c** noradrenaline and **d** serotonin content (in ng/mg

of proteins) in the superficial layers of the superior colliculus (SC) showing significant increase in noradrenaline in EphA3KI/KI animals compared to EphA3KI/+ and WT littermates. * $p < 0.05$ KW test

specific, as all other paradigms tested, namely vision, visuospatial orientation, sensorimotor function, motivation, learning and memory as well as exploratory behavior and anxiety were similar in WT, EphA3^{KI/+} and EphA3^{KI/KI} mice. Defective response inhibition could be the consequence of enhanced levels of noradrenaline that we detected in the superficial layers of the SC of EphA3^{KI/KI} mice. Enhanced noradrenaline levels in the SC could alter the behavior of the EphA3^{KI/KI} mice by modulating the signal-to-noise ratio in this structure (Mooney et al. 1990; Tan et al. 1999) and thereby changing its level of activation (Dommett et al. 2009). In hamsters, in vivo and in vitro studies demonstrated a suppression of collicular neuron response upon noradrenaline application (Mooney et al. 1990; Tan et al. 1999). In rats, Sato and Kayama reported that iontophoretically applied noradrenaline exerts an excitatory action, indicating an increase of the signal-to-noise ratio, in accordance with our hypothesis (Sato and Kayama 1983). Whether noradrenaline increases or decreases the signal-to-noise ratio in the superficial layers of the SC is still debated. However, it clearly affects the processing of salient stimuli in a context-specific manner (Sato and Kayama 1983; Mooney et al. 1990; Tan et al. 1999).

The increase in noradrenaline was specific to the superficial layers of the SC, where the retinotopy is duplicated. Moreover, the increase only concerned noradrenaline, whereas other monoamines including dopamine, serotonin and adrenaline showed similar concentrations for all

genotypes and brain regions. The increase in noradrenaline was not accompanied by changes in transcript levels of genes involved in monoamine metabolism. Therefore, we hypothesize that the increase of noradrenaline in the superficial layers of the SC may be the consequence of the duplication of the RGCs projections, which are functional, as shown by optical intrinsic imaging (Triplett et al. 2009). Previous studies revealed that RGC axons release noradrenaline upon activation (Osborne and Patel 1985). Alternatively, the increase may come from a duplication of projections from the *locus coeruleus* (LC), the major source of noradrenaline in the brain, to the superficial layers of the SC (Takemoto et al. 1978; Fritschy et al. 1990). Whether LC projections to the SC are duplicated is unknown as the mapping of the LC to the SC is hindered by the small size and specific sub-nuclei organization of the LC. However, it appears possible given that cortico-collicular projections are also duplicated in the EphA3^{KI/KI} animals although projecting V1 neurons do not express ectopic EphA3 (Triplett et al. 2009). RGCs project to different brain areas, including lateral geniculate nucleus (LGN) and non-image forming structures such as the suprachiasmatic nucleus (SCN), the medial tegmental nucleus (MTN) or the olivary pretectal nucleus (OPN). Triplett and colleagues show no targeting defects in the LGN of Isl2-EphA3 animals (Triplett et al. 2009). The same group recently demonstrated that among 1 % of RGCs projecting to the SCN (the intrinsically photoreceptive RGCs—ipRGCs), 3 % are

Isl2-positive and that these SCN-targeting Isl2-positive RGCs only transiently innervate the SCN during the development (Triplett et al. 2014). MTN and OPN also show innervation by Isl2-positive RGCs at early postnatal stages which is pruned by P6 (Triplett et al. 2014). The behavioral and molecular changes in EphA3^{KI/KI} mice including defective response inhibition and noradrenaline enrichment in the superficial layers of the SC phenocopy some of the symptoms observed in ADHD patients, specifically the adult and predominantly inattentive-type (Barkley 1997; Aron and Poldrack 2005; Biederman and Faraone 2005; Bekker et al. 2005; Fisher et al. 2011; American Psychiatric Association 2013). These symptoms are also main features of Autism Spectrum Disorder (ASD) (Murray 2010). Our findings support the hypothesis that adult ADHD patients present collicular hyperstimulation leading to the appearance of impulsivity and attentional impairments (Overton 2008; Miller 2009; Dommert et al. 2009). Moreover, they are in line with the idea that dysregulation of the central noradrenergic systems contributes to the pathophysiology of ADHD (Biederman and Spencer 1999). Currently, progress on the etiology, diagnosis and treatment of ADHD is hindered by the limited number of experimental models. Most of the available rodent models are based on impaired monoaminergic transmission (van der Kooij and Glennon 2007; Sontag et al. 2010) and present some of the phenotypic features of ADHD patients. Our findings suggest that EphA3^{KI/KI} animals may serve as a new model to study ADHD pathology and complement the limited arsenal of ADHD/ADD-related experimental approaches to understand and treat these neuropsychologic diseases.

Acknowledgments The authors thank Dr. Sophie Reibel-Foisset, Nicolas Lethenet and Laurence Huck (Chronobiotron, Unité Mixte de Service 3415, Centre National de la Recherche Scientifique, Strasbourg) for animal care and Pedwin Pallet for help with recordings of the optokinetic reflex. This work was supported by Partner University Fund (M.R.), Centre National de la Recherche Scientifique (CNRS) and Université de Strasbourg (UdS). Publication costs are supported by the Neurex network (TriNeuron – Program Interreg IV Upper Rhine) <http://www.neurex.org>.

Conflict of interest The authors report no biomedical financial interests or potential conflicts of interest.

Open Access This article is distributed under the terms of the Creative Commons Attribution License which permits any use, distribution, and reproduction in any medium, provided the original author(s) and the source are credited.

References

- American Psychiatric Association (2013) Diagnostic and statistical manual of mental disorders, 5th edn. doi: [10.1176/appi.books.9780890423349](https://doi.org/10.1176/appi.books.9780890423349)
- Aron AR, Poldrack RA (2005) The cognitive neuroscience of response inhibition: relevance for genetic research in attention-deficit/hyperactivity disorder. *Biol Psychiatry* 57:1285–1292. doi:[10.1016/j.biopsych.2004.10.026](https://doi.org/10.1016/j.biopsych.2004.10.026)
- Barkley RA (1997) Behavioral inhibition, sustained attention, and executive functions: constructing a unifying theory of ADHD. *Psychol Bull* 121:65–94
- Barkley RA (2004) Driving impairments in teens and adults with attention-deficit/hyperactivity disorder. *Psychiatr Clin North Am* 27:233–260. doi:[10.1016/S0193-953X\(03\)00091-1](https://doi.org/10.1016/S0193-953X(03)00091-1)
- Bekker EM, Overtoom CCE, Kooij JJS et al (2005) Disentangling deficits in adults with attention-deficit/hyperactivity disorder. *Arch Gen Psychiatry* 62:1129–1136. doi:[10.1001/archpsyc.62.10.1129](https://doi.org/10.1001/archpsyc.62.10.1129)
- Bevins N, Lemke G, Reber M (2011) Genetic dissection of EphA receptor signaling dynamics during retinotopic mapping. *J Neurosci* 31:10302–10310. doi:[10.1523/JNEUROSCI.1652-11.2011](https://doi.org/10.1523/JNEUROSCI.1652-11.2011)
- Biederman J, Faraone SV (2005) Attention-deficit hyperactivity disorder. *Lancet* 366:237–248. doi:[10.1016/S0140-6736\(05\)66915-2](https://doi.org/10.1016/S0140-6736(05)66915-2)
- Biederman J, Spencer T (1999) Attention-deficit/hyperactivity disorder (ADHD) as a noradrenergic disorder. *Biol Psychiatry* 46:1234–1242. doi:[10.1016/S0006-3223\(99\)00192-4](https://doi.org/10.1016/S0006-3223(99)00192-4)
- Binns KE (1999) The synaptic pharmacology underlying sensory processing in the superior colliculus. *Prog Neurobiol* 59:129–159
- Boeuf J, Trigo JM, Moreau P-H et al (2009) Attenuated behavioural responses to acute and chronic cocaine in GASP-1-deficient mice. *Eur J Neurosci* 30:860–868. doi:[10.1111/j.1460-9568.2009.06865.x](https://doi.org/10.1111/j.1460-9568.2009.06865.x)
- Brown A, Yates PA, Burrola P et al (2000) Topographic mapping from the retina to the midbrain is controlled by relative but not absolute levels of EphA receptor signaling. *Cell* 102:77–88. doi:[10.1016/S0092-8674\(00\)00012-X](https://doi.org/10.1016/S0092-8674(00)00012-X)
- Chamberlain SR, Sahakian BJ (2007) The neuropsychiatry of impulsivity. *Curr Opin Psychiatry* 20:255–261. doi:[10.1097/YCO.0b013e3280ba4989](https://doi.org/10.1097/YCO.0b013e3280ba4989)
- Crawley JN (2007) What's Wrong With My Mouse: Behavioral Phenotyping of Transgenic and Knockout Mice. Wiley, USA. doi:[10.1111/j.1601-183X.2008.00424_1.x](https://doi.org/10.1111/j.1601-183X.2008.00424_1.x)
- Diamond A (2005) Attention-deficit disorder (attention-deficit/hyperactivity disorder without hyperactivity): a neurobiologically and behaviorally distinct disorder from attention-deficit/hyperactivity disorder (with hyperactivity). *Dev Psychopathol* 17:807–825. doi:[10.1017/S0954579405050388](https://doi.org/10.1017/S0954579405050388)
- Dommert EJ, Overton PG, Greenfield SA (2009) Drug therapies for attentional disorders alter the signal-to-noise ratio in the superior colliculus. *Neuroscience* 164:1369–1376. doi:[10.1016/j.neuroscience.2009.09.007](https://doi.org/10.1016/j.neuroscience.2009.09.007)
- Dottori M, Hartley L, Galea M et al (1998) EphA4 (Sek1) receptor tyrosine kinase is required for the development of the corticospinal tract. *Proc Natl Acad Sci USA* 95:13248–13253
- Douglas RM, Alam NM, Silver BD et al (2005) Independent visual threshold measurements in the two eyes of freely moving rats and mice using a virtual-reality optokinetic system. *Vis Neurosci* 22:677–684. doi:[10.1017/S0952523805225166](https://doi.org/10.1017/S0952523805225166)
- Feldheim DA (2004) Loss-of-function analysis of EphA receptors in retinotectal mapping. *J Neurosci* 24:2542–2550. doi:[10.1523/JNEUROSCI.0239-03.2004](https://doi.org/10.1523/JNEUROSCI.0239-03.2004)
- Feldheim DA, Kim YI, Bergemann AD et al (2000) Genetic analysis of ephrin-A2 and ephrin-A5 shows their requirement in multiple aspects of retinocollicular mapping. *Neuron* 25:563–574
- Fisher T, Aharon-Peretz J, Pratt H (2011) Disregulation of response inhibition in adult attention deficit hyperactivity disorder (ADHD): an ERP study. *Clin Neurophysiol* 122:2390–2399. doi:[10.1016/j.clinph.2011.05.010](https://doi.org/10.1016/j.clinph.2011.05.010)

- Fritschy JM, Geffard M, Grzanna R (1990) The response of noradrenergic axons to systemically administered DSP-4 in the rat: an immunohistochemical study using antibodies to noradrenaline and dopamine-beta-hydroxylase. *J Chem Neuroanat* 3:309–321
- Fuentes LJ (2001) Selective attention deficit in schizophrenia. *Rev Neurol* 32:387–391
- Gandhi NJ, Katnani HA (2011) Motor functions of the superior colliculus. *Annu Rev Neurosci* 34:205–231. doi:10.1146/annurev-neuro-061010-113728
- Gibson EJ, Walk RD (1960) The “visual cliff”. *Sci Am* 202:64–71
- Gubner NR, Wilhelm CJ, Phillips TJ, Mitchell SH (2010) Strain differences in behavioral inhibition in a Go/No-go task demonstrated using 15 inbred mouse strains. *Alcohol Clin Exp Res* 34:1353–1362. doi:10.1111/j.1530-0277.2010.01219.x
- Himelstein J, Newcorn JH, Halperin JM (2000) The neurobiology of attention-deficit hyperactivity disorder. *Front Biosci* 5:461–478
- Holmes NP, Spence C (2005) Multisensory integration: space, time and superadditivity. *Curr Biol CB* 15:R762–R764. doi:10.1016/j.cub.2005.08.058
- Huberman AD, Niell CM (2011) What can mice tell us about how vision works? *Trends Neurosci* 34:464–473. doi:10.1016/j.tins.2011.07.002
- King AJ, Schnupp JW, Thompson ID (1998) Signals from the superficial layers of the superior colliculus enable the development of the auditory space map in the deeper layers. *J Neurosci Off J Soc Neurosci* 18:9394–9408
- Kleinhans NM, Richards T, Johnson LC et al (2011) fMRI evidence of neural abnormalities in the subcortical face processing system in ASD. *NeuroImage* 54:697–704. doi:10.1016/j.neuroimage.2010.07.037
- Lemke G, Reber M (2005) Retinotectal mapping: new insights from molecular genetics. *Annu Rev Cell Dev Biol* 21:551–580. doi:10.1146/annurev.cellbio.20.022403.093702
- Loos M, Staal J, Schoffelmeier ANM et al (2010) Inhibitory control and response latency differences between C57BL/6 J and DBA/2 J mice in a Go/No-Go and 5-choice serial reaction time task and strain-specific responsivity to amphetamine. *Behav Brain Res* 214:216–224. doi:10.1016/j.bbr.2010.05.027
- May PJ (2006) The mammalian superior colliculus: laminar structure and connections. *Prog. Brain Res* 151:321–378
- Mendoza J, Pévet P, Challet E (2008) High-fat feeding alters the clock synchronization to light. *J Physiol* 586:5901–5910. doi:10.1113/jphysiol.2008.159566
- Meredith MA, Stein BE (1985) Descending efferents from the superior colliculus relay integrated multisensory information. *Science* 227:657–659
- Meziane H, Devigne C, Tramu G, Soumireu-Mourat B (1993) Effects of anti-CCK-8 antiserum on acquisition and retrieval by mice in an appetitive task. *Peptides* 14:67–73
- Meziane H, Dodart JC, Mathis C et al (1998) Memory-enhancing effects of secreted forms of the beta-amyloid precursor protein in normal and amnesic mice. *Proc Natl Acad Sci USA* 95:12683–12688
- Miller L (2009) Perspectives on sensory processing disorder: a call for translational research. *Front Integr Neurosci*. doi:10.3389/neuro.07.022.2009
- Mooney RD, Bennett-Clarke C, Chiaia NL et al (1990) Organization and actions of the noradrenergic input to the hamster’s superior colliculus. *J Comp Neurol* 292:214–230. doi:10.1002/cne.902920205
- Moreau P-H, Cosquer B, Jeltsch H et al (2008) Neuroanatomical and behavioral effects of a novel version of the cholinergic immunotoxin mu p75-saporin in mice. *Hippocampus* 18:610–622. doi:10.1002/hipo.20422
- Murray MJ (2010) Attention-deficit/hyperactivity disorder in the context of autism spectrum disorders. *Curr Psychiatry Rep* 12:382–388. doi:10.1007/s11920-010-0145-3
- Osborne NN, Patel S (1985) The presence of dopamine- β -hydroxylase-like enzyme in the vertebrate retina. *Neurochem Int* 7:51–56
- Overton PG (2008) Collicular dysfunction in attention deficit hyperactivity disorder. *Med Hypotheses* 70:1121–1127. doi:10.1016/j.mehy.2007.11.016
- Reber M, Burrola P, Lemke G (2004) A relative signalling model for the formation of a topographic neural map. *Nature* 431:847–853. doi:10.1038/nature02957
- Ross KC, Coleman JR (2000) Developmental and genetic audiogenic seizure models: behavior and biological substrates. *Neurosci Biobehav Rev* 24:639–653
- Sato H, Kayama Y (1983) Effects of noradrenaline applied iontophoretically on rat superior collicular neurons. *Brain Res Bull* 10:453–457
- Sontag TA, Tucha O, Walitza S, Lange KW (2010) Animal models of attention deficit/hyperactivity disorder (ADHD): a critical review. *ADHD Atten Deficit Hyperact Disord* 2:1–20. doi:10.1007/s12402-010-0019-x
- Sperry RW (1963) Chemoaffinity in the orderly growth of nerve fiber patterns and connections. *Proc Natl Acad Sci USA* 50:703–710
- Stein BE (1984) Development of the superior colliculus. *Annu Rev Neurosci* 7:95–125
- Stein BE, Stanford TR, Rowland BA (2009) The neural basis of multisensory integration in the midbrain: its organization and maturation. *Hear Res* 258:4–15. doi:10.1016/j.heares.2009.03.012
- Takemoto I, Sasa M, Takaori S (1978) Role of the locus coeruleus in transmission onto anterior colliculus neurons. *Brain Res* 158:269–278
- Tan H, Mooney RD, Rhoades RW (1999) Effects of norepinephrine upon superficial layer neurons in the superior colliculus of the hamster: in vitro studies. *Vis Neurosci* 16:557–570
- Thaler JP, Koo SJ, Kania A et al (2004) A postmitotic role for Isl-class LIM homeodomain proteins in the assignment of visceral spinal motor neuron identity. *Neuron* 41:337–350
- Triplett JW, Owens MT, Yamada J et al (2009) Retinal input instructs alignment of visual topographic maps. *Cell* 139:175–185. doi:10.1016/j.cell.2009.08.028
- Triplett JW, Phan A, Yamada J, Feldheim DA (2012) Alignment of multimodal sensory input in the superior colliculus through a gradient-matching mechanism. *J Neurosci* 32:5264–5271. doi:10.1523/JNEUROSCI.0240-12.2012
- Triplett JW, Wei W, Gonzalez C et al (2014) Dendritic and axonal targeting patterns of a genetically-specified class of retinal ganglion cells that participate in image-forming circuits. *Neural Dev* 9:2. doi:10.1186/1749-8104-9-2
- Van der Kooij MA, Glennon JC (2007) Animal models concerning the role of dopamine in attention-deficit hyperactivity disorder. *Neurosci Biobehav Rev* 31:597–618. doi:10.1016/j.neubiorev.2006.12.002
- Wallace MT, Meredith MA, Stein BE (1993) Converging influences from visual, auditory, and somatosensory cortices onto output neurons of the superior colliculus. *J Neurophysiol* 69:1797–1809
- Yassine N, Lazaris A, Dorner-Ciossek C et al (2013) Detecting spatial memory deficits beyond blindness in tg2576 Alzheimer mice. *Neurobiol Aging* 34:716–730. doi:10.1016/j.neurobiolaging.2012.06.016

Estimating the location and size of retinal injections from orthogonal images of an intact retina.

Hjorth, J. J., Savier, E., Sterratt, D. C., Reber, M., & Eglén, S. J. (2015) *BMC neuroscience*, 16(1), 80

To study the formation of a topographic map during development, precise tracing techniques are required, notably to establish the relationship between the origin of projections and the position that they target. To investigate visual map formation, coordinates in the retina have to be matched to coordinates in the collicular space.

The SC can be considered as a planar surface on the medial part, but the retina is a spherical object. To obtain retinal coordinates, the retina has to be flat mounted after dissection. This method induces a lot of error. Indeed, in addition to its tediousness, coordinates have to be projected along the nasal-temporal axis, inducing a reduction in dimension. To optimize the acquisition of these coordinates, an algorithm that preserves the native coordinate system was developed.

This algorithm, IntactEye, calculates the location of an injection site from two views (top and side) of an intact retina. This method improved the accuracy of measurements in the retina, leading to a more precise mapping of the retino-collicular projections.

SOFTWARE

Open Access



Estimating the location and size of retinal injections from orthogonal images of an intact retina

J. J. Johannes Hjorth¹, Elise Savier², David C. Sterratt³, Michaël I Reber^{2,4} and Stephen J. Eglén^{1,4*} 

Abstract

Background: To study the mapping from the retina to the brain, typically a small region of the retina is injected with a dye, which then propagates to the retina's target structures. To determine the location of the injection, usually the retina is dissected out of the eye, flattened and then imaged, causing tears and stretching of the retina. The location of the injection is then estimated from the image of the flattened retina. Here we propose a new method that avoids dissection of the retina.

Results: We have developed IntactEye, a software package that uses two orthogonal images of the intact retina to locate focal injections of a dye. The two images are taken while the retina is still inside the eye. This bypasses the dissection step, avoiding unnecessary damage to the retina, and speeds up data acquisition. By using the native spherical coordinates of the eye, we avoid distortions caused by interpreting a curved structure in a flattened coordinate system. Our method compares well to the projection method and to the Retistruct package, which both use the flattened retina as a starting point. We have tested the method also on synthetic data, where the injection location is known. Our method has been designed for analysing mouse retinas, where there are no visible landmarks for discerning retinal orientation, but can also be applied to retinas from other species.

Conclusions: IntactEye allows the user to precisely specify the location and size of a retinal injection from two orthogonal images taken of the eye. We are solving the abstract problem of locating a point on a spherical object from two orthogonal images, which might have applications outside the field of neuroscience.

Keywords: Retinotopic mapping, Retinal injection, Native coordinate system

Background

The connections from the retina are topographically organised into maps in the brain, meaning nearby cells in the retina project to neighbouring cells in each target structure [1]. To study the connectivity of the retina and its targets we need a reliable system to specify retinal locations precisely. This is complicated by a lack of visible retinal landmarks that are consistent between individuals. Furthermore, the curvature of the eye means we

cannot simply represent a location on the retina in Cartesian coordinates, as this would lead to distortions.

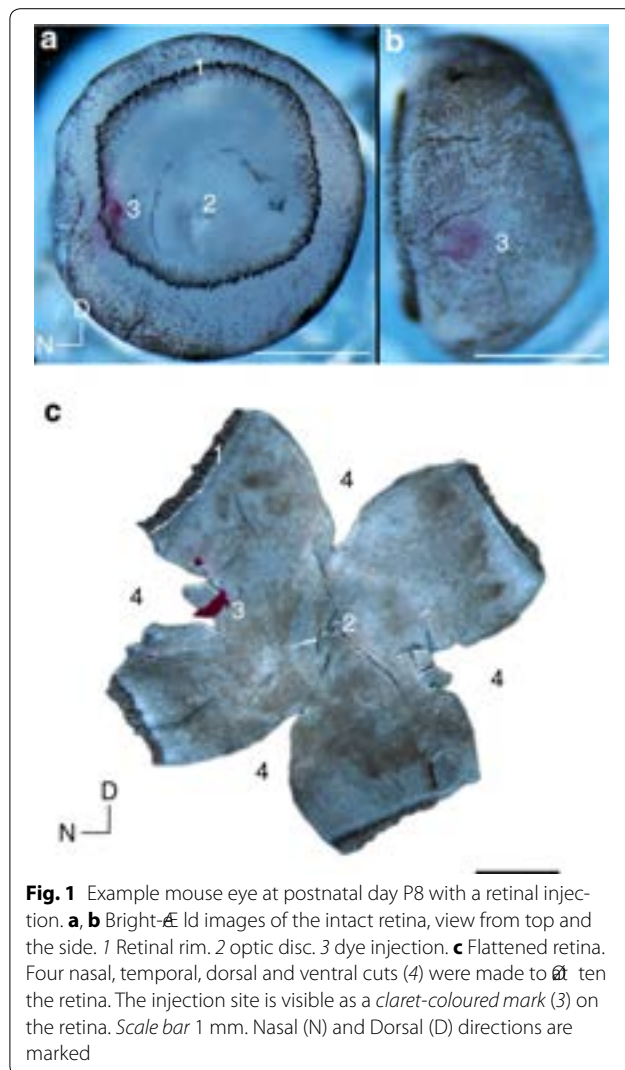
The retinal projections to the brain have been studied extensively as a model system for self-organisation of the brain [1±3]. The most widely-used technique to analyse retinotopy is to inject a dye into a small region of the eye to label a region of the retina (Fig. 1A, B). The dye is then transported through retinal axons to label target structures [4±6]. Although this method is over twenty years old [7], it is still commonly used today [8]. A common alternative for assessing retinotopic map order is to use imaging techniques [9]. However, these imaging methods require the retina to generate visual responses, around postnatal day 10 in mouse, by which time the mouse retinocollicular map has already been established.

*Correspondence: sje30@cam.ac.uk

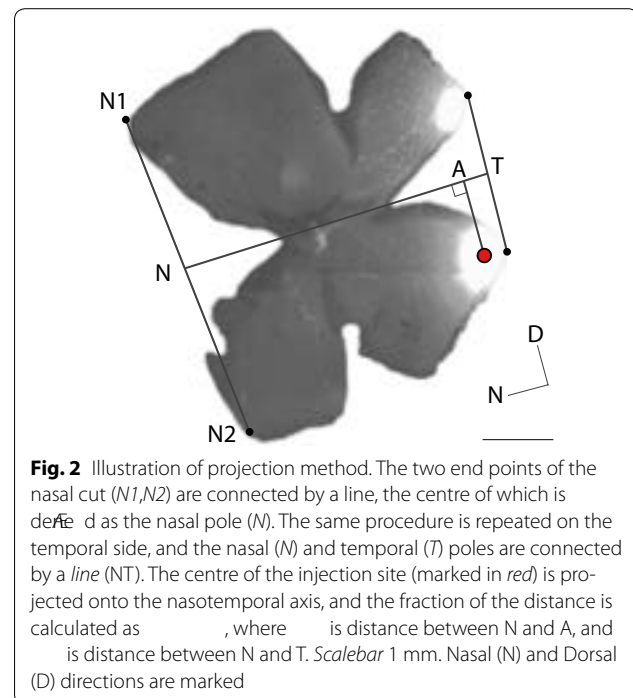
[§]Michaël I Reber and Stephen J. Eglén contributed equally to this work

⁴ Université de Strasbourg Institut d'Études Avancées, 5 rue Blaise Pascal, 67084 Strasbourg, France

Full list of author information is available at the end of the article



To determine the location of the dye injection in the retina, it is dissected out and flattened so that it can be imaged (Fig. 1C) [10]. This is a delicate procedure and the flattening causes distortions and tears in the retina. The retinal location of the injection is then estimated from the image using the projection method [5, 6] or Retistruct [11]. In the projection method the location of the nasotemporal axis is best estimated based on the vestigial nictitating membrane at the nasal pole, and then the location of the injection site is projected onto the nasotemporal (NT) axis. The injection location is reported as a fraction of the NT axis, measured from the nasal pole (Fig. 2). The dorsoventral axis is calculated by orthogonal projection of the NT axis. This projection method uses a Cartesian coordinate system to describe a curved surface, which leads to distortions. To address this issue, the



Retistruct program [11] was developed recently independently from earlier work using relaxation techniques [12]. Retistruct refolds the retina back onto a sphere to try and recover the original geometry. Internally it minimizes an energy function such that the stretching of the surface is as small as possible. Using Retistruct's mapping of the flattened image onto the sphere the injection site can be specified in the native three dimensional coordinates of the eye without distortions due to incompatible coordinate systems.

Retistruct is a significant improvement over the projection method, however, it still requires the retina to be dissected out and flattened. It also requires manual labelling of the outline of the retina. Here we propose a method that bypasses the need to dissect out the retina from the eye. Instead of using one image of the flattened retina, the IntactEye method uses two orthogonal images of the intact retina. With the help of two user-placed wire-frame spheres that are aligned with the pictures of the eye, IntactEye can calculate the location of the marked injection site in the 3D coordinate frame of the eye. The accuracy of the IntactEye method compares well with both the projection method and Retistruct. By avoiding the retinal ex vivo flattening, the acquisition is faster and we also reduce measurement artefacts and increase reproducibility and reliability. The IntactEye method is developed with the retina in mind, but we solve a general problem of locating a point in a three dimensional sphere from two images, which could have applications outside neuroscience.

Implementation

In the next section we describe how to use the IntactEye method. We then describe the animal procedures used, and describe two other approaches of analysis that we compare to the IntactEye method. We also describe the new wedge coordinate system used to determine the location of the retinal injection. The last section describes the verification of the IntactEye method using both known experimental retinal landmarks and synthetic data.

Installation

IntactEye is free to download from [13]. An archived version of our program is also available from <http://dx.doi.org/10.6084/m9.figshare.1605574>. The zip file contains the source code and some example images. This article acts as the main documentation for the program. Unpack the zip file, then start MATLAB. In the MATLAB GUI click the "Set path" icon, and add the IntactEye directory to the path. Alternatively this can be done from the command line by executing `addpath('your/path/to/IntactEye'); savepath`.

Preparation of images

To localise a retinal injection using IntactEye two images of the intact retina, with the injection site visible, must be prepared. We suggest one taken from the top looking down at the iris, and a second one taken from the side. For mouse we recommend a small cut at the vestigial nictitating membrane as a nasal marker. Make sure this cut is visible in at least one of the two images. The two images can be loaded separately or as a part of a composite image. The software reads images in tiff, png and jpeg format. The images need to have the same magnification and either have the same height or width so they can be automatically merged.

How to use the software

A video of the following four-step procedure can be found on YouTube [14].

Step 1 Open up Matlab and type `IntactEye` to start the program. In the user interface click "Load Image". This brings up a dialog box to select which composite file to load. Alternatively, "Load Images" allows you to load the two views from two separate files. The images of the eye are displayed with two wire-frame spheres overlaid. The "Left Eye"/"Right Eye" button lets the user select if it is a left or right eye that is being analysed; this switches the dorsoventral (DV) axis accordingly.

Step 2 Using the computer mouse, the wire-frame spheres can be interactively resized and repositioned (Fig. 3). The left mouse button is used when the sphere is resized (by clicking and dragging on the axis handles) or moved (by clicking and dragging the centre). The

right mouse button is used when rotating the wire-frame sphere. There are also two sliders to adjust the rim angle and rotate the eye around its central axis. If a nasal cut was made, it must be aligned with the nasal marker. The wire-frame spheres can be temporarily hidden by clicking the "Hide" button. Clicking the button again shows the wire-frame spheres. If the nasal cut is only visible in the top view, then the injection can sometimes be used to help align the second sphere.

Step 3 Once the spheres match the images of the eye, the next step is to mark the injection site. Start by marking it in the top view by clicking "Mark top" and then clicking on the injection location. A line is then displayed in the side view with the possible locations. Click "Mark side" and place a mark in the side view and the program computes the nasal and dorsal positions.

Step 4 Click "Save" to create a MAT file with the eye image as well as the location of the wire-frame and injection. This information can be accessed by using the "Reload" button to return to a previously saved state. The "Export Figure" button saves a 2D picture of the injection location (and, optionally, extent) in polar coordinates, as well as an image with the wire-frame spheres overlaid on the original images.

Experimental protocol

To test the IntactEye method we collected two sets of retinal images from mouse. First we dissected out and imaged the intact retina, then we performed additional dissection to acquire images of the flattened retina that could be analysed for comparison.

C57/Bl6 mice were housed at the Chronobiotron, CNRS UPS 3415, Strasbourg, under a 12/12 h light/dark cycle. All procedures were in accordance with European community (2010/63/EU) guidelines. Official agreement number for animal experimentation was 01831.01 (MR). Standard laboratory rodent food and water were available *ad libitum*.

Neuronal lipophilic tracer injection and dissection procedure were performed as previously described [15]. Small volumes (30 ± 50 nl) of 1,1-dioctadecyl-3,3,3,3-tetramethylindocarbocyanine perchlorate (DiI) were injected in the left retina of P7-P8 C57/Bl6 mice. DiI was dissolved in dimethylformamide, loaded into a pulled glass pipette, and pressure injected into the retina using a Picospritzer. After 16 to 18 h, animals were euthanized by a lethal dose of pentobarbital (800 mg/kg), perfused with 4 % PFA and decapitated. The head skin was removed and a cut was made at the level of the nictitating membrane (Np) indicating the nasal pole of the retina. Oculomotor muscles were then cut and the tilted forceps were used to enucleate the eye. Cornea, sclera and pigmented epithelium were then delicately removed using

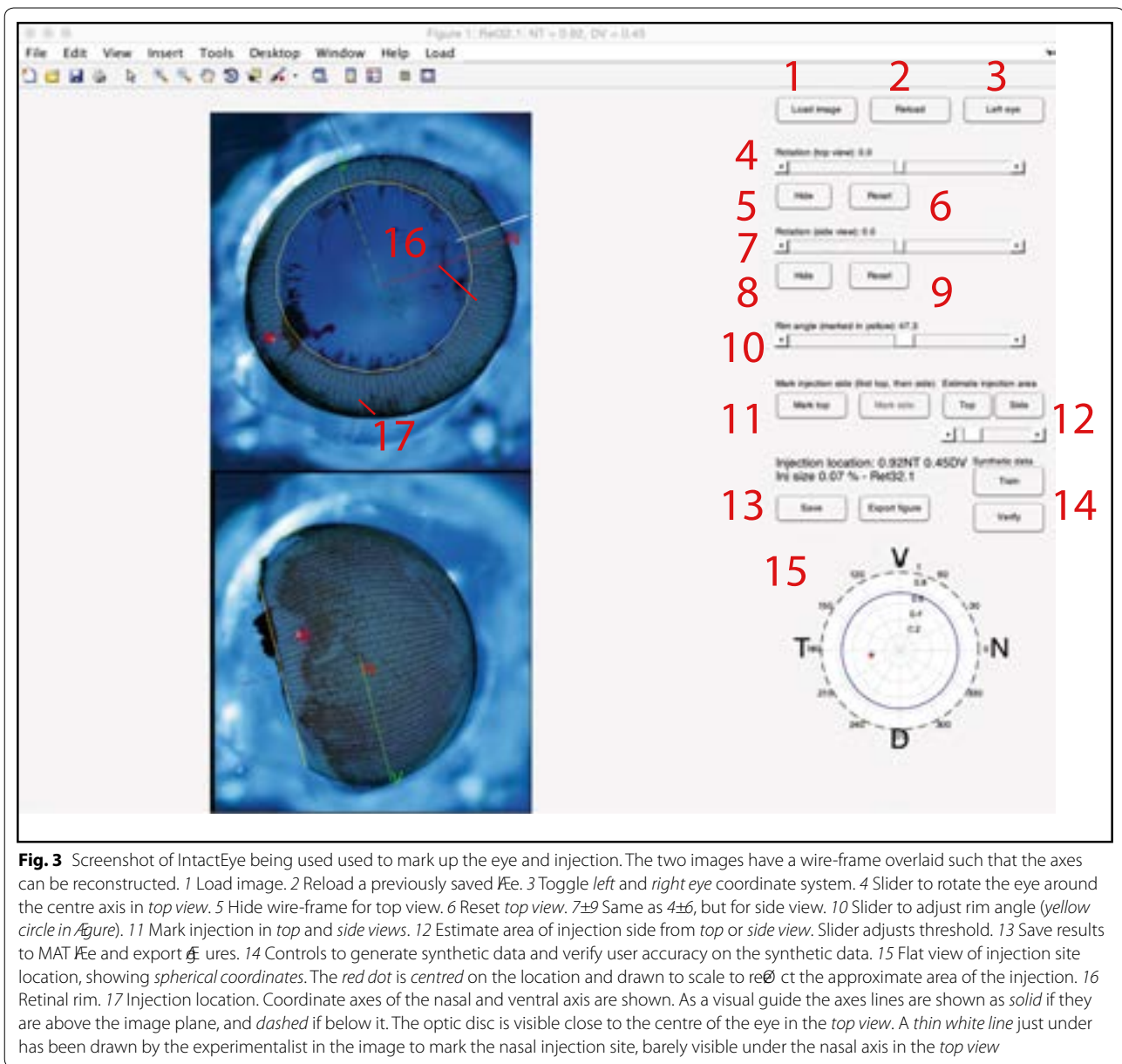


Fig. 3 Screenshot of IntactEye being used used to mark up the eye and injection. The two images have a wire-frame overlaid such that the axes can be reconstructed. 1 Load image. 2 Reload a previously saved file. 3 Toggle left and right eye coordinate system. 4 Slider to rotate the eye around the centre axis in top view. 5 Hide wire-frame for top view. 6 Reset top view. 7-9 Same as 4±6, but for side view. 10 Slider to adjust rim angle (yellow circle in figure). 11 Mark injection in top and side views. 12 Estimate area of injection side from top or side view. Slider adjusts threshold. 13 Save results to MAT file and export figures. 14 Controls to generate synthetic data and verify user accuracy on the synthetic data. 15 Flat view of injection site location, showing spherical coordinates. The red dot is centred on the location and drawn to scale to reflect the approximate area of the injection. 16 Retinal rim. 17 Injection location. Coordinate axes of the nasal and ventral axis are shown. As a visual guide the axes lines are shown as solid if they are above the image plane, and dashed if below it. The optic disc is visible close to the centre of the eye in the top view. A thin white line just under has been drawn by the experimentalist in the image to mark the nasal injection site, barely visible under the nasal axis in the top view

tweezers, revealing the retina. The intact retina was then photographed from a top-down and a side view, showing the injection site (Fig. 1A, B) using a Zeiss binocular coupled to digital camera. These can then be analysed using IntactEye.

The projection method (Fig. 2) and Retistruct both require additional steps to be performed. For flat-mount dissection (Fig. 1C), cardinal cuts (temporal, dorsal and ventral) were performed according to the original nasal cut. The retina was then flattened on a coverslip and mounted onto a glass slide. A picture at low magnification of the full flat-mounted retina was taken using Zeiss

Axioskop 2. These flattened images can then be used with the projection method or Retistruct.

Projection method

The projection method [5, 6] is a standard method used to estimate the location of the nasotemporal axis based on the nasal cut and the optic disc (Fig. 2). In the image of the flattened retina, the two nasal points (N1, N2) that were separated by the cut are reconnected by a straight line. The middle of this line is defined as the nasal pole (N). The same procedure is applied to define the temporal pole (T). A second line is drawn from N to T. This line

(NT), which runs from the nasal pole to the temporal pole via the optic disc, defines the nasotemporal axis. The injection location is projected onto this line and the position (A) reported as a fraction of the whole nasotemporal axis (f), where r is the length of the line NA).

Retistruct method

The Retistruct method [11] is used here as a control to evaluate our method. Retistruct's starting point is a flattened retina. The user provides the algorithm with a mark-up of the periphery of the retina indicating where the cuts and tears were. This information is used to fold the flattened retina back onto a sphere. The refolding takes into account the rim angle and is done so as to minimize the amount of stretching and compression of the retinal image. The location of the injection is then calculated in the native 3D space of the eye.

IntactEye method

By using two images taken from different angles, the location of an injection mark in an eye can be found without flattening the retina. To estimate the view angle for each of the images, the user needs to indicate where the eye is positioned and which way it is turned. This is done by placing a wire-frame eye-ball over the image of the intact retina. The controls in the program allow the user to rotate the eye along the three axes and to adjust the lengths a , b , and c of the semi-axes of the ellipsoid. The

rim angle (Fig. 4) of the eye-opening is manually adjusted to improve the fit between the wire-frame model and the image of the eye. By marking the position of the injection in the top image ((x_1, y_1)), the location of the injection site can be narrowed down to a line segment between (x_1, y_1) and (x_2, y_2) perpendicular to the imaging plane, where r is the largest radius of the ellipsoid. The view transform is

$$V = R_z(\vartheta) R_y(\vartheta) R_x(\vartheta) \tag{1}$$

where for rotation ϑ ϑ ϑ around the x , y , z -axis the rotation matrix is

$$\begin{pmatrix} \cos \vartheta & 0 & \sin \vartheta \\ 0 & 1 & 0 \\ \sin \vartheta & 0 & \cos \vartheta \end{pmatrix} \begin{pmatrix} \cos \vartheta & \sin \vartheta & 0 \\ -\sin \vartheta & \cos \vartheta & 0 \\ 0 & 0 & 1 \end{pmatrix} \begin{pmatrix} \cos \vartheta & \sin \vartheta & 0 \\ 0 & 0 & 1 \\ \sin \vartheta & \cos \vartheta & 0 \end{pmatrix} \tag{2}$$

and \mathbf{v} is a vector. The inverse transform is

$$V^{-1} = R_x^{-1}(\vartheta) R_y^{-1}(\vartheta) R_z^{-1}(\vartheta) \tag{3}$$

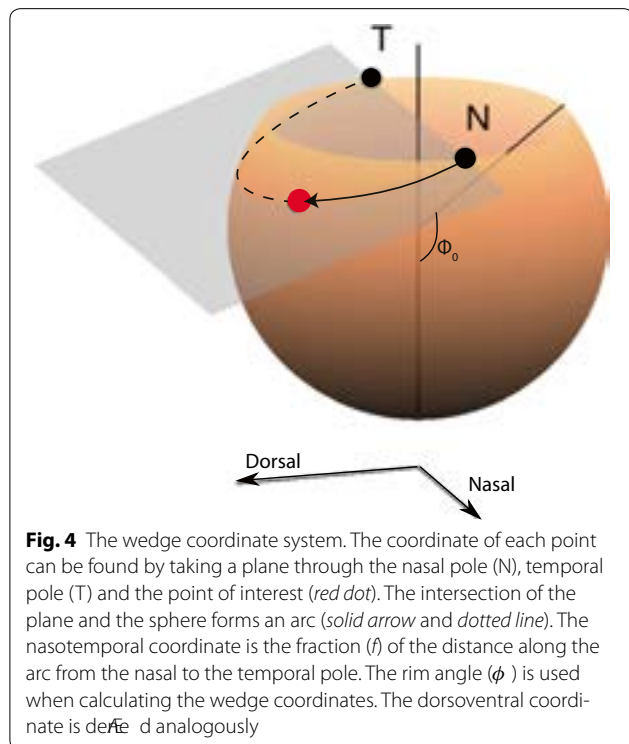
and the line representing possible locations for the injection in the eye frame runs from (x_1, y_1) to (x_2, y_2) . By plotting this line in the second view overlaid on the eye, we can quickly establish which point in 3D space corresponds to the injection. This method relies on accurately placing the two wire-frame eyes on top of the real images.

Internally the program stores the coordinates of the injection ((x, y, z)) in Cartesian coordinates in the coordinate frame of the eye (E). The program also stores the viewing transforms for each of the two views, which tracks the 3D rotation and the translation of the spheres.

Wedge coordinate system

A coordinate system which defines arcs running from the nasal to the temporal poles, along which the fractional distance f from nasal to temporal can be measured. A fractional distance from the dorsal to the ventral poles can be defined analogously. This section is presented for information only; the user can use the program without studying the new coordinate system.

Assume the retina is oriented as shown in Fig. 4, with the rim lying at a colatitude of ϕ measured from the south pole. Each point on the surface of the curtailed sphere can be reached by a system of coordinates (ψ, f) where ψ is the angle to the vertical made by a plane passing through the nasal and temporal poles and f is the fractional distance along the circle defined by the intersection of this plane and the curtailed sphere. Assuming a sphere of unit radius, the forward transformation from



wedge coordinates ψ to Cartesian coordinates (x, y, z) is:

$$\begin{pmatrix} \rho \cos \alpha \\ -\rho \sin \alpha \\ \rho \end{pmatrix} \begin{pmatrix} \psi \\ \psi \\ \psi \end{pmatrix} \begin{pmatrix} \pi - \alpha \\ \pi - \alpha \\ \pi - \alpha \end{pmatrix} \quad (4)$$

where

$$\begin{aligned} \rho &= \sqrt{\phi^2 + \psi^2} \\ \alpha &= \arctan\left(\frac{\phi}{\psi}\right) \end{aligned} \quad (5)$$

Here ρ is the radius of the circular arc whose centre is $(0,0,0)$, and α is the value of the angular parameter along the circle at the rim.

To invert (x, y, z) back to ψ the following equations are used:

$$\begin{aligned} \psi &= \frac{-y}{\alpha - \alpha} \\ \alpha &= \frac{-z}{\pi - \alpha} \end{aligned} \quad (6)$$

where

$$\left\{ \begin{aligned} \alpha &\in [0, \pi] \\ \psi &\in [0, \pi] \end{aligned} \right. \quad (7)$$

Internally, IntactEye uses Cartesian coordinates, and the inverse transformation (Eqs. 6, 7) is used to generate the output. The forward transformation (Eqs. 4, 5) is given as reference.

Injection area estimation

As well as reporting the location of the centre of the retinal injection, the area can also be estimated from either the top view or the side view, as long as the entire injection site is visible. IntactEye automatically converts the image from RGB into the L*A*B* colour space, which has one value for lightness and the other two for colour hues. The lightness value is discarded. If the injection centre in the image is located at (p,q) then the distance in colour space for a pixel at (i,j) is calculated as

$$\sqrt{(h_i - h_p)^2 + (h_j - h_q)^2} \quad (8)$$

where h_i, h_j, h_p, h_q are the hue values. The image is thresholded (default threshold 5) so that only the parts with similar colour hue to the injection centre are selected. To find the corresponding points on the sphere,

IntactEye takes a line through each injection pixel, perpendicular to the image plane, and finds its intersection with the eye ellipsoid. This is done by calculating

$$\left(\begin{aligned} & \\ & - \end{aligned} \right) \quad (9)$$

(where a, b, c are the lengths of the semi-axes of the ellipsoid) for 2000 points on the line, and picking the one with the smallest v . The fraction of the total area of the eye is reported as the injection size. The injection area is calculated using MATLAB's built in alpha hull [16] function (alphaShape); this functionality requires matlab version 2014b or newer; older versions of matlab will not calculate the area of injections, but can still calculate the location.

Synthetic data

We generated a set of synthetic data to train the user, and also to verify the accuracy of the method. The length of the semi-axes of the ellipsoid representing each eye are drawn from a normal distribution (μ, σ) , corresponding to a P12 mouse eye [11]. The rim angle defining the opening was sampled from a normal distribution (μ, σ) . For the top and side views, the view angle and location was varied approximately within a range of 0° around the x and y axis (normal distribution (μ, σ)) and freely rotating around the z-axis. The nasal cut was marked with a M. The location of the injection centre (spherical coordinates $\theta \in [0, \pi], \phi \in [0, 2\pi]$) was randomized from a uniform distribution. The injection site was represented by 100 points, with spherical coordinates sampled from a normal distribution centered on the injection centre, and with standard deviation σ . Any points placed above the rim were discarded. Three observers were asked to estimate the location of the centre of the injection site in synthetic data. The user-provided location and the known location were then compared.

Locating the optic disc

By using the location of the optic disc as a known landmark close to the geometric centre of the eye [17] we can estimate the accuracy of the Retistruct and IntactEye. Images where the optic disc was not clearly visible were excluded from this verification step.

Results and discussion

We have created a software package named "IntactEye" to calculate the location of a retinal injection from two orthogonal pictures of an intact retina. IntactEye lets the user manually place two reference wire-frame spheres on the images of the eye. The program reports the nasotemporal and dorsoventral coordinates of the injection as a

fraction along the respective axes using our wedge coordinate system (Fig. 4). The injection size is reported as a fraction of the area of the retina.

To compare IntactEye with the projection method and Retistruct, a set of wild type mouse retinas (N = 11) which had been imaged both before and after α -attenuation was analysed. Fig. 5 compares the position estimates from the three methods, for the nasotemporal axis (A) and the dorsoventral axis (B). We see that there is a good correspondence between all three measures, but there is a larger variation in the dorsoventral coordinates than in the nasotemporal coordinates (compare Pearson correlation coefficients in Table 1). For the projection method the nasal cut and α -attenuation will cause a larger distortion

of the dorsoventral axis than the nasotemporal axis due to the direction of the cut.

We assess the accuracy of the IntactEye using two methods. First we used the location of the optic disc, a known retinal landmark. The optic disc was visible in six out of eleven images investigated. By marking the optic disc in the images using IntactEye we estimated the location as (mean \pm SD) nasotemporal and dorsoventral (Fig. 6). This is comparable to the results from Retistruct when applied to the same retinas: nasotemporal and dorsoventral (Fig. 6).

We also created synthetic images of eyes with label injections where the exact location was known. This allowed us to assess the variability with the IntactEye method that comes from flattening the spheres to the image of an idealised eye. Three observers each marked a unique set of synthetic data. Figure 7 shows the known NT (DV) coordinates on the x-axis and the corresponding estimates on the y-axis. We see a good correspondence between the true location and the estimated position in the synthetic data (Pearson correlation coefficient 0.98

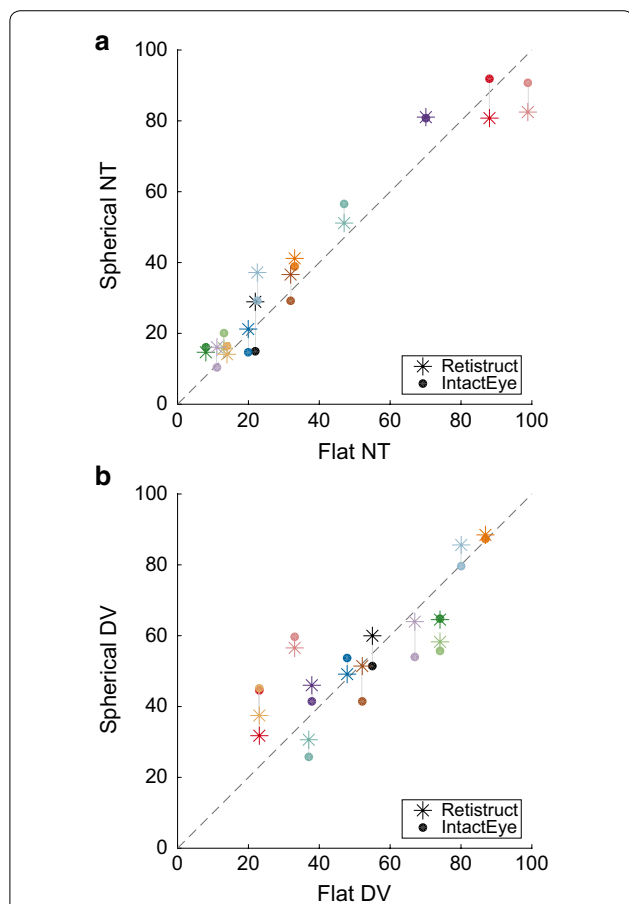


Fig. 5 Comparison of nasotemporal and dorsoventral coordinates for retinal injections derived from three different methods. **a** The coordinates on the flattened retina from the projection method are shown on the x-axis and the NT coordinates on the spherical eye from both Retistruct and the IntactEye method are shown on the y-axis. **b** As in **a**, but for the DV axis. Points estimated from the same eye are shown in the same colour and connected by a thin grey line. The diagonal line shows the case when the coordinates in the flattened and spherical coordinate system agree

Table 1 Pearson correlation coefficient for NT (DV) coordinates between the three methods for data shown in Fig. 5

	Retistruct	IntactEye
Projection	0.97 (0.88)	0.98 (0.74)
IntactEye	0.98 (0.92)	\pm

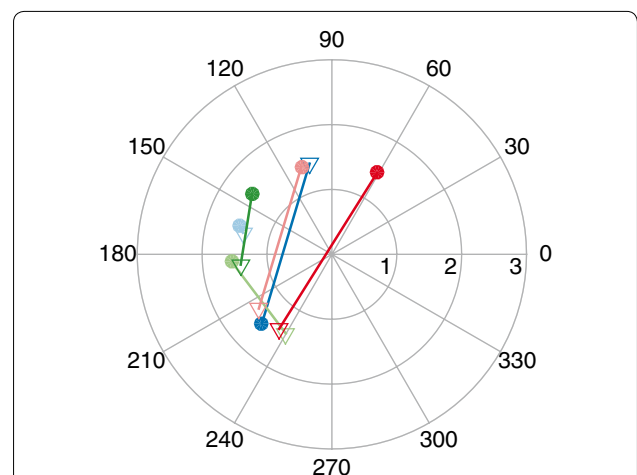
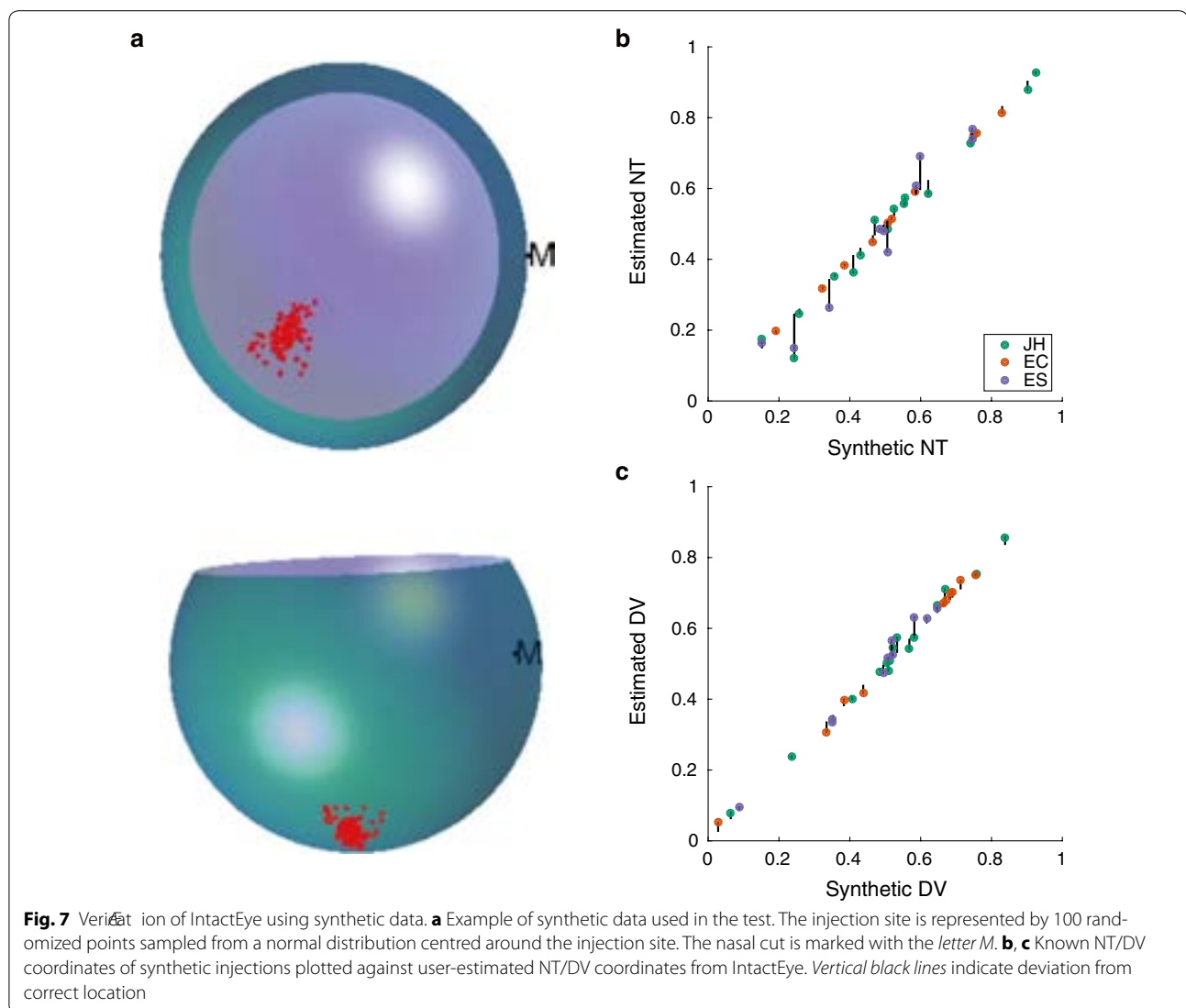


Fig. 6 Estimating the precision of the IntactEye method by locating the optic disc. The optic disc is located in the centre of the eye and was visible in 6 out of 11 retinas. For each of the six retinas, the optic disc location was estimated in polar coordinates using IntactEye (triangles) and Retistruct (filled circles). Lines connect two estimates from the same retina. In all six cases, The optic discs were located within 2° of the geometric centre; by comparison the rim is located at 127° and so the error in locating the optic disc was under 2 %



and 0.99 for NT and DV axis). These images are relatively clean, lacking deformations of the eye and imperfections such as debris and limited depth of field. However, it provides us with images where the centre of the injection is known and allows us to test misalignment of the wireframe spheres onto the images of the eye.

Limitations

Each point that is localised using IntactEye must be uniquely identified in both images of the retina. Because of this limitation the IntactEye method is best suited for finding single injections and other distinct landmarks. If more than one distinct region is labelled with the same dye, it may be difficult to uniquely identify the same region in the two different images. This is known as the correspondence problem in stereo vision [18]. This may

limit the use to anterograde injections where the retinal marking is focused. For retrograde injections in animals where the label is spread over a large region of the retina (e.g. when topographic maps are perturbed, such as Figure 4 of [19]), it is currently better to dissect the retina and then use a program like Retistruct, which analyses the entire retina and can generate density estimates.

Future work

By using the IntactEye method we can locate the centre of a single injection from images taken from any two distinct views where the injection is visible. The program currently only tracks one injection, but could be extended to handle multiple injections of different coloured dyes. This, together with the area estimation, might allow the processing of focal retrograde injections as well, as long

as they are wholly visible in the images, potentially by allowing for additional views of the retina.

The manual placement and alignment of the wireframes takes a few minutes, and is a candidate for automation. However currently the time-intensive part is the data acquisition; for example dissecting out the retina and flattening procedures takes 10 ± 15 min.

An alternative method to our current problem of locating an injection site might be to image the entire eye to generate e.g. a z-stack of images. Although this would avoid the need for any retinal dissection, it does not in itself solve the subsequent problem of registering the retinal location in a standard coordinate space. Therefore, generating volumetric images of eyes would not allow the injection sites to be compared meaningfully with each other. By contrast, if a z-stack is already available for an eye, it should be possible (resolution permitting) to extract two orthogonal images suitable for our program.

Conclusions

We have developed a method that uses two images of an intact retina to derive the location of a retinal injection. This bypasses the need to cut and flatten the retina, improving the accuracy of the localisation as the tissue undergoes less distortion, and saving the experimentalist time. By analysing the data in a coordinate system native to the shape of the eye, we avoid the problem of representing a spherical structure in a flat coordinates. To verify our results we analysed the data in three different ways. We found good correspondence between the coordinates of our IntactEye method and of Retistruct, which uses flattened images and then folds them back onto a sphere. Both methods produce coordinates in the native curved space of the eye. We have solved the abstract problem of deducing the location of a point on a spherical object from two images, and implemented it for our use analysing mouse retinæ, where there are no discernable landmarks for orientation within the retina. It can however be used in other species where retinal landmarks are available, such as the corneal marks in goldfish. Furthermore, this technique might have clinical applications to human retinas, where a reliable coordinate system is required for describing retinal locations, based for example on MRI images. Finally, as our approach is to treat the retina as a simple geometrical, rather than neuronal object, we imagine this technique can be applied straightforwardly to a wide range of fields outside of neuroscience.

Availability and requirements

Project name: IntactEye. Project home page: <http://github.com/hjorthmedh/IntactEye>. Archived version available at: <http://dx.doi.org/10.6084/m9.figshare.1605574>. Operating system(s): Any platform that runs

MATLAB 2014b or later (tested on mac, linux and windows). Programming language: MATLAB. Other requirements: None. Any restrictions to use by non-academics: GPL/MIT.

Abbreviations

N: nasal; T: temporal; D: dorsal; V: ventral; NT: nasotemporal axis; DV: dorsoventral axis.

Authors' contributions

JJJH and DCS designed the algorithm. JJJH wrote the code. ES and MR performed the experiments. JJJH, ES, MR, SJE evaluated the technique. JJJH, DCS, ES, MR, SJE wrote the manuscript. All authors read and approved the final manuscript.

Author details

¹ Cambridge Computational Biology Institute, University of Cambridge, Wilberforce Road, Cambridge CB3 0WA, UK. ² Institute of Cellular and Integrative Neuroscience, CNRS UPR 3212, 5 rue Blaise Pascal, 67084 Strasbourg, France. ³ Institute for Adaptive and Neural Computation, School of Informatics, University of Edinburgh, 10 Crichton Street, Edinburgh EH8 9AB, UK. ⁴ Université de Strasbourg Institut d'études Avancées, 5 rue Blaise Pascal, 67084 Strasbourg, France.

Acknowledgements

SJE and MR gratefully acknowledge the support of the University of Strasbourg Institute for Advanced Study (USIAS). SJE and JJJH were supported by the Wellcome Trust (grant number 083205). The authors wish to thank Elise Cotterill for analysing synthetic data for verification of accuracy.

Competing interests

The authors declare that they have no competing interests.

Received: 12 June 2015 Accepted: 5 November 2015

Published online: 22 November 2015

References

- McLaughlin T, O'Leary DDM. Molecular gradients and development of retinotopic maps. *Annu Rev Neurosci*. 2005;28:327–5. doi:[10.1146/annurev.neuro.28.061604.135714](https://doi.org/10.1146/annurev.neuro.28.061604.135714).
- Chklovskii DB, Koulakov AA. Maps in the brain: what can we learn from them? *Annu Rev Neurosci*. 2004;27:369–92. doi:[10.1146/annurev.neuro.27.070203.144226](https://doi.org/10.1146/annurev.neuro.27.070203.144226).
- Goodhill GJ, Xu J. The development of retinotectal maps: a review of models based on molecular gradients. *Network*. 2005;16:53–4.
- Simon DK, O'Leary DDM. Development of topographic order in the mammalian retinocollicular projection. *J Neurosci*. 1992;12:1212–23.
- Brown A, Yates PA, Burrola P, Ortucò D, Vaidya A, Jessell TM, Pfaff SL, O'Leary DDM, Lemke G. Topographic mapping from the retina to the midbrain is controlled by relative but not absolute levels of EphA receptor signaling. *Cell*. 2000;102:773–8. doi:[10.1016/S0092-8674\(00\)00012-X](https://doi.org/10.1016/S0092-8674(00)00012-X).
- Reber M, Burrola P, Lemke G. A relative signalling model for the formation of a topographic neural map. *Nature*. 2004;431:847–53. doi:[10.1038/nature02957](https://doi.org/10.1038/nature02957).
- Nakamura H, O'Leary DDM. Inaccuracies in initial growth and arborization of chick retinotectal axons followed by course corrections and axon remodeling to develop topographic order. *J Neurosci*. 1989;9:3776–85.
- Suetterlin P, Drescher U. Target-independent ephrinA/EphA-mediated axon-axon repulsion as a novel element in retinocollicular mapping. *Neuron*. 2014;84(4):740–52. doi:[10.1016/j.neuron.2014.09.023](https://doi.org/10.1016/j.neuron.2014.09.023).
- Cang J, Wang L, Stryker MP, Feldheim DA. Roles of Ephrin-as and structured activity in the development of functional maps in the superior colliculus. *J Neurosci*. 2008;28:11015–23. doi:[10.1523/JNEUROSCI.2478-08.2008](https://doi.org/10.1523/JNEUROSCI.2478-08.2008).
- Ullmann JFP, Moore BA, Temple SE, Fernandez-Juricic E, Collin SP. The retinal wholemount technique: a window to understanding the brain and behaviour. *Brain Behav Evol*. 2012;79:264–4.

11. Sterratt DC, Lyngholm D, Willshaw DJ, Thompson ID. Standard anatomical and visual space for the mouse retina: computational reconstruction and transformation of flattened retinæ with the Retistruct package. *PLoS Comput Biol*. 2013;9:1002921. doi:10.1371/journal.pcbi.1002921.
12. Curcio CA, Sloan KR, Meyers D. Computer methods for sampling, reconstruction, display and analysis of retinal whole mounts. *Vision Res*. 1989;29:529-40. doi:10.1016/0042-6989(89)90039-4.
13. Hjorth J.: Github Repository for IntactEye. <https://github.com/Hjorthmedh/IntactEye/archive/master.zip>.
14. Hjorth J. IntactEye Instruction Video. <https://www.youtube.com/watch?v=dn3MqbRjS1Q>.
15. Bevin N, Lemke G, Reber M. Genetic dissection of EphA receptor signaling dynamics during retinotopic mapping. *J Neurosci*. 2011;31:10302-11. doi:10.1523/JNEUROSCI.1652-11.2011.
16. Edelsbrunner H, Kirkpatrick D, Seidel R. On the shape of a set of points in the plane. *IEEE Trans Inform Theor*. 1983;29:551-60. doi:10.1109/TIT.1983.1056714.
17. Dräger UC, Olsen JF. Ganglion cell distribution in the retina of the mouse. *Invest Ophthalmol Vis Sci*. 1981;20:285-93.
18. Marr D, Poggio T. Cooperative computation of stereo disparity. *Science*. 1976;194(4262):283-7. doi:10.1126/science.968482.
19. McLaughlin T, Torborg CL, Feller MB, O'Leary DDM. Retinotopic map refinement requires spontaneous retinal waves during a brief critical period of development. *Neuron*. 2003;40:1147-60. doi:10.1016/S0896-6273(03)00790-6.

**Submit your next manuscript to BioMed Central
and take full advantage of:**

- Convenient online submission
- Thorough peer review
- No space constraints or color figure charges
- Immediate publication on acceptance
- Inclusion in PubMed, CAS, Scopus and Google Scholar
- Research which is freely available for redistribution

Submit your manuscript at
www.biomedcentral.com/submit



Savier, E., Eglén, S.J., Perraut, M., Pfrieger, F.W., Reber, M., *submitted*

Isl2-ephrin-A3KI mouse model

To gain insights on the role of the retinal ephrin-As gradient, a knock-in mouse model was generated: the Isl2-ephrin-A3KI. In this model, 50% of RGCs over-express ephrin-A3 due to the pattern of expression of Islet-2. As a consequence, the Isl2-ephrin-A3KI has two distinct populations of RGCs: one with endogenous levels of ephrin-As (ephrin-A2/A3/A5), and one over-expressing ephrin-A3 in addition. This over-expression quantitatively disrupts the retinal ephrin-A gradient.

Molecular characterization of the Isl2-ephrin-A3KI mouse model

The Isl2-ephrin-A3KI mouse model was characterized by immunostaining and qPCR to assess the over-expression of ephrin-A3. No perturbation was found concerning endogenous ephrin-A expression; mRNA levels of ephrin-A3 in the retina are increased in mutants as compared to wild-types and a strong ephrin-A3 immunostaining colocalize with Isl2 + RGCs. Taken together, these results validated the Isl2-ephrinA3KI mouse model.

Isl2-ephrin-A3KI retino-collicular map

Using lipophilic tracer injections (Dil) and IntactEye (Hjorth et al., 2015), the retino-collicular map was measured in wild-type, heterozygote, and homozygote mutants. Each injection site in the retina is associated to its corresponding projection site in the SC. The map obtained in mutants did not reveal any particular phenotype when compared to the wild-type. These results suggest that retinal ephrin-A3 is not involved in the formation of the retino-collicular map.

Isl2-ephrin-A3KI cortico-collicular map:

Previous studies have revealed an implication of ephrin-As in the formation of the cortico-collicular map (Cang et al., 2005a), and that alignment onto the retino-collicular map depends on the retinal inputs (Triplett et al., 2009). From a developmental aspect, projections from V1 reach the SC after the establishment of the retino-collicular map. Full duplication of the retino-collicular map in Isl2-EphA3KI homozygous mice leads to a duplication of the cortico-collicular map, which originally suggested that activity drives the alignment of both maps (Triplett et al., 2009). Considering these results, the cortico-collicular map was characterized in the Isl2-ephrin-A3KI mouse model with focal Dil injections in V1 at P15, when this map is mature. Interestingly, duplications were observed in 47% of homozygous animals and 43% of heterozygous animals, in the absence of a retino-collicular duplication. In addition, the distance separation is doubled in homozygous animals as compared to heterozygous (7 and 13% of rostral-caudal collicular axis), suggesting an effect that depends on the number of alleles. These observations suggest that molecular signaling plays an important role in the alignment of cortico-collicular projections, in addition to activity. A plausible mechanism is the transportation of retinal ephrin-As to the SC, giving instructions to ingrowing cortical axons. The delay in the formation of both maps is in favor of such a mechanism.

Isl2-EphA3KI x Isl2-ephrin-A3KI retino-collicular map

The Isl2-ephrin-A3KI was crossed with the Isl2-EphA3KI, which expresses EphA3 in the same subpopulation of RGCs. This mutation (Isl2-EphA3KI) leads to a full duplication of the retino-collicular map in homozygous, and a partial duplication in heterozygous animals, with systematic duplication on the caudal pole of the SC, and single termination zones at the rostral pole (Brown et al., 2000; Reber

et al., 2004). Mapping of the retino-collicular projections revealed a single map, with single termination zones along the rostral-caudal axis in the double mutant, reversing the *Isl2-EphA3KI/+* phenotype. This rescue suggests that ephrin-A3/EphA3 co-expression in the same RGC leads to an inactivation of the EphA3 receptor.

***Isl2-EphA3KI x Isl2-ephrin-A3KI* cortico-collicular map**

The cortico-collicular map was also assessed in double mutants. In these animals, no duplications were found, rescuing the *Isl2-ephrin-A3KI/+* phenotype, which confirms joint inactivation of ephrin-A3 ligand and EphA3 receptor.

In silico modeling

To further validate the mechanistic model that was suggested, a computational model was adapted and used to test the results that were obtained. The original model (Koulakov and Tsigankov, 2004) allows for the formation of the retino-collicular map, according to EphA/ephrinA gradients and correlated activity. To reproduce the formation of the cortico-collicular map, the model was extended as follows: 1) Formation of the retino-collicular map 2) Transposition of the retinal ephrin-A gradient to the SC 3) Formation of the cortico-collicular map by interaction between cortical EphAs and transposed ephrin-As. This modeling reproduces the formation of the wild-type cortico-collicular map, but also our findings, with a penetrance and a distance separation similar to the observations in both homozygous and heterozygous *Isl2-ephrin-A3KI*.

A Molecular Mechanism for the Topographic Alignment of Convergent Neural Maps

Elise Savier ^a, Stephen J. Eglan ^{b,c}, Martine Perraut ^a, Frank W. Pfrieger ^a and Michael Reber ^{a,c,*}

^a CNRS UPR3212 – Institute of Cellular & Integrative Neuroscience, Strasbourg, 67084, France

^b Cambridge Computational Biology Institute, Department of Applied Mathematics and Theoretical Physics, University of Cambridge, Cambridge, CB3 0WA, United Kingdom.

^c University of Strasbourg Institute of Advanced Study, Strasbourg, 67084, France.

* Contact: michael.reber@inserm.fr

Abstract

The processing of sensory information requires the proper alignment of neural maps throughout the brain. In the superficial layers of the superior colliculus of the midbrain, converging anterograde axonal projections from ganglion cells in the eye and retrograde projections from neurons in visual cortex must be aligned to form a visuotopic map, but the basic mechanisms that mediate this convergent alignment remain elusive. In a new mouse model, ectopic expression of ephrin-A3 in a subset of retinal ganglion cells does not affect retinocollicular map development but disrupts corticocollicular map alignment onto the retinocollicular map, creating a visuotopic mismatch. In vivo inactivation of ectopically expressed retinal ephrin-A3 restores a wild-type corticocollicular map. Theoretical analyses using a new mapping algorithm model both map formation and alignment, and recapitulate our experimental observations in normal and aberrant conditions. The algorithm is based on a leading sensory map, the retinocollicular map, which carries intrinsic molecular information, the retinal ephrin-As, to the superior colliculus. These ephrin-As subsequently topographically align ingrowing visual cortical axons to the retinocollicular map, allowing the corticocollicular map to compensate for retinocollicular mapping variability.

28 Brain function relies on efficient processing of sensory information, which in turn requires the proper
29 formation and interaction of multiple sensory maps of the world. The superior colliculus (SC) of the
30 midbrain is a major hub for sensory processing as it receives organized inputs from visual, auditory,
31 and somatosensory modalities¹. The SC is a laminated structure controlling visuo-spatial orientation
32 and attention^{1,2}. As such, defective sensory processing in the SC has been associated with psychiatric
33 conditions³. Visual information reaches the superficial layers of the SC, which are innervated both by
34 retinal ganglion cells (RGCs - the retino-collicular projection) and by layer V neurons of the primary
35 visual cortex V1 (the cortico-collicular projection). During development, the retino-collicular map forms
36 during the first post-natal week followed by the cortico-collicular map which develops between P6 and
37 P12⁴. These visuotopic maps must be aligned to ensure efficient modulation of the SC's response by
38 V1 inputs^{5,6}. It has been suggested that the formation of the visuotopy is a stochastic process
39 instructed by a balanced contribution of molecular cues and correlated neuronal activity^{4,7-11}. However
40 the basic principles and underlying molecular mechanisms governing the alignment of converging
41 maps have not yet been fully identified. Potential candidates are gradients of Eph tyrosine kinase
42 receptors and their membrane-bound ligands, the ephrins, already known to control retino-collicular
43 map formation. In the mouse, EphA4/A5/A6 receptors are present on projecting RGCs in a low-nasal
44 to high-temporal gradient. RGC axons are repelled upon EphAs activation by collicular ephrin-
45 A2/A3/A5, expressed in a low-rostral to high-caudal gradient in the SC^{12,13}. Counter-gradients of
46 ligands (ephrin-A2/A3/A5) and receptors (EphA3/A4/A7) are also present in the RGCs and the SC
47 respectively, but their role remains controversial¹⁴⁻¹⁷. In V1, gradients of EphA4/A7, running from high-
48 lateral to low-medial have also been shown and evidence from genetic analyses suggests their
49 involvement in the development of the cortico-collicular projections^{18,19}. Moreover, the formation of the
50 cortico-collicular map requires retinal input^{4,20}, but again, the underlying molecular mechanism
51 remains elusive. Here, we analyze the role of retinal ephrin-As gradients in visuotopic map formation
52 in the SC using new transgenic mice in which ephrin-A3 is ectopically expressed specifically in Isl2(+)
53 RGCs. Surprisingly, Isl2-ephrin-A3KI mice exhibit a normal retino-collicular/geniculate maps and
54 normal ipsi/ contra-lateral projections. In marked contrast, the formation of the cortico-collicular map

55 was severely disrupted, leading to a mix of single and duplicated projections and generating a
56 mismatch with the retino-collicular map. The causal role of ephrin-A3 -ectopic expression was further
57 confirmed when in vivo inactivation by co-expressed EphA3 receptor in the same Isl2(+) RGCs
58 restored a wild-type map. Theoretical modelling recapitulated the observed visuotopic abnormalities
59 induced by ephrin-A3 ectopic expression and therefore validated the basic principle and mechanism of
60 map alignment.

61

62 **Results**

63 **Knock-in mice for ephrin-A3 ectopic expression in Isl2(+) RGCs show normal retino-collicular** 64 **and retino-geniculate projections.**

65 To test the role of retinal ephrin-A ligands in visuotopic map formation, we generated knock-in mice by
66 insertion of a full length ephrin-A3 cDNA into the 3'-UTR region of the Islet-2 gene locus
67 (Supplementary Fig. 1a), similar to a previous approach²¹. Immunohistochemical staining confirmed
68 selective ectopic expression of ephrin-A3 in somata and axons of Isl2(+) RGCs in postnatal day 1 (P1)
69 and P8 ephrin-A3 homozygous knock-in (ephrin-A3KI/KI) mice compared to wild-type (WT) littermates
70 (Fig. 1a-f) without affecting Islet-2 expression at P1 (Fig. 1g,h). Ephrin-A3KI/KI mice present two sub-
71 populations of RGCs: Isl2 (-) cells, expressing wild-type levels of ephrin-A3 and Isl2(+) cells
72 expressing additional ephrin-A3 (Fig. 1e-f,i-n). Ephrin-A3 is observed on RGC neurites in vitro (Fig.
73 1o, o'). Ectopic expression of ephrin-A3 in Isl2(+) RGCs did not induce perceptible changes in
74 synaptic layers nor in retinal organization (Fig. 2a,b). Quantitative RGC-specific transcript (mRNA)
75 analyses confirmed a two-fold increase of ephrin-A3 and normal levels of ephrin-A2/A5 in ephrin-
76 A3KI/KI mutants when compared to WT littermates (Fig. 2c). Together, these data confirmed ectopic
77 expression of ephrin-A3 in Isl2(+) RGCs in our new mouse model.

78 To study retino-collicular map formation, we performed focal Dil anterograde labelling in the retina of
79 P7 mice and analyzed the termination zones (TZs) in the SC at P8, as described²¹⁻²⁴. For quantitative
80 analysis, we measured the locations of the termination zones along the rostral-caudal axis of the SC
81 and the location of the focal Dil injections along the nasal-temporal axis of the retina (Supplementary

82 Fig. 1b,c). Plotting these values in Cartesian coordinates, as described previously, revealed normal
83 retino-collicular maps in ephrinA3KI/KI and ephrin-A3KI/+ mice similar to WT littermates (Fig. 3a).
84 Retrograde labelling confirmed that axons from both Isl2(-) and Isl2(+) RGCs project to the SC (Fig.
85 3b-g). Moreover, anterograde focal injections show normal retino-geniculate mapping (Fig. 3h-k) and
86 labelling by full-eye fills showed normal retino-collicular/geniculate eye-specific segregation (Fig. 3l-o')
87 in ephrin-A3KI/KI similarly to WT littermates. These results demonstrated that ectopic expression of
88 retinal ephrin-A3 in Isl2(+) RGCs does not disturb the formation of the retino-collicular/geniculate
89 mapping nor the eye-specific segregation.

90
91 **Cortico-collicular maps are duplicated in Isl2-ephrin-A3KI mutants**

92 To test whether retinal ephrin guidance cues influence the formation of the V1 cortico-collicular map,
93 we traced cortico-collicular projections from V1 cortex by focal Dil injection in P14 mice and analyzed
94 the location of the TZs in the SC at P15. Quantitative analyses revealed a remarkable duplication of
95 the cortico-collicular map along the rostral-caudal axis of the SC in 47% of ephrin-A3KI/KI (n = 9/19,
96 Fig. 4a) and 43% of ephrin-A3KI/+ (n = 7/16, Fig. 4b) animals when compared to WT littermates (n =
97 9, Fig. 4c). If this heterogeneity is caused by genetic variation between animals, the same type of
98 projections (either single or duplicated) should be observed in both colliculi of a given animal. This
99 was not observed in 60% of ephrin-A3KI/KI (n = 3/5) and 57% of ephrin-A3KI/+ (n = 4/7) animals when
100 we traced the cortico-collicular projections in both left and right colliculi (Fig. 4d). Therefore, genetic
101 variation is unlikely to contribute to map heterogeneity between animals which is rather the
102 consequence of a stochastic process of map formation, as suggested previously¹¹. In 40% of ephrin-
103 A3KI/KI animals showing the same type of projections between colliculi, all of these projections were
104 duplicated whereas in the ephrin-A3KI/+ animals, the remaining 43% presented only single projections
105 in both left and right colliculi, suggesting an effect of the level of ephrin-A3 ectopic expression onto

106 cortico-collicular map duplication. As expected, all WT animals tested (n = 4) showed single
107 projections in both colliculi (Fig. 4d).

108 Next, we calculated the average distance of separation (ΔS_{exp}) between the duplicated maps in
109 Isl2-ephrin-A3KI mutants as a percentage of the rostral-caudal axis of the SC (Fig. 4a,b). This
110 revealed a significant two-fold difference in map separation between ephrin-A3KI/KI (ΔS_{exp} median =
111 13 %, n = 9) and ephrin-A3KI/+ (ΔS_{exp} median = 7 %, n = 7) animals which correlates with the
112 presence of one or two alleles of Isl2-ephrin-A3 (Fig. 4e). Since Isl2 is not expressed in the cortex,
113 these results indicate that ephrin-A3 ectopic expression in Isl2(+) RGC axons destabilizes the
114 stochastic process of cortico-collicular mapping leading to map duplication in Isl2-ephrin-A3KI
115 animals. This in turn implies that V1 EphA+ cortical axons sense the alternating ephrin-A3 levels on
116 RGCs terminals by direct contact with these terminals in the SC¹⁸. Anterograde labelling from retina
117 and V1 cortex showed that both cortical and retinal axons terminals overlap in the superficial layers of
118 the SC (Fig. 4f)^{4,25}. Retrograde labelling confirmed that the cortico-collicular projections originate from
119 layer V neurons in V1 cortex in P14 ephrin-A3KI/KI animals (Supplementary Fig. 2a). Transcript
120 analyses in colliculi and V1 cortices revealed normal levels of ephrinA2/A3/A5 and EphA4/A7
121 receptors in ephrin-A3KI/KI compared to WT littermates at P7 (Supplementary Fig. 2b) excluding
122 indirect effects caused by local changes of gene expression. No bi-cistronic expression of Isl2-ephrin-
123 A3 in either SC or V1 cortex of WT and ephrin-A3KI/KI animals could be detected (Supplementary Fig.
124 2c) ruling out any indirect effects of ectopic ephrin-A3 ectopic expression.

125

126 **In vivo cis-inactivation of ephrin-A3 ectopic expression restores a wild-type cortico-collicular** 127 **map**

128 If the defective cortico-collicular maps in the Isl2-ephrin-A3KI animals were solely due to ephrin-A3
129 ectopic expression in Isl2(+) RGCs, then inactivation of this ectopic expression should rescue the
130 phenotype and restore a wild-type map. Previous work showed that co-expression of ephrin-A3 ligand
131 and EphA3 receptor in the same cell leads to their mutual inactivation through cis-masking²⁶. To
132 accomplish this in vivo, we generated double heterozygous mice carrying ephrin-A3 on one allele of

133 the *Isl2*-2 gene and EphA3 on the second allele (*ephrin-A3KI/EphA3KI*). Immunohistochemical
134 staining confirmed co-expression of ephrin-A3 and EphA3 in acutely isolated double heterozygous
135 RGCs (Fig. 5a). Importantly, previous studies demonstrated that ectopic expression of the EphA3
136 receptor in *Isl2*(+) RGCs in heterozygous *EphA3KI/+* animals results in a duplicated retino-collicular
137 map (Supplementary Fig. 3)²¹. Remarkably, *ephrin-A3KI/EphA3KI* double-mutant mice exhibited a
138 rescued, non-duplicated retinocollicular map, and at the same time, a rescued, non-duplicated cortico-
139 collicular map (Fig. 5b,c). This double restoration of the two maps indicates that cortico-collicular
140 defects in *Isl2*-*ephrin-A3KI* animals were caused by ectopic expression of ephrin-A3 in *Isl2*(+) RGCs
141 and were restored by concomitant expression of EphA3. The cis-inactivation mechanism was cross-
142 validated by the observation of a normal retino-collicular map in the *ephrin-A3KI/EphA3KI* double
143 mutant mice, indicating EphA3 inactivation (Fig. 5c). To further evaluate any residual ephrinA3 or
144 EphA3 signaling activity, we generated *ephrin-A3KI/EphA3KIxEphA4KO* compound mutants. In these
145 mice, decreasing the overall level of retinal EphA receptors by suppressing EphA4 expression would
146 reveal subtle changes in retinal EphA signaling strength^{22,23}. According to the Relative Signaling model
147 in the *EphA3KI/+::EphA4KO* animals analyzed previously²² any residual EphA3 signaling on map
148 formation would generate duplicated retinal TZs, particularly in the caudal part of the SC where nasal
149 RGCs axons, expressing low levels of EphA receptors, project. Anterograde Dil tracing revealed no
150 duplications, even in the caudal pole of the SC, in *ephrin-A3KI/EphA3KI::EphA4+/-* and *ephrin-*
151 *A3KI/EphA3KI::EphA4-/-* compound mutants confirming inactivation of EphA3 and ephrin-A3 (Fig.
152 5d,e). Altogether, these results suggest that EphA3 and ephrin-A3 ectopic expression in the same
153 RGCs lead to their mutual inactivation and confirm that cortico-collicular mapping duplications
154 observed in *Isl2*-*ephrin-A3KI* animals are the consequence of retinal ephrin-A3 ectopic expression.

155

156 **In silico modelling and theoretical analysis of cortico-collicular map alignment**

157 Our results suggest that the level of ephrin-A3 on RGC projections innervating the SC influences the
158 mapping and alignment of the cortico-collicular projections. To simulate the mechanism of map
159 alignment, we created a 3-step Map Alignment model based on an algorithm originally developed to

160 model the retino-collicular mapping^{8,9,11}. Our version generates first the retino-collicular map based on
161 retinal EphA receptors and collicular ephrin-A graded expression. The second step transposes the
162 retinal ephrin-A gradients onto the rostral-caudal axis of the SC according to the layout of the retino-
163 collicular map generated in step one. In the third step, the cortico-collicular map is generated based
164 on cortical EphA receptors expression and the transposed retinal ephrin-As in the SC. Each map is
165 generated by a stochastic process based on balanced forces between repelling EphAs forward
166 signaling and associating correlated neuronal activity^{8,9,11} (see Experimental Procedures). To improve
167 the validity of our model, we replaced the theoretical values of the retinal EphAs and ephrin-As
168 gradients previously used^{7,8,11,27} by our experimental quantification of retinal EphA mRNAs²² ($R_{A(x)}^{\text{retina}}$)
169 and ephrin-A mRNAs ($L_{A(x)}^{\text{retina}}$) (Fig. 6a,b, Box1). $L_{A(x)}^{\text{retina}}$ equations were derived from semi-
170 quantitative in situ hybridization as described²² (Fig. 6a, b) and from our transcripts analyses
171 measuring the relative expression levels of ephrin-As in acutely isolated RGCs (Fig. 2c). In
172 accordance with previous work¹⁵⁻¹⁷, we observed graded expression of ephrin-A2 and A5 along the
173 nasal-temporal axis of the retina, whereas ephrin-A3 is homogeneously expressed in WT animals
174 (Fig. 6a, b).

175 Curve fitting using MATLAB revealed the equation $L_{A(x)}^{\text{retina WT}}$ modelling WT retinal ephrin-As
176 ligands (Box 1, equations 1-4). The two-fold increase of ephrin-A3 in ephrin-A3KI/KI RGCs compared
177 to WT (Fig. 2c) was included into the model by adding a constant ΔL_{A3} to $L_{A(x)}^{\text{retina WT}}$ thus generating
178 the $L_{A(x)}^{\text{retina KI}}$ alternating ectopic expression in the Isl2-ephrin-A3KI retinas (Box 1, equation 5, 6). The
179 3-step Map Alignment model simulates the sequential mapping of 100 RGCs onto a 1D array of 100
180 SC neurons along the rostral caudal axis, followed by 100 V1 cortical neurons innervating the SC. We
181 made two assumptions: (1) endogenous collicular ephrin-As were no longer active for incoming V1
182 axons as they have been engaged previously in RGCs axon guidance by binding to retinal EphAs
183 (forward signaling) which leads to the cleavage of their extracellular domains²⁸, (2) retinal ephrin-A3
184 expression alone cannot provide positional information in the SC as its expression is not graded in the
185 RGCs. Consequently, a proportion of graded retinal ephrin-A2/A5 acts together with ephrin-A3 to
186 provide positional information in the SC. Initially, the TZs of all RGCs and V1 axons in the SC are

187 generated randomly and exchanged with a probability proportional to the degree to which the switch
188 reduces the energy of the system^{7,8,11} (see Experimental Procedures for detailed description of the
189 model). After 10^7 iterations per run ($n = 20$ runs) for each genotype, stable and organized retino-
190 collicular maps were formed (Fig. 7a,d,g). Thereafter, a proportion of retinal ephrin-As gradients were
191 transposed in the SC (Fig. 7b,e,h). After this transposition, the cortico-collicular maps are generated in
192 a similar fashion (Fig. 7c,f,i). We further analyzed the theoretical cortico-collicular maps using a linear
193 regression (Fig. 7c,f,i, red lines) and an exclusion parameter EP (Fig. 7f,i, dashed grey lines) which
194 corresponds to the variability of the WT single map (Fig. 7c, dashed grey lines, $\sigma_{WT} = 2.18\%$) added to
195 the genotype-specific average map separation (ΔS_{exp}) calculated for Isl2-ephrin-A3KI animals (Fig. 4f;
196 $EP_{KI/KI} = 15.18\%$; $EP_{KI/+} = 9.18\%$; Fig. 6f,i). The points, simulating the position of the cortico-collicular
197 TZs along the rostral-caudal axis of the SC, located outside EP correspond to duplicated projections
198 whereas the points located within EP correspond to single projections (Fig. 7f,i). The percentages of
199 duplicated projections generated by the model for ephrin-A3KI/KI and ephrin-A3KI/+ were similar to
200 the percentages of observed duplications (Fig. 4a,b) (one sample t-test, ephrin-A3KI/KI, $P = 0.17$;
201 ephrin-A3KI/+, $P = 0.22$; Fig. 7j).

202 These results indicated that the 3-step Map Alignment model simulates both the retino- and
203 cortico-collicular mapping and accurately recapitulates the normal and defective visual maps. It
204 predicts the stochastic nature of the mapping abnormalities in ephrin-A3KI/+ and ephrin-A3KI/KI
205 animals due to the ephrin-A3 ectopic expression in a subset of RGCs. Hence the model provides

206 further evidence that retinal ephrin-A3 contributes to the alignment of the cortico-collicular map by
207 providing positional information in the SC for ingrowing V1 axons carrying EphAs.

208

209 **Discussion**

210 Using mouse molecular genetics and theoretical modelling, we describe a molecular mechanism and
211 associated principles governing the alignment of converging neural maps in the brain.

212 **Retinal ephrin-A3 in cortico-collicular mapping**

213 We showed that modestly elevated expression of ephrin-A3 exclusively in a subset of RGCs disturbed
214 cortico-collicular map alignment in the SC, pointing to a mechanism where retinal ephrin-A3 provides
215 positional information to ingrowing V1 cortico-collicular axons. Further confirmation came from the
216 genetic inactivation of over-expressed ephrin-A3 using co-expressed EphA3 receptor. Trans-binding of
217 ephrin-As and EphAs could be abolished through cis-interaction when EphA3/ephrin-A3, are co-
218 expressed in the same cell, including RGCs^{26,29-33}. We therefore generated double heterozygous
219 mutants, ephrin-A3KI/EphA3KI. The strength of this approach resides in the fact that each individual
220 ephrin-A3KI/+ and EphA3KI/+ mutant shows robust visuotopic map abnormalities^{4,11,21-23}. The
221 presence of wild-type retino- and cortico-collicular maps in the ephrin-A3KI/EphA3KI double
222 heterozygous mutants provides compelling evidence that both ephrin-A3 and EphA3 were inactivated
223 in Isl2(+) RGCs. Further evidence of ephrin-A3/EphA3 inactivation came from the presence of normal
224 retino-collicular maps in compound mutants ephrin-A3KI/EphA3KI::EphA4 knock-outs. These results,
225 together with the normal expression levels of collicular and cortical EphA receptors and ephrin-As
226 ligands in Isl2-ephrin-A3KI animals, confirmed the causal role of retinal ephrin-A3 ectopic expression
227 on cortico-collicular alignment defects and suggested that retinal projections play an instructive role in
228 cortico-collicular map formation.

229 The heterogeneity of the cortico-collicular phenotype in the Isl2-ephrin-A3KI mutants, revealed
230 by a mix of single and duplicated projections, is in accordance with previous data showing a variable
231 penetrance of the retinotopic mapping abnormalities in constitutive or conditional ephrin-As knock-
232 outs³⁴⁻³⁶. Such variable penetrance of the mutant phenotype can be explained by the stochastic nature

233 of map formation driven by opposing forces resulting from EphA signaling, which tends to separate
234 neighboring RGCs through repulsion, and correlated neuronal activity, which tends to reinforce
235 neighboring RGCs projections on adjacent target cells^{4,35}. The general pattern of V1 collicular
236 projections (Fig. 4a-c) is consistent with the involvement of cortical EphA receptors gradients (high-
237 lateral to low-medial)¹⁸ repelled by low-rostral to high-caudal ephrin-As gradients of retinal origin in the
238 SC (forward signaling). In the *Isl2-ephrin-A3KI* animals, retinal ephrin-A3 oscillation in the SC
239 organizes neighbor-neighbor relationships of V1 axons through repulsion locally inducing a small
240 distance of map duplication. Our model is consistent with retinal matching, suggesting that retinal
241 inputs are required for proper cortico-collicular mapping^{4,13,20}.

242 In our model, retinal inputs carry molecular cues, ephrin-A3 and likely other retinal ephrin-As,
243 to provide positional information for ingrowing V1 axons (Fig. 8). Retinal ephrin-As act then together
244 with correlated neuronal activity pattern shared between RGCs and V1 axons^{4,13} for cortico-collicular
245 map alignment. Triplett and colleagues³⁷ also suggested a gradient-matching model which posits that
246 collicular ephrin-As are required for the mapping of somatosensory inputs to the SC which behave
247 similarly to the retino-collicular projections as they also require collicular ephrin-As³⁷. In contrast, the
248 requirement of collicular ephrin-As for cortico-collicular mapping is unlikely. In this particular scenario,
249 cortico-collicular projections in previously characterized *EphA3KI/KI* mutants would have led to a
250 single TZ in the SC, leading to a mismatch between cortico- and retino-collicular maps which was not
251 observed^{4,13}. More investigations are required, in particular using conditional ephrin-As knock-outs, to
252 identify the role of ephrin-As from input structures versus collicular ephrin-As in the formation of the
253 sensory maps across the layers of the SC.

254 **Retinal ephrin-A3 in retino-collicular mapping**

255 The presence of non-duplicated retino-collicular maps in both *ephrin-A3KI/+* and *ephrin-A3KI/KI*
256 mutants, as revealed by Dil tracing, suggests that retinal ephrin-A3 does not play a significant role in
257 the formation of this map, consistent with previous work on ephrin-A3-null mutants²⁷. Several
258 hypotheses have been raised as to how retinal ephrin-As may participate in retino-collicular map
259 formation using *in vitro*, *ex vivo* and *in vivo* approaches in mouse and chick. For example, ephrin-As

260 on RGC axons are activated by collicular EphAs (reverse signaling), leading to axon repulsion³⁸⁻⁴⁰ or
261 branch inhibition in the SC⁴¹. In our mouse model, this mechanism would generate a segregation
262 between Isl2(-) and Isl2(+) RGC axons in the SC, the latter being more repelled by collicular EphAs.
263 However, such a segregation did not occur, excluding the involvement of retinal ephrin-A3 in such
264 reverse signaling. In vitro and in vivo transfection analyses in chick suggested that retinal ephrin-A3
265 bind to co-expressed retinal EphAs in the same RGCs leading to inactivation/masking of the EphA
266 receptors rendering those axons are less sensitive to ephrin-As binding in the target tissue^{29-32,42,43}.

267 In our model, this mechanism would lead to a stronger inactivation of the EphA4/A5/A6
268 receptors in the Isl2(+) RGCs expressing high levels of ephrin-A3, compared to RGCs with normal
269 ephrin-A3 expression level. According to the Relative Signaling model, distinct RGCs population with
270 different levels of active EphAs should generate a duplicated retino-collicular map (partial or full)²¹⁻²³.
271 However, we did not observe any retino-collicular mapping defects regardless of the mutant
272 genotypes, suggesting that ephrin-A3 ectopic expression does not inactivate co-expressed
273 EphA4/A5/A6 receptors in RGCs, although we showed specific inactivation of EphA3, suggesting
274 specific interactions in *cis* between ephrin-A/EphA pairs as previously observed^{26,33,43}. Conditional
275 ablation revealed that high retinal ephrin-A5 on nasal RGCs axons prevents temporal RGC axons
276 from targeting the caudal SC through fiber-fiber interaction³⁶. In our mice, such mechanism would
277 have generated a local duplication between Isl2(+) and Isl2(-) RGCs or an extension of the TZs in the
278 SC which was not observed, suggesting that retinal ephrin-A3 is not involved in fiber-fiber interaction.
279 However, these results do not exclude the contribution of the fiber-fiber interaction mechanism to map
280 development. Together with recent results³⁶, our data suggest also that retinal ephrin-A3 and ephrin-
281 A5 present distinct functions in visuotopic mapping, suggesting a member-specific role of retinal
282 ephrin-As in map formation. This is in contrast with retinal EphA receptors which are considered as
283 functionally interchangeable^{22,23}.

284 **Theoretical modelling further confirms mapping mechanism**

285 Previous work modelled the stochastic nature of retino-collicular map formation based on the
286 Koulakov model^{8,9,11}. Here, we have substantially modified this algorithm using our measured ephrin-A

287 expression data instead of theoretical values ,and simulated the retino- and cortico-collicular mapping
288 process sequentially. We assumed that retinal ephrin-A3 expression alone cannot provide positional
289 information, due to its homogeneous expression profile in WT RGCs. Therefore other ephrin-As or
290 other guidance molecules, either retinal or collicular, must participate in the regulation of map
291 alignment. Although retinal ephrin-A5 has been recently shown to participate in RGCs fiber-fiber
292 interactions³⁶ we cannot exclude that a given proportion is also involved in map alignment. Moreover,
293 contribution of endogenous collicular ephrin-As to cortico-collicular map alignment seems unlikely as
294 these mediated previous RGCs axons guidance. Therefore, we chose to retain 80% of the retinal
295 ephrin-A5 level and 100% of retinal ephrin-A2/A3 levels in the algorithm. The 3-step Map Alignment
296 model replicates features of both retino- and cortico-collicular maps observed in WT and Isl2-ephrin-
297 A3KI animals. It validates a stochastic mechanism of retinal-dependent molecular cues, involving
298 ephrin-A3, providing positional information in the SC for V1 axons which may then coordinate with
299 correlated neuronal activity⁴ to align visuotopic maps.

300 These data raise important new questions as to the function of the different endogenous
301 ephrin-As in the formation of topographic maps, requiring additional development of cell-specific gene
302 targeting approaches. From a functional standpoint, this new principle may serve as a general
303 framework for sensory map alignment, where positional information, carried by the leading map, acts
304 together with correlated activity, enabling fine adjustments of the subsequent projections alignment
305 and therefore compensating for subtle mapping variations.

306 **Methods**

307 **Generation of the Isl2-ephrin-A3KI mice, animals and housing.**

308 The targeting construct containing a ribosomal entry site (IRES) followed by the mouse ephrin-A3
309 ORF-SV40polyA and the selection cassette PGK-Neo was inserted by homologous recombination in
310 the 3' untranslated region of the Islet-2 gene locus as previously performed²¹. The mouse line was
311 generated by the Mouse Clinic Institute, project IR3483 (Illkirch-France) in a C57/Bl6J background.
312 Mice were hosted in a 12h/12h light-dark condition, fed ad lib. at the CNRS UMS3415 Chronobiotron
313 (Strasbourg – France). All procedures were in accordance with national (council directive 87/848,
314 October 1987) and European community (2010/63/EU) guidelines. Official agreement number for
315 animal experimentation is A67-395, protocol number 01831.01 (M.R). Males and females C57/Bl6J
316 ephrin-A3KI, EphA3KI and EphA4KO mice and pups were genotyped by PCR from genomic DNA
317 from tail biopsies as described previously²². Primers are available upon request. All experiments were
318 made blind to genotype.

319 **Projections analysis/mapping.**

320 Anterograde and retrograde Dil (1,1-dioctadecyl-3,3,3,3-tetramethylindocarbocyanine perchlorate)
321 and/or retrograde CTB-488 (Cholera Toxin B subunit-Alexa 488) labelling were performed as
322 described^{4,22}. Whole-mount SC were processed as described and TZs were plotted along the rostral-
323 caudal axis on Cartesian coordinates (y axis)²². For cortico-collicular map analyses, sagittal vibratome
324 sections were performed on P14 SC and TZs were plotted along the rostral-caudal axis on Cartesian
325 coordinates (y axis). Retinas were dissected and imaged using Zeiss Axioscope 2 and Axiovision
326 software. Retinal coordinates of the Dil injections were calculated using IntactEye algorithm²⁴,
327 confirmed using the projection method²² and plotted on Cartesian coordinates (x axis). V1 cortices
328 were photographed as whole-mount and focal injections plotted along the V1 lateral-medial axis (x
329 axis)⁴. Retino-collicular and cortico-collicular maps were generated using non-parametric smoothing
330 technique, termed LOESS smoothing⁴⁴, to estimate the profile of the one-dimensional mapping either
331 from retina to SC, or from V1 to SC. To estimate the variability in a mapping containing N data points,
332 we repeat the procedure N times with N-1 datapoints, each time dropping a different datapoint. This is

333 termed a "leave-one-out" method and was used in the R statistical computing environment. Scripts are
334 available upon request. Retino-geniculate and binocular tracings were performed as described²⁷ on
335 ephrin-A3KI/KI (n = 4) and WT (n = 3) P7 animals.

336 **Immunohistochemistry.**

337 Retinas were dissected after animal perfusion with PFA4%, post-fixed O/N in PFA4%, cryoprotected in
338 PFA4%/sucrose 30% for several hours at 4°C. Retinas were cryostat-sectioned (14-18 µm) and
339 processed for immunohistochemistry. Briefly, sections were incubated in blocking solution
340 (PBS1X/BSA1%/serum10%) for 1hr at RT then incubated with primary antibody O/N at 4°C in
341 PBS1X/BSA1%/serum1%. The following day, sections were washed (3X5' in PBS1X at RT) and
342 incubated for 1hr at RT with secondary Alexa-labelled antibodies in PBS1X/BSA1%/serum1%. After 3
343 washes at RT (3X5' PBS1X), slides were mounted in Aqua-Polymount (Polysciences Europe GmbH,
344 Eppelheim, Germany) and visualized under a confocal microscope (Leica SP5 II, Leica Microsystems,
345 Wetzlar, Germany). Sections were imaged using Leica LASAF software. Antibodies: anti-Isl2 (ref. LS-
346 C165303), anti-ephrin-A3 (ref. LS-C6547) and anti-EphA3 (ref. LS-C150188) at respectively 1/400,
347 1/300 and 1/100 dilutions (LifeSpan Biosciences Inc., Seattle, WA), anti-ephrin-A3 (ref. 36-7500,
348 1/200, Invitrogen, Invitrogen Co., Camarillo, CA), anti-synaptophysin (ref. S5768, 1/200, Sigma), anti-
349 rabbit Alexa 488 / anti-goat Alexa 594 (1/500, Invitrogen, Invitrogen Co., Camarillo, CA)

350 **Quantitative RT-PCR.**

351 V1 cortices, superficial layers of the SC and retinas were freshly dissected. Retinas were cut in three
352 equal pieces along the NT axis (Nasal, Central, Temporal RGCs) and RGCs acutely isolated^{45,46}. Total
353 RNA was extracted and quantified as previously described³. Relative quantification was performed
354 using the comparative Delta Ct method. Triplicates were run for each sample and concentration for the
355 target gene and for two housekeeping genes (hypoxanthine-guanine phosphoribosyl transferase -
356 HPRT and glyceraldehyde 3-phosphate dehydrogenase – GAPDH) were computed. Primer
357 sequences are: ephrin-A2 (forward: TCCCCCTTGATCATGTGACCT, reverse:
358 GGTAGGTAGCTCCCCTTCCT), ephrin-A5 (forward: TTGATGGGTACAGTGCCTGC, reverse:
359 TTCCGAGAACTTCAGCGGTC), ephrin-A3 (forward: TATGAATTCCATGCCGGCCAA, reverse:

360 GCAGACGAACACCTTCATCCT), EphA4 (forward: GAGGCTCCTGTGTCAACAACT, reverse:
361 AGTTGCCAATGGGTACCAGC), EphA7 (forward: TCCTCCTTAGTCGAGGTCCG, reverse:
362 GCCACTCTCCTTCTGCACTG)

363 **Retinal ganglion cell isolation.**

364 P3/P4 retinas were freshly dissected and RGCs were isolated and purified (>99%) as previously
365 described^{45,46}. After isolation, RGCs were either treated for RNA extraction or fixed with PFA4% 15' at
366 RT and processed for immunohistochemistry. Stainings were performed and cells were visualized as
367 described above.

368 **Semi-quantitative in situ hybridization and gradient fitting.**

369 Analysis of ephrin-As expression was performed as previously described²² on nasal-temporal 20um
370 thick sections of P1/P2 WT retinas. Probes used were: mouse ephrin-A2 (NM007909.3, 879bp, pos.
371 387-1266), mouse ephrin-A3 (NM010108, 791bp, pos. 208-999) and ephrin-A5 (NM207654, 696bp,
372 pos. 189-885). Experimental values (mean +SD, ephrin-A2/A3/A5, for each ephrin-As, n = 18 sections
373 total, 3 sections/retina, from 6 retinas -2 left, 2 right- from 3 animals were plotted along the nasal-
374 temporal axis and fitted using MATLAB (curve fitting application).

375 **In silico replication of the duplication of the cortico-collicular map.**

376 The Koulakov model^{8,9} was used to simulate the formation of both the retino- and cortico-collicular maps
377 in the presence of an oscillatory ephrin-A gradient in the target structure. Each brain structure (retina,
378 SC, V1) is modelled as a 1-d array of 100 neurons in each network. Two maps are generated: first, the
379 map from retina to SC; second, the map from V1 to SC. Each map is modelled sequentially in the same
380 way. This model consists in the minimization of affinity potential (E) which is computed as follow:

$$381 \quad E = E_{\text{act}} + E_{\text{chem}}$$

382 At each step, this potential is minimized by switching two randomly chosen axons probabilistically
383 according to the degree such a switch reduces the energy in the system by Delta E (ΔE). The
384 probability of switching, p, is given by: $p = 1 / (1 + e^{(4\Delta E)})$

385 E_{chem} is expressed as follow:

$$386 \quad E_{\text{chem}} = \sum_i \in \text{synapses} \alpha [R_A(i) - R_A(r')] [L_A(i) - L_A(r')]$$

387 where α is the strength ($\alpha = 200$), $R_A(i)$ the receptor concentration in the retina and $L_A(r')$ the ligand
388 concentration at the corresponding position in the SC.

389 The contribution of activity-dependent process is modelled as:

$$390 E_{act} = -\gamma/2 \sum_{i \in \text{synapses}} C_{ij} U(r'_i r'_j)$$

391 where $\gamma = 1$ is the strength parameter, C_{ij} is the cross-correlation of neuronal activity between two
392 RGCs during retinal waves, and U simulates the overlap between two SC cells. Here, we use $C_{ij} =$
393 $e^{(-r/R)}$, where r is the retinal distance between axons i and j , $R = 0.11 \times N$, and $U(r') = e^{(-r'^2/2d^2)}$, where r'
394 is the distance between two SC points and $d = 3$.

395 Receptor and ligand gradients were modelled as follow:

$$396 \text{ Retinal EphAs gradients}^{22} \quad R_{A(x)}^{\text{retina}} = 0.26e^{0.023x} + 1.05$$

$$397 \text{ Cortical V1 EphAs gradients}^{7,8} \quad R_{A(x)}^{\text{V1}} = e^{(-x/N)} - e^{x/(N-2)}$$

$$398 \text{ Collicular ephrin-As gradients}^{7,8} \quad L_{A(x)}^{\text{SC}} = e^{(x-N)/N} - e^{(-x-N)/N}$$

399 $L_{A(x)}^{\text{retina}}$ is the ephrin-A gradient which was modelled by an exponential fitting the in situ hybridization
400 data. This retinal ephrin-A gradient is translated to the SC for the simulation of the cortico-collicular
401 map.

$$402 \text{ Retinal ephrin-As gradients (see Results): } L_{A(x)}^{\text{retina}} = 0.56e^{0.14x} + 0.54e^{0.08x} + 0.44$$

403 where $x = 1 \dots N$ is the coordinate along the NT axis.

404 Oscillatory gradient was generated by randomly attributing to 50% of collicular cells an overexpression
405 of ephrinA3 (ΔL_{A3}) with $\Delta L_{A3} = 0.44$ for homozygotes and $\Delta L_{A3} = 0.22$ for heterozygotes. Iterations
406 were ran for 10^7 epochs. Codes and scripts are available upon request.

407 **Quantitative analysis of theoretical maps.**

408 To determine the amount of duplication that could be found in heterozygotes and homozygotes
409 mutants a linear regression was calculated using implemented functions in Matlab. The residuals were
410 then used to calculate the percentage of duplication. Duplication were considered when values were
411 outside EP = 9.18 % for ephrin-A3KI/+ and EP = 15.18 % for ephrin-A3KI/KI, which corresponds to the
412 averaged experimental distances measured between duplicated termination zones (ΔS_{exp}) to which
413 was added the wild-type map variability (average of residuals, $\sigma_{WT} = 2.18$ %, $n = 20$ runs). Twenty runs

414 were performed and averaged to find the proportion of duplicated termination zones for Isl2-ephrin-
415 A3KI.

416 **Data/Codes Availability.**

417 All relevant data in the manuscript and supplementary files are available from authors upon request.

418 Codes for the Leave-One-Out method and for the 3-Step Alignment model are available upon request.

419 **References:**

- 420 1. May, P.J. The mammalian superior colliculus: laminar structure and connections. *Prog. Brain Res.*
421 Elsevier, pp 321–378 (2006).
- 422 2. Krauzlis, R.J., Lovejoy, L.P. & Zenon, A. Superior colliculus and visual spatial attention. *Annu. Rev.*
423 *Neurosci.* **36**, 165-82 (2013).
- 424 3. Mathis, C. *et al.* Defective response inhibition and collicular noradrenaline enrichment in mice with
425 duplicated retinotopic map in the superior colliculus. *Brain Struct. Funct.* **220**, 1573-84 (2015).
- 426 4. Triplett, J.W., Owens, M.T., Yamada, J., Lemke, G., Cang, J., Stryker, M.P. & Feldheim, D.A.
427 Retinal input instructs alignment of visual topographic maps. *Cell* **139**, 175-85 (2009).
- 428 5. Zhao, X., Liu, M. & Cang, J. Visual cortex modulates the magnitude but not the selectivity of
429 looming-evoked responses in the superior colliculus of awake mice. *Neuron* **84**, 202-13 (2014).
- 430 6. Liang, F., Xiong, X.R., Zhang, L.I. & Tao, H.W. Sensory cortical control of a visually induced arrest
431 behaviour via corticotectal projections. *Neuron* **86**, 755-767 (2015).
- 432 7. Chandrasekaran, A.R., Plas, D.T., Gonzalez, E. & Crair, M.C. Evidence for an instructive role of
433 retinal activity in retinotopic map refinement in the superior colliculus of the mouse. *J. Neurosci.* **25**,
434 6929-38 (2005).
- 435 8. Tsigankov, D.N. & Koulakov, A.A. A unifying model for activity-dependent and activity-independent
436 mechanisms predicts complete structure of topographic maps in ephrin-A deficient mice. *J.*
437 *Comput. Neurosci.* **21**, 101-14 (2006).
- 438 9. Tsigankov, D. N. & Koulakov, A.A. Sperry versus Hebb: topographic mapping in *Isl2/EphA3* mutant
439 mice. *BMC Neurosci.* **29**, 11-155 (2010).
- 440 10. Ackman, J.B. & Crair, M.C. Role of emergent neural activity in visual map development. *Curr.*
441 *Opin. Neurobiol.* **24**, 166–175 (2014).
- 442 11. Owens, M.T., Feldheim, D.A., Stryker, M.P. & Triplett, J.W. Stochastic Interaction between Neural
443 Activity and Molecular Cues in the Formation of Topographic Maps. *Neuron* **87**, 1261-73 (2015).
- 444 12. Lemke, G. & Reber, M. Retinotectal mapping: new insights from molecular genetics. *Annu. Rev.*
445 *Cell Dev. Biol.* **21**, 551–580 (2005).
- 446 13. Cang, J. & Feldheim, D.A. Developmental mechanisms of topographic map formation and
447 alignment. *Annu. Rev. Neurosci.* **36**, 51–77 (2013).
- 448 14. Feldheim, D.A. & O’Leary, D.D.M. Visual map development: bidirectional signalling, bifunctional
449 guidance molecules, and competition. *Cold Spring Harb. Perspect. Biol.* **2**, a001768 (2010).
- 450 15. Triplett, J.W. & Feldheim, D.A. Eph and ephrin signalling in the formation of topographic maps.
451 *Semin. Cell Dev. Biol.* **23**, 7–15 (2012).
- 452 16. Suetterlin, P., Marler, K.M. & Drescher, U. Axonal ephrinA/EphA interactions, and the emergence
453 of order in topographic projections. *Semin. Cell Dev. Biol.* **23**, 1–6 (2012).
- 454 17. Weth, F., Fiederling, F., Gebhardt, C. & Bastmeyer, M. Chemoaffinity in topographic mapping
455 revisited--is it more about fiber-fiber than fiber-target interactions? *Semin. Cell Dev. Biol.* **35**, 126–
456 135 (2014).

- 457 18. Cang, J., Kaneko, M., Yamada, J., Woods, G., Stryker, M.P. & Feldheim D.A. Ephrin-as guide the
458 formation of functional maps in the visual cortex. *Neuron* **48**, 577-89 (2005).
- 459 19. Wilks, T.A., Rodger, J. & Harvey, A.R. A role for ephrin-As in maintaining topographic organization
460 in register across interconnected central visual pathways. *Eur J Neurosci.* **31**, 613-22 (2010).
- 461 20. Khachab, M.Y. & Bruce, L.L. The development of corticocollicular projections in anophthalmic
462 mice. *Brain Res. Dev. Brain Res.* **14**, 179-92 (1999).
- 463 21. Brown, A., Yates, P.A., Burrola, P., Ortuño, D., Vaidya, A., Jessell, T.M., Pfaff, S.L., O'Leary, D.D.
464 & Lemke, G. Topographic mapping from the retina to the midbrain is controlled by relative but not
465 absolute levels of EphA receptor signalling. *Cell* **102**, 77–88 (2000).
- 466 22. Reber, M., Burrola, P. & Lemke, G. A relative signalling model for the formation of a topographic
467 neural map. *Nature* **431**, 847–853 (2004).
- 468 23. Bevins, N., Lemke, G. & Reber, M. Genetic dissection of EphA receptor signalling dynamics during
469 retinotopic mapping. *J. Neurosci.* **31**, 10302–10 (2011).
- 470 24. Hjorth, J.J., Sterratt, D.C., Cutts, C.S., Willshaw, D.J. & Eglon, S.J. Quantitative assessment of
471 computational models for retinotopic map formation. *Dev. Neurobiol.* **75**, 641-66 (2015).
- 472 25. Phillips, M.A., Colonnese, M.T., Goldberg, J., Lewis, L.D., Brown, E.N. & Constantine-Paton, M. A
473 synaptic strategy for consolidation of convergent visuotopic maps. *Neuron.* **71**, 710-24 (2011).
- 474 26. Falivelli, G., Lisabeth, E.M., Rubio de la Torre, E., Perez-Tenorio, G., Tosato, G., Salvucci, O. &
475 Pasquale, E.B. Attenuation of eph receptor kinase activation in cancer cells by coexpressed ephrin
476 ligands. *PLoS One* **29**, e81445 (2013).
- 477 27. Pfeiffenberger, C., Yamada, J. & Feldheim, D.A. Ephrin-As and patterned retinal activity act
478 together in the development of topographic maps in the primary visual system. *J. Neurosci.* **26**,
479 12873-84 (2006).
- 480 28. Janes, P.W., Saha, N., Barton, W.A., Kolev, M.V., Wimmer-Kleikamp, S.H., Nievergall, E., Blobel,
481 C.P., Himanen, J.P., Lackmann, M. and Nikolov, D.B. Adam meets Eph: an ADAM substrate
482 recognition module acts as a molecular switch for ephrin cleavage in trans. *Cell* **123**, 291-304
483 (2005).
- 484 29. Connor, R.J., Menzel, P. & Pasquale, E.B. Expression and Tyrosine Phosphorylation of Eph
485 Receptors Suggest Multiple Mechanisms in Patterning of the Visual System. *Dev. Biol.* **193**, 21–35
486 (1998).
- 487 30. Hornberger, M.R. *et al.* Modulation of EphA receptor function by coexpressed ephrinA ligands on
488 retinal ganglion cell axons. *Neuron* **22**, 731–742 (1999).
- 489 31. Menzel, P., Valencia, F., Godement, P., Dodelet, V.C. & Pasquale, E.B. Ephrin-A6, a new ligand
490 for EphA receptors in the developing visual system. *Dev. Biol.* **230**, 74–88 (2001).
- 491 32. Carvalho, R.F., Beutler, M., Marler, K.J.M., Knöll, B., Becker-Barroso, E., Heintzmann, R., Ng, T. &
492 Drescher, U. Silencing of EphA3 through a cis interaction with ephrinA5. *Nat. Neurosci.* **9**, 322–330
493 (2006).
- 494 33. Klein, R. & Kania, A. Ephrin signalling in the developing nervous system. *Curr. Opin. Neurobiol.*
495 **27**, 16-24 (2014).
- 496

- 497 34. Feldheim, D.A., Kim, Y.I., Bergemann, A.D., Frisén, J., Barbacid, M. & Flanagan, J.G. Genetic
498 analysis of ephrin-A2 and ephrin-A5 shows their requirement in multiple aspects of retinocollicular
499 mapping. *Neuron* **25**, 563-74 (2000).
- 500 35. Cang, J., Niell, C.M., Liu, X., Pfeifferberger, C., Feldheim, D.A. & Stryker, M.P. Selective
501 disruption of one Cartesian axis of cortical maps and receptive fields by deficiency in ephrin-As and
502 structured activity. *Neuron* **57**, 511-23 (2008).
- 503 36. Suetterlin, P. & Drescher, U. Target-independent ephrina/EphA-mediated axon-axon repulsion as
504 a novel element in retinocollicular mapping. *Neuron* **84**, 740–752 (2014).
- 505 37. Triplett, J.W., Phan, A., Yamada, J. & Feldheim, D.A. Alignment of multimodal sensory inputs in
506 the superior colliculus through a gradient-matching mechanism. *J. Neurosci.* **32**, 5264-71 (2012).
- 507 38. Rashid, T., Upton, A.L., Blentic, A., Ciossek, T., Knöll, B., Thompson, I.D. & Drescher, U.
508 Opposing gradients of ephrin-As and EphA7 in the superior colliculus are essential for topographic
509 mapping in the mammalian visual system. *Neuron* **47**, 57–69 (2005).
- 510 39. Lim, Y.-S., McLaughlin, T., Sung, T.-C., Santiago, A., Lee, K.-F. & O'Leary, D.D.M. p75(NTR)
511 mediates ephrin-A reverse signalling required for axon repulsion and mapping. *Neuron* **59**, 746–
512 758 33 (2008).
- 513 40. Yoo, S., Kim, Y., Noh, H., Lee, H., Park, E. & Park, S. Endocytosis of EphA receptors is essential
514 for the proper development of the retinocollicular topographic map. *EMBO J.* **30**, 1593-607 (2011).
- 515 41. Yates, P.A., Roskies, A.L., McLaughlin, T. & O'Leary, D.D. Topographic-specific axon branching
516 controlled by ephrin-As is the critical event in retinotectal map development. *J. Neurosci.* **21**, 8548–
517 8563 (2001).
- 518 42. McLaughlin, T. & O'Leary, D.D. Functional consequences of coincident expression of EphA
519 receptors and ephrin-A ligands. *Neuron* **22**, 636-9 (1999).
- 520 43. Yin, Y., Yamashita, Y., Noda, H., Okafuji, T., Go, M.J. & Tanaka, H. EphA receptor tyrosine
521 kinases interact with co-expressed ephrin-A ligands in cis. *Neurosci. Res.* **48**, 285–296 (2004).
- 522 44. Efron, B. & Tibshirani, R. Statistical data in the computer age. *Science* **253**, 390-95 (1991).
- 523 45. Steinmetz, C.C., Buard, I., Claudepierre, T., Nägler, K. & Pfriederger, F.W. Regional variations in the
524 glial influence on synapse development in the mouse CNS. *J. Physiol.* **577**, 249–261 (2006).
- 525 46. Claudepierre, T., Koncina, E., Pfriederger, F.W., Bagnard, D., Aunis, D. & Reber, M. Implication of
526 neuropilin 2/semaphorin 3F in retinocollicular map formation. *Dev. Dyn.* **237**, 3394–3403 (2008).
- 527

528 **Acknowledgements:**

529 We thank G. Lemke for helpful comments, Dr. Sophie Reibel-Foisset and Laurence Huck (UMS 3415
530 CNRS – Chronobiotron, Strasbourg, France) for mouse colony management, Dr. Nick Bevins and Dr.
531 Alexandre Charlet for technical help, Dr. Melinda Owens for providing the Koulakov/Triplett scripts in
532 MATLAB. This work was supported by CNRS and University of Strasbourg – Institute for Advanced
533 Study (M.R.).

534

535 **Author Contributions:**

536 E.S., M.P. and M.R. performed the experiments. S.E. generated the Leave-One-Out algorithm. E.S.,
537 S.E and M.R. generated the theoretical modelling. E.S., S.E. F.W.P. and M.R. analyzed the results.
538 M.R. wrote the manuscript with the participation of all the authors.

539

540 **Competing financial interests**

541 Authors declare having no competing financial interest

542

543 **Materials and Correspondence**

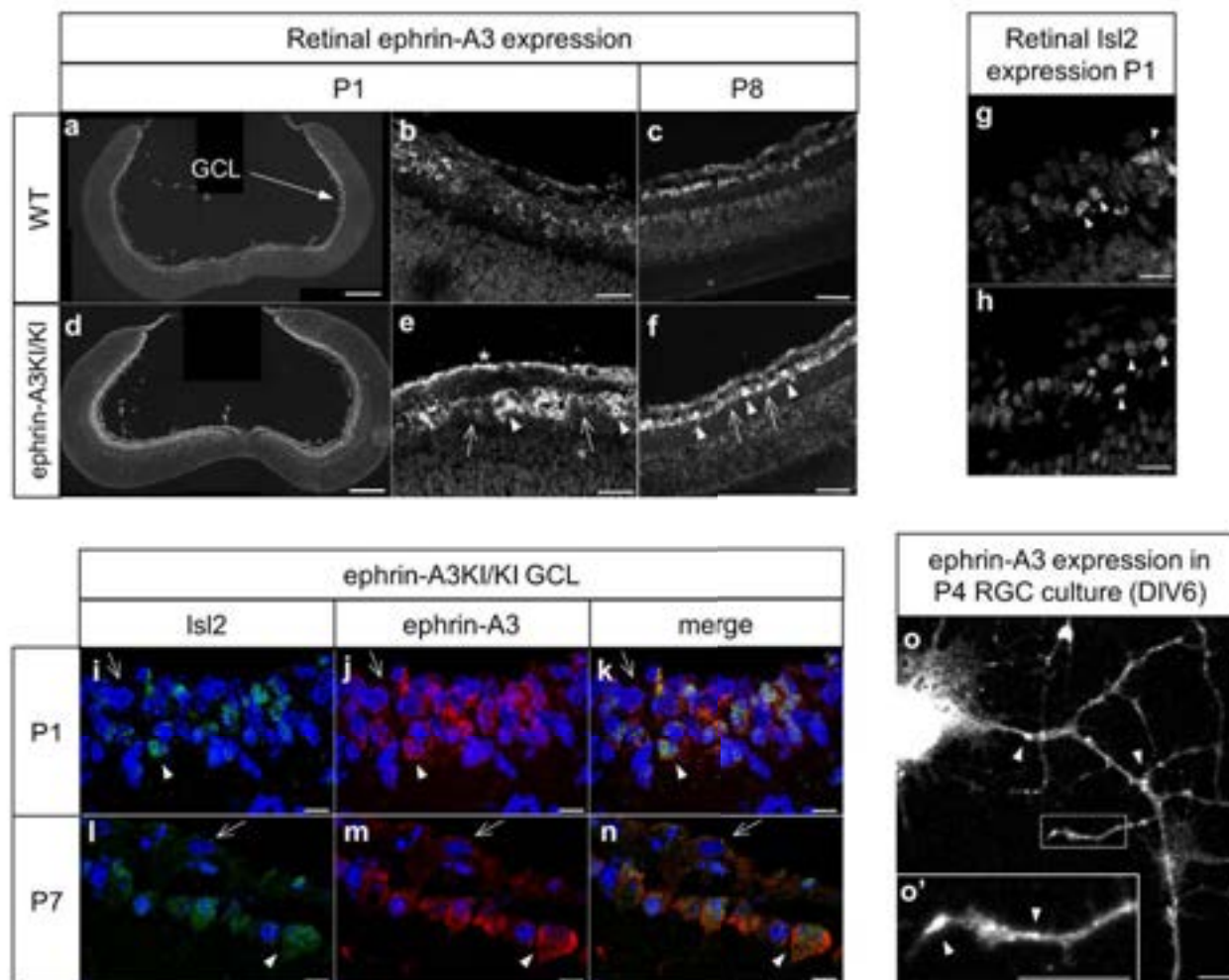
544 Material requests and correspondence should be addressed to M.R. email: michael.reber@inserm.fr

545

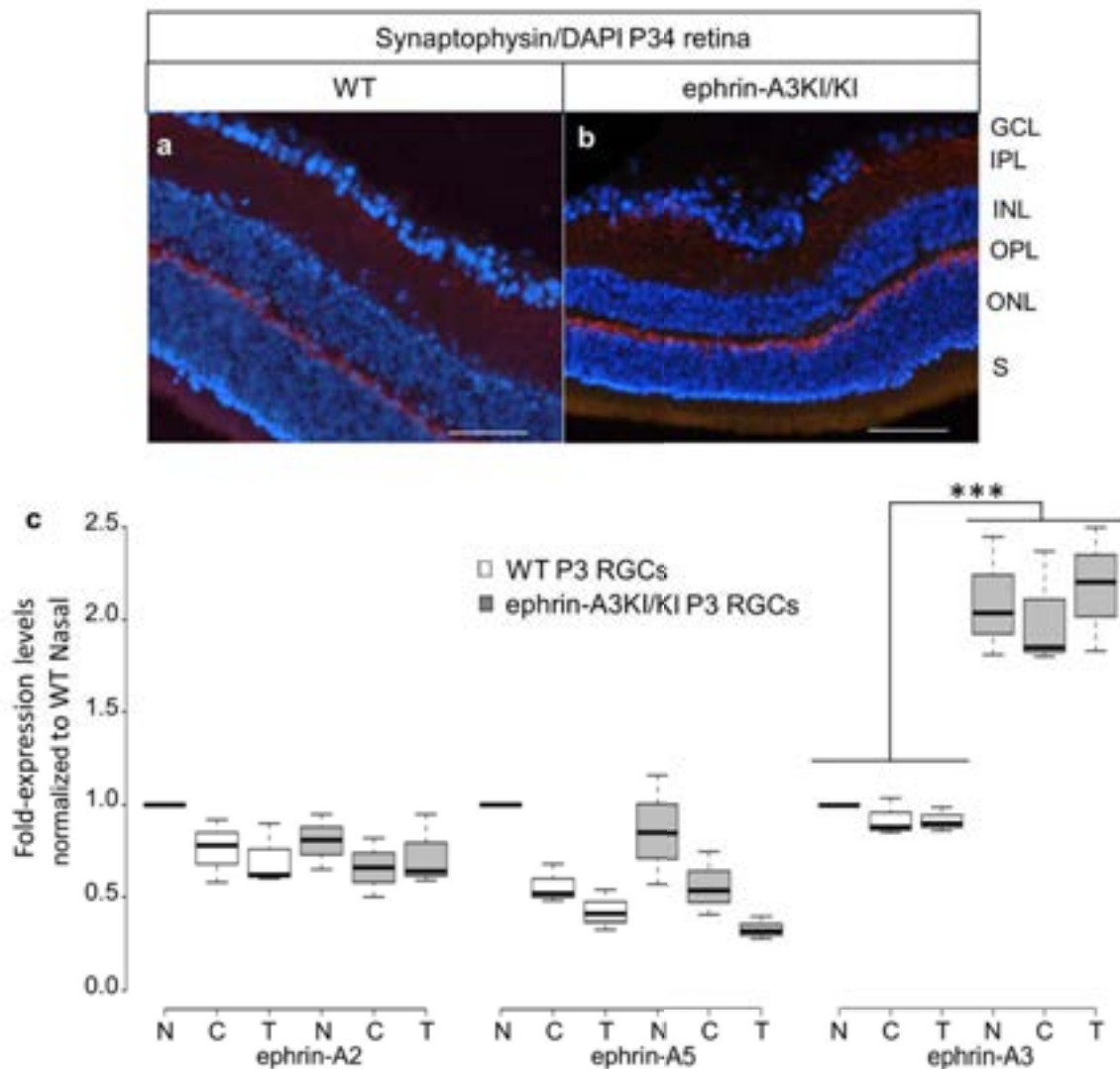
546

547

548

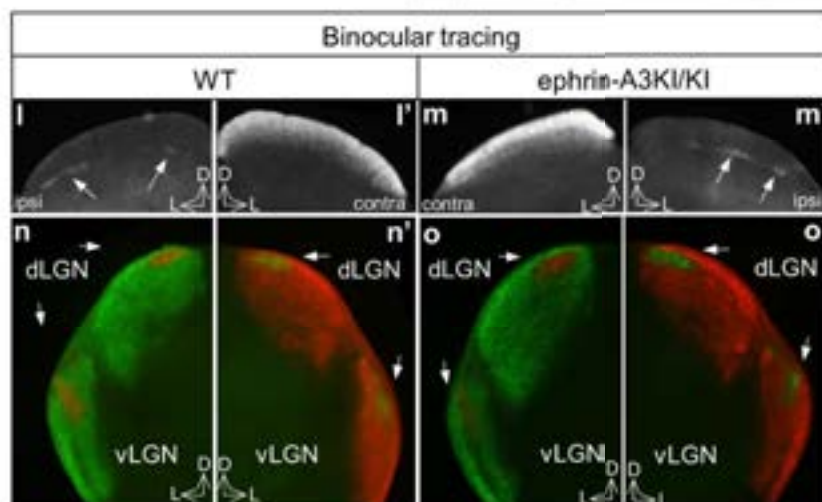
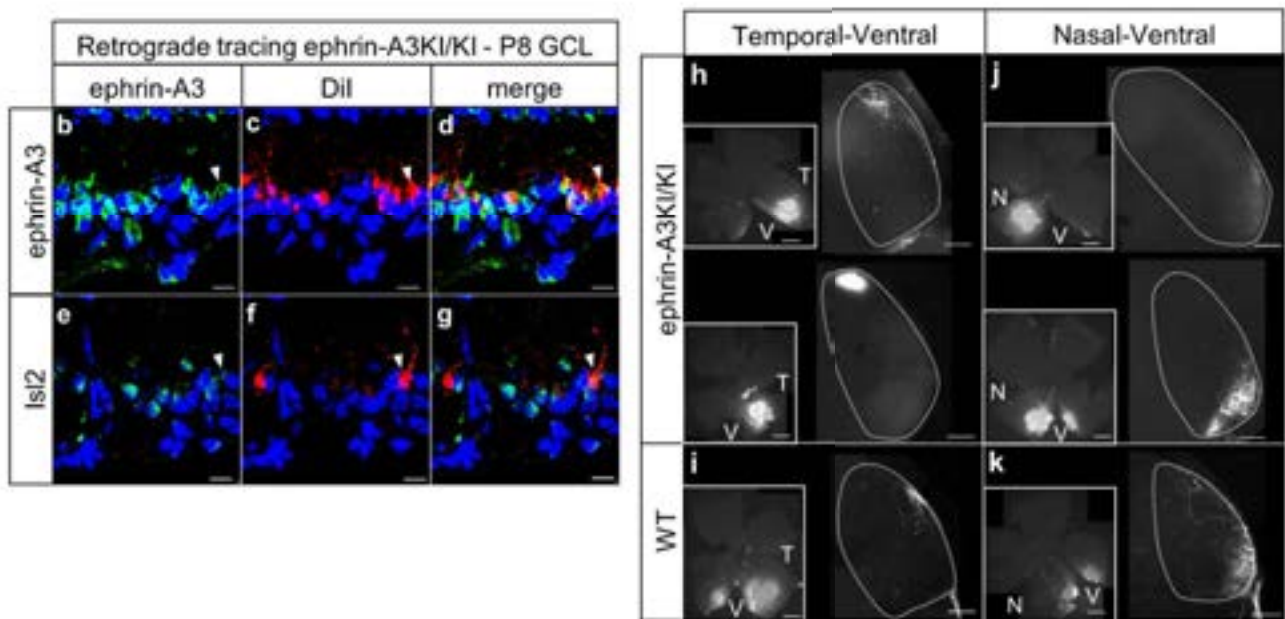
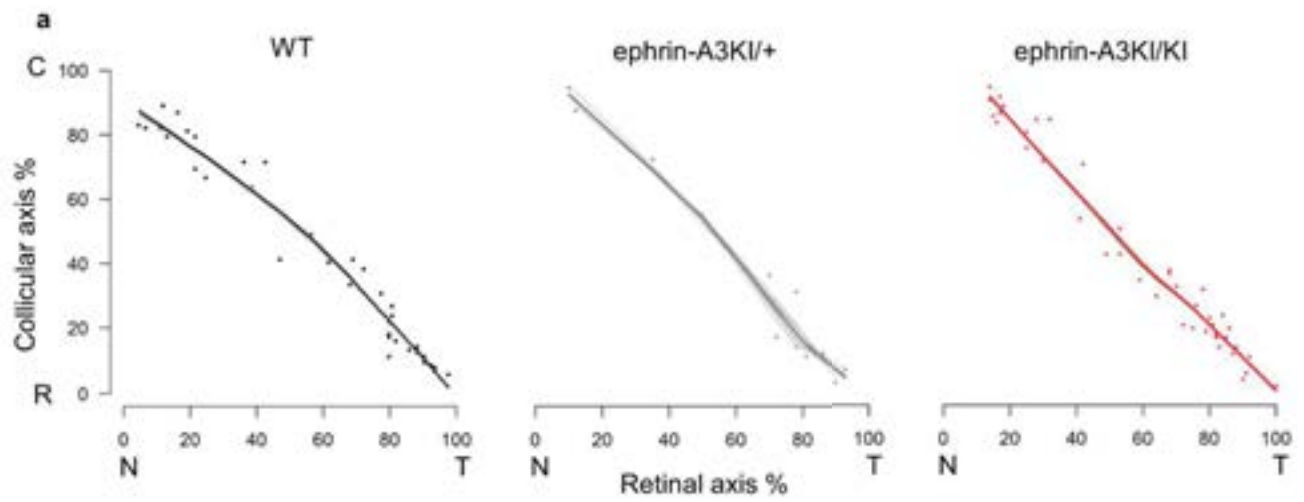


550 **Figure 1 Validation of the ephrin-A3KI/KI model I.** (a-f) Immunostaining of ephrin-A3 in P1 (a, b)
 551 and P8 (c) WT (n = 3 animals) and P1 (d, e) and P8 (f) ephrin-A3KI/KI (n = 5 animals) RGCs. In (e, f)
 552 arrows indicate ephrin-A3 WT expression level in RGCs, arrowheads indicate ephrin-A3 ectopic
 553 expression in RGCs and asterisk indicates high ephrin-A3 labelling in the fiber layer. Scale bars
 554 represent 200 μm (a, d), 20 μm (b-f). (g-h) Immunostaining of Islet-2 in P1 WT (n = 3 animals) (g) and
 555 ephrin-A3KI/KI (n = 5 animals) (h) RGCs. Arrowheads indicate Isl2(+) RGCs. Scale bars represent 20
 556 μm. (i-n) Immunostaining of Islet-2 (i, l), ephrin-A3 (j, m) and merged (k, n) in P1 and P7 ephrin-
 557 A3KI/KI (n = 5 animals) RGCs. Arrowheads indicate Isl2(+) / high ephrin-A3 RGCs. Arrows indicate
 558 Isl2 (-) / wild-type ephrin-A3 expressing RGCs. Scale bars represent 10 μm. (o, o') ephrin-A3
 559 immunostaining on P4 RGC in culture (DIV 6) (n = 4 animals). Arrowheads indicate stained neurites.
 560 Scale bars represent 10 μm. GCL, ganglion cell layer, RGC, retinal ganglion cell.

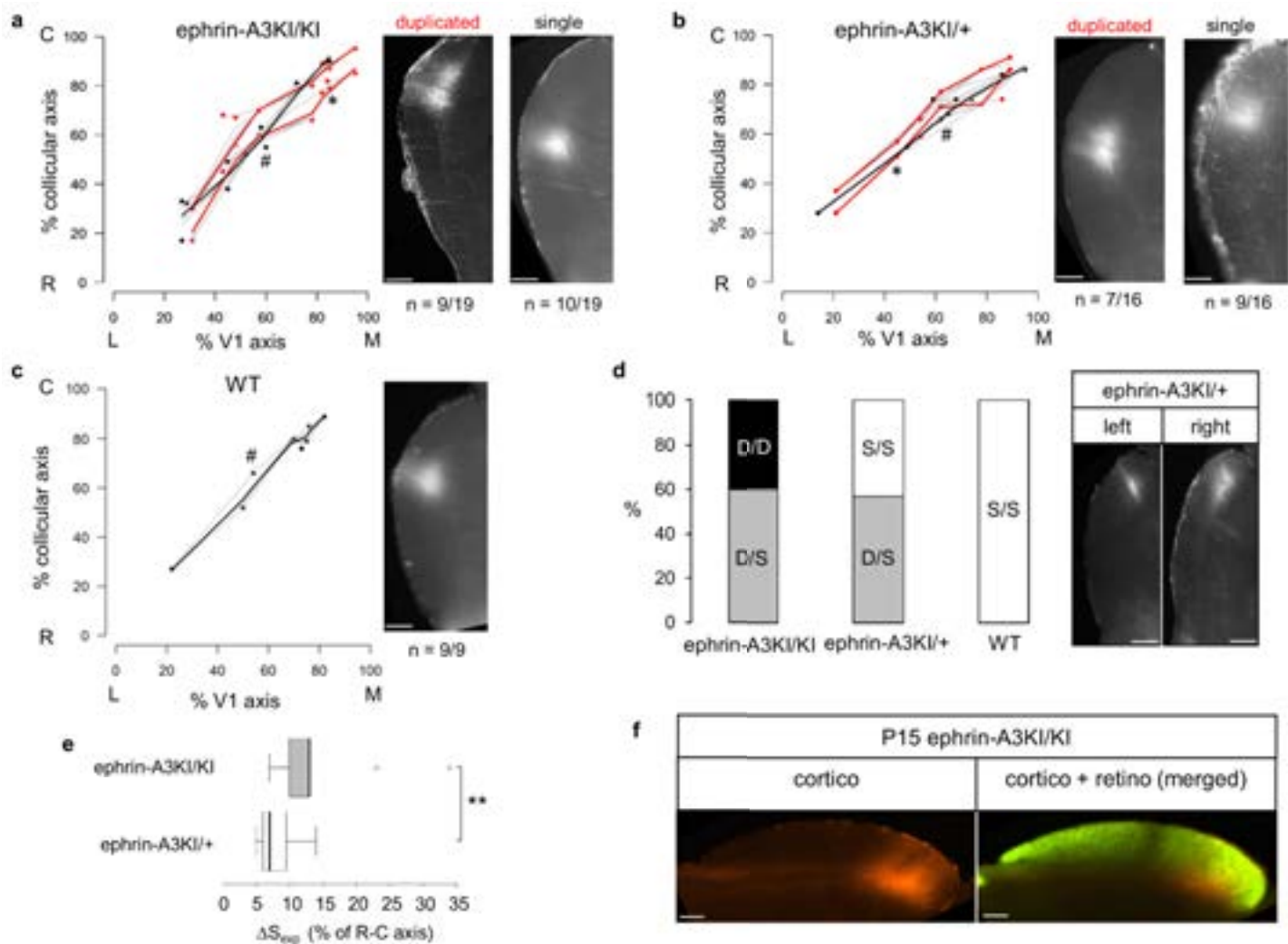


562 **Figure 2 Validation of the ephrin-A3KI/KI model II.** (a, b) Synaptophysin and DAPI staining in P34
 563 WT (n = 4 animals) (a) and ephrin-A3KI/KI (n = 4 animals) (b) retinas. Scale bars represent 50 μm. (c)
 564 Ephrin-As expression relative to WT nasal from nasal (N), central (C) and temporal (T) RGCs and
 565 normalized against GAPDH and HPRT in P3 WT and ephrin-A3KI/KI (WT, n = 6 animals / 12 retinas;
 566 ephrin-A3KI/KI, n = 8 animals / 16 retinas, variables are normally distributed, two-way ANOVA: ephrin-
 567 A2 genotype $F_{11,3} = 1.79$, $p = 0.11$; ephrin-A5 genotype $F_{11,3} = 2.08$, $p = 0.07$; ephrin-A3 genotype $F_{11,3}$
 568 $= 8.11$, $***p < 0.001$). WT, wild-type; GCL, ganglion cell layer; IPL, inner plexiform layer; INL, inner
 569 nuclear layer; OPL, outer plexiform layer; ONL, outer nuclear layer; S, outer and inner segments.

570



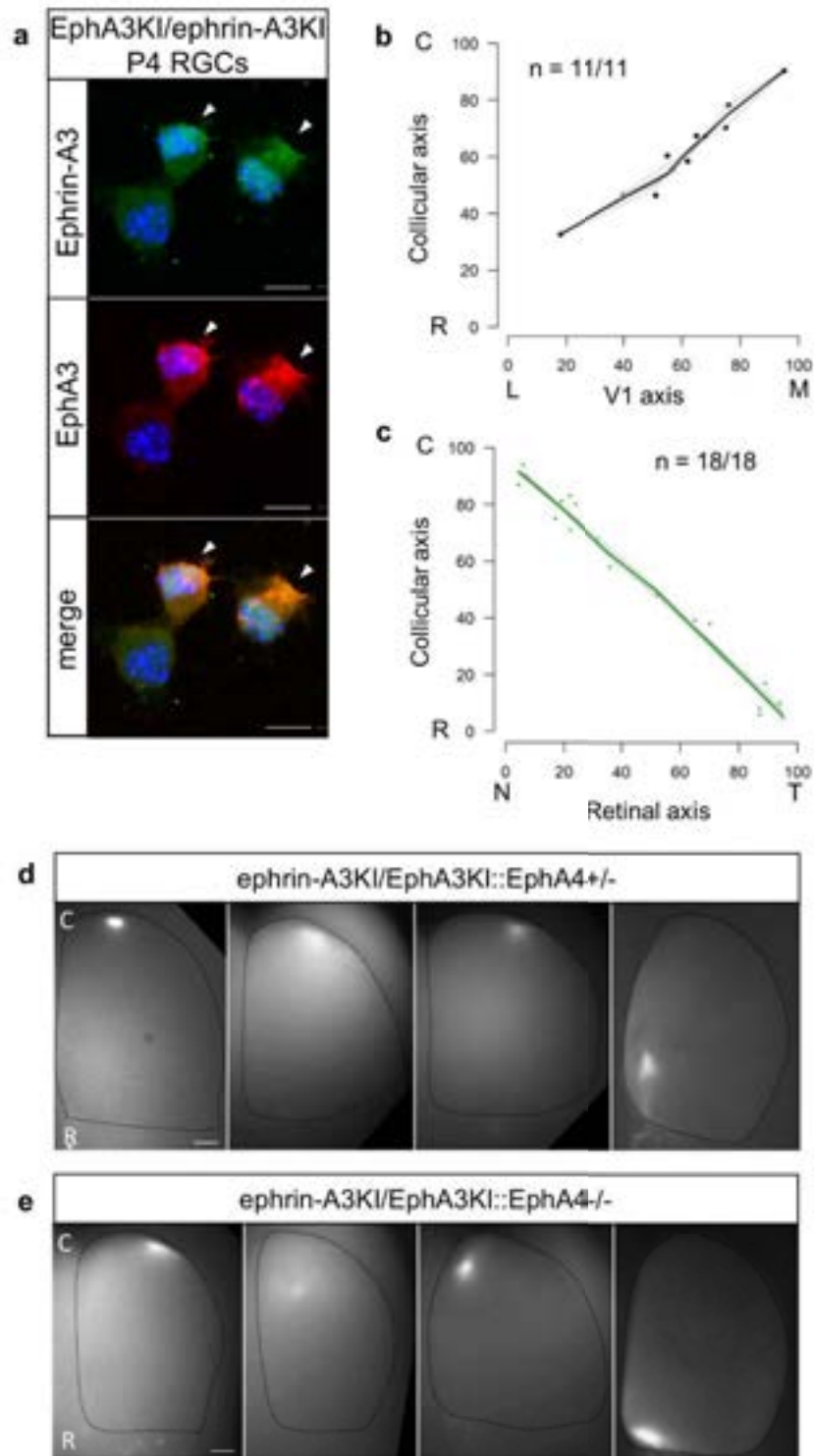
572 **Figure 3 Anterograde mapping and retrograde Dil labelling in P8 animals.** (a) Retino-collicular
573 maps generated by the Leave-One-Out method at P8 in WT (n = 38 animals), ephrin-A3KI/+ (n = 15
574 animals) and ephrin-A3KI/KI (n = 43 animals) mutants. (b-g) P8 Dil retrograde labelling coupled to
575 immuno-staining of ephrin-A3 (b-d) and Isl2 (e-g) in ephrin-A3KI/KI (n = 4 animals) mutant retinas.
576 Arrowheads indicate Isl2(+) / high ephrin-A3 Dil labelled RGCs. Scale bars represent 10 μ m. (h-k)
577 Anterograde focal Dil injections showing no difference in retino-geniculate mapping from the temporal-
578 ventral (T-V) (h, i) and nasal-ventral (N-V) (j, k) retinal quadrants between ephrin-A3KI/KI (n = 4
579 animals) and WT (n = 4 animals) P8 littermates. Scale bars represent 400 μ m. (l-o') Anterograde full-
580 eye injections showing normal binocular projections in P8 WT (n = 3 animals) SC (l, l'), LGN (n, n')
581 and in ephrin-A3KI/KI (n = 4 animals) SC (m, m') and LGN (o, o'). WT, wild-type; T, temporal; N,
582 nasal; R, rostral; C, caudal, vLGN, ventral lateral geniculate nuclei; dLGN, dorsal lateral geniculate
583 nuclei.
584



586

587 **Figure 4 Anterograde cortico-collicular mapping in P14 animals.** (a-c) Cortico-collicular maps
 588 generated by the Leave-One-Out method at P15 in ephrin-A3KI/KI (n = 19 animals) (a), ephrin-A3KI/+
 589 (n = 16 animals) (b) and WT (n = 9 animals) (c) mutant littermates. Right panels in a, b and c show an
 590 example of duplicated and/or single cortical TZs in collicular sagittal sections in different animals. The
 591 corresponding coordinates are labelled by an asterisk (duplicated) or a hashtag (single). Scale bars
 592 represent 400 μ m. (d) Percentage of heterogeneous duplicated/single (D/S) or homogeneous
 593 single/single or duplicated/duplicated (S/S or D/D) projections in both colliculi of the same animal
 594 (ephrin-A3KI/KI, n = 5 animals; ephrin-A3KI/+, n = 7 animals; WT, n = 4 animals). Right panel show an
 595 example of cortico-collicular TZs from left and right colliculi in a P15 ephrin-A3KI/+ animal. Scale bars
 596 represent 400 μ m. (e) Mean separation between duplicated maps measured experimentally (ΔS_{exp}) in

597 ephrin-A3KI/KI (median = 13 %, 1st quartile = 10 %, 3rd quartile = 13 %, n = 9 animals) and ephrin-
598 A3KI/+ (median = 7 %, 1st quartile = 6 %, 3rd quartile = 9.5 % n = 7 animals) (non-parametric Mann &
599 Whitney test, ** p = 0.020). (f) Sagittal section of P15 ephrin-A3KI/KI (n = 4 animals) Dil labelled
600 cortical projection (left) and merged image of CTB-488 full-eye fill and cortical Dil projection (right).
601 Scale bars represent 200 μ m. L, lateral; M, medial; R, rostral; C, caudal; S, single; D, duplicated.
602

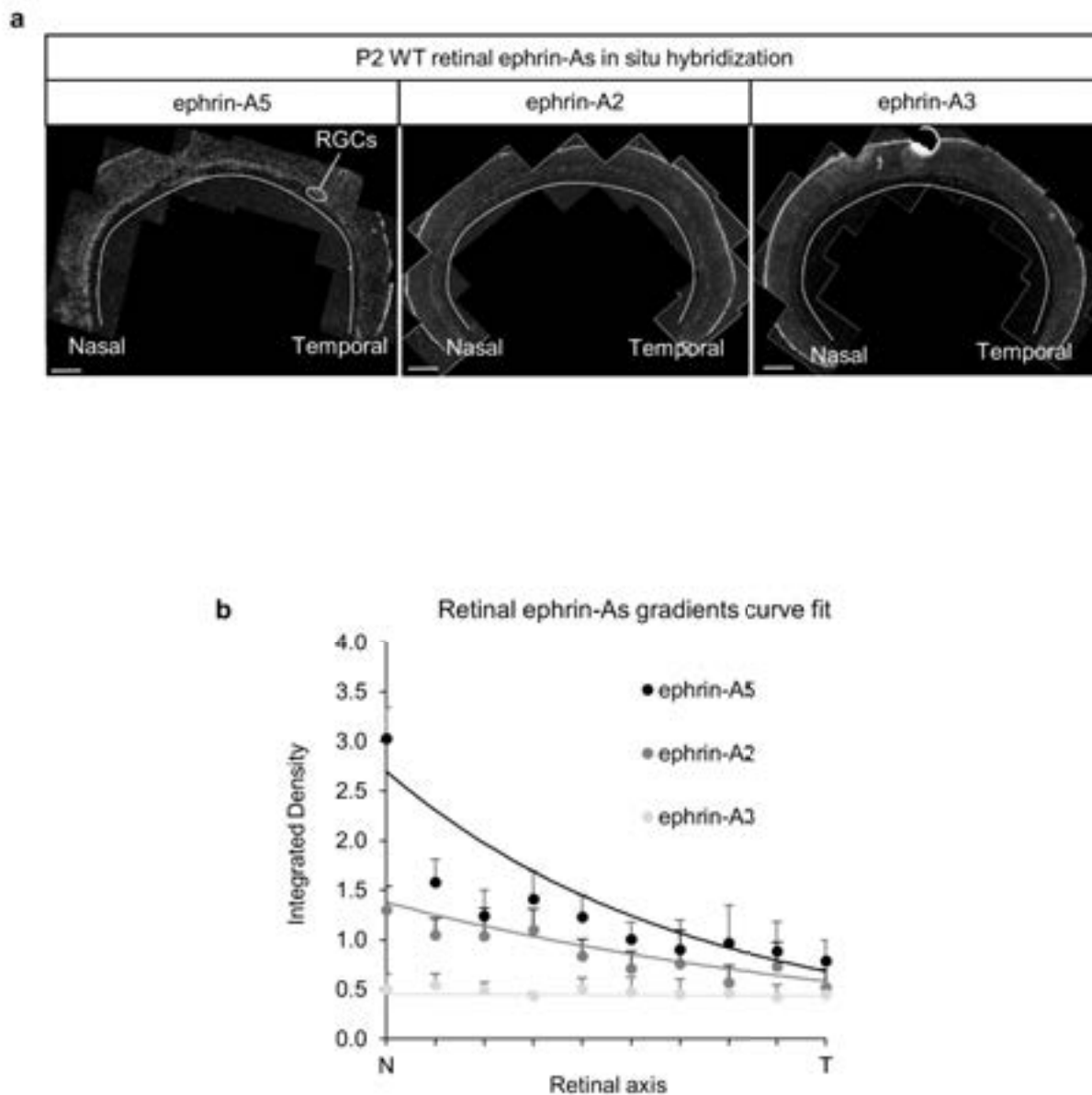


604

605 **Figure 5 Retino- and cortico-collicular maps in ephrin-A3KI/EphA3KI double heterozygous and**

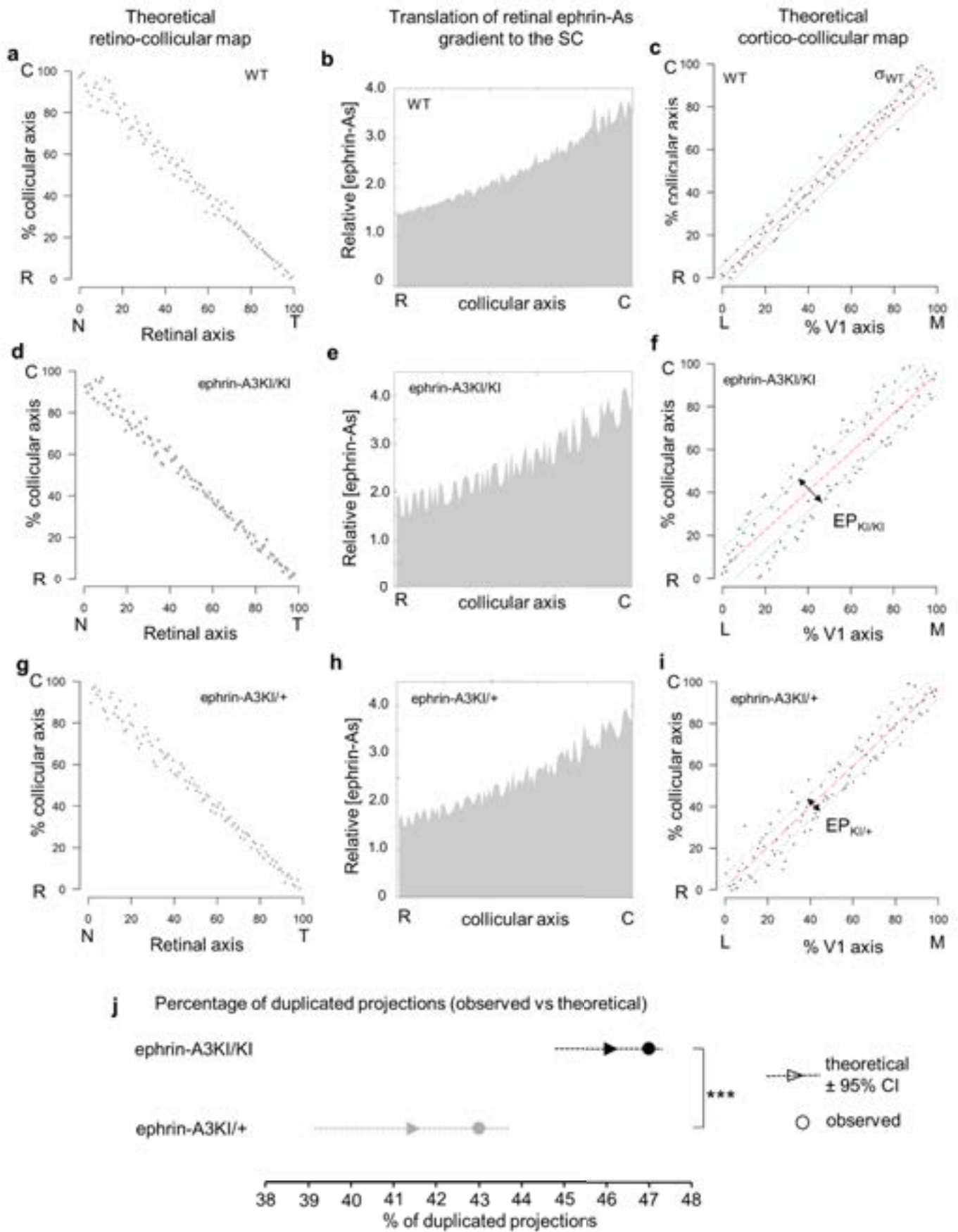
606 **compound ephrin-A3KI/EphA3KI::EphA4KO mutants. (a) Co-immunostaining of ephrin-A3 and**

607 EphA3 in P4 acutely isolated EphA3KI/ephrin-A3KI (n = 8 animals / 15 retinas) RGCs. Arrowheads
608 indicate EphA3/ephrin-A3 co-expression in the same RGCs. Scale bars represent 10 μ m. **(b, c)**
609 Retino-collicular (n = 11 animals) **(b)** and cortico-collicular (n = 18 animals) **(c)** maps generated by the
610 Leave-One-Out method at P8 and P15 respectively in EphA3KI/ephrin-A3KI double mutants. **(d, e)**
611 Retino-collicular projections in P8 ephrin-A3KI/EphA3KI::EphA4+/- (n = 6 animals) **(d)** and ephrin-
612 A3KI/EphA3KI::EphA4 -/- (n = 6 animals) **(e)** mutants. Scale bars represent 200 μ m. T, temporal; N,
613 nasal; R, rostral; C, caudal; L, lateral; M, medial; RGCs, retinal ganglion cells.
614

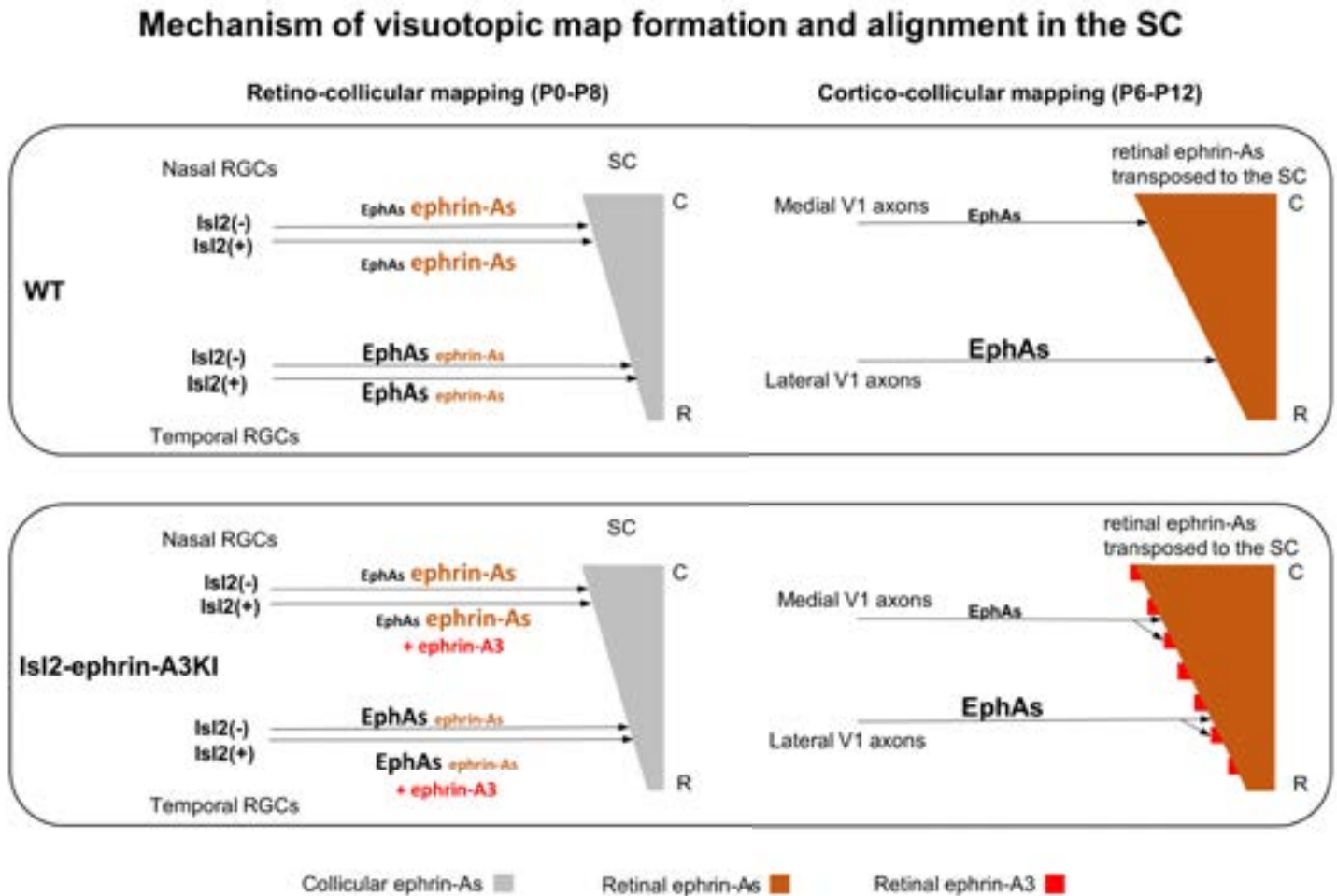


616 **Figure 6 Retinal ephrin-As quantification.** (a) Section of P2 mouse retina (n = 6 retinas from 3
 617 animals) hybridized with ephrin-A5, ephrin-A2 and ephrin-A3 probes. Quantification was performed for
 618 10 segments of the RGC layer along the nasal-temporal axis. Scale bar, 100 μ m. (b) ephrin-A5, A2
 619 and A3 expression profile (dots) fitted by the equations (lines) corresponding to equations (1), (2) and
 620 (3) respectively in Box 1.

621



623 **Figure 7 Theoretical analysis and modelling. (a-i)** Retino- **(a, d, g)** and cortico- **(c, f, i)** collicular
624 maps generated by the 3-step Map Alignment model in WT **(a, c)**, ephrin-A3KI/KI **(d, f)** and ephrin-
625 A3KI/+ **(g, i)** after $n = 20$ runs and 10^7 iteration/run. Translated retinal ephrin-As gradients (% retinal
626 expression: ephrin-A2 = 100%, ephrin-A3 = 100% and ephrin-A5 = 80%) into the SC in WT **(b)**,
627 ephrin-A3KI/KI **(e)** and ephrin-A3KI/+ **(h)**. Red lines in **(c, f, i)** represent the linear regression.
628 Variability of the WT map in **(c)** is calculated by $\sigma_{WT} = 2.18\%$. Grey lines in **(f, i)** represent the
629 exclusion parameter (EP) corresponding to $EP = \sigma_{WT} + \Delta S_{exp}$: $EP_{KI/KI} = 15.18\%$, $EP_{KI/+} = 9.18\%$. **(j)**
630 Dot plot representation of the percentage of duplicated cortico-collicular projections (observed versus
631 theoretical) for $n = 20$ runs in ephrin-A3KI/KI (experimental = 47%, $n = 9$ animals; theoretical mean =
632 46.1 %, $\pm 95\%CI = 1.2\%$, one sample t-test, $t = 1.42$, 19 d.f., $P = 0.17$) and ephrin-A3KI/+
633 (experimental = 43%, $n = 7$ animals; theoretical mean = 41.4%, $\pm 95\%IC = 2.4\%$, variables are
634 normally distributed, one sample t-test, $t = 1.28$, 19 d.f., $P = 0.22$) (theoretical ephrin-A3KI/+ vs ephrin-
635 A3KI/KI, two-sample t-test, $t = 3.4$, 38 d.f., *** $P = 0.0016$).
636



638 **Figure 8.** Schematic representation of the map alignment mechanism. RGCs axons in WT and ephrin-
 639 A3KI animals project to the SC during the first postnatal week and form the retino-collicular map
 640 through forward signaling activated by collicular ephrin-As and fiber-fiber interactions (left side). In
 641 both WT and ephrin-A3KI animals, the retino-collicular map is single and coherent. In WT and ephrin-
 642 A3KI, each RGCs axon is loaded with a different concentration of retinal ephrin-As (high-nasal, low-
 643 temporal) carried to the SC. Due to the coherence of the retino-collicular map, a smooth retinal ephrin-
 644 As gradient is formed in the SC in WT, whereas in ephrin-A3KI animals, Isl2+ RGC axons carry extra
 645 ephrin-A3 (in red) which creates an oscillatory retinal ephrin-As gradient once transposed in the SC
 646 (right side). During cortico-collicular mapping, V1 axons carrying EphA receptors are facing a smooth
 647 gradient of retinal ephrin-As in the SC, leading to a single coherent map in WT. In ephrin-A3KI
 648 animals, V1 axons carrying EphA receptors are facing an oscillatory gradient of retinal ephrin-As (due

649 to ectopic expression of ephrin-A3 in Isl2+ RGCs) which leads to the duplication of the cortico-
650 collicular map (43% in ephrin-A3KI/+ and 47% in ephrin-A3KI/KI) through local neighbor–neighbor
651 relationships of V1 axons via repulsion. Abbreviations, C, caudal; R, rostral; WT, wild-type.
652

Box 1

Best fit equations:

$$(1) \quad L_{A5(x)}^{\text{retina}} = 0.56 e^{(-0.14x)} \quad (R^2 = 0.99)$$

$$(2) \quad L_{A2(x)}^{\text{retina}} = 0.54 e^{(-0.08x)} \quad (R^2 = 0.97)$$

$$(3) \quad L_{A3(x)}^{\text{retina}} = 0.44 \quad (R^2 = 0.99)$$

Total ephrin-As gradients in the WT retina:

$$L_{A(x)}^{\text{retina WT}} = L_{A5(x)}^{\text{retina}} + L_{A2(x)}^{\text{retina}} + L_{A3(x)}^{\text{retina}}$$

$$(4) \quad L_{A(x)}^{\text{retina WT}} = 0.56 e^{(-0.14x)} + 0.54 e^{(-0.08x)} + 0.44$$

Total ephrin-As gradients in the mutants retina:

$$\begin{aligned} L_{A(x)}^{\text{retina KI}} &= L_{A(x)}^{\text{retina WT}} + \Delta L_{A3} \text{ with } \Delta L_{A3} = 0.22 \text{ for ephrin-A3KI/+} \\ &\text{and } \Delta L_{A3} = 0.44 \text{ for ephrin-A3KI/KI} \end{aligned}$$

$$(5) \quad L_{A(x)}^{\text{retina KI/+}} = 0.56 e^{(-0.14x)} + 0.54 e^{(-0.08x)} + 0.44 + 0.22$$

$$(6) \quad L_{A(x)}^{\text{retina KI/KI}} = 0.56 e^{(-0.14x)} + 0.54 e^{(-0.08x)} + 0.44 + 0.44$$

653 **Box 1. Best fit equations of retinal ephrin-As graded expression.**

Complementary data

Due to space restriction in the manuscript for “A mechanism for sensory map alignment in the midbrain.”, some results were excluded. In this section, supplementary materials are provided regarding the role of retinal ephrin-As in cortico-collicular map formation and alignment.

Ephrin-A3 expression on retinal ganglion cells axons

To detect the presence of ephrin-A3 on RGCs axons in ephrin-A3KI/KI animals, we performed a immunohistochemistry using two mouse specific ephrin-A3 antibody (LSBio LS-C6547 or Invitrogen 36-7500), after Dil RGCs labeling, in P2 and P8 SC parasagittal sections. As shown below, incoming RGC axons can be observed (in red). Labeling with ephrin-A3 shows a specific staining in collicular cells but no co-staining on Dil labelled RGCs axons.

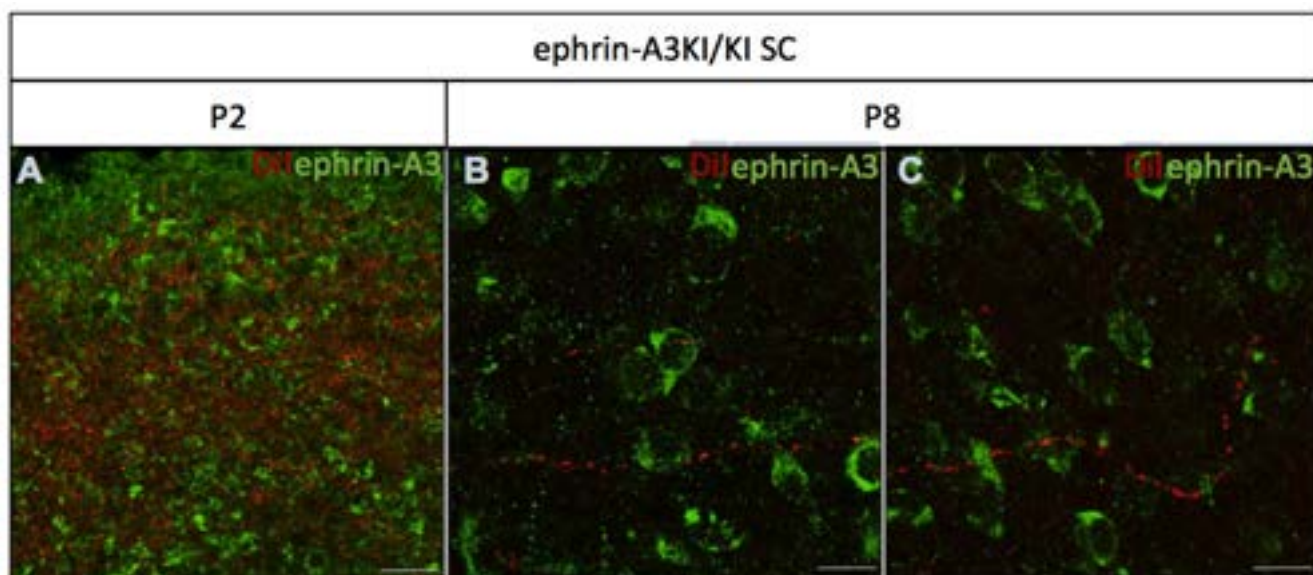


Figure 22: Ephrin-A3 expression on RGCs entering the superior colliculus. Ephrin-A3 immunostaining (green) after RGC Dil labelling by subretinal injection (red). SC parasagittal sections from P2 (A) and P8 (B and C) Isl2-ephrinA3KI/KI animals. Scale bars: 30 μ m (A), 10 μ m (B, C).

In addition, ephrin-A3 immunohistochemistry was performed on P3 ephrin-A3KI/KI optic nerve longitudinal sections (proximal, medial and distal of the optic cup), using signal amplification (streptavidin/biotin). As shown below, specific ephrin-A3 labeling could be detected on fibers within the proximal and medial part of the optic nerve, but not in the distal part, suggesting that ephrin-A3 is not detectable on RGCs axons. The absence of staining in the distal part suggests that ephrin-A3 ligands are spread along the axons, and reach a low concentration that lies below the immunohistochemistry detection limit.

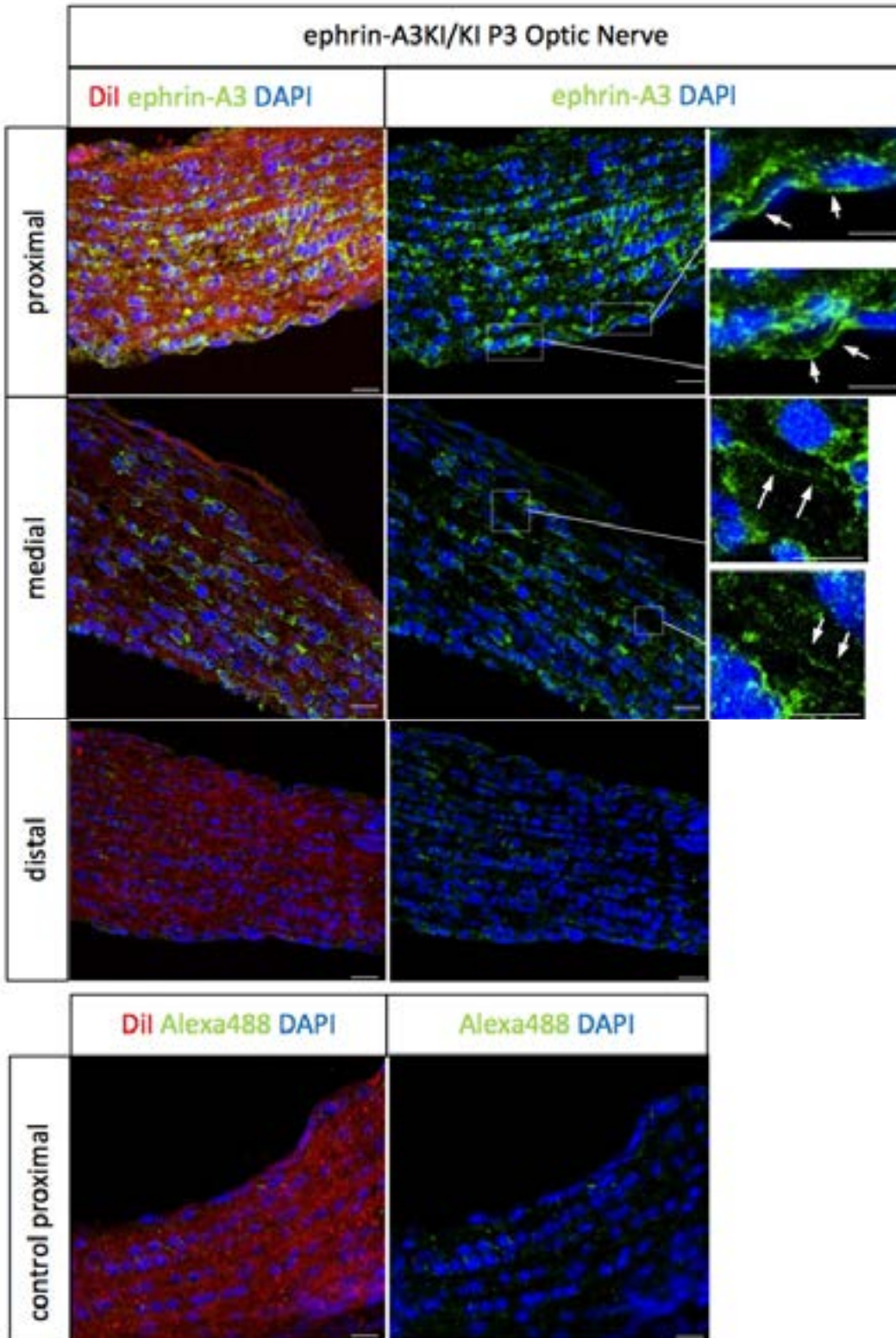


Figure 23: Ephrin-A3 expression on optic nerve. Ephrin-A3 immunostaining (green) after RGC Dil labelling by subretinal injection (red) and DAPI staining (blue). Proximal, medial and distal part of the optic nerve from P3 *Isl2-ephrinA3KI/KI* animals. Controls performed omitting primary antibody. Scale bars: 30µm, insets, 10µm.

A similar issue was raised in Triplet et al. (2009) -Figure S4- in EphA3KI/KI mice. In these animals, the dramatic collicular phenotype (full duplication) should generate two different retinal ephrin-A gradients, one covering the rostral half of the SC (running from low-rostral to high-mid-SC) and the other covering the caudal half (running from low mid-SC to high-caudal). However, no such staining could be detected.

The failure to detect retinal ephrin-A3, and more generally any retinal EphAs/ephrin-As, in situ on RGCs axons traveling within the colliculus may be the consequence of the spreading of these molecules along the axons, which then generates a low concentration locally precluding any detection using conventional immunohistochemical methods. Another explanation for the absence of detection could be a specific folding of these proteins along the axon, masking the epitope.

Ephrin-A3 expression in the superior colliculus

The expression of ephrin-A3 in the SC is still debatable. As shown below, Suetterlin and Drescher (2014) (Sup. Figures S1H, I) suggested that there is no ephrin-A3 expression in retino-recipient layers of the SC at P2.

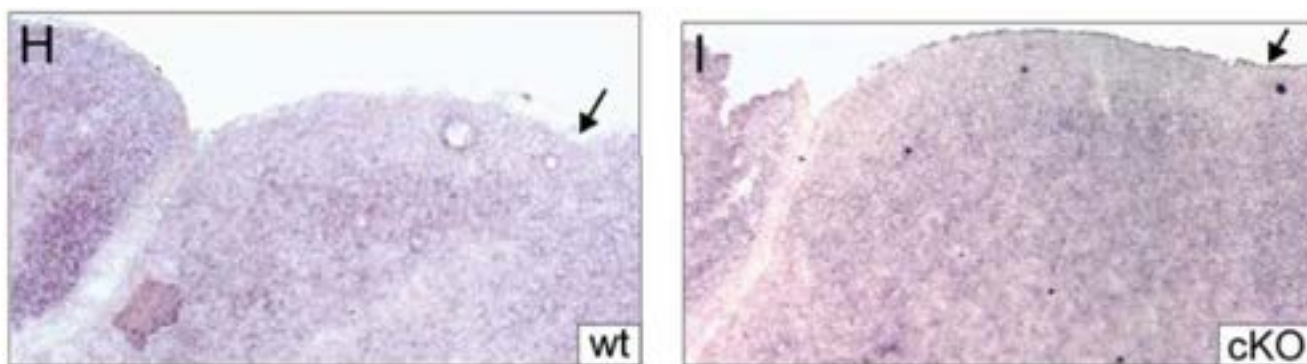


Figure 24: EphrinA3 expression in the superior colliculus. mRNA *in situ* data for ephrin-A3 performed at P2 in wild-type and conditional knock-out for ephrin-A5 in the superior colliculus, adapted from Suetterlin and Drescher, 2014.

In contrast, a snapshot from the Allen Brain Atlas shows ephrin-A3 expression using *in situ* hybridization at P4 and P14 in retino-recipient layers, along the rostral-caudal axis of the SC. We used the scale bar as provided by Allen Brain Atlas to measure the ephrin-A3 expression in the SC at P4 and P14. Ephrin-A3 expression appears between 200 and 280 μm below the surface of the SC, which corresponds to the retino-recipient layer – dashed lines) lying 50-400 μm beneath the surface of the SC.

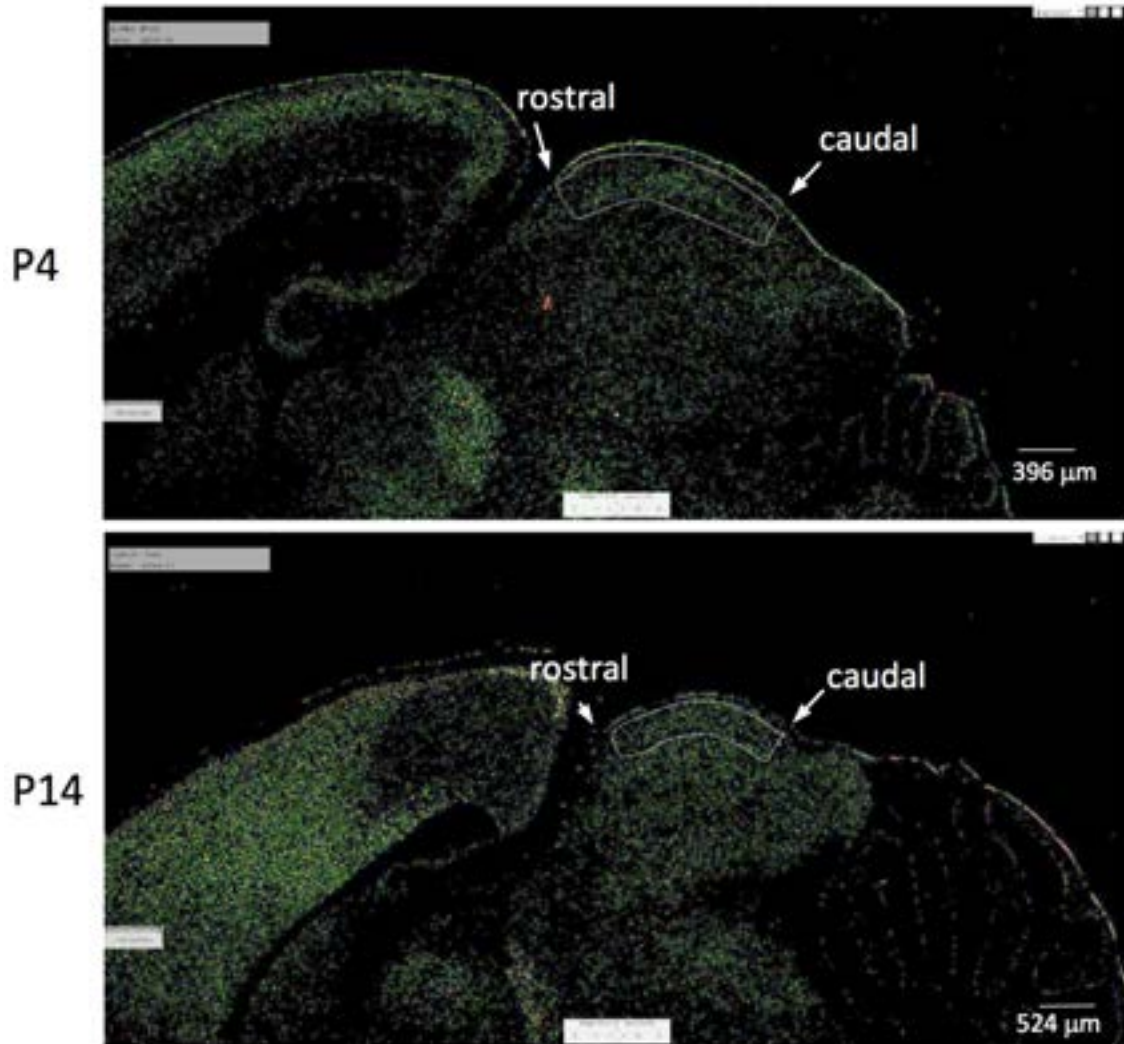


Figure 25: Ephrin-A3 expression in the superior colliculus. In situ hybridization at P4 and P14 in the superior colliculus. Adapted from the Allen Brain Atlas.

Careful examination and appropriate measurements of the data from Pfeiffenberger et al. (2006) (Supp. Figure 1 D, E, F) and Triplett et al. (2012) (Figure 5A, B, F) shown below also suggest that ephrin-A3 is expressed in the retino-recipient layers of the SC (although some controversies exist regarding the expression profile).

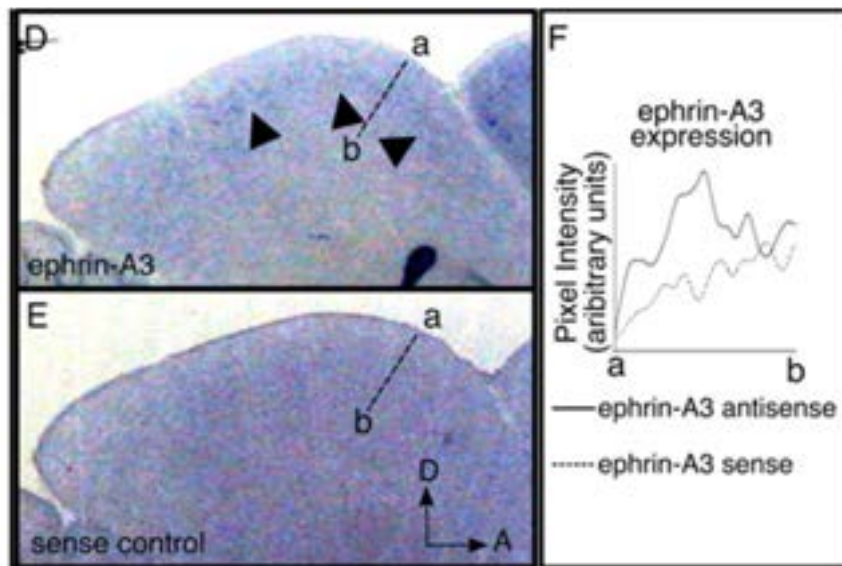


Figure 26: Ephrin-A3 staining in the superior colliculus.

(D, E) Ephrin-A3 is expressed at low levels in the developing SC. P1 sagittal sections treated with ephrin-A3 antisense (D) or ephrin-A3 sense (E) probes reveal a low level of uniform expression in deep layers of the SC. Arrowheads identify the region of ephrin-A3 expression. The dotted lines in (D) and (E) denote the region analyzed by the intensity plot shown in (F), with “a” and “b” corresponding to “a” and “b” along the x-axis of the plot. The plot shows a small increase in intensity in the antisense tracing associated with the region of ephrin-A3 expression. D, dorsal; A, anterior; Adapted from Pfeiffenberger et al., 2006.

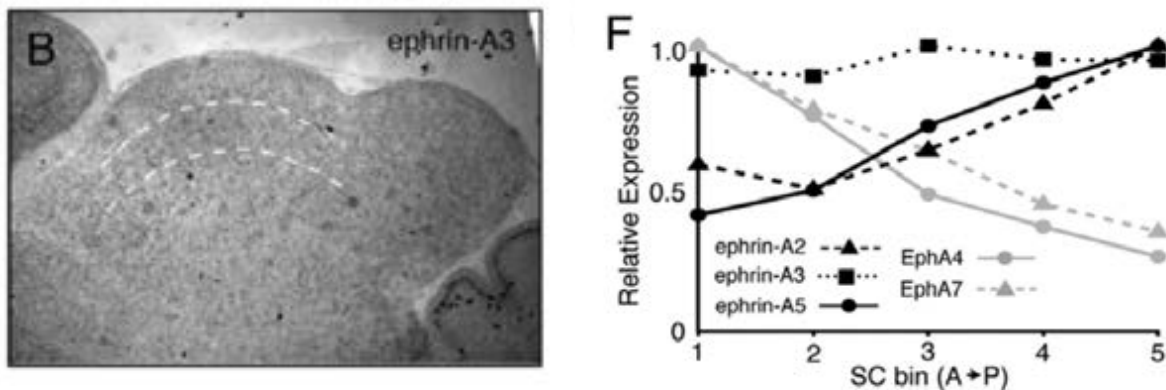


Figure 27: Ephrin-A3 staining in the superior colliculus.

Parasagittal sections through the SC, marked by arrows, of postnatal day 4 wild-type pups stained for ephrin-A3 (B). F. Quantification of the relative expression levels in the SC across the anteroposterior axis. Adapted from Triplett et al., 2012.

In addition to the work previously described, we performed multiple ephrin-A3 antibody staining in the SC at different time points, using two ephrin-A3 antibodies, (LSBio-C6547 and Invitrogen 36-7500) which gave specific staining on retinal sections (Fig.1, 2). Below are examples of P3, P8 and P14 collicular sections stained with an ephrin-A3 antibody. A clear staining can be detected on collicular cells within the retino-recipient layers (note that no fiber-like, nor termination zones-like staining can be observed).

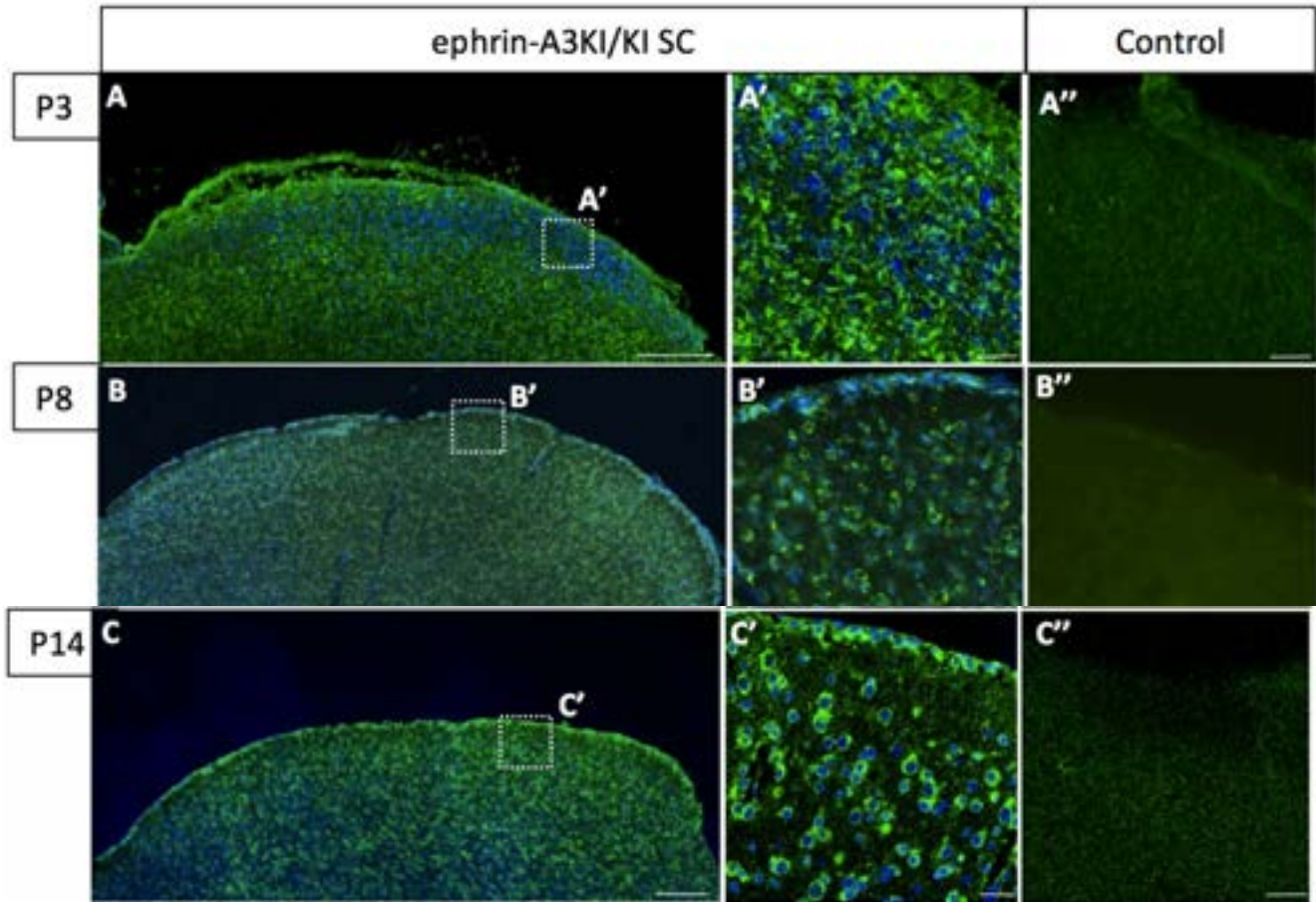


Figure 28: EphrinA3 immunostaining in the superior colliculus. **A.** Ephrin-A3 immunostaining at P3 in the superior colliculus. **A'**. Inset of superficial layers at higher magnification. **A''.** Control omitting primary antibody. **B.** Ephrin-A3 immunostaining at P8 in the superior colliculus. **B'**. Inset of superficial layers at higher magnification. **B''.** Control omitting primary antibody. **C.** Ephrin-A3 immunostaining at P14 in the superior colliculus. **C'**. Inset of superficial layers at higher magnification. **C''.** Control omitting primary antibody. (scale bars: 200 μ m (A, B, C), 30 μ m (A' – C'')).

Altogether, these data suggest that ephrin-A3 is homogeneously expressed in the retino-recipient layers of the SC during retino- and cortico-collicular map formation, although at a lower level compared to ephrin-A2 and ephrin-A5.

Termination zones morphology in *Isl2-ephrin-A3KI/KI*

In addition to measuring retino-collicular termination zone position along the rostral-caudal axis, the lamina targeting as well as extension was also assessed in wild-type and *Isl2-ephrin-A3KI/KI* animals. Overall, no significant differences could be found between wild-type TZs and homozygous animals at different location along the rostral-caudal axis of the superior colliculus.

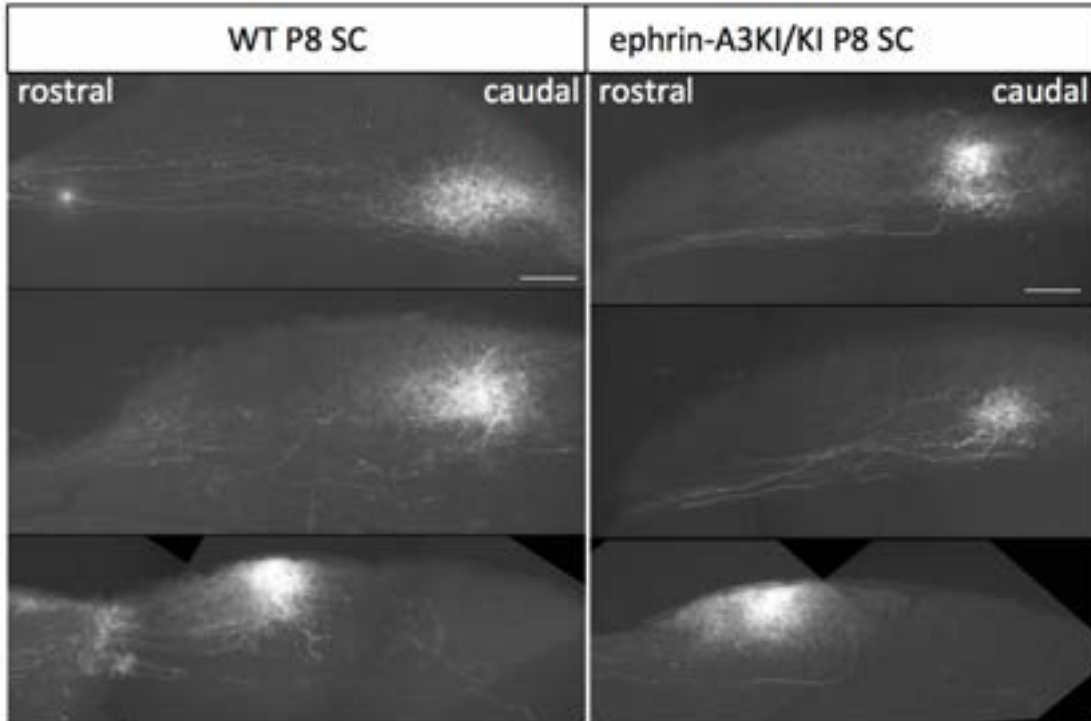


Figure 29: Morphology of the retinal ganglion cells termination zones in the superior colliculus. Superior colliculus parasagittal sections in Dil injected animal in the retina at P7. Left panel. Wild-type termination zones in the superficial layers of the superior colliculus ending in the caudal, medial and rostral pole of the superior colliculus. **Right panel.** *Isl2-ephrin-A3KI/KI* termination zones in the superficial layers of the superior colliculus ending in the caudal, medial and rostral pole of the superior colliculus. (scale bars: 200 μ m)

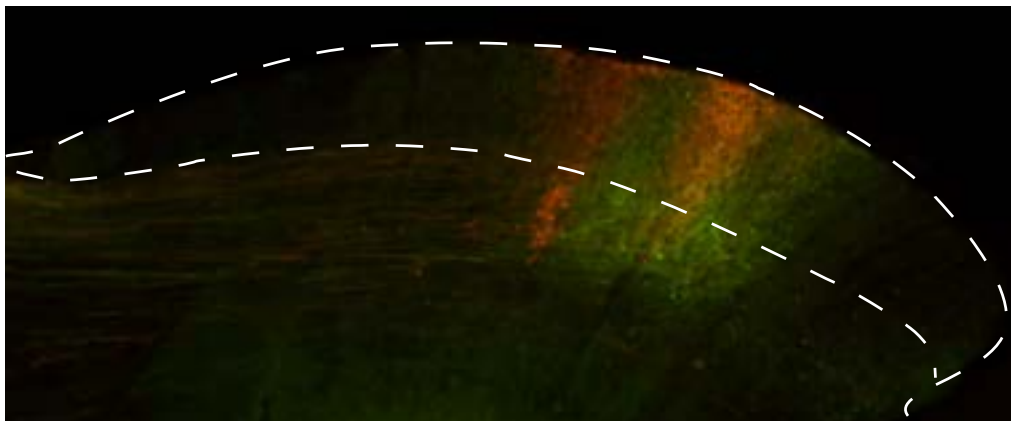


Figure 30: Cortico- and retino-collicular termination zones. Retinal and cortical inputs targets to the upper superficial SGS: sagittal section of the superior colliculus, AAV1-CAG-tdTomato (red) and AAV9-Synapsin-GFP (green) transfection of retinal and cortical inputs. Dashed line: SC boundary and limits between the superficial layers and optic layer.

Distance separation in cortico-collicular duplication in *Isl2-ephrin-A3KI/+* and *KI/KI*

We further analyzed the average distance of duplication in both *ephrin-A3KI/+* and *ephrin-A3KI/KI* mutant cortico-collicular maps. A two-fold difference in average duplication distance between *ephrin-A3KI/+* and *ephrin-A3KI/KI*, can be found, which is relevant with the presence of 1 or 2 alleles of *Isl2-ephrin-A3* (gene dosage effect). However, as shown below, this distance slightly varies along the rostral-caudal axis of the SC and becomes similar for both genotypes in the caudal-most 20% of the SC (from 80% to 100% on x axis).

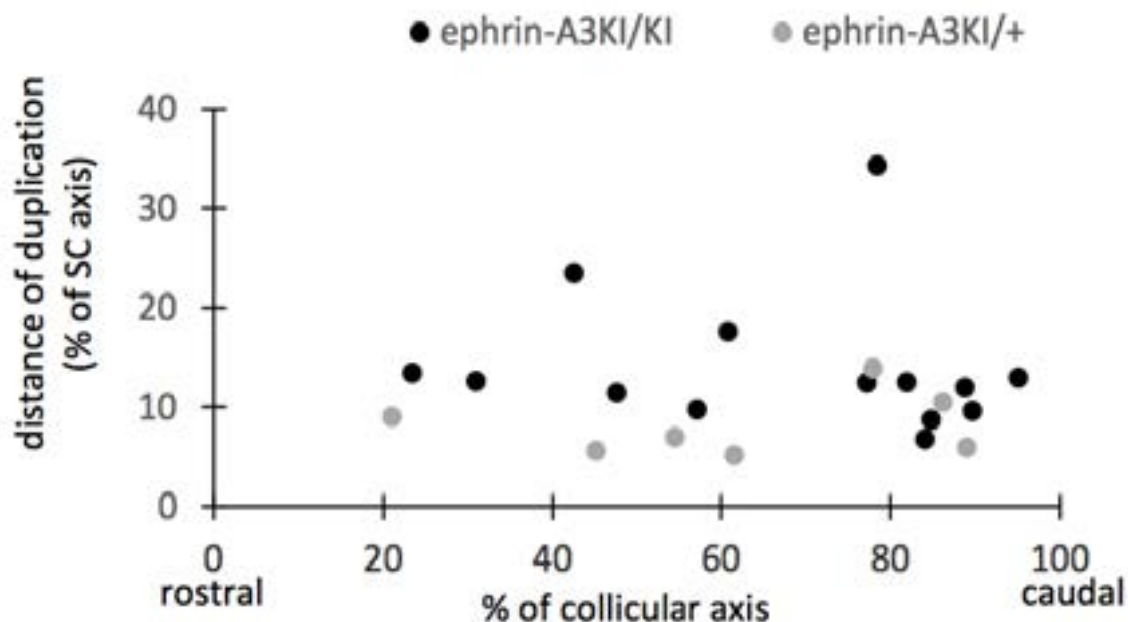


Figure 31: Distance separation between cortico-collicular termination zones in the superior colliculus in *Isl2-ephrin-A3KI*. Duplication distance is expressed as a percentage of the total length of the rostral-caudal axis and matched with position along the rostro-caudal axis of the superior colliculus. In grey, heterozygous, in black, homozygous.

This observation is in accordance with the Relative Signaling model characterized in Brown et al. (2000) and conceptualized in Reber et al. (2004) and Bevins et al. (2011) which predicts the variation of the duplication distance and the occurrence of a collapse point according to a Relative EphA signaling threshold. Although no collapse points are observed in cortico-collicular mapping in *ephrin-A3KI* animals, this model seems, in which EphA forward signaling on V1 axons mediates cortico-collicular mapping, seems to apply. In contrast to the EphA3KI model where differences in relative EphA signaling on RGCs axons is provided by oscillatory EphA3 receptors on RGCs, in the *ephrin-A3KI* model, the difference in relative EphA signaling on V1 axons is provided by oscillatory retinal ephrin-A3 transposed to the SC. An increase in the relative difference of retinal ephrin-As (between *Isl2+* and *Isl2-* RGCs for example in compound mutant *ephrin-A3KI/ephrin-A5* retinal KO) may generate a collapse point in the cortico-collicular map.

Retino-collicular map in *Isl2-ephrin-A3KI* x *EphA4KO*

To test whether ectopic ephrin-A3 may cis-interact with endogenous EphA receptors during the formation of the retino-collicular map, the *Isl2-ephrin-A3KI* were crossed with the *EphA4KO*. EphA4 accounts for the majority of EphAs expressed in the retina and is ungraded. If ephrin-A3 over-expression level was not sufficient to induce a phenotype through cis interaction with EphA5 or EphA6, lowering the overall level of EphAs in the retina should increase this difference and reveal duplications. According to the relative signalling model, cis interaction of ephrin-A3 with endogenous EphAs in the *Isl2-ephrin-A3KI* would lead to two distinct populations of RGCs with different levels of functional EphA receptors: wild-type, with endogenous level of EphA and the *Isl2+*, which express ephrin-A3 in which retinal EphAs would be silenced by cis-interaction. This would generate an oscillatory gradient of retinal EphAs, similar to the *Isl2-EphA3KI*, and induce duplications in the retino-collicular map. The retino-collicular map was assessed in *Isl2-ephrin-A3KI/+;EphA4-/-* and *Isl2-ephrin-A3KI/KI;EphA4-/-* (Figure 32). In these two compound mutants, no duplication were found, suggesting that retinal ephrin-A3 does not silence retinal EphAs.

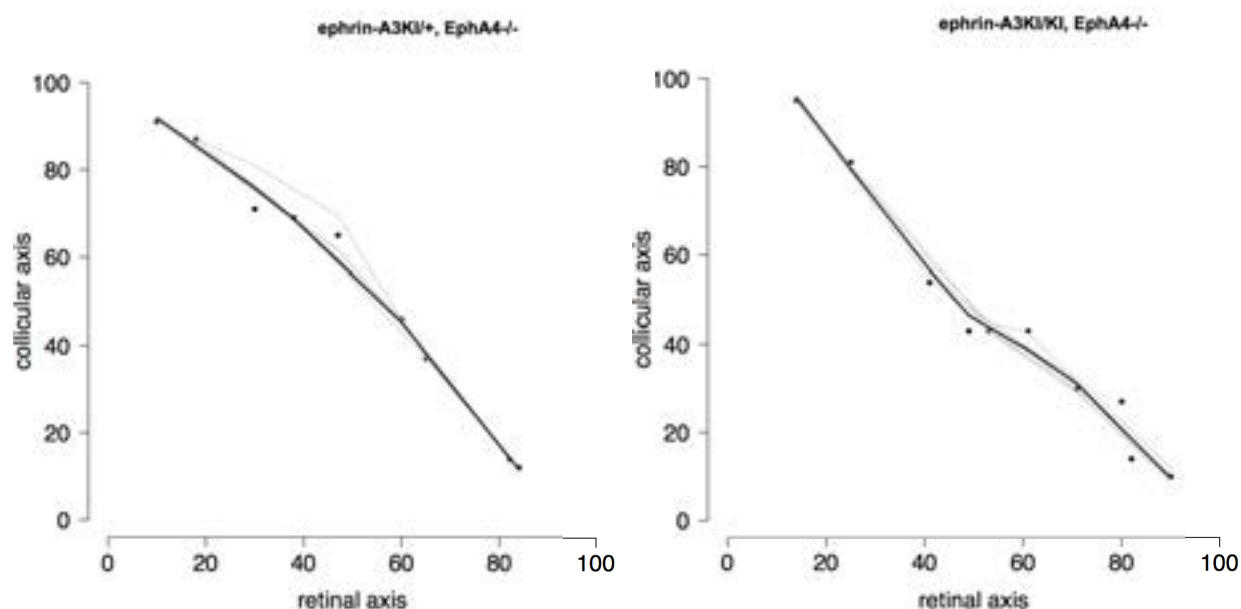


Figure 32: Retino-collicular map of *Isl2-ephrin-A3KI* x *EphA4KO*. Retino-collicular maps generated by the Leave-One-Out method at P8 in *Isl2-ephrin-A3KI/+* x *EphA4-/-* (left) and *Isl2-ephrin-A3KI/KI* x *EphA4-/-* (right).

In silico modelling of the Isl2-EphA3KI cortico-collicular map.

To test the validity of the three-step map alignment model, the Isl2-EphA3KI retino- and cortico-collicular map was modeled. These animals have a fully duplicated retino- and cortico-collicular map as demonstrated through anatomical and functional studies. We hypothesized that the duplication of the cortico-collicular map in the Isl2-EphA3KI is due to the redistribution of retinal ephrin-As in the superior colliculus, according to the duplicated retino-collicular map. Using the three-step map alignment model, we were able to replicate the full duplication of the cortico-collicular map (Figure 33) with retinal ephrin-As guiding cortical axons.

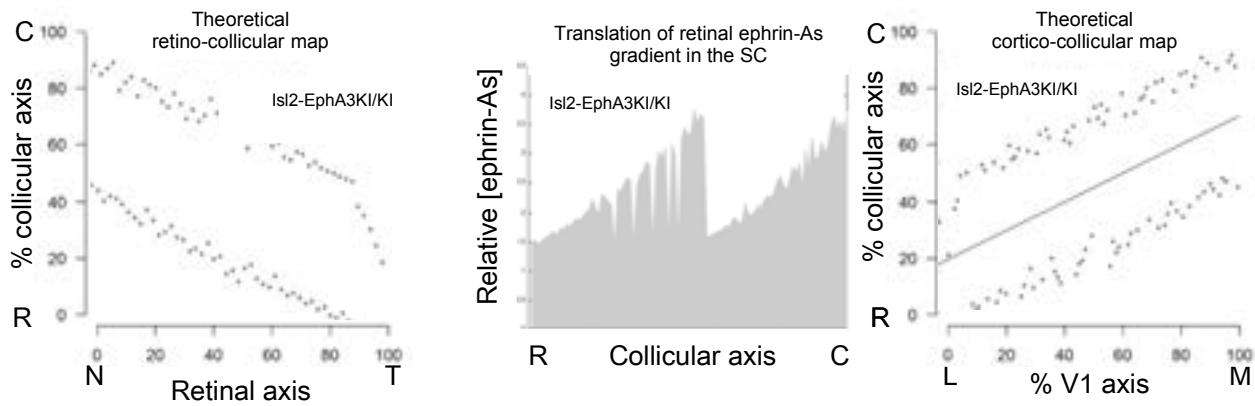


Figure 33: In silico modeling of the retino- and cortico-collicular map of Isl-EphA3KI/KI. Retino- and cortico-collicular maps generated by the 3-step Map Alignment model in Isl2-EphA3KI/KI. Left. Retino-collicular map in Isl2-EphA3KI/KI. Duplications are found along the entire rostral-caudal axis. Center. Transposed retinal ephrin-As gradient in the superior colliculus. Right. Cortico-collicular map of Isl2-EphA3KI/KI. Duplication can be found along the entire rostral-caudal axis.

Discussion

Our results highlight another form of plasticity and adaptability in the formation of connections during development. Indeed, a molecular disruption localized in the source, the retina, can lead to an unaltered phenotype in the target (here the SC), but induce defects in the feedback projections emanating from V1. The cortico-collicular map formation is subsequent to the formation of the retino-collicular map, allowing an adaptability prior to sensory experience. This interdependence relies on precise timing in the establishment of the maps, and pinpoints how adaptive this process is. To explain molecular mechanisms driving such plasticity, we suggest that the gradients of retinal ephrin-As are transposed to the SC, where they can be read by entering cortical fibers. These findings also highlight an unsuspected role for retinal ephrin-As, which have also been involved in axon-axon interaction-mediated competition.

Role of counter-gradients in the visual system

Map interdependence

The idea that counter-gradients of EphA and ephrin-As participate in map alignment came from their expression pattern, as well as the fact that most regions in the nervous system are both the target and the projecting areas. This feature requires a precise alignment of projections because they carry information that needs to be spatially matched. Recent work also demonstrated an interdependence of subsequent mapping processes. The study of topographic maps in other systems has revealed that their formation depends on each other (Grant et al., 2016; Shanks et al., 2016). The sequential development, the transfer topographic information, and the alignment suggests a common signaling framework that has to account for potential variation during development and adaptability.

Role of retinal ephrin-As

Several hypotheses have been raised over the last two decades about the role of retinal ephrin-As (discussed in detail in the submitted manuscript above). Some work suggested that retinal ephrin-As are involved in cis-masking, which could lead to a sharpening of the EphA retinal gradient. However, most demonstrations come from *in vitro* experiments whereby EphA and ephrin-As are co-expressed at high levels in the same cell. Recent experiments in which ephrin-A is specifically ablated in either the retina or the superior colliculus, do not show targeting defects when ephrin-A5 is not expressed in the retina. This suggests a minimal role for a retinal ephrin-A counter-gradient in the reshaping of the EphA receptor gradient (Suetterlin and Drescher, 2014). However, retinal ephrin-As could play an important role during the overshooting phase, where they could desensitize nasal axons by cis-binding, in order to reach the caudal part of the SC.

Duplication or termination zone extension

The effect of retinal ephrin-A3 on axonal outgrowth through reverse signaling, has not yet been addressed. Following the hypothesis of a role of retinal ephrin-As in outgrowth promotion, the level at which ephrin-A3 expression is driven in the Isl2-ephrin-A3KI may induce growth promotion, leading to an increase in the axonal arborization of retinal terminals in the SC, which has not been observed in the Isl2-ephrin-A3KI animals. Addressing this question *in vivo* seems quite challenging. However, *in vitro* assays quantifying the effect of ephrin-A3 could partially answer this question. In addition, the presence of duplication or TZs extension in the retino-collicular map induced by retinal ephrin-A3 ectopic expression seems unlikely, as shown previously (complementary data, figure 29).

Dose-dependent effect of ephrin-A3 in cortico-collicular mapping

To assess in a quantitative manner the effect of ephrin-A3 over-expression on distance separation in the cortico-collicular map, it would be interesting to perform similar experiments in the ephrin-A5 retinal KO model. This would increase the ephrin-A ratio between Isl2-positive and negative RGCs expressing the endogenous levels of ephrin-As. This increase in the ephrin-A ratio may lead to an increase in the duplication distance of the cortico-collicular map. In the absence of such a phenotype, one can hypothesize a differential role; thus testing the effect of ephrin-A3 on an ephrin-A2KO background would also be of interest. Both experiments would further confirm the participation of retinal ephrin-As in the mapping of cortico-collicular projections.

Distance separation in the Isl2-ephrin-A3:

When compared to this Isl2-EphA3KI, the distance separation observed is noticeably smaller (20% for Isl2-EphA3KI heterozygotes, and 7 and 13% for Isl2-ephrin-A3KI heterozygotes and homozygotes, respectively) even if expression is regulated by the same gene. The duplication distance observed in the Isl2-EphA3KI/KI mice (Brown et al., 2000) is the consequence of a segregation between cells over-expressing EphA3, and cells expressing endogenous level of EphAs through forward EphA signaling at the level of the entire RGC population. The smaller duplication of the cortico-collicular map, with roughly a 45% penetrance, as observed in the ephrin-A3KI animals, occurs locally due to the oscillation of retinal ephrin-A3 in the SC that organizes local neighbor-neighbor relationships of V1 axons via repulsion. Such an effect at a local level may explain the small distance in the map duplication in ephrin-A3KI.

Interestingly, a 2-fold increase on distance separation is observed between Isl2-ephrin-A3KI homozygotes and heterozygotes, which corroborates with the presence of 1 or 2 alleles of Isl2-ephrin-A3, suggesting a gene dosage effect. However, the distance separation slightly varies along the rostral-caudal axis of the SC and becomes similar for both genotypes in the caudal-most 20% of the SC (from 80% to 100% on x axis).

This difference can be explained with the Relative Signaling model (Bevins et al., 2011; Brown et al., 2000; Reber et al., 2004), which predicts variation in the duplication distances. Indeed, the over-expression of ephrinA3 is constant across the entire collicular space, which leads to a variation in the signaling ratio. This should also apply for EphA forward signaling on V1 axons mediating cortico-collicular mapping. In contrast to the EphA3KI model whereby differences in relative EphA signaling on RGCs axons is provided by oscillatory EphA3 receptor expression on RGCs in the ephrin-A3KI model, the difference in relative EphA signaling on V1 axons is provided by oscillatory retinal ephrin-A3 transposed to the SC, which might dampen local variations.

An increase in the relative difference of retinal ephrin-As (between Isl2+ and Isl2- RGCs for example in compound mutant Isl2-ephrin-A3KI/ephrin-A5 retinal KO) may generate a collapse point in the cortico-collicular map. In addition, no difference in the occurrence of duplications was found as a function of localization along the rostral-caudal axis.

EphA3/ephrin-A3 double mutants

To demonstrate the full inactivation of EphA3 in the Isl2-ephrin-A3KI/EphA3KI, these animals were crossed with the EphA4KO. According to the phenotype of the Isl2EphA3KI/+ x EphA4KO, in which distance separation is increased, this should have induced the same effect if a residual amount of EphA3 is available. Given that both EphA3KI/ephrin-A3KI double mutants and EphA3KI/ephrin-A3;EphA4KO compound mutants present systematically single retino-collicular projections – particularly in the caudal pole of the SC – this provides compelling evidence that signaling through

ectopic EphA3 is inactivated.

Cis interaction in vivo

The silencing of EphA3 by ephrin-A3 in the Isl2-ephrin-A3/EphA3 suggests a cis-interaction between these molecules. This interaction could be specific to this particular pair since no phenotype on the retino-collicular map can be observed. Indeed, if ephrin-A3 could interact with other EphAs, this would lead to a decrease in the EphA receptors available, and a segregation between the Isl2 positive and the wild-type population of RGCs. However, since EphA3 is not endogenously expressed in RGCs, interactions with ephrin-A3 could be caused by an insertion of this receptor in the same microdomains as ephrin-A3, where they can interact specifically, whereas endogenous receptors (EphA4/A5/A6) are segregated.

Role of retinal ephrin-As in the alignment of visual maps

To date only a few analyses have been performed on the cortico-collicular map formation in EphA/ephrin-A mutants (Triplett et al., 2009; Wilks et al., 2010). In the Isl2-EphA3KI, the interpretation was that the alignment occurred by retinal-matching of the activity pattern of the duplicated retino-collicular map. In ephrin-As KO, the cortico-collicular ectopic termination zone could be observed with a lower incidence than in the retino-collicular map. The interpretation was that not all of the retino-collicular ectopic termination zones are functional, which made them unable to drive the alignment of the cortico-collicular projections. The lower occurrence of the ectopic termination could be due to the redistribution of remaining ephrin-As ligands in the SC, which could dampen the relative difference in expression. A specific role of ephrin-A3 could not be excluded. The analysis of single full ephrin-A3KO has been performed (Pfeiffenberger et al., 2006), and did not reveal any effect on retino-collicular mapping, which does not exclude an altered cortico-collicular map. It must be emphasized that these results were obtained from full ephrin-As knock-out, precluding any relevant conclusions concerning the specific role of retinal ephrin-As in cortico-collicular map alignment. From this perspective, it would be interesting to see the effect of a specific loss of retinal ephrin-As using ephrin-As conditional knock-out animals.

Generation of an oscillatory gradient in the SC

Redistribution of retinal ephrin-As carried by retinal axons could indeed dampen the oscillatory expression of these ligands through overlapping TZs. Nevertheless, the variability in the degree of overlap will create smaller or larger areas containing high levels of retinal ephrin-A3. This phenomenon may participate towards the incomplete penetrance of the cortico-collicular phenotype, and may explain the reduced distance separation when compared to Isl2-EphA3KI.

A similar issue was raised in the Isl2-EphA3KI/KI mice (Triplett et al., 2009). In these animals, the dramatic collicular phenotype (full duplication) should generate two different retinal ephrin-A gradients; one covering the rostral half of the SC (running from low-rostral to high-mid-SC) and the other covering the caudal half (running from low mid-SC to high-caudal). However, no such staining could be detected.

The failure to detect retinal ephrin-A3, and more generally any retinal EphAs/ephrin-As *in situ* on RGC axons traveling within the colliculus may be the consequence of the spreading of these molecules along the axons, which then generates a low concentration locally, precluding any detection using conventional immunohistochemical methods. Another explanation for the absence of detection could be a specific folding of these proteins along the axon, masking the epitope.

Possible alteration of the retino-geniculate pathway

Duplications observed in the SC of incoming projections from the V1 could be due to an abnormal mapping of the retino-geniculate pathway, which would then be transferred to feedback projections from V1. To test this eventuality, Dil injections were performed in the retina, and their TZs were assessed in the dLGN. No abnormalities were observed, suggesting that retinal ephrin-A3 is unlikely to participate in the formation retino-geniculate topography.

Gradient matching and retinal-matching model

To date, two alternative hypothesis have been suggested to account for duplication of the cortico-collicular map: gradient matching and retinal-matching (Cang and Feldheim, 2013).

Gradient matching hypothesis suggests that collicular ephrin-As interact with cortical EphAs and lead to the formation of the cortico-collicular map. This seems unlikely regarding the results obtained in the *Isl2-EphA3KI*, since ephrin-As collicular expression is unaltered and a duplication of the cortico-collicular projections can be observed. This is in favor of retinal matching, where activity drives the formation of the cortico-collicular map. However, if molecular information is (at least in part) carried by retinal axons, the rearrangement of the retinal ephrin-A gradient through the duplication of the retino-collicular map accounts for the duplication of the cortico-collicular map and explains the phenotype observed in the *Isl2-EphA3KI*.

In addition, *in silico* modeling of the *Isl2-EphA3KI* using the three-step model revealed that a duplication of the cortico-collicular can be obtained through the segregation of the *Isl2* positive and wild-type RGCs and the consequent resorting of retinal ephrin-As.

Timing is everything

In the absence of a complete expression profile at the different time points during development, deciphering the respective role for each EphA and ephrin-As is quite difficult. Much evidence has accumulated that different Ephs and ephrins are implicated in different functions. Gradients are dynamic since homogeneous or graded expression can be found at different developmental stages, and eventually a disappearance of some of these gradients in adulthood. However no information is available concerning the expression profiles at the protein level, which could greatly vary with internalization of both receptors and changes in translation dynamics. In addition, this could have major effects if we assume that ephrin-A levels have attractive and repulsive properties according to their expression levels, or if the balance between reverse and forward signaling is an important factor in the formation of a topographic map.

The formation of visual maps is a highly dynamic and sequential process, in which the timing of the different actors plays an essential role. One likely timeline for the formation of such maps, is:

- Overshooting. Cis masking could be required at this particular time point. Indeed if reverse signaling is involved in retino-collicular mapping through a repulsive effect, nasal axons, carrying high levels of ephrin-As could probably not enter the SC and reach the caudal pole. Localization of EphA/ephrin-As close to each other would silence both, which could be later on segregated in different micro-domains and could therefore be involved in both forward and reverse signaling
- Repulsive interaction through reverse signaling between ingrowing axons (fiber-fiber interaction) that would mediate competition

- Threshold effect due to the probability of interactions between the different levels of EphAs and ephrin-As, to prevent extension and induce the retraction of overshooting. This signaling should be relative
- Branching extension at the local topographically correct location through interactions with BDNF
- Refinement by correlated activity

When, but also where.

In addition to the need for information on the expression dynamics of EphAs and ephrin-As during the formation of the visuotopic maps, the precise location of these molecules would also be required. The overshooting phase could be explained by a delay in the transport of receptors and ligands, which would still be in the translation phase before they are carried along the axon where they can signal. The amount of EphAs/ephrin-As mRNA translated and the location of their insertion in the axonal membrane (distal, proximal) seems to be critical. According to the proportion localized (either on axonal arborization or along axons), different types of interactions could be considered. In addition, if EphA receptors are internalized as they interact with ephrin-As, this could lead to a decrease in signaling during the formation of the map.

Similarly, our results suggest a cis-interaction between EphA3 and ephrin-A3 *in vivo*, leading to silencing of both partners; but since EphA3 is not normally expressed in RGCs, this could induce a different segregation of the receptor along the axon when compared to the wild-type situation.

Stochasticity in molecular guidance

Our results also point toward an adaptability of the developmental program, and highlights the existence of inter-individual variations. Another recent study, (Owens et al., 2015), showed that the interplay between activity and molecular cues could lead to differences at the individual level. The formation of topographic maps during development can be viewed as a dynamical system, where different forces are combined until an equilibrium is reached. This equilibrium, even if the system shows robustness, can be shifted toward a breaking point and induce a chaotic behavior.

Stochasticity is found at different levels during map formation. During a receptor/ligands interaction, thermal noise is believed to induce errors at the molecular level. EphA and ephrin-A amounts can only be detected and integrated by the ingrowing axons, through the indirect and noisy process of chance encounters with a limited number of receptors on the sensing device (Goodhill, 2016).

Gradients are not enough

There are limits regarding the information content and the robustness of signaling that can be carried by linear or exponential gradients. The systematic investigation and quantification of gradients regarding one particular axis probably induced a bias, regarding their actual shape and expression profile. Diffusion occurs in all directions so it seems more likely that EphA and ephrin-A gradients when stretched in the second dimension of the structure are rather concentric, which would explain the exponential shape. This could also account for the rostral-caudal axis perturbation as observed in EphB2KO (Hindges et al., 2002), and some dorsal-ventral perturbations as observed in ephrin-A2/A5KO (Feldheim et al., 2000).

Mapping of retino-collicular projections is probably a more complex process than that which can be carried by a single class of molecules. The causal effect of gradient perturbation remains to be fully demonstrated, since other actors are probably involved. To ensure robustness other mechanisms

need to be involved. Activity is not required for the establishment of a rough topography (Benjumbeda et al., 2013), but seems critical in refinement.

Different processes for different maps.

The results obtained in the *Isl2-ephrin-A3KI* raises questions regarding the implication of correlated activity in refinement of the cortico-collicular map. Indeed, a spontaneous correlated activity pattern seems unlikely to occur between the retinal and the cortical inputs, since a delay would be introduced between the mono- (Retina → SC) and the tri-synaptic pathway (Retina → dLGN → V1 → SC). This would explain the presence of duplications with short distance separations observed, since these eTZs cannot be eliminated through correlated activity. According to spike-time dependent plasticity (STDP), connections are either strengthened or weakened according to both the temporal window as well as the order of pre- and post-firing. In addition, activity-dependent refinement through STDP probably eliminates eTZ in ephrin-As KO in a particular distance, and reinforces them past a critical zone. This suggests that a minimal distance is required for the stabilization these connections and as consequence, eTZs far from the correct topographic site are not eliminated.

Similarly, the mapping of the rostral-caudal axis and the dorsal-ventral seems to occur through different processes. Indeed, the nasal-temporal one is specifically disrupted in ephrin-As KO in the V1 (Cang et al., 2008b). The presence of a dorsal-ventral patterning in the optical nerve, a presorting of axons, also suggest different mapping mechanisms for the different classes of Ephs (Plas et al., 2005).

Different EphAs and ephrin-As for different functions.

Over-expression of ephrin-A3 in *Isl2+* RGCs does not seem to lead to inactivation of endogenous EphAs, suggesting a high specificity of EphA/ephrin-A interactions in cis. Such specificity in cis-binding between given ephrin- A/EphA pairs have been shown previously (Carvalho et al., 2006; Yin et al., 2004) in different cell types, including RGCs. Cis-inactivation of endogenous EphA4/A5/A6 receptors by over-expressed ephrin-A3 would generate a distinct population of RGCs expressing different levels of active EphA receptors that would lead – according to the Relative Signaling mechanism (Bevins et al., 2011; Brown et al., 2000; Reber et al., 2004) – to the formation of a duplicated (partial of full) retino-collicular map. In ephrin-A3KI, such duplications are not observed in the retino-collicular map, suggesting that ephrin-A3 does not cis-inactivate endogenous retinal EphA receptors. To further confirm this, retino-collicular projections from compound mutants ephrin-A3KI/KI;EphA4KO were also assessed. Here, decreasing the overall level of retinal EphA receptors by suppressing EphA4 expression (in EphA4^{+/-} and EphA4^{-/-} backgrounds) would reveal a cis-interaction with endogenous EphA5/A6, which will lead retino-collicular map duplication. An effect on map duplication should be particularly pronounced in the nasal pole of the retina (projecting caudally in the SC), where EphA5/A6 are expressed at very low levels compared to EphA4. As shown below, in both ephrin-A3KI/KI;EphA4^{+/-} and ephrin-A3KI/KI;EphA4^{-/-}, retino-collicular maps are not duplicated, suggesting that ephrin-A3 does not cis-inactivate endogenous EphA5/A6 receptors.

Behavior of the *Isl2-EphA3KI*

The behavioral study conducted in the *Isl2-EphA3KI* mouse model is to date, the only one conducted in an animal model in which the retinotopy is specifically altered in the SC. In other models with an EphA/ephrin-A disruption, the targeting is global, which can lead to an impairment in many different brain structures/pathways. The fact that the representation of the visual space is specifically

altered in the SC, has allowed the investigation of its implication in behavior. The results are quite remarkable and demonstrates that even if vision is unaltered, some specific behavioral defects related to visual attention can be found in these animals.

However, since both the retino- and the cortico-collicular maps are fully duplicated in these animals, specific projections that are involved cannot be addressed; however a partial duplication of both retino- and cortico-collicular maps is not sufficient to induce significant attentional deficits. In addition, a recent study demonstrated that when mice are trained to run constantly on a spinning disk, an arrest behavior (stop in locomotion) can be induced by solely activating the cortico-collicular fibers (Liang et al., 2015). As a consequence, it would be very interesting to perform the same behavioral tests in the *Isl2-ephrin-A3KI* mouse model in which the disruption is specific for the cortico-collicular map. The mismatch between both maps might induce conflicting behavioral outputs in tasks with a distractor.

Functional imaging

The results obtained at an anatomical level might not show significant functional changes, as ectopic sites might not be strengthened by correlated activity, and as a consequence, only make a small contribution to the function. Optical intrinsic imaging might not be able to reveal a duplication of the cortico-collicular map, since the relative contribution of the retino- and the cortico-collicular map to the overall signal is to date not known, and anesthesia is known to decrease cortical signals. In addition the distance separation might not be sufficient to reveal an alteration in the retinotopy, according to the spatial resolution. However a 2-photon calcium imaging approach, with a specific labeling of the cortico-collicular projections, might allow the investigation of these duplications.

References

- Ackman, J.B., Burbridge, T.J., and Crair, M.C. (2012). Retinal waves coordinate patterned activity throughout the developing visual system. *Nature* 490, 219–225.
- Akrouh, A., and Kerschensteiner, D. (2013). Intersecting Circuits Generate Precisely Patterned Retinal Waves. *Neuron* 79, 322–334.
- Aletta, J.M., and Greene, L.A. (1988). Growth cone configuration and advance: a time-lapse study using video-enhanced differential interference contrast microscopy. *J. Neurosci. Off. J. Soc. Neurosci.* 8, 1425–1435.
- Applebury, M.L., Antoch, M.P., Baxter, L.C., Chun, L.L., Falk, J.D., Farhangfar, F., Kage, K., Krzystolik, M.G., Lyass, L.A., and Robbins, J.T. (2000). The murine cone photoreceptor: a single cone type expresses both S and M opsins with retinal spatial patterning. *Neuron* 27, 513–523.
- Armstrong, R.A. (2011). Visual signs and symptoms of progressive supranuclear palsy. *Clin. Exp. Optom.* 94, 150–160.
- Arnall, S., Cheam, L.Y., Smart, C., Rengel, A., Fitzgerald, M., Thivierge, J.P., and Rodger, J. (2010). Abnormal strategies during visual discrimination reversal learning in ephrin-A2(-/-) mice. *Behav. Brain Res.* 209, 109–113.
- Arvanitis, D., and Davy, A. (2008). Eph/ephrin signaling: networks. *Genes Dev.* 22, 416–429.
- Aston-Jones, G., and Cohen, J.D. (2005). An integrative theory of locus coeruleus-norepinephrine function: adaptive gain and optimal performance. *Annu. Rev. Neurosci.* 28, 403–450.
- Attardi, D.G., and Sperry, R.W. (1963). Preferential selection of central pathways by regenerating optic fibers. *Exp. Neurol.* 7, 46–64.
- Baden, T., Schubert, T., Chang, L., Wei, T., Zaichuk, M., Wissinger, B., and Euler, T. (2013). A Tale of Two Retinal Domains: Near-Optimal Sampling of Achromatic Contrasts in Natural Scenes through Asymmetric Photoreceptor Distribution. *Neuron* 80, 1206–1217.
- Baden, T., Berens, P., Franke, K., Román Rosón, M., Bethge, M., and Euler, T. (2016). The functional diversity of retinal ganglion cells in the mouse. *Nature* 529, 345–350.
- Bansal, A., Singer, J.H., Hwang, B.J., Xu, W., Beaudet, A., and Feller, M.B. (2000). Mice lacking specific nicotinic acetylcholine receptor subunits exhibit dramatically altered spontaneous activity patterns and reveal a limited role for retinal waves in forming ON and OFF circuits in the inner retina. *J. Neurosci. Off. J. Soc. Neurosci.* 20, 7672–7681.
- Behan, M., Jourdain, A., and Bray, G.M. (1992). Calcium binding protein (calbindin D28k) immunoreactivity in the hamster superior colliculus: ultrastructure and lack of co-localization with GABA. *Exp. Brain Res.* 89, 115–124.
- Behan, M., Steinhacker, K., Jeffrey-Borger, S., and Meredith, M.A. (2002). Chemoarchitecture of GABAergic neurons in the ferret superior colliculus. *J. Comp. Neurol.* 452, 334–359.
- Benjumbeda, I., Escalante, A., Law, C., Morales, D., Chauvin, G., Muca, G., Coca, Y., Marquez, J., Lopez-Bendito, G., Kania, A., et al. (2013). Uncoupling of EphA/ephrinA Signaling and Spontaneous Activity in Neural Circuit Wiring. *J. Neurosci.* 33, 18208–18218.

- Bevins, N., Lemke, G., and Reber, M. (2011). Genetic Dissection of EphA Receptor Signaling Dynamics during Retinotopic Mapping. *J. Neurosci.* *31*, 10302–10310.
- Bi, G.Q., and Poo, M.M. (1998). Synaptic modifications in cultured hippocampal neurons: dependence on spike timing, synaptic strength, and postsynaptic cell type. *J. Neurosci. Off. J. Soc. Neurosci.* *18*, 10464–10472.
- Biederman, J. (2005). Attention-Deficit/Hyperactivity Disorder: A Selective Overview. *Biol. Psychiatry* *57*, 1215–1220.
- Birgbauer, E., Cowan, C.A., Sretavan, D.W., and Henkemeyer, M. (2000). Kinase independent function of EphB receptors in retinal axon pathfinding to the optic disc from dorsal but not ventral retina. *Dev. Camb. Engl.* *127*, 1231–1241.
- Blankenship, A.G., Ford, K.J., Johnson, J., Seal, R.P., Edwards, R.H., Copenhagen, D.R., and Feller, M.B. (2009). Synaptic and extrasynaptic factors governing glutamatergic retinal waves. *Neuron* *62*, 230–241.
- Bolton, A.D., Murata, Y., Kirchner, R., Kim, S.-Y., Young, A., Dang, T., Yanagawa, Y., and Constantine-Paton, M. (2015). A Diencephalic Dopamine Source Provides Input to the Superior Colliculus, where D1 and D2 Receptors Segregate to Distinct Functional Zones. *Cell Rep.* *13*, 1003–1015.
- Bonhoeffer, F., and Huf, J. (1980). Recognition of cell types by axonal growth cones in vitro. *Nature* *288*, 162–164.
- Bonhoeffer, F., and Huf, J. (1982). In vitro experiments on axon guidance demonstrating an anterior-posterior gradient on the tectum. *EMBO J.* *1*, 427–431.
- Bonhoeffer, F., and Huf, J. (1985). Position-dependent properties of retinal axons and their growth cones. *Nature* *315*, 409–410.
- Brace, L.R., Kraev, I., Rostron, C.L., Stewart, M., Overton, P.G., and Dommett, E.J. (2015). Altered visual processing in a rodent model of Attention-Deficit Hyperactivity Disorder. *Neuroscience* *303*, 364–377.
- Braisted, J.E., McLaughlin, T., Wang, H.U., Friedman, G.C., Anderson, D.J., and O’leary, D.D. (1997). Graded and lamina-specific distributions of ligands of EphB receptor tyrosine kinases in the developing retinotectal system. *Dev. Biol.* *191*, 14–28.
- Briggs, F., Mangun, G.R., and Usrey, W.M. (2013). Attention enhances synaptic efficacy and the signal-to-noise ratio in neural circuits. *Nature* *499*, 476–480.
- Brown, A., Yates, P.A., Burrola, P., Ortuño, D., Vaidya, A., Jessell, T.M., Pfaff, S.L., O’Leary, D.D., and Lemke, G. (2000). Topographic mapping from the retina to the midbrain is controlled by relative but not absolute levels of EphA receptor signaling. *Cell* *102*, 77–88.
- Bruckner, K., Pasquale, E.B., and Klein, R. (1997). Tyrosine Phosphorylation of Transmembrane Ligands for Eph Receptors. *Science* *275*, 1640–1643.
- Buhusi, M., Demyanenko, G.P., Jannie, K.M., Dalal, J., Darnell, E.P.B., Weiner, J.A., and Maness, P.F. (2009). ALCAM Regulates Mediolateral Retinotopic Mapping in the Superior Colliculus. *J. Neurosci.* *29*, 15630–15641.

Bush, J.O., and Soriano, P. (2009). Ephrin-B1 regulates axon guidance by reverse signaling through a PDZ-dependent mechanism. *Genes Dev.* 23, 1586–1599.

Butts, D.A., and Rokhsar, D.S. (2001). The information content of spontaneous retinal waves. *J. Neurosci. Off. J. Soc. Neurosci.* 21, 961–973.

del Campo, N., Chamberlain, S.R., Sahakian, B.J., and Robbins, T.W. (2011). The Roles of Dopamine and Noradrenaline in the Pathophysiology and Treatment of Attention-Deficit/Hyperactivity Disorder. *Biol. Psychiatry* 69, e145–e157.

Cang, J., and Feldheim, D.A. (2013). Developmental Mechanisms of Topographic Map Formation and Alignment. *Annu. Rev. Neurosci.* 36, 51–77.

Cang, J., Kaneko, M., Yamada, J., Woods, G., Stryker, M.P., and Feldheim, D.A. (2005a). Ephrin-As Guide the Formation of Functional Maps in the Visual Cortex. *Neuron* 48, 577–589.

Cang, J., Rentería, R.C., Kaneko, M., Liu, X., Copenhagen, D.R., and Stryker, M.P. (2005b). Development of Precise Maps in Visual Cortex Requires Patterned Spontaneous Activity in the Retina. *Neuron* 48, 797–809.

Cang, J., Wang, L., Stryker, M.P., and Feldheim, D.A. (2008a). Roles of Ephrin-As and Structured Activity in the Development of Functional Maps in the Superior Colliculus. *J. Neurosci.* 28, 11015–11023.

Cang, J., Niell, C.M., Liu, X., Pfeifferberger, C., Feldheim, D.A., and Stryker, M.P. (2008b). Selective Disruption of One Cartesian Axis of Cortical Maps and Receptive Fields by Deficiency in Ephrin-As and Structured Activity. *Neuron* 57, 511–523.

Carandini, M., Shimaoka, D., Rossi, L.F., Sato, T.K., Benucci, A., and Knopfel, T. (2015). Imaging the Awake Visual Cortex with a Genetically Encoded Voltage Indicator. *J. Neurosci.* 35, 53–63.

Carter-Dawson, L.D., and LaVail, M.M. (1979). Rods and cones in the mouse retina. I. Structural analysis using light and electron microscopy. *J. Comp. Neurol.* 188, 245–262.

Carvalho, R.F., Beutler, M., Marler, K.J.M., Knöll, B., Becker-Barroso, E., Heintzmann, R., Ng, T., and Drescher, U. (2006). Silencing of EphA3 through a cis interaction with ephrinA5. *Nat. Neurosci.* 9, 322–330.

Chandrasekaran, A.R. (2005). Evidence for an Instructive Role of Retinal Activity in Retinotopic Map Refinement in the Superior Colliculus of the Mouse. *J. Neurosci.* 25, 6929–6938.

Chenau, G., and Henkemeyer, M. (2011). Forward signaling by EphB1/EphB2 interacting with ephrin-B ligands at the optic chiasm is required to form the ipsilateral projection. *Eur. J. Neurosci.* 34, 1620–1633.

Cheng, H.J., and Flanagan, J.G. (1994). Identification and cloning of ELF-1, a developmentally expressed ligand for the Mek4 and Sek receptor tyrosine kinases. *Cell* 79, 157–168.

Cheng, H.-J., Nakamoto, M., Bergemann, A.D., and Flanagan, J.G. (1995). Complementary gradients in expression and binding of ELF-1 and Mek4 in development of the topographic retinotectal projection map. *Cell* 82, 371–381.

Cheng, T.-W., Liu, X.-B., Faulkner, R.L., Stephan, A.H., Barres, B.A., Huberman, A.D., and Cheng, H.-J. (2010). Emergence of Lamina-Specific Retinal Ganglion Cell Connectivity by Axon Arbor Retraction

and Synapse Elimination. *J. Neurosci.* *30*, 16376–16382.

Cherry, T.J., Trimarchi, J.M., Stadler, M.B., and Cepko, C.L. (2009). Development and diversification of retinal amacrine interneurons at single cell resolution. *Proc. Natl. Acad. Sci.* *106*, 9495–9500.

Chklovskii, D.B., and Koulakov, A.A. (2004). MAPS IN THE BRAIN: What Can We Learn from Them? *Annu. Rev. Neurosci.* *27*, 369–392.

Clascá, F., Rubio-Garrido, P., and Jabaudon, D. (2012). Unveiling the diversity of thalamocortical neuron subtypes: Thalamocortical neuron diversity. *Eur. J. Neurosci.* *35*, 1524–1532.

Clements, K.M., Devonshire, I.M., Reynolds, J.N.J., and Overton, P.G. (2014). Enhanced visual responses in the superior colliculus in an animal model of attention-deficit hyperactivity disorder and their suppression by d-amphetamine. *Neuroscience* *274*, 289–298.

Cline, H. (2003). Sperry and Hebb: oil and vinegar? *Trends Neurosci.* *26*, 655–661.

Colonnese, M.T., and Constantine-Paton, M. (2006). Developmental period for N-methyl-D-aspartate (NMDA) receptor-dependent synapse elimination correlated with visuotopic map refinement. *J. Comp. Neurol.* *494*, 738–751.

Colonnese, M.T., and Khazipov, R. (2010). “Slow activity transients” in infant rat visual cortex: a spreading synchronous oscillation patterned by retinal waves. *J. Neurosci. Off. J. Soc. Neurosci.* *30*, 4325–4337.

Constantine-Paton, M., and Law, M.I. (1978). Eye-specific termination bands in tecta of three-eyed frogs. *Science* *202*, 639–641.

Cook, P.M., Prusky, G., and Ramoa, A.S. (1999). The role of spontaneous retinal activity before eye opening in the maturation of form and function in the retinogeniculate pathway of the ferret. *Vis. Neurosci.* *16*, 491–501.

Coombs, J., van der List, D., Wang, G.-Y., and Chalupa, L.M. (2006). Morphological properties of mouse retinal ganglion cells. *Neuroscience* *140*, 123–136.

Cooper, M.A., Crockett, D.P., Nowakowski, R.S., Gale, N.W., and Zhou, R. (2009). Distribution of EphA5 receptor protein in the developing and adult mouse nervous system. *J. Comp. Neurol.* *514*, 310–328.

Cowan, C.A., and Henkemeyer, M. (2001). The SH2/SH3 adaptor Grb4 transduces B-ephrin reverse signals. *Nature* *413*, 174–179.

Cowan, C.A., Yokoyama, N., Bianchi, L.M., Henkemeyer, M., and Fritsch, B. (2000). EphB2 guides axons at the midline and is necessary for normal vestibular function. *Neuron* *26*, 417–430.

Cowan, C.W., Shao, Y.R., Sahin, M., Shamah, S.M., Lin, M.Z., Greer, P.L., Gao, S., Griffith, E.C., Brugge, J.S., and Greenberg, M.E. (2005). Vav family GEFs link activated Ephs to endocytosis and axon guidance. *Neuron* *46*, 205–217.

Cruz-Martín, A. (2014). A dedicated circuit links direction-selective retinal ganglion cells to the primary visual cortex. *Nature* *507*, 358–361.

Cutsuridis, V., Kumari, V., and Ettinger, U. (2014). Antisaccade performance in schizophrenia: a neural model of decision making in the superior colliculus. *Front. Neurosci.* *8*.

- Davis, S., Gale, N.W., Aldrich, T.H., Maisonpierre, P.C., Lhotak, V., Pawson, T., Goldfarb, M., and Yancopoulos, G.D. (1994). Ligands for EPH-related receptor tyrosine kinases that require membrane attachment or clustering for activity. *Science* 266, 816–819.
- Davy, A. (2000). Ephrin-A5 modulates cell adhesion and morphology in an integrin-dependent manner. *EMBO J.* 19, 5396–5405.
- Davy, A., Gale, N.W., Murray, E.W., Klinghoffer, R.A., Soriano, P., Feuerstein, C., and Robbins, S.M. (1999). Compartmentalized signaling by GPI-anchored ephrin-A5 requires the Fyn tyrosine kinase to regulate cellular adhesion. *Genes Dev.* 13, 3125–3135.
- Davy, A., Aubin, J., and Soriano, P. (2004). Ephrin-B1 forward and reverse signaling are required during mouse development. *Genes Dev.* 18, 572–583.
- Demb, J.B., and Singer, J.H. (2015a). Functional Circuitry of the Retina. *Annu. Rev. Vis. Sci.* 1, 263–289.
- Demb, J.B., and Singer, J.H. (2015b). Functional Circuitry of the Retina. *Annu. Rev. Vis. Sci.* 1, 263–289.
- Dent, E.W., and Gertler, F.B. (2003). Cytoskeletal Dynamics and Transport in Growth Cone Motility and Axon Guidance. *Neuron* 40, 209–227.
- Deschamps, C., Morel, M., Janet, T., Page, G., Jaber, M., Gaillard, A., and Prestoz, L. (2010). EphrinA5 protein distribution in the developing mouse brain. *BMC Neurosci.* 11, 105.
- Dhande, O.S., Hua, E.W., Guh, E., Yeh, J., Bhatt, S., Zhang, Y., Ruthazer, E.S., Feller, M.B., and Crair, M.C. (2011). Development of Single Retinofugal Axon Arbors in Normal and 2 Knock-Out Mice. *J. Neurosci.* 31, 3384–3399.
- Dhande, O.S., Bhatt, S., Anishchenko, A., Elstrott, J., Iwasato, T., Swindell, E.C., Xu, H.-P., Jamrich, M., Itoharu, S., Feller, M.B., et al. (2012). Role of adenylate cyclase 1 in retinofugal map development. *J. Comp. Neurol.* 520, 1562–1583.
- Dhande, O.S., Estevez, M.E., Quattrochi, L.E., El-Danaf, R.N., Nguyen, P.L., Berson, D.M., and Huberman, A.D. (2013). Genetic dissection of retinal inputs to brainstem nuclei controlling image stabilization. *J. Neurosci. Off. J. Soc. Neurosci.* 33, 17797–17813.
- Dhande, O.S., Stafford, B.K., Lim, J.-H.A., and Huberman, A.D. (2015). Contributions of Retinal Ganglion Cells to Subcortical Visual Processing and Behaviors. *Annu. Rev. Vis. Sci.* 1, 291–328.
- Diaz, E., Yang, Y.H., Ferreira, T., Loh, K.C., Okazaki, Y., Hayashizaki, Y., Tessier-Lavigne, M., Speed, T.P., and Ngai, J. (2003). Analysis of gene expression in the developing mouse retina. *Proc. Natl. Acad. Sci.* 100, 5491–5496.
- Dickson, B.J. (2002). Molecular mechanisms of axon guidance. *Science* 298, 1959–1964.
- Dommett, E.J., Overton, P.G., and Greenfield, S.A. (2009). Drug therapies for attentional disorders alter the signal-to-noise ratio in the superior colliculus. *Neuroscience* 164, 1369–1376.
- Douglas, R.J., and Martin, K.A.C. (2004). NEURONAL CIRCUITS OF THE NEOCORTEX. *Annu. Rev. Neurosci.* 27, 419–451.
- Dräger, U.C. (1975). Receptive fields of single cells and topography in mouse visual cortex. *J. Comp.*

Neurol. 160, 269–290.

Dräger, U.C., and Hubel, D.H. (1975). Physiology of visual cells in mouse superior colliculus and correlation with somatosensory and auditory input. *Nature* 253, 203–204.

Dräger, U.C., and Hubel, D.H. (1976). Topography of visual and somatosensory projections to mouse superior colliculus. *J. Neurophysiol.* 39, 91–101.

Dravis, C., Yokoyama, N., Chumley, M.J., Cowan, C.A., Silvany, R.E., Shay, J., Baker, L.A., and Henkemeyer, M. (2004). Bidirectional signaling mediated by ephrin-B2 and EphB2 controls urorectal development. *Dev. Biol.* 271, 272–290.

Drescher, U., Kremoser, C., Handwerker, C., Löschinger, J., Noda, M., and Bonhoeffer, F. (1995). In vitro guidance of retinal ganglion cell axons by RAGS, a 25 kDa tectal protein related to ligands for Eph receptor tyrosine kinases. *Cell* 82, 359–370.

Dütting, D., Handwerker, C., and Drescher, U. (1999). Topographic Targeting and Pathfinding Errors of Retinal Axons Following Overexpression of EphrinA Ligands on Retinal Ganglion Cell Axons. *Dev. Biol.* 216, 297–311.

Egea, J., Nissen, U.V., Dufour, A., Sahin, M., Greer, P., Kullander, K., Mrsic-Flogel, T.D., Greenberg, M.E., Kiehn, O., Vanderhaeghen, P., et al. (2005). Regulation of EphA 4 kinase activity is required for a subset of axon guidance decisions suggesting a key role for receptor clustering in Eph function. *Neuron* 47, 515–528.

Eglen, S.J., Demas, J., and Wong, R.O.L. (2003). Mapping by waves. Patterned spontaneous activity regulates retinotopic map refinement. *Neuron* 40, 1053–1055.

Ellis, C., Kasmi, F., Ganju, P., Walls, E., Panayotou, G., and Reith, A.D. (1996). A juxtamembrane autophosphorylation site in the Eph family receptor tyrosine kinase, Sek, mediates high affinity interaction with p59fyn. *Oncogene* 12, 1727–1736.

Ellis, E.M., Gauvain, G., Sivyer, B., and Murphy, G.J. (2016). Shared and Distinct Retinal Input to the Mouse Superior Colliculus and Dorsal Lateral Geniculate Nucleus. *J. Neurophysiol.* jn.00227.2016.

Elowe, S., Holland, S.J., Kulkarni, S., and Pawson, T. (2001). Downregulation of the Ras-Mitogen-Activated Protein Kinase Pathway by the EphB2 Receptor Tyrosine Kinase Is Required for Ephrin-Induced Neurite Retraction. *Mol. Cell. Biol.* 21, 7429–7441.

Endo, T., Yanagawa, Y., Obata, K., and Isa, T. (2003). Characteristics of GABAergic neurons in the superficial superior colliculus in mice. *Neurosci. Lett.* 346, 81–84.

Euler, T., Haverkamp, S., Schubert, T., and Baden, T. (2014). Retinal bipolar cells: elementary building blocks of vision. *Nat. Rev. Neurosci.* 15, 507–519.

Famiglietti, E.V. (1992). Dendritic co-stratification of ON and ON-OFF directionally selective ganglion cells with starburst amacrine cells in rabbit retina. *J. Comp. Neurol.* 324, 322–335.

Fang, W.B., Brantley-Sieders, D.M., Hwang, Y., Ham, A.-J.L., and Chen, J. (2008). Identification and Functional Analysis of Phosphorylated Tyrosine Residues within EphA2 Receptor Tyrosine Kinase. *J. Biol. Chem.* 283, 16017–16026.

Feinberg, E.H., and Meister, M. (2015). Orientation columns in the mouse superior colliculus. *Nature* 519, 229–232.

- Feldheim, D.A. (2004). Loss-of-Function Analysis of EphA Receptors in Retinotectal Mapping. *J. Neurosci.* *24*, 2542–2550.
- Feldheim, D.A., Vanderhaeghen, P., Hansen, M.J., Frisén, J., Lu, Q., Barbacid, M., and Flanagan, J.G. (1998). Topographic guidance labels in a sensory projection to the forebrain. *Neuron* *21*, 1303–1313.
- Feldheim, D.A., Kim, Y.-I., Bergemann, A.D., Frisén, J., Barbacid, M., and Flanagan, J.G. (2000). Genetic analysis of ephrin-A2 and ephrin-A5 shows their requirement in multiple aspects of retinocollicular mapping. *Neuron* *25*, 563–574.
- Feller, M.B. (1999). Spontaneous correlated activity in developing neural circuits. *Neuron* *22*, 653–656.
- Feller, M.B. (2002). The role of nAChR-mediated spontaneous retinal activity in visual system development. *J. Neurobiol.* *53*, 556–567.
- Feller, M.B., Wellis, D.P., Stellwagen, D., Werblin, F.S., and Shatz, C.J. (1996). Requirement for cholinergic synaptic transmission in the propagation of spontaneous retinal waves. *Science* *272*, 1182–1187.
- Feller, M.B., Butts, D.A., Aaron, H.L., Rokhsar, D.S., and Shatz, C.J. (1997). Dynamic processes shape spatiotemporal properties of retinal waves. *Neuron* *19*, 293–306.
- Firl, A., Sack, G.S., Newman, Z.L., Tani, H., and Feller, M.B. (2013). Extrasynaptic glutamate and inhibitory neurotransmission modulate ganglion cell participation during glutamatergic retinal waves. *J. Neurophysiol.* *109*, 1969–1978.
- Firl, A., Ke, J.-B., Zhang, L., Fuerst, P.G., Singer, J.H., and Feller, M.B. (2015). Elucidating the Role of All Amacrine Cells in Glutamatergic Retinal Waves. *J. Neurosci.* *35*, 1675–1686.
- Firth, S.I., Wang, C.-T., and Feller, M.B. (2005). Retinal waves: mechanisms and function in visual system development. *Cell Calcium* *37*, 425–432.
- Flanagan, J.G. (2006). Neural map specification by gradients. *Curr. Opin. Neurobiol.* *16*, 59–66.
- Flanagan, J.G., and Vanderhaeghen, P. (1998). The ephrins and Eph receptors in neural development. *Annu. Rev. Neurosci.* *21*, 309–345.
- Ford, K.J., Félix, A.L., and Feller, M.B. (2012). Cellular mechanisms underlying spatiotemporal features of cholinergic retinal waves. *J. Neurosci. Off. J. Soc. Neurosci.* *32*, 850–863.
- Frisén, J., Yates, P.A., McLaughlin, T., Friedman, G.C., O’Leary, D.D., and Barbacid, M. (1998). Ephrin-A5 (AL-1/RAGS) is essential for proper retinal axon guidance and topographic mapping in the mammalian visual system. *Neuron* *20*, 235–243.
- Gale, S.D., and Murphy, G.J. (2014). Distinct representation and distribution of visual information by specific cell types in mouse superficial superior colliculus. *J. Neurosci. Off. J. Soc. Neurosci.* *34*, 13458–13471.
- Gale, N.W., Holland, S.J., Valenzuela, D.M., Flenniken, A., Pan, L., Ryan, T.E., Henkemeyer, M., Strebhardt, K., Hirai, H., Wilkinson, D.G., et al. (1996). Eph Receptors and Ligands Comprise Two Major Specificity Subclasses and Are Reciprocally Compartmentalized during Embryogenesis. *Neuron* *17*, 9–19.

- Galli, L., and Maffei, L. (1988). Spontaneous impulse activity of rat retinal ganglion cells in prenatal life. *Science* 242, 90–91.
- Gao, E., DeAngelis, G.C., and Burkhalter, A. (2010). Parallel Input Channels to Mouse Primary Visual Cortex. *J. Neurosci.* 30, 5912–5926.
- Gebhardt, C., Bastmeyer, M., and Weth, F. (2012). Balancing of ephrin/Eph forward and reverse signaling as the driving force of adaptive topographic mapping. *Development* 139, 335–345.
- Genander, M., Halford, M.M., Xu, N.-J., Eriksson, M., Yu, Z., Qiu, Z., Martling, A., Greicius, G., Thakar, S., Catchpole, T., et al. (2009). Dissociation of EphB2 Signaling Pathways Mediating Progenitor Cell Proliferation and Tumor Suppression. *Cell* 139, 679–692.
- Ghosh, K.K., Bujan, S., Haverkamp, S., Feigenspan, A., and Wässle, H. (2004). Types of bipolar cells in the mouse retina. *J. Comp. Neurol.* 469, 70–82.
- Gierer, A. (1983). Model for the Retino-Tectal Projection. *Proceedings of the Royal Society B: Biological Sciences* 218, 77–93.
- Gierer, A. (1987). Directional cues for growing axons forming the retinotectal projection. *Development* 101, 479–489.
- Glickfeld, L.L., Andermann, M.L., Bonin, V., and Reid, R.C. (2013). Cortico-cortical projections in mouse visual cortex are functionally target specific. *Nat. Neurosci.* 16, 219–226.
- Goldberg, D.J., and Burmeister, D.W. (1986). Stages in axon formation: observations of growth of *Aplysia* axons in culture using video-enhanced contrast-differential interference contrast microscopy. *J. Cell Biol.* 103, 1921–1931.
- González-Soriano, J., González-Flores, M.L., Contreras-Rodríguez, J., Rodríguez-Veiga, E., and Martínez-Sainz, P. (2000). Calbindin D28k and parvalbumin immunoreactivity in the rabbit superior colliculus: an anatomical study. *Anat. Rec.* 259, 334–346.
- Goodhill, G.J. (2016). Can Molecular Gradients Wire the Brain? *Trends Neurosci.* 39, 202–211.
- Gowan, J.D., Coizet, V., Devonshire, I.M., and Overton, P.G. (2008). d-Amphetamine depresses visual responses in the rat superior colliculus: a possible mechanism for amphetamine-induced decreases in distractibility. *J. Neural Transm.* 115, 377–387.
- Grant, E., Hoerder-Suabedissen, A., and Molnár, Z. (2016). The Regulation of Corticofugal Fiber Targeting by Retinal Inputs. *Cereb. Cortex* 26, 1336–1348.
- Greferath, U., Canty, A.J., Messenger, J., and Murphy, M. (2002). Developmental expression of EphA4-tyrosine kinase receptor in the mouse brain and spinal cord. *Gene Expr. Patterns GEP* 2, 267–274.
- Grubb, M.S., Rossi, F.M., Changeux, J.P., and Thompson, I.D. (2003). Abnormal functional organization in the dorsal lateral geniculate nucleus of mice lacking the beta 2 subunit of the nicotinic acetylcholine receptor. *Neuron* 40, 1161–1172.
- Hansen, M.J., Dallal, G.E., and Flanagan, J.G. (2004). Retinal axon response to ephrin-as shows a graded, concentration-dependent transition from growth promotion to inhibition. *Neuron* 42, 717–730.
- Harting, J.K., Huerta, M.F., Hashikawa, T., and van Lieshout, D.P. (1991). Projection of the

- mammalian superior colliculus upon the dorsal lateral geniculate nucleus: Organization of tectogeniculate pathways in nineteen species. *J. Comp. Neurol.* 304, 275–306.
- Hattar, S., Kumar, M., Park, A., Tong, P., Tung, J., Yau, K.-W., and Berson, D.M. (2006). Central projections of melanopsin-expressing retinal ganglion cells in the mouse. *J. Comp. Neurol.* 497, 326–349.
- Hattori, M., Osterfield, M., and Flanagan, J.G. (2000). Regulated cleavage of a contact-mediated axon repellent. *Science* 289, 1360–1365.
- Haustead, D.J., Lukehurst, S.S., Clutton, G.T., Bartlett, C.A., Dunlop, S.A., Arrese, C.A., Sherrard, R.M., and Rodger, J. (2008). Functional topography and integration of the contralateral and ipsilateral retinocollicular projections of ephrin-A/- mice. *J. Neurosci. Off. J. Soc. Neurosci.* 28, 7376–7386.
- Hebb, D.O. (2002). *The organization of behavior: a neuropsychological theory* (Mahwah, NJ: Erlbaum).
- Henkemeyer, M., Orioli, D., Henderson, J.T., Saxton, T.M., Roder, J., Pawson, T., and Klein, R. (1996). Nuk Controls Pathfinding of Commissural Axons in the Mammalian Central Nervous System. *Cell* 86, 35–46.
- Hilbig, H., Merbach, M., Krause, J., Gärtner, U., and Stubbe, A. (2000). Dendritic organization of neurons of the superior colliculus in animals with different visual capability. *Brain Res. Bull.* 51, 255–265.
- Himanen, J.-P., Chumley, M.J., Lackmann, M., Li, C., Barton, W.A., Jeffrey, P.D., Vearing, C., Geleick, D., Feldheim, D.A., Boyd, A.W., et al. (2004). Repelling class discrimination: ephrin-A5 binds to and activates EphB2 receptor signaling. *Nat. Neurosci.* 7, 501–509.
- Himmelstein, J., Newcorn, J.H., and Halperin, J.M. (2000). The neurobiology of attention-deficit hyperactivity disorder. *Front. Biosci. J. Virtual Libr.* 5, D461–D478.
- Hindges, R., McLaughlin, T., Genoud, N., Henkemeyer, M., and O’Leary, D.D. (2002). EphB forward signaling controls directional branch extension and arborization required for dorsal-ventral retinotopic mapping. *Neuron* 35, 475–487.
- Hjorth, J.J.J., Savier, E., Sterratt, D.C., Reber, M., and Eglen, S.J. (2015). Estimating the location and size of retinal injections from orthogonal images of an intact retina. *BMC Neurosci.* 16.
- Hofbauer, A., and Dräger, U.C. (1985). Depth segregation of retinal ganglion cells projecting to mouse superior colliculus. *J. Comp. Neurol.* 234, 465–474.
- Holland, S.J., Gale, N.W., Mbamalu, G., Yancopoulos, G.D., Henkemeyer, M., and Pawson, T. (1996). Bidirectional signalling through the EPH-family receptor Nuk and its transmembrane ligands. *Nature* 383, 722–725.
- Holmberg, J., Genander, M., Halford, M.M., Annerén, C., Sondell, M., Chumley, M.J., Silvany, R.E., Henkemeyer, M., and Frisén, J. (2006). EphB Receptors Coordinate Migration and Proliferation in the Intestinal Stem Cell Niche. *Cell* 125, 1151–1163.
- Honda, H. (2003). Competition between retinal ganglion axons for targets under the servomechanism model explains abnormal retinocollicular projection of Eph receptor-overexpressing or ephrin-lacking mice. *J. Neurosci.* 23, 10368–10377.

- Hong, Y.K., Kim, I.-J., and Sanes, J.R. (2011). Stereotyped axonal arbors of retinal ganglion cell subsets in the mouse superior colliculus. *J. Comp. Neurol.* *519*, 1691–1711.
- Hope, R.A., Hammond, B.J., and Gaze, R.M. (1976). The Arrow Model: Retinotectal Specificity and Map Formation in the Goldfish Visual System. *Proc. R. Soc. B Biol. Sci.* *194*, 447–466.
- Hornberger, M.R., Dütting, D., Ciossek, T., Yamada, T., Handwerker, C., Lang, S., Weth, F., Huf, J., Weis sel, R., Logan, C., et al. (1999). Modulation of EphA receptor function by coexpressed ephrinA ligands on retinal ganglion cell axons. *Neuron* *22*, 731–742.
- Huai, J., and Drescher, U. (2001). An ephrin-A-dependent Signaling Pathway Controls Integrin Function and Is Linked to the Tyrosine Phosphorylation of a 120-kDa Protein. *J. Biol. Chem.* *276*, 6689–6694.
- Huang, L., and Pallas, S.L. (2001). NMDA antagonists in the superior colliculus prevent developmental plasticity but not visual transmission or map compression. *J. Neurophysiol.* *86*, 1179–1194.
- Hubel, D.H., and Wiesel, T.N. (1962). Receptive fields, binocular interaction and functional architecture in the cat's visual cortex. *J. Physiol.* *160*, 106–154.
- Huberman, A.D., and Niell, C.M. (2011). What can mice tell us about how vision works? *Trends Neurosci* *34*, 464–473.
- Huberman, A.D., Stellwagen, D., and Chapman, B. (2002). Decoupling eye-specific segregation from lamination in the lateral geniculate nucleus. *J. Neurosci. Off. J. Soc. Neurosci.* *22*, 9419–9429.
- Huberman, A.D., Wang, G.-Y., Liets, L.C., Collins, O.A., Chapman, B., and Chalupa, L.M. (2003). Eye-specific retinogeniculate segregation independent of normal neuronal activity. *Science* *300*, 994–998.
- Huberman, A.D., Murray, K.D., Warland, D.K., Feldheim, D.A., and Chapman, B. (2005). Ephrin-As mediate targeting of eye-specific projections to the lateral geniculate nucleus. *Nat. Neurosci.* *8*, 1013–1021.
- Huberman, A.D., Manu, M., Koch, S.M., Susman, M.W., Lutz, A.B., Ullian, E.M., Baccus, S.A., and Barres, B.A. (2008). Architecture and Activity-Mediated Refinement of Axonal Projections from a Mosaic of Genetically Identified Retinal Ganglion Cells. *Neuron* *59*, 425–438.
- Huberman, A.D., Wei, W., Elstrott, J., Stafford, B.K., Feller, M.B., and Barres, B.A. (2009). Genetic Identification of an On-Off Direction- Selective Retinal Ganglion Cell Subtype Reveals a Layer-Specific Subcortical Map of Posterior Motion. *Neuron* *62*, 327–334.
- Inayat, S., Barchini, J., Chen, H., Feng, L., Liu, X., and Cang, J. (2015). Neurons in the Most Superficial Lamina of the Mouse Superior Colliculus Are Highly Selective for Stimulus Direction. *J. Neurosci.* *35*, 7992–8003.
- Isa, T. (2002). Intrinsic processing in the mammalian superior colliculus. *Curr. Opin. Neurobiol.* *12*, 668–677.
- Isa, T., and Saito, Y. (2001). The direct visuo-motor pathway in mammalian superior colliculus; novel perspective on the interlaminar connection. *Neurosci. Res.* *41*, 107–113.
- Janes, P.W., Saha, N., Barton, W.A., Kolev, M.V., Wimmer-Kleikamp, S.H., Nievergall, E., Blobel, C.P., Himanen, J.-P., Lackmann, M., and Nikolov, D.B. (2005). Adam meets Eph: an ADAM substrate recognition module acts as a molecular switch for ephrin cleavage in trans. *Cell* *123*, 291–304.

- Kaas, J.H. (1997). Topographic maps are fundamental to sensory processing. *Brain Res. Bull.* *44*, 107–112.
- Kalatsky, V.A., and Stryker, M.P. (2003). New Paradigm for Optical Imaging. *Neuron* *38*, 529–545.
- Katz, L.C., and Shatz, C.J. (1996). Synaptic activity and the construction of cortical circuits. *Science* *274*, 1133–1138.
- Kay, J.N. (2011). Retinal ganglion cells with distinct directional preferences differ in molecular identity, structure, and central projections. *J Neurosci* *31*, 7753–7762.
- Kerschensteiner, D. (2016). Glutamatergic Retinal Waves. *Front. Neural Circuits* *10*.
- Khachab, M.Y., and Bruce, L.L. (1999). The development of corticocollicular projections in anophthalmic mice. *Brain Res. Dev. Brain Res.* *114*, 179–192.
- Kim, I.J., Zhang, Y., Yamagata, M., Meister, M., and Sanes, J.R. (2008a). Laminar restriction of retinal ganglion cell dendrites and axons: subtype-specific developmental patterns revealed with transgenic markers. *Nature* *452*, 478–482.
- Kim, I.-J., Zhang, Y., Yamagata, M., Meister, M., and Sanes, J.R. (2008b). Molecular identification of a retinal cell type that responds to upward motion. *Nature* *452*, 478–482.
- Kim, I.-J., Zhang, Y., Meister, M., and Sanes, J.R. (2010). Laminar Restriction of Retinal Ganglion Cell Dendrites and Axons: Subtype-Specific Developmental Patterns Revealed with Transgenic Markers. *J. Neurosci.* *30*, 1452–1462.
- Kirkby, L.A., Sack, G.S., Firl, A., and Feller, M.B. (2013). A Role for Correlated Spontaneous Activity in the Assembly of Neural Circuits. *Neuron* *80*, 1129–1144.
- Knoll, B. (2004). Src Family Kinases Are Involved in EphA Receptor-Mediated Retinal Axon Guidance. *J. Neurosci.* *24*, 6248–6257.
- Kondo, S., and Ohki, K. (2015). Laminar differences in the orientation selectivity of geniculate afferents in mouse primary visual cortex. *Nat. Neurosci.* *19*, 316–319.
- Koulakov, A.A., and Tsigankov, D.N. (2004). A stochastic model for retinocollicular map development. *BMC Neurosci.* *5*, 30.
- Krauzlis, R.J., Lovejoy, L.P., and Zénon, A. (2013). Superior Colliculus and Visual Spatial Attention. *Annu. Rev. Neurosci.* *36*, 165–182.
- Kullander, K., Mather, N.K., Diella, F., Dottori, M., Boyd, A.W., and Klein, R. (2001). Kinase-dependent and kinase-independent functions of EphA4 receptors in major axon tract formation in vivo. *Neuron* *29*, 73–84.
- Langer, T.P., and Lund, R.D. (1974). The upper layers of the superior colliculus of the rat: A Golgi study. *J. Comp. Neurol.* *158*, 405–435.
- Leamey, C.A., Merlin, S., Lattouf, P., Sawatari, A., Zhou, X., Demel, N., Glendinning, K.A., Oohashi, T., Sur, M., and Fässler, R. (2007). *Ten_m3* regulates eye-specific patterning in the mammalian visual pathway and is required for binocular vision. *PLoS Biol.* *5*, e241.
- Lee, J.-Y., Choi, J.-S., Ahn, C.-H., Kim, I.-S., Ha, J.-H., and Jeon, C.-J. (2006). Calcium-binding

protein calretinin immunoreactivity in the dog superior colliculus. *Acta Histochem. Cytochem.* **39**, 125–138.

Lee, P.H., Helms, M.C., Augustine, G.J., and Hall, W.C. (1997). Role of intrinsic synaptic circuitry in collicular sensorimotor integration. *Proc. Natl. Acad. Sci. U. S. A.* **94**, 13299–13304.

Liang, F., Xiong, X.R., Zingg, B., Ji, X., Zhang, L.I., and Tao, H.W. (2015). Sensory Cortical Control of a Visually Induced Arrest Behavior via Corticotectal Projections. *Neuron* **86**, 755–767.

Lim, Y.-S., McLaughlin, T., Sung, T.-C., Santiago, A., Lee, K.-F., and O’Leary, D.D.M. (2008). p75NTR Mediates Ephrin-A Reverse Signaling Required for Axon Repulsion and Mapping. *Neuron* **59**, 746–758.

Lin, B., Wang, S.W., and Masland, R.H. (2004). Retinal ganglion cell type, size, and spacing can be specified independent of homotypic dendritic contacts. *Neuron* **43**, 475–485.

Liu, C.J., Chaturvedi, N., Barnstable, C.J., and Dreyer, E.B. (1996). Retinal Thy-1 expression during development. *Invest. Ophthalmol. Vis. Sci.* **37**, 1469–1473.

Liu, Y.-J., Ehrenguber, M.U., Negwer, M., Shao, H.-J., Cetin, A.H., and Lyon, D.C. (2013). Tracing Inputs to Inhibitory or Excitatory Neurons of Mouse and Cat Visual Cortex with a Targeted Rabies Virus. *Curr. Biol.* **23**, 1746–1755.

Lomber, S.G., Payne, B.R., and Cornwell, P. (2001). Role of the superior colliculus in analyses of space: superficial and intermediate layer contributions to visual orienting, auditory orienting, and visuospatial discriminations during unilateral and bilateral deactivations. *J. Comp. Neurol.* **441**, 44–57.

Lovejoy, L.P., and Krauzlis, R.J. (2010). Inactivation of primate superior colliculus impairs covert selection of signals for perceptual judgments. *Nat Neurosci* **13**, 261–266.

Lund, R.D. (1966). The occipitotectal pathway of the rat. *J. Anat.* **100**, 51–62.

Lund, R.D. (1972). Anatomic studies on the superior colliculus. *Invest. Ophthalmol. Vis. Sci.* **11**, 434–441.

Luo, L., and Flanagan, J.G. (2007). Development of Continuous and Discrete Neural Maps. *Neuron* **56**, 284–300.

Lur, G., Vinck, M.A., Tang, L., Cardin, J.A., and Higley, M.J. (2016). Projection-Specific Visual Feature Encoding by Layer 5 Cortical Subnetworks. *Cell Rep.* **14**, 2538–2545.

Maffei, L., and Galli-Resta, L. (1990). Correlation in the discharges of neighboring rat retinal ganglion cells during prenatal life. *Proc. Natl. Acad. Sci. U. S. A.* **87**, 2861–2864.

Maiorano, N.A., and Hindges, R. (2013). Restricted perinatal retinal degeneration induces retina reshaping and correlated structural rearrangement of the retinotopic map. *Nat. Commun.* **4**.

Marcus, R.C., Gale, N.W., Morrison, M.E., Mason, C.A., and Yancopoulos, G.D. (1996). Eph family receptors and their ligands distribute in opposing gradients in the developing mouse retina. *Dev. Biol.* **180**, 786–789.

Marler, K.J., Poopalasundaram, S., Broom, E.R., Wentzel, C., and Drescher, U. (2010). Pro-neurotrophins secreted from retinal ganglion cell axons are necessary for ephrinA-p75NTR-mediated axon guidance. *Neural Develop.* **5**, 30.

- Marler, K.J.M., Becker-Barroso, E., Martinez, A., Llovera, M., Wentzel, C., Poopalasundaram, S., Hindges, R., Soriano, E., Comella, J., and Drescher, U. (2008). A TrkB/EphrinA Interaction Controls Retinal Axon Branching and Synaptogenesis. *J. Neurosci.* *28*, 12700–12712.
- Marquardt, T., Shirasaki, R., Ghosh, S., Andrews, S.E., Carter, N., Hunter, T., and Pfaff, S.L. (2005). Coexpressed EphA Receptors and Ephrin-A Ligands Mediate Opposing Actions on Growth Cone Navigation from Distinct Membrane Domains. *Cell* *121*, 127–139.
- Marshel, J.H., Garrett, M.E., Nauhaus, I., and Callaway, E.M. (2011). Functional Specialization of Seven Mouse Visual Cortical Areas. *Neuron* *72*, 1040–1054.
- Maskery, S., and Shinbrot, T. (2005). Deterministic and Stochastic Elements of Axonal Guidance. *Annu. Rev. Biomed. Eng.* *7*, 187–221.
- Masland, R.H. (1977). Maturation of function in the developing rabbit retina. *J. Comp. Neurol.* *175*, 275–286.
- Mathis, C., Savier, E., Bott, J.-B., Clesse, D., Bevins, N., Sage-Ciocca, D., Geiger, K., Gillet, A., Laux-Biehlmann, A., and Goumon, Y. (2014). Defective response inhibition and collicular noradrenaline enrichment in mice with duplicated retinotopic map in the superior colliculus. *Brain Struct. Funct.* 1–12.
- May, P.J. (2006). The mammalian superior colliculus: laminar structure and connections. In *Progress in Brain Research*, (Elsevier), pp. 321–378.
- McLaughlin, T., Torborg, C.L., Feller, M.B., and O’Leary, D.D.M. (2003). Retinotopic Map Refinement Requires Spontaneous Retinal Waves during a Brief Critical Period of Development. *Neuron* *40*, 1147–1160.
- Meister, M., Wong, R.O., Baylor, D.A., and Shatz, C.J. (1991). Synchronous bursts of action potentials in ganglion cells of the developing mammalian retina. *Science* *252*, 939–943.
- Métin, C., Godement, P., and Imbert, M. (1988). The primary visual cortex in the mouse: receptive field properties and functional organization. *Exp. Brain Res.* *69*, 594–612.
- Miao, H., Wei, B.R., Peehl, D.M., Li, Q., Alexandrou, T., Schelling, J.R., Rhim, J.S., Sedor, J.R., Burnett, E., and Wang, B. (2001). Activation of EphA receptor tyrosine kinase inhibits the Ras/MAPK pathway. *Nat. Cell Biol.* *3*, 527–530.
- Migani, P., Bartlett, C., Dunlop, S., Beazley, L., and Rodger, J. (2009). Regional and cellular distribution of ephrin-B1 in adult mouse brain. *Brain Res.* *1247*, 50–61.
- Miller, L. (2009). Perspectives on sensory processing disorder: a call for translational research. *Front. Integr. Neurosci.* *3*.
- Miller, E.D., Tran, M.N., Wong, G.K., Oakley, D.M., and Wong, R.O. (1999). Morphological differentiation of bipolar cells in the ferret retina. *Vis. Neurosci.* *16*, 1133–1144.
- Ming, G., Song, H., Berninger, B., Holt, C.E., Tessier-Lavigne, M., and Poo, M. (1997). cAMP-Dependent Growth Cone Guidance by Netrin-1. *Neuron* *19*, 1225–1235.
- Mize, R.R. (1992). The organization of GABAergic neurons in the mammalian superior colliculus. *Prog. Brain Res.* *90*, 219–248.
- Mize, R.R., Luo, Q., Butler, G., Jeon, C.-J., and Nabors, B. (1992). The calcium binding proteins

- parvalbumin and calbindin-D 28K form complementary patterns in the cat superior colliculus. *J. Comp. Neurol.* **320**, 243–256.
- Monschau, B. (1997). Shared and distinct functions of RAGS and ELF-1 in guiding retinal axons. *EMBO J.* **16**, 1258–1267.
- Mooney, R., Penn, A.A., Gallego, R., and Shatz, C.J. (1996). Thalamic Relay of Spontaneous Retinal Activity Prior to Vision. *Neuron* **17**, 863–874.
- Morin, L.P., and Studholme, K.M. (2014). Retinofugal projections in the mouse: Mouse Visual System. *J. Comp. Neurol.* **522**, 3733–3753.
- Mrsic-Flogel, T.D. (2005). Altered Map of Visual Space in the Superior Colliculus of Mice Lacking Early Retinal Waves. *J. Neurosci.* **25**, 6921–6928.
- Muir-Robinson, G., Hwang, B.J., and Feller, M.B. (2002). Retinogeniculate axons undergo eye-specific segregation in the absence of eye-specific layers. *J. Neurosci. Off. J. Soc. Neurosci.* **22**, 5259–5264.
- Nakamoto, M., Cheng, H.-J., Friedman, G.C., McLaughlin, T., Hansen, M.J., Yoon, C.H., O’Leary, D.D., and Flanagan, J.G. (1996). Topographically specific effects of ELF-1 on retinal axon guidance in vitro and retinal axon mapping in vivo. *Cell* **86**, 755–766.
- Nicol, X. (2006). Requirement of Adenylate Cyclase 1 for the Ephrin-A5-Dependent Retraction of Exuberant Retinal Axons. *J. Neurosci.* **26**, 862–872.
- Nicol, X., Voyatzis, S., Muzerelle, A., Narboux-Nême, N., Südhof, T.C., Miles, R., and Gaspar, P. (2007). cAMP oscillations and retinal activity are permissive for ephrin signaling during the establishment of the retinotopic map. *Nat. Neurosci.* **10**, 340–347.
- Niell, C.M., and Stryker, M.P. (2008). Highly selective receptive fields in mouse visual cortex. *J. Neurosci. Off. J. Soc. Neurosci.* **28**, 7520–7536.
- Nikonov, S.S., Kholodenko, R., Lem, J., and Pugh, E.N. (2006). Physiological Features of the S- and M-cone Photoreceptors of Wild-type Mice from Single-cell Recordings. *J. Gen. Physiol.* **127**, 359–374.
- O’Leary, D.D., Fawcett, J.W., and Cowan, W.M. (1986). Topographic targeting errors in the retinocollicular projection and their elimination by selective ganglion cell death. *J. Neurosci. Off. J. Soc. Neurosci.* **6**, 3692–3705.
- Overton, K.J., and Arbib, M.A. (1982). The Extended Branch-Arrow Model of the formation of retinotectal connections. *Biological Cybernetics* **45**, 157–175.
- Overton, P.G. (2008). Collicular dysfunction in attention deficit hyperactivity disorder. *Med. Hypotheses* **70**, 1121–1127.
- Owens, M.T., Feldheim, D.A., Stryker, M.P., and Triplett, J.W. (2015). Stochastic Interaction between Neural Activity and Molecular Cues in the Formation of Topographic Maps. *Neuron* **87**, 1261–1273.
- Palmer, A., Zimmer, M., Erdmann, K.S., Eulenburg, V., Porthin, A., Heumann, R., Deutsch, U., and Klein, R. (2002). EphrinB phosphorylation and reverse signaling: regulation by Src kinases and PTP-BL phosphatase. *Mol. Cell* **9**, 725–737.
- Penn, A.A., Riquelme, P.A., Feller, M.B., and Shatz, C.J. (1998). Competition in retinogeniculate patterning driven by spontaneous activity. *Science* **279**, 2108–2112.

- Petros, T.J., Shrestha, B.R., and Mason, C. (2009). Specificity and Sufficiency of EphB1 in Driving the Ipsilateral Retinal Projection. *J. Neurosci.* *29*, 3463–3474.
- Petros, T.J., Bryson, J.B., and Mason, C. (2010). Ephrin-B2 elicits differential growth cone collapse and axon retraction in retinal ganglion cells from distinct retinal regions. *Dev. Neurobiol.* *70*, 781–794.
- Pfeiffenberger, C., Cutforth, T., Woods, G., Yamada, J., Rentería, R.C., Copenhagen, D.R., Flanagan, J.G., and Feldheim, D.A. (2005). Ephrin-As and neural activity are required for eye-specific patterning during retinogeniculate mapping. *Nat. Neurosci.* *8*, 1022–1027.
- Pfeiffenberger, C., Yamada, J., and Feldheim, D.A. (2006). Ephrin-As and Patterned Retinal Activity Act Together in the Development of Topographic Maps in the Primary Visual System. *J. Neurosci.* *26*, 12873–12884.
- Phongphananee, P., Marino, R.A., Kaneda, K., Yanagawa, Y., Munoz, D.P., and Isa, T. (2014). Distinct local circuit properties of the superficial and intermediate layers of the rodent superior colliculus. *Eur. J. Neurosci.* *40*, 2329–2343.
- Pisauro, M.A., Dhruv, N.T., Carandini, M., and Benucci, A. (2013). Fast Hemodynamic Responses in the Visual Cortex of the Awake Mouse. *J. Neurosci.* *33*, 18343–18351.
- Plas, D.T., Visel, A., Gonzalez, E., She, W.-C., and Crair, M.C. (2004). Adenylate Cyclase 1 dependent refinement of retinotopic maps in the mouse. *Vision Res.* *44*, 3357–3364.
- Plas, D.T., Lopez, J.E., and Crair, M.C. (2005). Pretarget sorting of retinocollicular axons in the mouse. *J. Comp. Neurol.* *491*, 305–319.
- Polack, P.-O., and Contreras, D. (2012). Long-Range Parallel Processing and Local Recurrent Activity in the Visual Cortex of the Mouse. *J. Neurosci.* *32*, 11120–11131.
- Politis, M.J., Ederle, K., and Spencer, P.S. (1982). Tropism in nerve regeneration in vivo. Attraction of regenerating axons by diffusible factors derived from cells in distal nerve stumps of transected peripheral nerves. *Brain Res.* *253*, 1–12.
- Prestige, M.C., and Willshaw, D.J. (1975). On a Role for Competition in the Formation of Patterned Neural Connexions. *Proceedings of the Royal Society B: Biological Sciences* *190*, 77–98.
- Prusky, G.T., and Douglas, R.M. (2004). Characterization of mouse cortical spatial vision. *Vision Res.* *44*, 3411–3418.
- Rajan, I., and Cline, H.T. (1998). Glutamate receptor activity is required for normal development of tectal cell dendrites in vivo. *J. Neurosci. Off. J. Soc. Neurosci.* *18*, 7836–7846.
- Rash, B.G., and Grove, E.A. (2006). Area and layer patterning in the developing cerebral cortex. *Curr. Opin. Neurobiol.* *16*, 25–34.
- Rashid, T., Upton, A.L., Blentic, A., Ciossek, T., Knöll, B., Thompson, I.D., and Drescher, U. (2005). Opposing Gradients of Ephrin-As and EphA7 in the Superior Colliculus Are Essential for Topographic Mapping in the Mammalian Visual System. *Neuron* *47*, 57–69.
- Razak, K.A. (2003). NMDA Receptor Blockade in the Superior Colliculus Increases Receptive Field Size Without Altering Velocity and Size Tuning. *J. Neurophysiol.* *90*, 110–119.
- Reber, M., Burrola, P., and Lemke, G. (2004). A relative signalling model for the formation of a

topographic neural map. *Nature* **431**, 847–853.

Reh, T.A., and Constantine-Paton, M. (1985). Eye-specific segregation requires neural activity in three-eyed *Rana pipiens*. *J. Neurosci. Off. J. Soc. Neurosci.* **5**, 1132–1143.

Rhoades, R.W., Mooney, R.D., and Fish, S.E. (1985). Subcortical projections of area 17 in the anophthalmic mouse. *Brain Res.* **349**, 171–181.

Rivlin-Etzion, M. (2011). Transgenic mice reveal unexpected diversity of on-off direction-selective retinal ganglion cell subtypes and brain structures involved in motion processing. *J Neurosci* **31**, 8760–8769.

Rogers, J., Ciossek, T., Ullrich, A., West, E., Hoare, M., and Muir, E.. (1999). Distribution of the receptor EphA7 and its ligands in development of the mouse nervous system. *Mol. Brain Res.* **74**, 225–230.

Ross, K.C., and Coleman, J.R. (2000). Developmental and genetic audiogenic seizure models: behavior and biological substrates. *Neurosci. Biobehav. Rev.* **24**, 639–653.

Rossi, F.M., Pizzorusso, T., Porciatti, V., Marubio, L.M., Maffei, L., and Changeux, J.P. (2001). Requirement of the nicotinic acetylcholine receptor beta 2 subunit for the anatomical and functional development of the visual system. *Proc. Natl. Acad. Sci. U. S. A.* **98**, 6453–6458.

Runyan, C.A., Schummers, J., Van Wart, A., Kuhlman, S.J., Wilson, N.R., Huang, Z.J., and Sur, M. (2010). Response Features of Parvalbumin-Expressing Interneurons Suggest Precise Roles for Subtypes of Inhibition in Visual Cortex. *Neuron* **67**, 847–857.

Ruthazer, E.S., Akerman, C.J., and Cline, H.T. (2003). Control of axon branch dynamics by correlated activity in vivo. *Science* **301**, 66–70.

Sagvolden, T. (2000). Behavioral validation of the spontaneously hypertensive rat (SHR) as an animal model of attention-deficit/hyperactivity disorder (AD/HD). *Neurosci. Biobehav. Rev.* **24**, 31–39.

Sahin, M., Greer, P.L., Lin, M.Z., Poucher, H., Eberhart, J., Schmidt, S., Wright, T.M., Shamah, S.M., O'Connell, S., Cowan, C.W., et al. (2005). Eph-Dependent Tyrosine Phosphorylation of Ephexin1 Modulates Growth Cone Collapse. *Neuron* **46**, 191–204.

Sanes, J.R., and Masland, R.H. (2015). The Types of Retinal Ganglion Cells: Current Status and Implications for Neuronal Classification. *Annu. Rev. Neurosci.* **38**, 221–246.

Schuett, S., Bonhoeffer, T., and Hübener, M. (2002). Mapping retinotopic structure in mouse visual cortex with optical imaging. *J. Neurosci. Off. J. Soc. Neurosci.* **22**, 6549–6559.

Shah, R.D., and Crair, M.C. (2008). Retinocollicular Synapse Maturation and Plasticity Are Regulated by Correlated Retinal Waves. *J. Neurosci.* **28**, 292–303.

Shamah, S.M., Lin, M.Z., Goldberg, J.L., Estrach, S., Sahin, M., Hu, L., Bazalakova, M., Neve, R.L., Corfas, G., Debant, A., et al. (2001). EphA Receptors Regulate Growth Cone Dynamics through the Novel Guanine Nucleotide Exchange Factor Ephexin. *Cell* **105**, 233–244.

Shanks, J.A., Ito, S., Schaevitz, L., Yamada, J., Chen, B., Litke, A., and Feldheim, D.A. (2016). Corticothalamic Axons Are Essential for Retinal Ganglion Cell Axon Targeting to the Mouse Dorsal Lateral Geniculate Nucleus. *J. Neurosci.* **36**, 5252–5263.

- Shatz, C.J., and Stryker, M.P. (1988). Prenatal tetrodotoxin infusion blocks segregation of retinogeniculate afferents. *Science* 242, 87–89.
- Siegel, F., Heimel, J.A., Peters, J., and Lohmann, C. (2012). Peripheral and central inputs shape network dynamics in the developing visual cortex in vivo. *Curr. Biol.* CB 22, 253–258.
- Simon, D.K., and O’leary, D.D. (1992). Development of topographic order in the mammalian retinocollicular projection. *J. Neurosci.* 12, 1212–1232.
- Simon, D.K., Prusky, G.T., O’Leary, D.D., and Constantine-Paton, M. (1992). N-methyl-D-aspartate receptor antagonists disrupt the formation of a mammalian neural map. *Proc. Natl. Acad. Sci. U. S. A.* 89, 10593–10597.
- Song, H., Ming, G., He, Z., Lehmann, M., McKerracher, L., Tessier-Lavigne, M., and Poo, M. (1998). Conversion of neuronal growth cone responses from repulsion to attraction by cyclic nucleotides. *Science* 281, 1515–1518.
- Song, H.J., Ming, G.L., and Poo, M.M. (1997). cAMP-induced switching in turning direction of nerve growth cones. *Nature* 388, 275–279.
- Sontag, T.A., Tucha, O., Walitza, S., and Lange, K.W. (2010). Animal models of attention deficit/hyperactivity disorder (ADHD): a critical review. *ADHD Atten. Deficit Hyperact. Disord.* 2, 1–20.
- Sperry, R.W. (1963). Chemoaffinity in the orderly growth of nerve fiber patterns and connections. *Proc. Natl. Acad. Sci. U. S. A.* 50, 703.
- Sprague, J.M., and Meikle, T.H. (1965). THE ROLE OF THE SUPERIOR COLLICULUS IN VISUALLY GUIDED BEHAVIOR. *Exp. Neurol.* 11, 115–146.
- Stafford, B.K., Sher, A., Litke, A.M., and Feldheim, D.A. (2009). Spatial-Temporal Patterns of Retinal Waves Underlying Activity-Dependent Refinement of Retinofugal Projections. *Neuron* 64, 200–212.
- Stellwagen, D., and Shatz, C.J. (2002). An Instructive Role for Retinal Waves in the Development of Retinogeniculate Connectivity. *Neuron* 33, 357–367.
- Stubblefield, E.A., Costabile, J.D., and Felsen, G. (2013). Optogenetic investigation of the role of the superior colliculus in orienting movements. *Behav. Brain Res.* 255, 55–63.
- Suetterlin, P., and Drescher, U. (2014). Target-Independent EphrinA/EphA-Mediated Axon-Axon Repulsion as a Novel Element in Retinocollicular Mapping. *Neuron* 84, 740–752.
- Sun, C., Speer, C.M., Wang, G.-Y., Chapman, B., and Chalupa, L.M. (2008a). Epibatidine application in vitro blocks retinal waves without silencing all retinal ganglion cell action potentials in developing retina of the mouse and ferret. *J. Neurophysiol.* 100, 3253–3263.
- Sun, C., Warland, D.K., Ballesteros, J.M., van der List, D., and Chalupa, L.M. (2008b). Retinal waves in mice lacking the 2 subunit of the nicotinic acetylcholine receptor. *Proc. Natl. Acad. Sci.* 105, 13638–13643.
- Sun, W., Deng, Q., Levick, W.R., and He, S. (2006). ON direction-selective ganglion cells in the mouse retina: ON DSGCs in the mouse retina. *J. Physiol.* 576, 197–202.
- Sun, W., Tan, Z., Mensh, B.D., and Ji, N. (2015). Thalamus provides layer 4 of primary visual cortex with orientation- and direction-tuned inputs. *Nat. Neurosci.* 19, 308–315.

- Sutherland, K.R., Alsop, B., McNaughton, N., Hyland, B.I., Tripp, G., and Wickens, J.R. (2009). Sensitivity to delay of reinforcement in two animal models of attention deficit hyperactivity disorder (ADHD). *Behav. Brain Res.* *205*, 372–376.
- Szél, á., Röhlich, P., Gaffé, A.R., Juliusson, B., Aguirre, G., and Van Veen, T. (1992). Unique topographic separation of two spectral classes of cones in the mouse retina: TOPOGRAPHIC SEPARATION OF MOUSE RETINAL CONES. *J. Comp. Neurol.* *325*, 327–342.
- Tan, Z., Sun, W., Chen, T.-W., Kim, D., and Ji, N. (2015). Neuronal Representation of Ultraviolet Visual Stimuli in Mouse Primary Visual Cortex. *Sci. Rep.* *5*, 12597.
- Tasic, B., Menon, V., Nguyen, T.N., Kim, T.K., Jarsky, T., Yao, Z., Levi, B., Gray, L.T., Sorensen, S.A., Dolbeare, T., et al. (2016). Adult mouse cortical cell taxonomy revealed by single cell transcriptomics. *Nat. Neurosci.* *19*, 335–346.
- Tessier-Lavigne, M. (1995). Eph receptor tyrosine kinases, axon repulsion, and the development of topographic maps. *Cell* *82*, 345–348.
- Tessier-Lavigne, M., Placzek, M., Lumsden, A.G., Dodd, J., and Jessell, T.M. (1988). Chemotropic guidance of developing axons in the mammalian central nervous system. *Nature* *336*, 775–778.
- Thakar, S., Chenuaux, G., and Henkemeyer, M. (2011). Critical roles for EphB and ephrin-B bidirectional signalling in retinocollicular mapping. *Nat. Commun.* *2*, 431.
- Thoreson, W.B., and Mangel, S.C. (2012). Lateral interactions in the outer retina. *Prog. Retin. Eye Res.* *31*, 407–441.
- Tohmi, M., Meguro, R., Tsukano, H., Hishida, R., and Shibuki, K. (2014). The Extrageniculate Visual Pathway Generates Distinct Response Properties in the Higher Visual Areas of Mice. *Curr. Biol.* *24*, 587–597.
- Torborg, C.L., and Feller, M.B. (2005). Spontaneous patterned retinal activity and the refinement of retinal projections. *Prog. Neurobiol.* *76*, 213–235.
- Torborg, C.L., Hansen, K.A., and Feller, M.B. (2005). High frequency, synchronized bursting drives eye-specific segregation of retinogeniculate projections. *Nat. Neurosci.* *8*, 72–78.
- Trappenberg, T.P., Dorris, M.C., Munoz, D.P., and Klein, R.M. (2001). A Model of Saccade Initiation Based on the Competitive Integration of Exogenous and Endogenous Signals in the Superior Colliculus. *J. Cogn. Neurosci.* *13*, 256–271.
- Triplett, J.W., Owens, M.T., Yamada, J., Lemke, G., Cang, J., Stryker, M.P., and Feldheim, D.A. (2009). Retinal Input Instructs Alignment of Visual Topographic Maps. *Cell* *139*, 175–185.
- Triplett, J.W., Pfeiffenberger, C., Yamada, J., Stafford, B.K., Sweeney, N.T., Litke, A.M., Sher, A., Koulakov, A.A., and Feldheim, D.A. (2011). Competition is a driving force in topographic mapping. *Proc. Natl. Acad. Sci.* *108*, 19060–19065.
- Triplett, J.W., Wei, W., Gonzalez, C., Sweeney, N.T., Huberman, A.D., Feller, M.B., and Feldheim, D.A. (2014). Dendritic and axonal targeting patterns of a genetically-specified class of retinal ganglion cells that participate in image-forming circuits. *Neural Develop.* *9*, 2.
- Tsigankov, D., and Koulakov, A.A. (2010). Sperry versus Hebb: Topographic mapping in *Isl2/EphA3* mutant mice. *BMC Neurosci.* *11*, 155.

- Upton, A.L., Salichon, N., Lebrand, C., Ravary, A., Blakely, R., Seif, I., and Gaspar, P. (1999). Excess of serotonin (5-HT) alters the segregation of ipsilateral and contralateral retinal projections in monoamine oxidase A knock-out mice: possible role of 5-HT uptake in retinal ganglion cells during development. *J. Neurosci. Off. J. Soc. Neurosci.* *19*, 7007–7024.
- Upton, A.L., Ravary, A., Salichon, N., Moessner, R., Lesch, K.-P., Hen, R., Seif, I., and Gaspar, P. (2002). Lack of 5-HT(1B) receptor and of serotonin transporter have different effects on the segregation of retinal axons in the lateral geniculate nucleus compared to the superior colliculus. *Neuroscience* *111*, 597–610.
- Vaney, D.I., Sivyer, B., and Taylor, W.R. (2012). Direction selectivity in the retina: symmetry and asymmetry in structure and function. *Nat. Rev. Neurosci.*
- Van Hooser, S.D. (2007). Similarity and diversity in visual cortex: is there a unifying theory of cortical computation? *Neurosci. Rev. J. Bringing Neurobiol. Neurol. Psychiatry* *13*, 639–656.
- Van Wyk, M., Wässle, H., and Taylor, W.R. (2009). Receptive field properties of ON- and OFF-ganglion cells in the mouse retina. *Vis. Neurosci.* *26*, 297.
- Vélez-Fort, M., Rousseau, C.V., Niedworok, C.J., Wickersham, I.R., Rancz, E.A., Brown, A.P.Y., Strom, M., and Margrie, T.W. (2014). The Stimulus Selectivity and Connectivity of Layer Six Principal Cells Reveals Cortical Microcircuits Underlying Visual Processing. *Neuron* *83*, 1431–1443.
- Volkow, N.D., Wang, G., Fowler, J.S., Logan, J., Gerasimov, M., Maynard, L., Ding, Y., Gatley, S.J., Gifford, A., and Franceschi, D. (2001). Therapeutic doses of oral methylphenidate significantly increase extracellular dopamine in the human brain. *J. Neurosci. Off. J. Soc. Neurosci.* *21*, RC121.
- von der Malsburg, C., and Willshaw, D.J. (1977). How to label nerve cells so that they can interconnect in an ordered fashion. *Proc. Natl. Acad. Sci. U.S.A.* *74*, 5176–5178.
- Wagor, E., Mangini, N.J., and Pearlman, A.L. (1980). Retinotopic organization of striate and extrastriate visual cortex in the mouse. *J. Comp. Neurol.* *193*, 187–202.
- Wahl, S., Barth, H., Ciossek, T., Aktories, K., and Mueller, B.K. (2000). Ephrin-A5 induces collapse of growth cones by activating Rho and Rho kinase. *J. Cell Biol.* *149*, 263–270.
- Wallace, M.T., Meredith, M.A., and Stein, B.E. (1993). Converging influences from visual, auditory, and somatosensory cortices onto output neurons of the superior colliculus. *J. Neurophysiol.* *69*, 1797–1809.
- Walter, J., Kern-Veits, B., Huf, J., Stolze, B., and Bonhoeffer, F. (1987a). Recognition of position-specific properties of tectal cell membranes by retinal axons in vitro. *Dev. Camb. Engl.* *101*, 685–696.
- Walter, J., Henke-Fahle, S., and Bonhoeffer, F. (1987b). Avoidance of posterior tectal membranes by temporal retinal axons. *Development* *101*, 909–913.
- Walter, J., Müller, B., and Bonhoeffer, F. (1990). Axonal guidance by an avoidance mechanism. *J. Physiol. (Paris)* *84*, 104–110.
- Wang, Q., and Burkhalter, A. (2007). Area map of mouse visual cortex. *J. Comp. Neurol.* *502*, 339–357.
- Wang, Q., Gao, E., and Burkhalter, A. (2011). Gateways of Ventral and Dorsal Streams in Mouse Visual Cortex. *J. Neurosci.* *31*, 1905–1918.

- Wei, Y., Tsigankov, D., and Koulakov, A. (2013). The molecular basis for the development of neural maps: Development of neural maps. *Ann. N. Y. Acad. Sci.* *1305*, 44–60.
- Weinl, C., Drescher, U., Lang, S., Bonhoeffer, F., and Lösschinger, J. (2003). On the turning of *Xenopus* retinal axons induced by ephrin-A5. *Dev. Camb. Engl.* *130*, 1635–1643.
- Weth, F., Fiederling, F., Gebhardt, C., and Bastmeyer, M. (2014). Chemoaffinity in topographic mapping revisited--is it more about fiber-fiber than fiber-target interactions? *Semin. Cell Dev. Biol.* *35*, 126–135.
- Wilks, T.A., Rodger, J., and Harvey, A.R. (2010). A role for ephrin-As in maintaining topographic organization in register across interconnected central visual pathways. *Eur. J. Neurosci.* *31*, 613–622.
- Williams, S.E., Mann, F., Erskine, L., Sakurai, T., Wei, S., Rossi, D.J., Gale, N.W., Holt, C.E., Mason, C.A., and Henkemeyer, M. (2003). Ephrin-B2 and EphB1 mediate retinal axon divergence at the optic chiasm. *Neuron* *39*, 919–935.
- Wong, R.O.L. (1999). RETINAL WAVES AND VISUAL SYSTEM DEVELOPMENT. *Annu. Rev. Neurosci.* *22*, 29–47.
- Wong, R.O., Meister, M., and Shatz, C.J. (1993). Transient period of correlated bursting activity during development of the mammalian retina. *Neuron* *11*, 923–938.
- Wong, R.O., Chernjavsky, A., Smith, S.J., and Shatz, C.J. (1995). Early functional neural networks in the developing retina. *Nature* *374*, 716–718.
- Wong, W.T., Myhr, K.L., Miller, E.D., and Wong, R.O. (2000). Developmental changes in the neurotransmitter regulation of correlated spontaneous retinal activity. *J. Neurosci. Off. J. Soc. Neurosci.* *20*, 351–360.
- Wurzman, R., Forcelli, P.A., Griffey, C.J., and Kromer, L.F. (2015). Repetitive grooming and sensorimotor abnormalities in an ephrin-A knockout model for Autism Spectrum Disorders. *Behav. Brain Res.* *278*, 115–128.
- Xiang, M., Zhou, L., Macke, J.P., Yoshioka, T., Hendry, S.H., Eddy, R.L., Shows, T.B., and Nathans, J. (1995). The Brn-3 family of POU-domain factors: primary structure, binding specificity, and expression in subsets of retinal ganglion cells and somatosensory neurons. *J. Neurosci. Off. J. Soc. Neurosci.* *15*, 4762–4785.
- Xu, N.-J., and Henkemeyer, M. (2009). Ephrin-B3 reverse signaling through Grb4 and cytoskeletal regulators mediates axon pruning. *Nat. Neurosci.* *12*, 268–276.
- Xu, H., Furman, M., Mineur, Y.S., Chen, H., King, S.L., Zenisek, D., Zhou, Z.J., Butts, D.A., Tian, N., Picciotto, M.R., et al. (2011). An Instructive Role for Patterned Spontaneous Retinal Activity in Mouse Visual Map Development. *Neuron* *70*, 1115–1127.
- Xu, H.-P., Burbridge, T.J., Ye, M., Chen, M., Ge, X., Zhou, Z.J., and Crair, M.C. (2016). Retinal Wave Patterns Are Governed by Mutual Excitation among Starburst Amacrine Cells and Drive the Refinement and Maintenance of Visual Circuits. *J. Neurosci.* *36*, 3871–3886.
- Yates, P.A., Roskies, A.L., McLaughlin, T., and O'Leary, D.D. (2001). Topographic-specific axon branching controlled by ephrin-As is the critical event in retinotectal map development. *J. Neurosci. Off. J. Soc. Neurosci.* *21*, 8548–8563.

- Yates, P.A., Holub, A.D., McLaughlin, T., Sejnowski, T.J., and O'Leary, D.D.M. (2004). Computational modeling of retinotopic map development to define contributions of EphA-ephrinA gradients, axon-axon interactions, and patterned activity. *J. Neurobiol.* *59*, 95–113.
- Yin, Y., Yamashita, Y., Noda, H., Okafuji, T., Go, M.J., and Tanaka, H. (2004). EphA receptor tyrosine kinases interact with co-expressed ephrin-A ligands in cis. *Neurosci. Res.* *48*, 285–295.
- Yoon, M. (1971). Reorganization of retinotectal projection following surgical operations on the optic tectum in goldfish. *Exp. Neurol.* *33*, 395–411.
- Young, T.R., Bourke, M., Zhou, X., Oohashi, T., Sawatari, A., Fässler, R., and Leamey, C.A. (2013). Ten-m2 is required for the generation of binocular visual circuits. *J. Neurosci. Off. J. Soc. Neurosci.* *33*, 12490–12509.
- Yu, H.H., Zisch, A.H., Dodelet, V.C., and Pasquale, E.B. (2001). Multiple signaling interactions of Abl and Arg kinases with the EphB2 receptor. *Oncogene* *20*, 3995–4006.
- Yun, M.E., Johnson, R.R., Antic, A., and Donoghue, M.J. (2003). EphA family gene expression in the developing mouse neocortex: regional patterns reveal intrinsic programs and extrinsic influence. *J. Comp. Neurol.* *456*, 203–216.
- Zhang, C., and McCALL, M.A. (2012). Receptor targets of amacrine cells. *Vis. Neurosci.* *29*, 11–29.
- Zhang, S., Xu, M., Kamigaki, T., Hoang Do, J.P., Chang, W.-C., Jenvay, S., Miyamichi, K., Luo, L., and Dan, Y. (2014). Long-range and local circuits for top-down modulation of visual cortex processing. *Science* *345*, 660–665.
- Zhang, Y., Kim, I.-J., Sanes, J.R., and Meister, M. (2012). The most numerous ganglion cell type of the mouse retina is a selective feature detector. *Proc. Natl. Acad. Sci.* *109*, E2391–E2398.
- Zheng, J., Lee, S., and Zhou, Z.J. (2004). A Developmental Switch in the Excitability and Function of the Starburst Network in the Mammalian Retina. *Neuron* *44*, 851–864.
- Zheng, J., Lee, S., and Zhou, Z.J. (2006). A transient network of intrinsically bursting starburst cells underlies the generation of retinal waves. *Nat. Neurosci.* *9*, 363–371.
- Zhou, Z.J. (2001). The function of the cholinergic system in the developing mammalian retina. *Prog. Brain Res.* *131*, 599–613.
- (1997). Unified nomenclature for Eph family receptors and their ligands, the ephrins. Eph Nomenclature Committee. *Cell* *90*, 403–404.

Rôle des éphrines-A rétiniennes dans la mise en place des cartes visuelles

Résumé

L'intégration sensorielle nécessite un alignement correct des cartes nerveuses dans le cerveau. Dans les couches superficielles du colliculus supérieur, situé dans le mésencéphale, des projections en provenance de la rétine ainsi que du cortex visuel primaire doivent être alignés, mais les mécanismes sous-jacents de ce processus demeurent à ce jour méconnus. Afin d'élucider ces mécanismes, éphrine-A3 a été sur-exprimée dans un modèle murin, dans une sous-population des cellules ganglionnaires de la rétine, induisant une disruption de l'alignement de la carte rétino-colliculaire sur la carte cortico-colliculaire. L'inactivation *in vivo* d'éphrine-A3 dans la rétine restaure un phénotype sauvage. Une analyse théorique utilisant un modèle informatique a permis la modélisation des données obtenues. Ces résultats ont permis l'identification d'un principe de base dans l'alignement des cartes et des mécanismes associés, validés par un modèle théorique.

Neuroscience, Développement, carte visuelle, éphrine-A, rétine, colliculus supérieur, cortex visuel primaire

Résumé en anglais

Efficient sensory processing requires correct alignment of neural maps throughout the brain. In the superficial layers of the superior colliculus in the midbrain, projections from retinal ganglion cells and V1 cortex must be aligned to form a visuotopic map, but the basic principle and underlying mechanism are elusive and still incomplete. In a new mouse model, over-expression of ephrin-A3 in a subset of retinal ganglion cells disrupts the cortico-collicular map alignment onto the retino-collicular map, creating a visuotopic mismatch. *In vivo* inactivation of retinal ephrin-A3 over-expression restores a wild-type cortico-collicular map. Theoretical analyses using an original algorithm models the stochastic nature of maps formation and alignment, and recapitulates our observations. Our results identify a basic principle for the alignment of converging maps and the associated mechanism, validated by a theoretical model.

Neuroscience, Development, Visual map, ephrinA, retina, superior colliculus, primary visual cortex